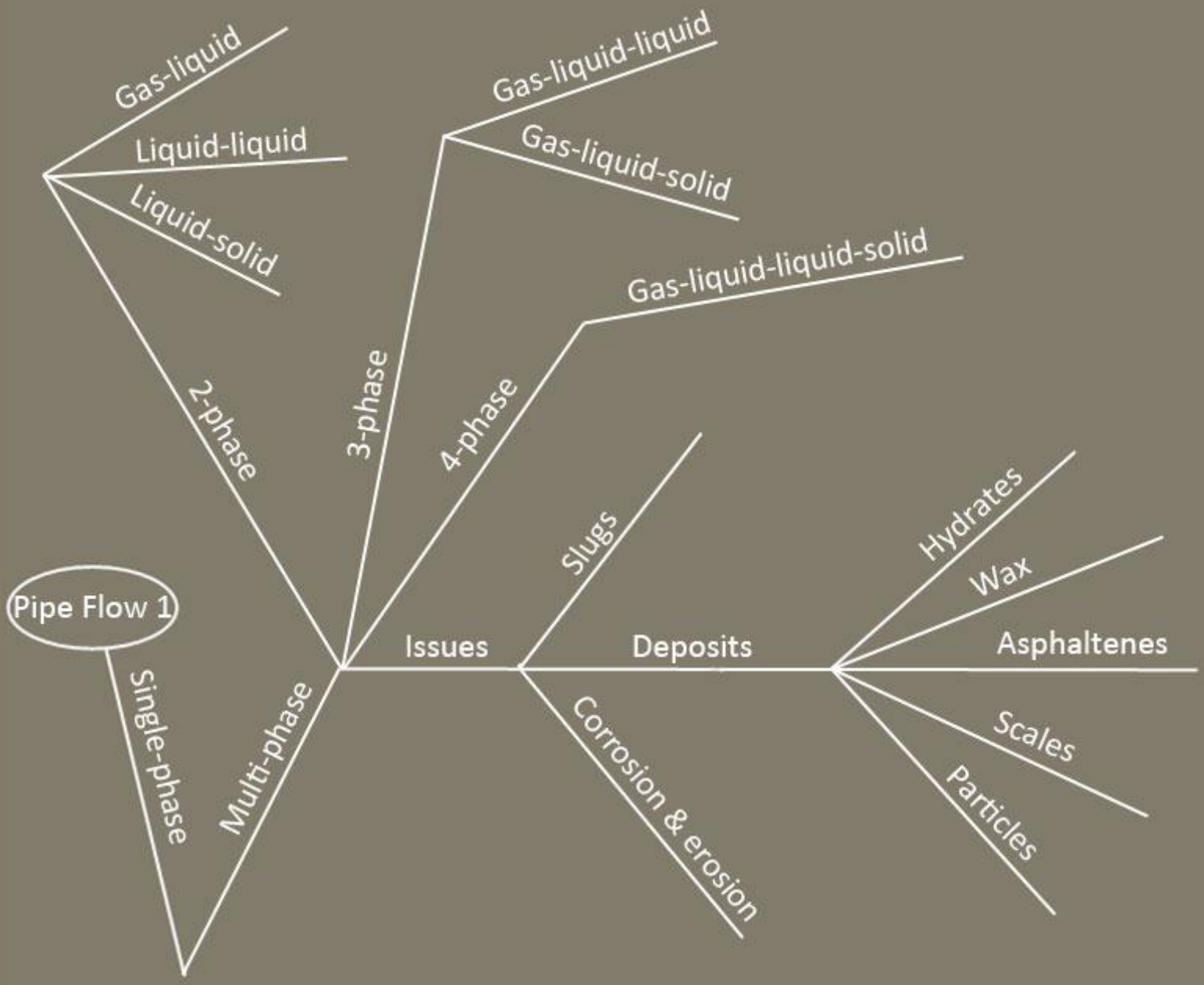

Pipe Flow 2

Multi-phase Flow Assurance

Ove Bratland

"It is now becoming urgent to train large numbers of young professionals from many different nations."
International Energy Agency, USA
About Oil & Gas Technologies for the future

Preface

This book was written during 2009. It is the final in a series of two, the first of which was titled *Pipe Flow 1, Single-phase Flow Assurance*.

Flow assurance – ensuring the fluid flows as intended in a pipe or a well – relies on well-established sciences like fluid mechanics, thermodynamics, mechanical engineering, chemical engineering, discrete mathematics, automation, and computer science. But even though the underlying sciences themselves are well established, flow assurance is developing very rapidly, and writing about it is a bit like shooting at a moving target. During the work with this book it has at times felt like keeping updated on all the latest developments took longer than evaluating and reporting them! Flow assurance is surely progressing faster than the average applied engineering discipline. It is easy to make a long list of important recent developments in each of the previously mentioned subject areas, even if only those which have had direct consequences to the flow assurance field are included.

In mathematics, for instance, numerical methods for solving hyperbolic equations develop constantly, and the improvements generally allow us to make faster, more robust and standardized solutions. Also in the field of mathematics, our understanding of whether the conservation equations are hyperbolic or not in all situations is currently far from perfect, and new articles regarding that are published regularly. Getting it wrong can lead to the simulations crashing or results becoming inaccurate or outright misleading. The list of exciting challenges continues into fluid mechanics, chemical engineering, and the other fields. This book intends building on the most important of these developments while using the latest in contemporary science.

I have included a **Suggested Reading List** at the end of the book, but it contains no books covering flow assurance. To my knowledge this book is presently the only one intending to cover flow assurance for both two-phase, three-phase, and (very briefly)

four-phase flow. There are some good general books on multi-phase flow, but flow assurance is so complex it requires taking advantage of all reasonable simplifications specific to our system. We deal primarily with circular or annular cross-sections, and that has important implications for how best to simplify. The most common models are one-dimensional or quasi two-dimensional, and the flow regimes they can deal with are reduced to a finite number of pre-defined types. More advanced and also more general 2D or 3D models may play an important role in the future, but they are currently restricted to research work or studies of short sections of the flow-path.

The same can be said about the relevant fluids' chemical properties: The goal determines the simplifications we employ. Researchers most interested in fluid mechanics usually prefer very simplified chemical models. That is a natural choice if you desire isolating some detail dealing with turbulence, say, and focus the investigation accordingly. But any useful model for flow assurance calculations on real systems must include rigorous chemical property data and correlations. The phenomena we deal with are highly characteristic of *petroleum fluids flowing in pipes or wells*, and the models have to be designed accordingly. General multi-phase flow theory is not specific enough to include all relevant considerations. Chemical models are also only adequate for our purpose if seen in the context of the actual flow.

Numerous research articles dealing with specific flow assurance problems have been published, but it is hard to learn a subject from articles alone. Mathematicians use slightly different notations than mechanical engineers, and chemists are somewhat different from both groups. Each discipline also tends to build on its own sorts of simplifications, and binding the different sciences together is in many ways a science in itself.

At the time of this publication, an internet search for '*flow assurance*' generates an amazing number of responses, and a very significant amount of them turns out to be companies interested in employing flow assurance engineers. The petroleum industry in general faces a distorted age pyramid, with a large percentage of the most skilled professionals reaching retirement age within the next decade. It appears the industry has an image problem which makes it less attractive to young educated people than 'greener' industries, at least is some countries. The psychology involved is understandable, but the logic less so. Having travelled quite a lot and observed the oil and gas industry at work in many countries, maybe most illustratively during a three year stay in Azerbaijan, I have become convinced that sound management and proper technology can make a huge difference regarding environmental impact. Knowledge is the key to good energy management in the petroleum industry just as in other

industries, and whether we like it or not, those working in the middle of it are best positioned to make a positive difference.

One thing to keep in mind for anyone who is in the process of making a career choice is that the shortage of skilled engineers in the flow assurance field creates very favorable conditions for those who enter it. In addition, flow assurance offers unique possibilities for value creation while at the same time its complexity and fast development eliminates any risk of stagnation in the foreseeable future. That is undoubtedly a very motivating combination few other fields can match.

In an effort to lure more young professionals into the field of flow assurance, I have decided to make the digital version of both books available for free at my internet site drbratland.com.

As for the first book, I am thankful for any comments or corrections the reader might contribute, they can be directed to contact@drbratland.com.

Ove Bratland
January 2010

Acknowledgements

The author wishes to thank the following companies for various discussions and support during the work with these two books: StatoilHydro, SINTEF Petroleum Research AS, AspenTech, Simsci-Esscor, Institute for Energy Technology (IFE), SPT Group, Institut Francais du Petrole (IFP), Telvent, Schlumberger, University of Tulsa, Neotechnology Consultants, Flowmaster, and Advantica.

Thanks also to Prof. Leonid Zaichik for lengthy, open, and illuminating discussions regarding how to improve his and his colleagues' groundbreaking paper on a three-fluid model from 2004, particularly pertaining to liquid entrainment and droplet deposition.

Table of Contents

"A room without books is like a body without a soul."
Cicero, ca. 70 B.C.

1 Introduction

This chapter presents some background information, including:

- When we are likely to encounter multi-phase pipe flow
- Some multi-phase flow history
- Various sorts of flow regimes
- Flow regimes and flow regime diagrams
- Frequently encountered flow assurance challenges
- Some basic definitions

1.1 Multi-phase flow assurance

1.1.1 General

In the first book in this series, *Pipe Flow 1 Single-phase Flow Assurance*, we observed that dealing with single-phase pipe flow is relatively easy in most cases, and the methods for predicting how the fluid behaves are quite mature. There are still important issues requiring further investigation, for instance related to something as basic as determining a pipeline's friction and thereby its capacity, and progress certainly continues. But we rarely depend on any groundbreaking new developments in our flow models to perform the calculations required during planning, design, operator training, or operation of single-phase pipelines.

The technology for multi-phase flow is in a very different stage of development. Although multi-phase flow occurs in many industrial processes, methods of transporting multi-phase fluids through pipelines and wells – which is what this book

is about - has advanced rapidly in recent decades. Multi-phase petroleum wells have existed for a long time, and multi-phase flow plays an important role in the process industry, the nuclear industry, and many others. In spite of that, calculation methods have traditionally been relatively inaccurate and unreliable, at times balancing somewhere between art and science.

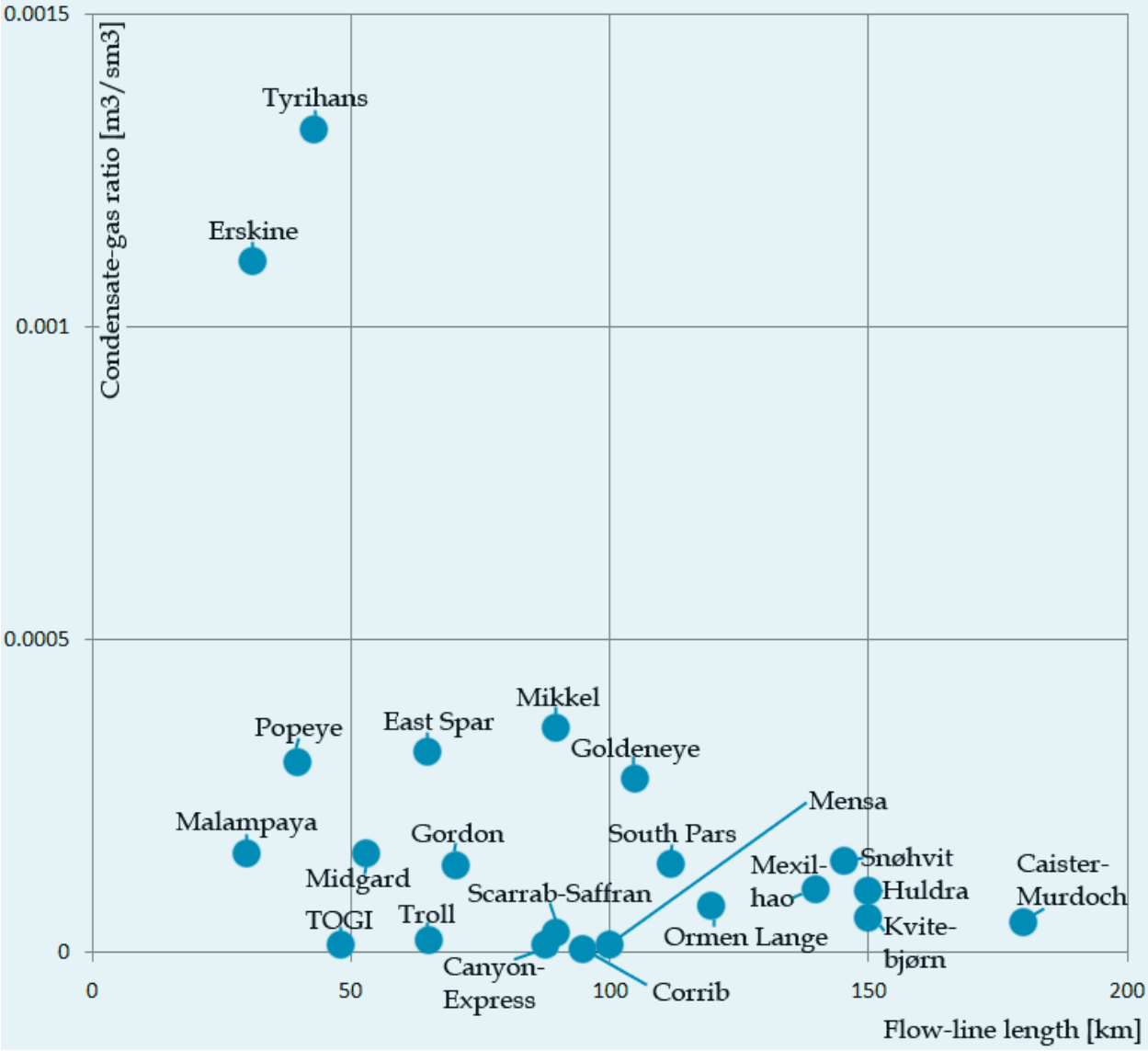

Figure 1.1.1. Current and future multiphase gas-condensate flow-lines plotted as function of flow-line length and condensate-gas flow ratio (the gas flow is defined at standard conditions, which is much higher than at actual pressure and temperature). Some of the fields in the diagram also produce water, and the flow in some of the lines is three-phase. The diagram shows clearly that current technology allows further transfer when the liquid content is low.

Better flow models are now available, and they are of great help both for predicting production rates, evaluating gas injection alternatives, avoiding problems with buildup of hydrates, wax, asphaltenes, scales, or particles. The models are also used to provide data for corrosion and erosion calculations. The best simulation models are based on cutting edge technology, incorporating very recent knowledge.

The latest advancements have benefitted and to a large extent also been driven by the petroleum industry, and it is now possible to transport un-separated gas-oil-water mixtures over quite long distances. This has already had enormous economical impact on some offshore developments, and multiphase flow-lines have in some cases replaced topside offshore installations. That is the case in the Snøhvit- and Ormen Lange-fields off the Norwegian coast, where transport distances are well above *100 km*. At Tyrihans, where production was started 2009, the flow-line length is at *43 km* relatively moderate in comparison, but the liquid to gas flow-rate ratio is much higher. The Tyrihans flow-line connects a new field to existing offshore structures, saving costs by avoiding new topside structures. At the Con Nam Son-field in Vietnam (outside the range of figure 1.1.1), some processing is done near the wellheads, but only to remove produced water. Sending gas and hydrocarbon liquid together in a 400 km two-phase flow-line to shore saves cost both because local processing is reduced (water separation is cheaper than gas-condensate-water separation) and because one line replaces two by transporting gas and condensate together.

Further technology improvements are likely to lead to even greater savings for other fields in the future. In some areas, for instance arctic areas in the north, ice conditions may mean that multi-phase transportation offers not only the most economical option, but even the only one technically feasible. Deep-water fields may also pose prohibitive technical challenges to local separation.

Multi-phase flow is often characterized by liquids and gases occurring simultaneously. Sometimes there are also solids in the mix. Strictly speaking all of the flow phenomena surrounding us are multi-phase since no fluid is so clean it does not contain at least microscopic particles. When we want to describe flow, one of the first challenges we face is therefore deciding whether we need a multi-phase model. As an example, consider the earth's atmosphere. The air contains some water, often in the form of moisture. As long as both air and water are in gas form, the gas-moisture mixture is single-phase and behaves quite similarly to dry air. Properties like density, compressibility, specific heat, and various others are slightly affected by the presence of the moisture, but the equations describing how it flows or how it exchanges heat with its surroundings are not. Describing such a fluid is rather similar to describing *dispersed*

multi-phase flow, for instance small gas bubbles mixed into oil: The gas and oil behave almost like one fluid, and even though dispersed flow is two-phase, a single-phase model can for many purposes approximate it quite well.

If air in the atmosphere is cooled down, droplets or ice crystals will sooner or later form, and the flow becomes two- or even three-phase. Meteorologists can deal with that by regarding the fluid as single-phase and average all properties accordingly, or they may use more advanced multi-phase models. Either way, everything becomes more complicated in that they need to consider such questions as where in time and space the droplets or ice crystals form, how they are distributed, how large they are, how the phase shift affects temperature, in addition to various other problems. No model can realistically describe each droplet or snowflake individually, so some sort of averaging is needed to simplify. Theory for how to average has a prominent place in some of the multi-phase literature.

When a scientist has constructed a model to the best of his ability, done calculations and interpreted the results, he is faced with one final problem: He must evaluate how reliable the results are. That is also a key requirement when designing a multi-phase flow-line, and it has many flow assurance implications. It is not adequate to embrace the results coming out of a commercial simulation tool without asking any critical questions. The tools currently available are very useful and have user friendly interfaces (Bratland, 2008), but they can usually not produce simple, reliable answers. The reason for this is that both the models and the input data rely on simplifications and approximations. As so often in engineering, it is essential to have a good understanding of the underlying assumptions and mechanisms and to investigate where the greatest uncertainties are likely to be found. Cross-checking the results as far as possible, a much more difficult task in multi-phase than in single-phase flow, is also essential.

In the case of meteorology, the undeniable answer will appear as the weather develops, and the models can be frequently updated and tuned to improve results. When dealing with oil and gas developments we are not so fortunate. The first simulations are often carried out years before the pipeline is even laid, at a time when the available input data is quite sparse. At the same time the consequences of inadequate predictions can be very costly and it is certainly possible to end up with a pipeline which cannot do the job it was designed for. Needless to say, it pays to make the best flow assurance efforts possible to minimize the risks.

1.1.2 Nuclear reactor multi-phase models

Much of the multi-phase flow theory used in the petroleum industry today rests on developments done to simulate the coolant water flow around nuclear reactors. Boiling in the reactor core – as in any steam boiler - leads to two-phase flow. It has long been known that different sorts of instabilities can occur, and such instabilities can disturb the heat removal. Various simulation codes have been developed to investigate such phenomena and other potentially hazardous incidents, for instance loss of feed-water. Without going into details, it is worth noting that the models developed for nuclear reactors – models any inquisitive practitioner in the field of multi-phase flow is likely to encounter - differ from those used for petroleum pipelines in several important ways:

Computer codes for nuclear reactors and transport pipelines differ in important ways.

- In nuclear reactors, things happen faster than in pipelines (seconds or minutes, as opposed to hours, days, or weeks). This makes explicit numerical solution methods and their correspondingly small time-steps more acceptable in the nuclear than in the petroleum industry. The short reaction times have implications for other aspects of the theory as well.
- Water is a single-component fluid with well-known properties, and in boilers, it only occurs in two phases. Well-flow, on the other hand, can contain gas, oil, water, as well as sand or other solids, and we therefore sometimes encounter four-phase flow in the petroleum industry. In addition, it is common that the fluid's composition is poorly known, particularly at early project stages.
- The pipes' elevation profiles are very important to how the fluid flows, and they are simple and well known in nuclear reactors. That is often not the case in multi-phase petroleum flows.

1.1.3 Multi-phase flow in the petroleum industry

In the reservoir in figure 1.1.2, the gas is at the top, and the oil further down. The high pressure can lead to some of the gas being dissolved in the oil, and it may start to be released when the pressure is reduced as the oil travels towards the surface via a borehole. To make reasonable flow calculations, we need to predict boiling and the release of gas dissolved in the oil, and these are phenomena to do with chemical properties, pressure, and temperature.

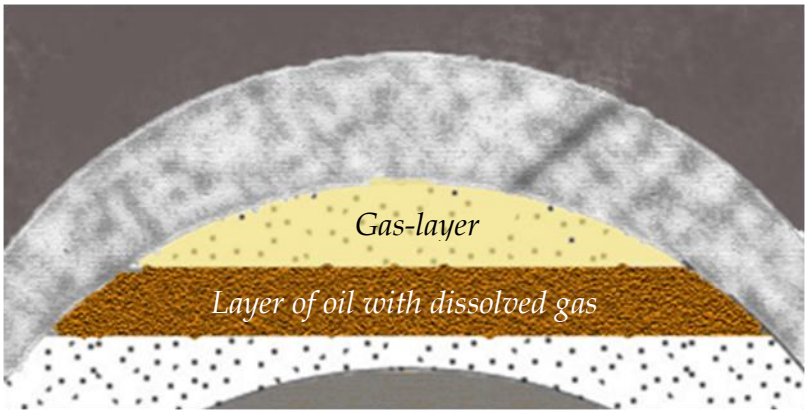

Figure 1.1.2. Petroleum reservoir with gas on top and oil below.

The pressure reduction experienced when hydrocarbons flow towards the wellhead is partly due to friction and partly due to increased elevation. Gas formation and expansion directly affect both the pressure and temperature.

In oil-producing wells we sometimes inject gas via annulus to help the oil rise to the surface. This can improve production rates and prolong the well's economical lifespan, but it can also lead to less stable flow. Some of the challenges involved are discussed later.

Keeping in mind that the well may also produce some water and/or particles, the well's elevation profile may have horizontal or even downhill sections, fluid may flow in at multiple locations, and the fluid composition may change over time, we realize that predicting the flow accurately can be very difficult.

Processing facilities are often not located by the wellhead, so the fluid sometimes continues through gathering networks and flow-lines. The pressures and temperatures in these networks can lead to deposits of hydrates, waxes, or other solids, and corrosion or slugging can also cause problems.

Sometimes we encounter multi-phase flow in pipelines carrying what was intended to be dry gas, and this can lead to similar problems. In less severe cases it simply results in altered pipe friction or reduced gas quality delivered to the customer, but the flow can also become truly multi-phase. In oil pipelines, the presence of gas bubbles, water, or particles can also make the flow multi-phase.

1.2 Two-phase flow

1.2.1 Flow regimes in horizontal pipes

One of the most challenging aspects of dealing with multi-phase flow is the fact that it can take many different forms. In the case of gas-liquid flow, the gas may appear as tiny amounts of small bubbles in the liquid. That kind of flow occurs when there is relatively little gas compared to liquid, at the same time as the liquid flows fast enough to create sufficient turbulence to mix the gas into the liquid faster than the gas can rise to the top of the pipe.

Another extreme occurs if tiny amounts of liquid droplets are carried by the gas. In that case part of the liquid becomes deposited on the pipe's surface and moves as a film in much the same way water moves on the windscreen of a car driving in the rain. Remember that since pressures can be high in pipelines, the gas density is typically much higher that what we are used to experience for air, and even moderate gas velocities can have great impact. Annular droplet flow can be relatively difficult to model accurately since the model needs to incorporate such effects as how fast the droplets are torn from the liquid film, how fast droplets settle on the liquid film, and how the liquid film affects the surface roughness between gas and liquid. In many cases, however, the resulting accuracy is acceptable for our purpose, since this kind of flow does not create the same sorts of problems as slugging does. But it can lead to the various secondary calculations of deposition or corrosion, which use results from the flow models as their input, becoming less accurate.

Figure 1.2.1 illustrates the flow regimes we can encounter in horizontal two-phase gas-liquid flow. Stratified flow has the strongest tendency to occur in downhill or horizontal flow with relatively small gas and liquid flow rates. If we increase the gas velocity, waves start to form, and these waves can get high enough to reach the top of the pipe. When that happens, the gas is throttled or even blocked for a moment so that the flow becomes discontinuous, thus leading to the formation of slugs or elongated bubbles. Slugs are generally unwanted because they can create significant pressure fluctuations, and they can also lead to gas and liquid arriving at the processing facilities unevenly, causing tanks to flood. Since gases have lower density and therefore lower heat capacity than liquids, gases cool faster, so the temperature

Slugs can cause problems by:
- **Creating pressure transients**
- **Leading to flooding at the receiving end**
- **Increasing deposits and corrosion**

reduction during periods of high gas content can more easily cause hydrates to form. The increased intermittent liquid velocity can also accelerate corrosion.

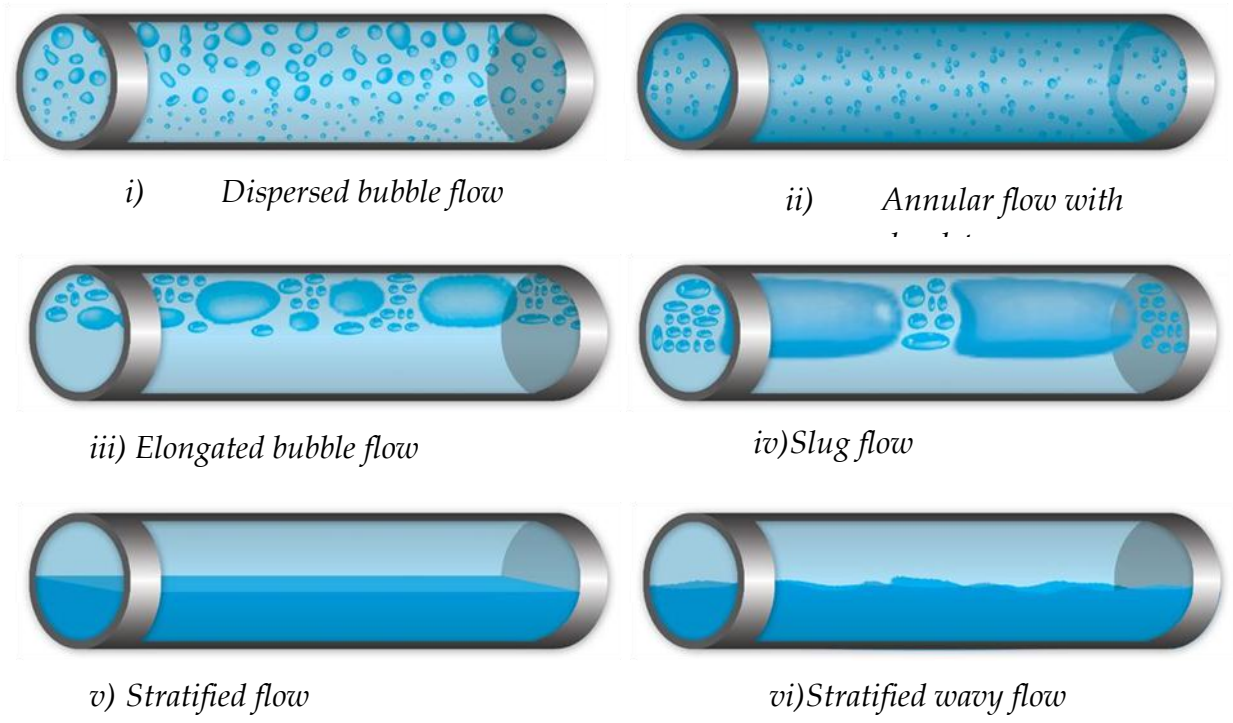

Figure 1.2.1. Gas-liquid flow regimes in horizontal pipes.

1.2.2 Slugging

Slugs forming in horizontal pipes of the sort illustrated on figure 1.2.1 iv) are called *hydrodynamic slugs*, and tend to be relatively short, typically less than 500 pipe diameters.

Another sort of slugs, referred to as *terrain generated slugs*, form when the pipe's elevation profile creates local elevation minima. Terrain generated slugs can have periods of several hours, and can originate in both wells and pipelines.

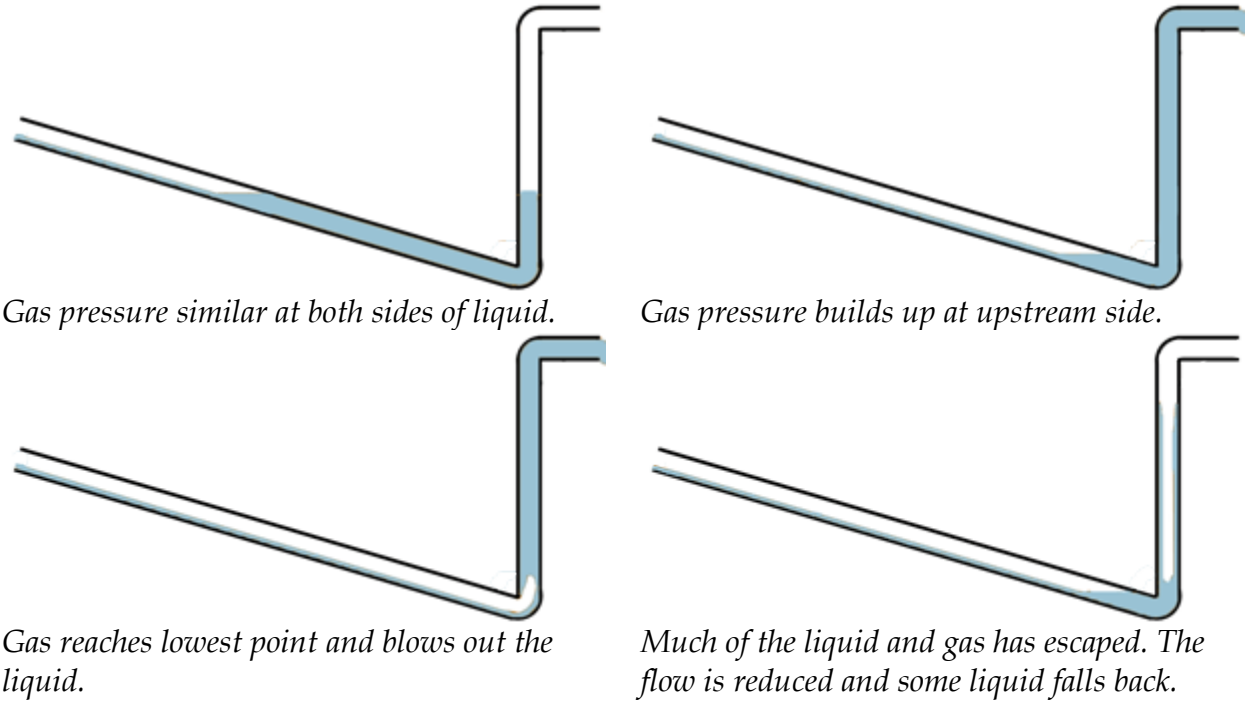

Figure 1.2.2. Terrain slug formation.

Liquid has a tendency to flow towards the low point and block the gas. The gas pressure builds until the gas reaches the low point and begins to escape into the liquid-filled uphill section. Once that occurs, the liquid column carried by the gas gets shorter and shorter, and it becomes easier for the pressure to push it further upwards. As a result, both the liquid and the gas accelerate out of the pipe.

Neither the downhill nor the uphill parts need to be as steep as illustrated here, a degree of elevation can be sufficient for this to happen. It can occur at any low point in the pipe, it does not have to be near the outlet. Risers may create these sorts of slugs if the seabed in front of the riser slopes downwards, and some sorts of risers are shaped like a J or U in order to allow floater movement.

The effect of slugging can be reduced by actively controlling the choke at the riser's outlet. Similar techniques have in some cases succeeded in countering the adverse effect of well slugs by actively controlling the wellhead choke.

Terrain generated slugs can have several hours time periods.

1.2.3 Flow regimes in vertical pipes

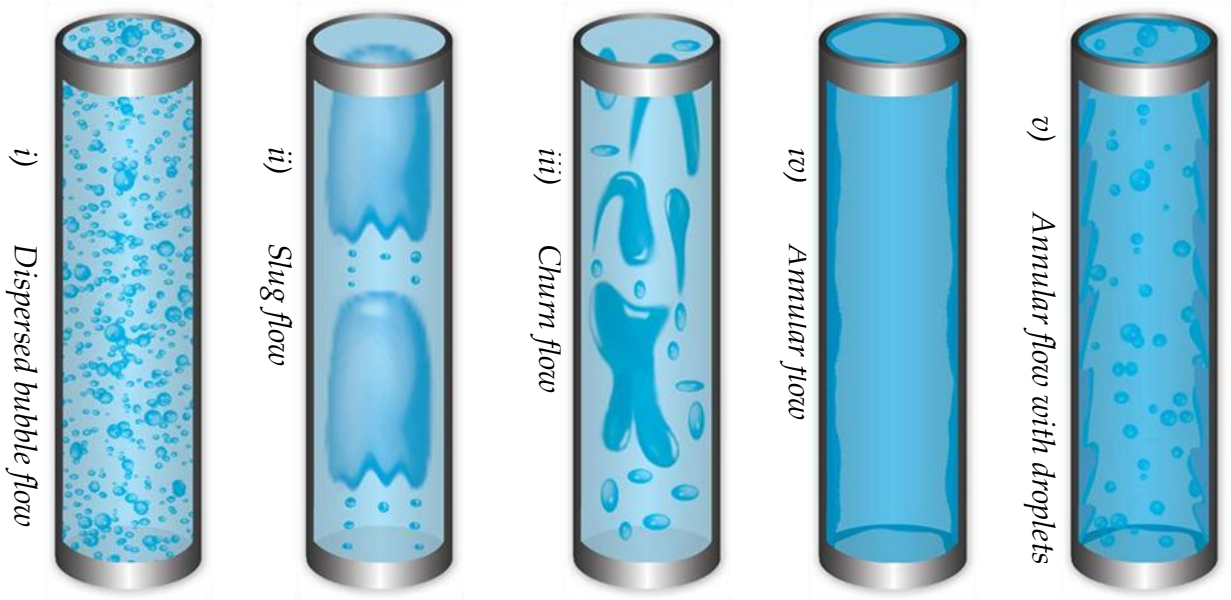

Figure 1.2.3. Gas-liquid flow regimes in vertical pipes.

The flow regimes occurring in vertical are similar to those in horizontal pipes, but one difference being that the there is no lower side of the pipe which the densest fluid 'prefers'. One of the implications this has is that stratified flow is not possible in vertical pipes.

Most of the published measurements have been carried out on horizontal and vertical pipes, which is also what we have shown flow regimes for here. Pipelines generally follow the terrain and most often have other inclinations, so the complexity is often larger than illustrated here.

1.2.4 Flow regime maps

Simulating pipes of any elevation involves determining what kind of flow regime we are facing as well as doing calculations for that particular regime. Flow regime maps of the sort shown in figure 1.2.4 are useful when we want to gain insight into the mechanisms creating the flow regimes.

Along the horizontal axis the *superficial gas velocity* $\alpha_G v_G$ has been plotted. That parameter is more thoroughly defined later, but for now, let us just consider it a way to

quantify the volumetric gas flow (or, by multiplying with the density, the gas mass flow). Along the vertical axis we have plotted the superficial liquid velocity.

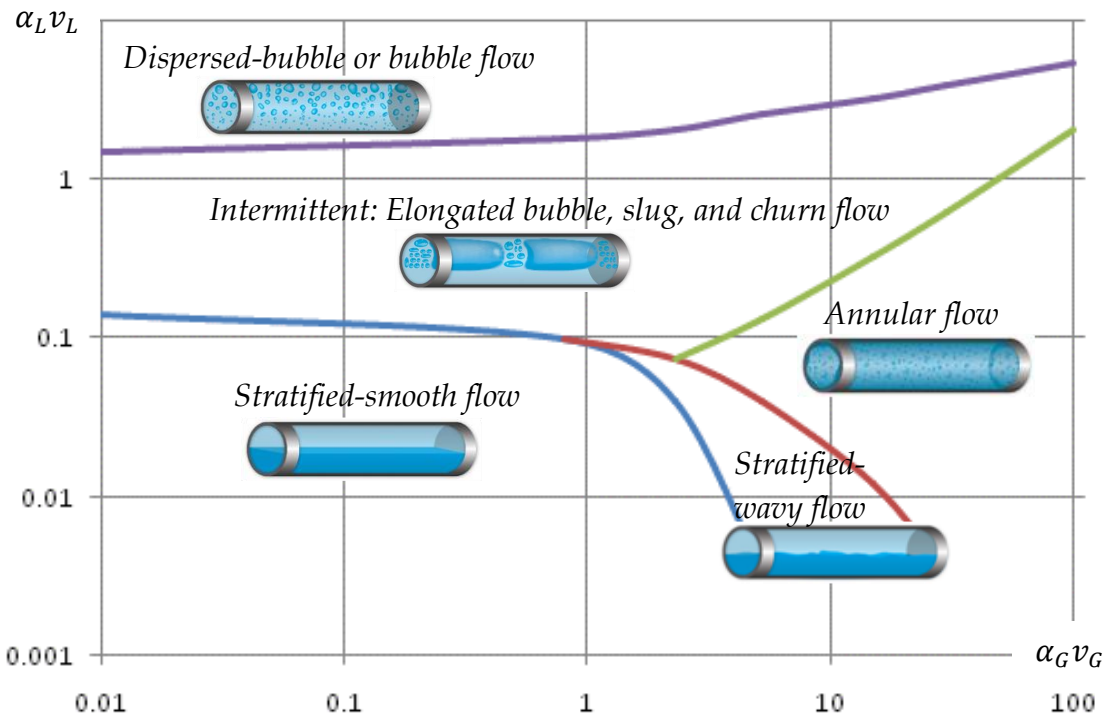

Figure 1.2.4. Example of steady-state flow regime map for a horizontal pipe.

We see that for very low superficial gas and liquid velocities the flow is stratified. That is not surprising: As the velocities approach zero, we expect the pipe to act as a long, horizontal tank with liquid at the bottom and gas on top. If we increase the gas velocity, waves start forming on the liquid surface. Due to the friction between gas and liquid, increasing the gas flow will also affect the liquid by dragging it faster towards the outlet and thereby reducing the liquid level. If we continue to increase the gas flow further, the gas turbulence intensifies until it rips liquid from the liquid surface so droplets become entrained in the gas stream, while the previously horizontal surface bends around the inside of the pipe until it covers the whole circumference with a liquid film. The droplets are carried by the gas until they occasionally hit the pipe wall and are deposited back into the liquid film on the wall. We will later learn how to model this process.

If the liquid flow is very high, the turbulence will be strong, and any gas tends to be mixed into the liquid as fine bubbles. For somewhat lower liquid flows, the bubbles float towards the top-side of the pipe and cluster. The appropriate mix of gas and liquid can then form *Taylor-bubbles*, which is the name we sometimes use for the large gas bubbles separating liquid slugs.

If the gas flow is constantly kept high enough, slugs will not form because the gas transports the liquid out so rapidly the liquid fraction stays low throughout the entire pipe. It is sometimes possible to take advantage of this and create *operational envelopes* that define how a pipeline should be operated, typically defining the minimum gas rate for slug-free flow.

Similar flow regime maps can be drawn for vertical pipes and pipes with uphill or downhill inclinations. Notice that even though numerous measured and theoretically estimated such maps are published in literature, and although they can be made dimensionless under certain conditions (Taitel & Dukler, 1976), no one has succeeded in drawing any general maps valid for all diameters, inclinations and fluid properties. Therefore a diagram valid for one particular situation (one point in one pipeline with one set of fluid data) is of little help when determining the flow regime for any other data set. That is why we need more general flow regime criteria rather than measured flow regime maps.

Flow regime maps are useful tools for getting an overview over which flow regimes we can expect for a particular set of input data. Each map is not, however, general enough to be valid for other data sets.

Characterizing flow regimes from visual observations in the laboratory is complicated as well, and the transitions are difficult to define accurately. To make matters worse, the flow regimes in figures 1.2.1 and 1.2.3 are not the only ones one may include when defining horizontal and vertical gas-liquid flow. Different researchers define different number of flow regimes during laboratory categorization, and the number of regimes implemented in simulations models is sometimes kept lower for simplicity. The flow regime selection shown here constitute therefore only one example of how they may be defined. Predicting the flow regime can be the least accurate part of multi-phase flow calculations.

Another difficulty comes from the fact that measurements, which are most abundant for small diameter pipes, are hard to scale up to larger diameters. This problem effects both flow regime determination and the modeling of each specific regime.

1.2.5 Flow in concentric and eccentric annulus

Sometimes we must deal with multi-phase flow in annular cross-sections. The phenomena and flow regimes encountered in such cases are principally the same as in pipes, but as explained in *Pipe Flow 1*, the frictions tend to be higher. The flow regime changes happen under somewhat different superficial velocities in annular compared to normal pipe flow.

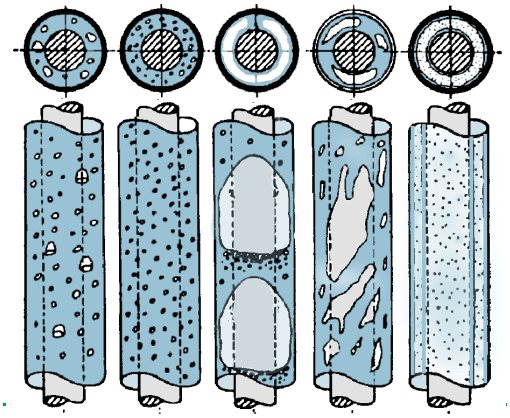

Figure 1.2.5 a) Various annular flow regimes in wellbores. Upward flow and concentric annulus.

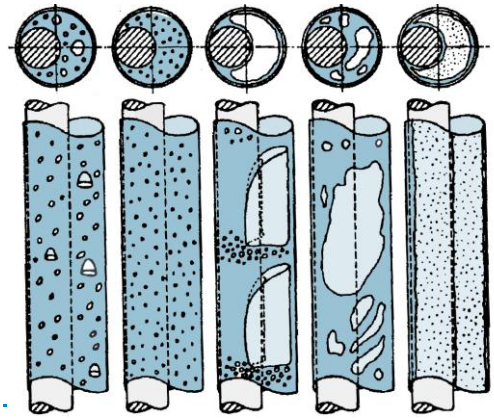

Figure 1.2.5 b) Various annular flow regimes in wellbores. Upward flow and fully eccentric annulus.

Two-phase flow can also occur when the pipe carries two liquids – oil and water, for instance - rather than a gas and a liquid. Liquids tend to have more similar density, and as chapter 13 will reveal, liquid-liquid flow can result in more flow regimes than those mentioned so far.

1.3 Three and four-phase flow

1.3.1 Types of three-phase and quasi four-phase flow

Three phase flow is most often encountered as a mixture of gas, oil and water. The presence of sand or other particles can result in four-phase flow, or we may have three-phase flow with solids instead of one of the other phases. Although sand has the potential to build up and affect the flow or even block it, the most common situation if sand is present is that the amounts are tiny. If we keep the velocities high enough, the sand is quickly transported out of the system, and we can often get away with neglecting the particles in the flow model. Instead, it is only taken into account in considerations to do with erosion or to establish minimum flow limits to avoid sand buildup. The three-phase flow our simulation models have to deal with are therefore primarily of the gas-liquid-liquid sort, and sand is only included – if at all - indirectly.

1.3.2 Three-phase flow regimes

Creating flow regime illustrations similar to those for gas-liquid flow in figures 1.2.1, 1.2.3, and 1.2.4 is very difficult for three-phase flow. Some authors have done so, but they end up with very complex illustrations of limited validity, and the pedagogical value is questionable. It may be more convenient to illustrate three-phase flow as shown in figure 1.3.1.

The diagram has been plotted in three dimensions, one for each phase. The vertical axis contains the gas superficial velocity as a fraction of the total superficial velocities. That superficial velocity fraction has been defined so that it becomes *1* for pure gas flow. For pure liquid (oil-water) flow, which corresponds to a straight line in the oil-water plane, the gas fraction is zero. Similarly, if the water content is zero, our operation point will be located somewhere on a line in the gas-oil plane, and so on for zero oil content. Operation points inside the triangle will correspond to three-phase flow.

The zero oil and zero water content planes in figure 1.3.1 correspond to gas-liquid flow regimes similar to those discussed in chapter 1.2. In the oil-water plane, the liquid-liquid mixture can show a very interesting property we have not mentioned yet: The oil can occur as isolated droplets dispersed in the continuous water. If we increase the oil content, the flow can suddenly switch to the opposite situation in a process called *phase inversion*. The dispersion's viscosity

Three-phase gas-liquid-liquid flow can in some cases be treated as two-phase gas-liquid flow in the simulation model.

tends to be quite similar to the continuous phase's viscosity, which normally is much higher for oil than for water. Whether we have an oil-in-water or water-in-oil dispersion is therefore very important to the mixture's viscosity, and we can observe significant viscosity 'jumps' when a phase inversion occurs. If we take a look at the modified Moody diagram, we see that the consequences of using inaccurate viscosity (and thereby inaccurate Reynolds number) in the friction calculations depend on where in the diagram our operational point is located – for relatively high Reynolds numbers and/or high surface roughness, it may have little or no influence.

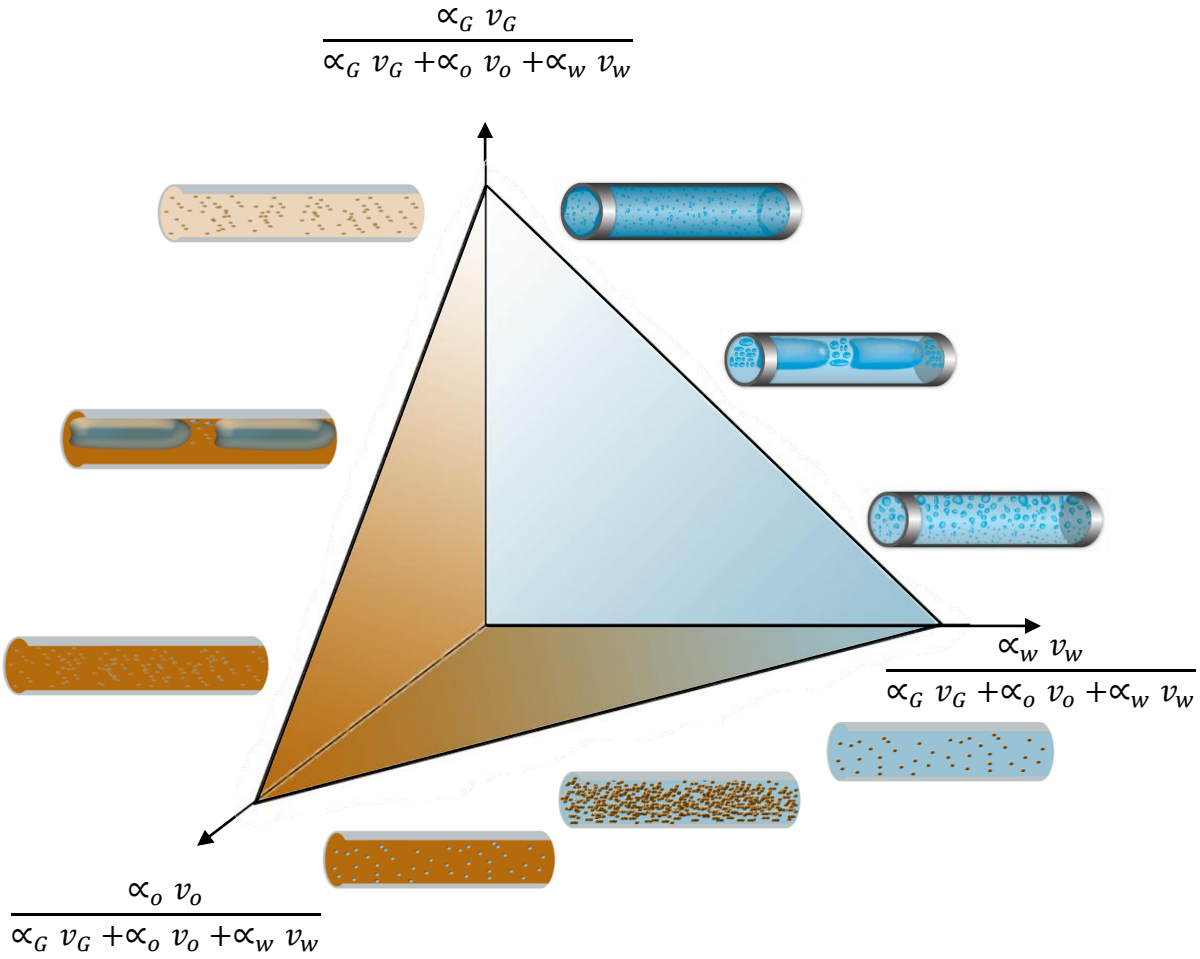

Figure 1.3.1. Three-phase gas-oil-water diagram for horizontal pipes. The illustrations along the borders show some (though not all) of the two-phase flow regimes possible for gas-oil (left border), gas-water (right border), and oil-water (lower border) flow. When all phases are present simultaneously, many more different flow regimes become possible.

We can also experience other liquid-liquid flow regimes, and the number of possible regimes becomes very large when we move upwards in the three-phase diagram. As a general rule, it is likely the liquids appear as one dispersed in the other if they occur in very different quantities. In some cases we can get reasonable results by treating the two liquids as one averaged liquid and reduce the problem to two-phase gas-liquid flow. Some of the commercial software treats three-phase gas-liquid-liquid flow in this way in all situations, but it can lead to quite inaccurate results for some flow regimes.

1.4 Typical flow assurance tasks

The various challenges involved in flow assurance for single-phase flow was discussed in *Pipe Flow 1*. In multi-phase flow, the most important additional challenges are related to slugging and the various phenomena which can block or even rupture the pipe. They are more thoroughly treated in later chapters, but some of the main issues are mentioned below:

Slugs: The challenge is to avoid, minimize, or design the system so that we can live with slugs.

Hydrates: Hydrates are ice-like structures which tend to form if the temperature falls below a certain value when gas molecules are in contact with water. We try to avoid steady-state hydrate formation (hydrates forming under normal circumstances) by injecting inhibitors, using thermo-insulation or even heating. We also attempt to optimize cooldown-times, allowing us sufficient time to take action in case of shutdown, but without increasing costs more than necessary. Achieving acceptable hydrate avoidance conditions at a minimum cost usually includes simulating the known or presumed fluid composition for various alternative anti-hydrate strategies and ranking the results. The solution must be flexible enough to be able to deal with uncertainties, and remediation methods in case of blockages are also normally considered.

Wax: Depending on the fluid's composition, paraffins in the oil can create challenges similar as for hydrates, the difference being that we may accept steady-state buildup and simply choose a high enough pigging frequency to scrape out built-up wax before the layer becomes thick enough to create problems.

Asphaltenes: This is also quite similar to dealing with hydrates or wax, but chemical properties making it a problem is encountered somewhat less frequently.

Scale: Scale deposits differ from the others mentioned above in that they are inorganic, come from produced water, and tend to be harder. Like the others, though, they can be prevented or removed by inhibitors and pigging. Chemicals can also be used to remove scales.

Corrosion and erosion: External corrosion is almost always of concern to steel pipelines, but it is beyond the scope of this book. Depending on what the pipe transports, internal corrosion is frequently also a concern. The chemistry involved in corrosion is very complex, and it remains a rapidly developing field. Corrosion is strongly affected by temperature, pressure, and velocity, and corrosion models can take such data from the flow models and use them as input. Pure erosion is usually not a problem in petroleum pipelines, but erosion in combination with corrosion can enhance each other to produce more damage than they would separately.

Multi-phase flow assurance is all about managing slugs, deposits, corrosion and erosion.

1.5 Some definitions

1.5.1 General

For the most part this book follows the definitions laid down in the first book, *Pipe Flow 1*. Multiphase flow also calls for additional definitions, some because they improve clarity, while others have become popular for less obvious reasons. This book tries to avoid jargon deemed to be of the second sort, but with some exceptions for terminology essential to understanding other relevant publications.

1.5.2 Volume fraction, holdup and water cut

When we have multiple phases passing through a cross-section of the pipe, each phase can obviously not cover more than a fraction of the area. If, for instance, a fourth of the cross-section is occupied by gas, we say the gas *area fraction* (or the *volume fraction,* since volume corresponds to area if the length of that volume is infinitely small) or simply the gas *fraction* $\alpha_G = 0.25$. If the remaining area is occupied by liquid, the liquid fraction has to be $\alpha_L = 1 - 0.25 = 0.75$.

Some authors choose to use a different name for liquid fraction and call it *liquid holdup* or simply *holdup*, while sticking to the *fraction*-terminology in case the fluid is a gas.

The term *water cut* is also used occasionally, particularly in describing a well's production. It means the ratio of water volumetric flow compared to the total volumetric liquid flow. Gas – if there is any – is not taken into account in this definition. Note that water cut does not in itself describe how much water there are in the liquid, since water and the other liquid(s) may flow at different velocities. Water cut refers to production rate fraction, not volume fraction. If the liquids are oil and water, the water cut is $\alpha_w v_w/(\alpha_o v_o + \alpha_w v_w)$.

1.5.3 Superficial velocity

In single-phase flow, we often define instantaneous average velocity (the average velocity at a particular point in time) as volumetric flow Q *[m³/s]* divided by pipe cross-sectional area A *[m²]*. That way, the average velocity directly reflects the volumetric flow.

In multi-phase flow, the part of the area occupied by one particular phase varies in space and time, so the flow is no longer proportional to the velocity at a given point. But if the gas phase occupies area $\alpha_G A$, we may define the average gas velocity in that part of the cross-section as $Q_G = \alpha_G A v_G$. By solving this equation for $\alpha_G v_G$, we define the gas' *superficial velocity* as:

$$\alpha_G v_G = \frac{Q_G}{A} \tag{1.5.1}$$

We see that the superficial velocity is proportional to the volumetric flow, and it can be regarded as the average instantaneous velocity the phase would have had if it occupied the whole cross-sectional area of the pipe. Since it often occupies only part of it, the superficial velocity tends to be lower than the actual average velocity.

1.5.4 Mixture velocity and density

The mixture (average) velocity in a mixture of N phases is defined as:

$$v_M = \sum_{k=1}^{N} \alpha_k v_k \tag{1.5.2}$$

We sometimes make use of the mixture (average) density, which is defined as:

$$\rho_M = \sum_{k=1}^{N} \alpha_k \rho_k \tag{1.5.3}$$

Other mixture properties or quantities can be defined in a similar fashion.

1.5.5 Various sorts of pipes

In this book, *pipe* is used with a broad meaning and includes what some authors may call channel, duct, conduit, tube, wellbore, line, riser, or hose. We sometimes also use *flow-line* or *gathering network* to emphasize that we are referring to the pipe(s) transporting produced gas/oil/water/sand from one or several wellhead(s) to the processing facility.

The multitude of names used to express *pipe* is worth keeping in mind when searching for related literature – the term 'vertical pipe slug', say, may not turn up in certain articles, even if 'vertical duct slug' does.

"Education is the best provision for old age."
Aristotle, 350 BC.

2 Conservation equations

The main equations for transient multi-phase flow with *N* phases:

- Mass conservation
- Momentum conservation
- Energy conservation
- Mass transfer between phases

2.1 Introduction

In the first book, *Pipe Flow 1*, we learned that *3* conservation equations - mass conservation, momentum conservation, and energy conservation – was sufficient to describe the main conservation principles governing transient single-phase flow. For multi-phase flow, the same three equations apply, but for each phase. Therefore, expect to need *6* equations to describe two-phase flow, *9* to describe three-phase flow, and so on. In practice it does not work quite like that, though, because we take advantage of some simplifications, and some phases may occur in more than one form (in annular flow, there can be both liquid droplets carried by the gas and a liquid film on the pipe wall). We also use additional equations - *closure correlations* - to describe how the phases interact with each other and the pipe wall, as well as to describe the fluid properties.

The simple illustration of multi-phase flow in figure 2.1.1 can for instance symbolize two-phase flow consisting of steam and water. Water can occupy more or less of the available space along the pipe, so we cannot assume the water cross section to be constant. In addition, water may turn into steam or vice versa, so we can no longer assume all water to enter via the control volume's boundaries – some may come from the steam inside the control volume. Although not shown on the figure, the pipe wall may also be perforated and allow fluid to pass through it.

In a more general case, we may have N different phases rather than only 2. We have seen that those phases can be distributed in several alternative ways – there can be bubbles, droplets, slugs, and various other sorts of fluid distributions. At this stage, though, we simply assume each phase to be continuous, without necessarily taking up the same cross-section everywhere along the pipe.

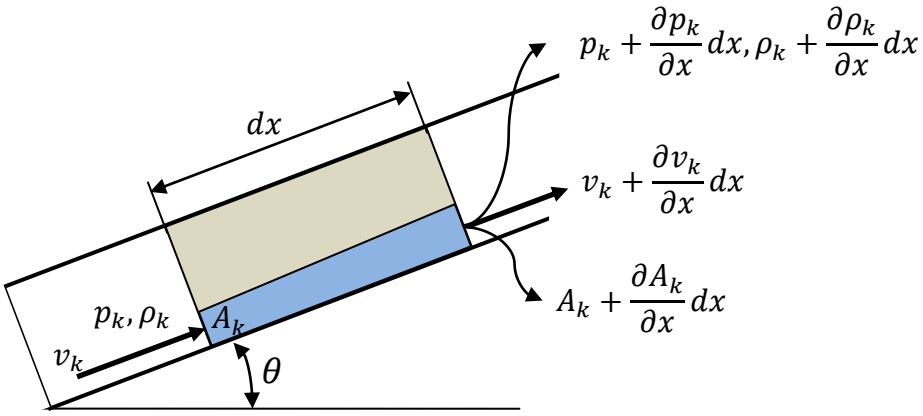

Figure 2.1.1. Compressible multi-phase pipe flow.

2.2 Mass conservation

Phase No. k is assumed to take up cross-sectional area A_k, while the total pipe cross-section is A. From that, we define the volume fraction as:

$$\propto_k \stackrel{\text{def}}{=} \frac{A_k}{A} \tag{2.2.1}$$

Analogy with the single-phase mass conservation equation implies that for each phase k in a multi-phase flow, the following must generally hold:

$$0 = \begin{matrix}\textit{accumulated}\\ \textit{mass}\end{matrix} + \begin{matrix}\textit{net mass flow into}\\ \textit{the control volume}\end{matrix} + \begin{matrix}\textit{mass from}\\ \textit{other phases}\end{matrix} + \begin{matrix}\textit{mass from}\\ \textit{other sources}\end{matrix} \tag{2.2.2}$$

$$0 = Adx\frac{\partial(\alpha_k\rho_k)}{\partial t} + Adx\frac{\partial}{\partial x}(\alpha_k\rho_k v_k) + \sum_{i=1}^{N,i\neq k}\dot{m}_{ki} + \dot{m}_{kW}$$

The term $\dot{m}_{ki}$ represents the interface mass flows from each of the other phases into phase k, and $\dot{m}_{kW}$ is mass flow into phase k from other sources such as inflow through perforations in a well. For simplicity, we omit the summation sign, and in effect let $\dot{m}_{ki}$ stand for the sum of all mass flows into phase k rather than each component of it.

We re-arrange equation 2.2.2 to:

$$\frac{\partial(\alpha_k\rho_k)}{\partial t} + \frac{\partial}{\partial x}(\alpha_k\rho_k v_k) = \frac{\dot{m}_{ki}}{Adx} + \frac{\dot{m}_{kW}}{Adx} \tag{2.2.3}$$

The continuity equations for each phase are very similar to the one for single-phase flow, but with two extra terms on the right hand side of the equation. They are *volume-specific mass flows*, and we denote them Γ_k *[kg/(s·m³)]*:

$$\frac{\partial(\alpha_k\rho_k)}{\partial t} + \frac{\partial(\alpha_k\rho_k v_k)}{\partial x} = \Gamma_{ki} + \Gamma_{kW} \tag{2.2.4}$$

The terms Γ_{ki} and Γ_{kW} therefore represent mass transfer per unit volume and time into phase k from all the other phases and from mass sources. Γ_{ki}, it follows, is in reality a sum of several sources and contains one source from each of the other phases the fluid consists of (although some or all may often be zero). In the special case that no part of the fluid changes phase and nothing flows in through perforations in the pipe wall, we obviously get $\Gamma_{ki} = 0$ and $\Gamma_{kW} = 0$.

Phase change cannot result in altered total mass, so one phase's gain must be another phase's loss. That can be expressed as:

$$\sum_{k=1}^{N} \Gamma_{ki} = 0 \tag{2.2.5}$$

In order to determine how each fraction appears, it is necessary to know each component's properties. In the simple case that the fluid consists only of water and steam, we have one *component*, H_2O, and two *phases*. The simulation program must have access to steam and water properties to determine how much condensation or boiling takes place and thereby quantify Γ_{ki}. In our models we generally neglect any chemical time delay involved when gas becomes liquid or vice-versa, and instead simply assume instantaneous equilibrium for the pressures, volumes, and temperatures involved. In chapters 17 and 18 we will discover that it is relatively complicated to model pressure-volume-temperature relationships for real petroleum fluids accurately, and in flow assurance calculations, it is common to use third-party software for that task.

Another useful relation follows from the definition of what a volume fraction is: The sum of all volume fractions must be *1* to fill the pipe's cross section. It is sometimes referred to as the *saturation constraint* and expressed as:

$$\sum_{k=1}^{N} \alpha_k = 1 \tag{2.2.6}$$

Equations 2.2.4 – 2.2.6 form the basis for mass conservation in multi-phase pipe flow.

2.2.1 Comparing single-phase and multi-phase mass conservation

As an example, let us consider single-phase flow as a special case of multi-phase flow by simply setting $N = 1$. Equation 2.2.6 implies that $\alpha_k = \alpha_1 = 1$. Equation 2.2.5 leads to

$\Gamma_{ki} = 0$. If nothing flows in through the pipe wall, $\Gamma_{kW} = 0$, and equation 2.2.4 simplifies to:

$$\frac{\partial \rho}{\partial t} + \frac{\partial (\rho v)}{\partial x} = 0 \tag{2.2.7}$$

As expected, this turns out to be the familiar mass conservation equation for single-phase flow.

2.2.2 Mass conservation for well mixed phases

Another interesting special case arises if the different phases are so well mixed that they travel at the same velocity. This can be the situation in a liquid containing a moderate amount of small bubbles, or in a liquid containing droplets of another, immiscible liquid. If the pipe also is un-perforated, then $\Gamma_{kW} = 0$ for all phases k.

By combining equations 2.2.4 and 2.2.5 it follows that:

$$\sum_{k=1}^{N} \frac{\partial (\alpha_k \rho_k)}{\partial t} + \sum_{k=1}^{N} \frac{\partial (\alpha_k \rho_k v_k)}{\partial x} = \frac{\partial}{\partial t} \sum_{k=1}^{N} (\alpha_k \rho_k) + \frac{\partial}{\partial x} \sum_{k=1}^{N} (\alpha_k \rho_k v_k) = 0 \tag{2.2.8}$$

The average density is obviously:

$$\bar{\rho} = \sum_{k=1}^{N} (\alpha_k \rho_k) \tag{2.2.9}$$

All velocities being identical implies:

$$\bar{\rho} v = \sum_{k=1}^{N} (\alpha_k \rho_k v_k) \tag{2.2.10}$$

When inserting equation 2.2.9 and 2.2.10 into 2.2.8, we get:

$$\frac{\partial \bar{\rho}}{\partial t} + \frac{\partial (\bar{\rho} v)}{\partial x} = 0 \tag{2.2.11}$$

This illustrates that mass conservation for well-mixed multi-phase-flow can be modeled as single-phase by simply using the average density – not a surprising result.

Although not shown here, other equations require us to modify other properties as well if we want to make the model complete. Even a very small amount of air in water, for instance, increases the compressibility and reduces the speed of sound dramatically.

2.3 Multi-phase momentum conservation

2.3.1 Main equations

Newton's second law applied to one phase can be written as:

$$\begin{array}{ccccc} \text{Mass} & \cdot & \text{acceleration} & = & \text{Sum of all forces} \\ A\alpha_k dx \rho_k & \cdot & \dfrac{dv_k}{dt} & = & \sum F_k \end{array} \tag{2.3.1}$$

Ordinary derivatives and partial derivatives relate to each other as:

$$dv_k = \frac{\partial v_k}{\partial t} dt + \frac{\partial v_k}{\partial x} dx \tag{2.3.2}$$

By dividing all terms in equation 2.3.2 with dt and also defining velocity as $dx/dt = v$, we get:

$$\frac{dv_k}{dt} = \left(\frac{\partial v_k}{\partial t} + v \frac{\partial v_k}{\partial x} \right) \tag{2.3.3}$$

We can now insert equation 2.3.3 into 2.3.1:

$$A\alpha_k dx\rho_k\left(\frac{\partial v_k}{\partial t}+v\frac{\partial v_k}{\partial x}\right)=\sum F_k \tag{2.3.4}$$

The derivative of a product can be re-formulated as:

$$\frac{\partial[(\alpha_k\rho_k)\cdot v_k]}{\partial t}=\alpha_k\rho_k\frac{\partial v_k}{\partial t}+v\frac{\partial(\alpha_k\rho_k)}{\partial t} \tag{2.3.5}$$

Hence:

$$\rho_k\alpha_k\frac{\partial v_k}{\partial t}=\frac{\partial(\rho_k\alpha_k v_k)}{\partial t}-v\frac{\partial(\rho_k\alpha_k)}{\partial t} \tag{2.3.6}$$

Similarly:

$$\alpha_k\rho_k v_k\frac{\partial v_k}{\partial x}=\frac{\partial(\alpha_k\rho_k {v_k}^2)}{\partial x}-v\frac{\partial(\alpha_k\rho_k v_k)}{\partial x} \tag{2.3.7}$$

Inserting equations 2.3.6 and 2.3.7 into 2.3.4 yields:

$$Adx\left(\frac{\partial(\alpha_k\rho_k v_k)}{\partial t}-v_k\frac{\partial(\alpha_k\rho_k)}{\partial t}+\frac{\partial(\alpha_k\rho_k {v_k}^2)}{\partial x}-v\frac{\partial(\alpha_k\rho_k v_k)}{\partial x}\right)=\sum F_k \tag{2.3.8}$$

By re-arranging the terms, this can be written as:

$$\frac{\partial(\alpha_k\rho_k v_k)}{\partial t}+\frac{\partial(\alpha_k\rho_k {v_k}^2)}{\partial x}-v\left[\frac{\partial(\rho_k\alpha_k)}{\partial t}+\frac{\partial(\alpha_k\rho_k v_k)}{\partial x}\right]=\frac{1}{Adx}\sum F_k \tag{2.3.9}$$

The terms in brackets turn out to be the left hand side of the mass conservation equation 2.2.4. Inserting that, we get:

$$\frac{\partial(\alpha_k \rho_k v_k)}{\partial t} + \frac{\partial(\alpha_k \rho_k {v_k}^2)}{\partial x} = v(\Gamma_{ki} + \Gamma_{kW}) + \frac{1}{Adx}\sum F_k \qquad (2.3.10)$$

It is not surprising that the mass transfer terms Γ_{ki} and Γ_{kW} turn up in the momentum conservation equation too. After all, the fluid going from one phase to another, Γ_{ki}, or flowing in through perforations in the pipe, Γ_{kW}, takes its momentum with it.

Thus far we have not discussed exactly which velocity v symbolizes, but it now appears to represent the velocity for the phases or external sources that transfer mass to phase k. Since Γ_{ki} is the sum of mass transfer from all other phases, v must be some sort of average when written in this general form. In practical calculations we would of course insert each phase's velocity. We need to keep in mind also that in our one-dimensional model, only axial momentum is included. This is further elaborated in chapter 3.2.

The different forces acting on the phase must be determined in order to quantify $\sum F_k$. As for single-phase flow, there are obviously going to be pressure, gravity, and friction forces. Since phase k is in contact with other phases, it is no longer only the pipe wall which can exert a friction force on it, and we get additional friction terms.

The next two force contributions may at first seem somewhat unfamiliar: Surface tension and a pressure correction term.

Surface tension is the force that makes it possible for some insects to walk on water. It also makes water 'prefer' to cluster and form drops rather than spread out as individual molecules when it is raining. Surface tension is caused by intermolecular forces trying to attract the molecules towards each other. In the bulk of the fluid, each molecule is pulled equally in all directions by neighboring liquid molecules, resulting in a net force of zero. At the surface, however, the molecules are pulled inwards by other molecules deeper inside the fluid, and they may not be attracted as intensely by the molecules in the neighboring medium (be it vacuum, another fluid or the pipe wall). In that case all molecules at the surface are subject to an inward force of molecular attraction. This results in a higher pressure at the inside. The liquid tries to achieve the lowest surface area possible, similar to a balloon when we pump air into it. Without attempting to dive fully into all details, let us just accept that surface tension can create forces both from other phases to phase k as well as from the pipe wall to phase k. A surface interface (a droplet surface, say) may stretch through a control volume boundary, and that can in

principle create some modeling problems, but we will ignore that for now. Also, note that the surface interfacial tension is a physical property with a value depending on the fluids or materials involved. Surface tension between water and vacuum, for instance, is not identical to surface tension between water and a particular hydrocarbon.

The surface tension is generally small compared to many other forces at work, and we will later see that in many cases it can be neglected. It can play a crucial role in some important phenomena, though, for instance the formation of droplets and bubbles or formation of short-wavelength surface waves, and it plays a role in determining the flow regime. This book's models neglect the surface tension forces in the main momentum balances, electing to deal with flow regime transitions in separate criteria. In the general momentum equations developed in this chapter, though, we include surface tension forces mainly to emphasize that they exists.

The various forces acting in phase *k* can then be expressed as:

$$\frac{1}{Adx}\sum F_k = F_{k\,pg} + F_{k\,g} + R_{ki} + R_{kW} + S_{ki} + S_{kW} \tag{2.3.11}$$

The different forces in the pipe's axial direction on phase k is as follows: $F_{k\,pg}$ is the pressure force due to a pressure gradient along the pipe, $F_{k\,g}$ is the gravity force along the pipe due to the pipe's inclination, R_{ki} is the friction force from other phases (the sum of contributions from each phase), R_{kW} is the friction force from the wall, S_{ki} is the force due to surface tension from all other phases (the sum of contributions from each phase), and S_{kW} is the surface tension force from the wall. Note that since $\sum F_k$ has the term $1/Adx$ in front of it, all the force terms on the right-hand side of equation 2.3.11 are on the volume-specific form, meaning they are forces pr. unit volume of pipe$[N/m^3]$.

Finding good approximations for each of the forces to be inserted into equation 2.3.11 is not easy. A correlation for the pressure force $F_{k\,pg}$, for instance, can in principle be found by looking at figure 2.1.1 and expressing the forces at each end of the studied element. That works fine as long as the phases are separated in layers in the way the figure indicates, but would obviously not be as straight-forward if one or several phases appeared as bubbles or droplets. Ignoring that problem for now, we simply calculate the volume-specific net force in the axial direction due to pressure on the surfaces on phase *k* as:

$$F_{k\,pg} = \frac{A\alpha_k p_k + F_{k\,int\,x} - A\left(\alpha_k + \frac{\partial \alpha_k}{\partial x}dx\right)\left(p_k + \frac{\partial p_k}{\partial x}dx\right)}{Adx} \tag{2.3.12}$$

$F_{k\,int\,x}$ is the internal axial force on phase k due to the pressure on the surface inside the control volume. That force depends both on how the *pressure on* and *the shape of* the phase vary from inlet to outlet of the control volume, and they are both unknown. As an example, consider a situation where the pressure on the outside of phase k and the fraction of phase k vary linearly from the control volume's inlet to outlet. In that case, the average pressure will be $p_k + 1/2\ \partial p_k/\partial x \cdot dx$, and the effective area on which the axial force works is $A\partial\alpha_k/\partial x \cdot dx$. Inserting that into equation 2.3.12, we get:

$$F_{k\,pg} = -\alpha_k \frac{\partial p_k}{\partial x} - \frac{1}{2}\frac{\partial \alpha_k}{\partial x}\frac{\partial p_k}{\partial x}dx \tag{2.3.13}$$

If we assume other pressure distributions, we will see that it only alters the factor in front of the last term in equation 2.3.13. If we ignore higher order terms, any axial pressure distribution inside the control element would lead to the same result, namely:

$$F_{k\,pg} = -\alpha_k \frac{\partial p_k}{\partial x} \tag{2.3.14}$$

The volume-specific gravity-force is very similar to how it was for single-phase flow:

$$F_{k\,g} = \frac{-A\alpha_k dx \rho_k g \sin\theta}{Adx} \tag{2.3.15}$$

This can be expressed as:

$$F_{k\,g} = -\alpha_k \rho_k g \sin\theta \tag{2.3.16}$$

The other forces are less meaningful to express in a general way and have to be considered after the flow regime has been determined. If we simply combine equations 2.3.10, 2.3.11, 2.3.14 and 2.3.16, we get:

$$\frac{\partial(\alpha_k \rho_k v_k)}{\partial t} + \frac{\partial(\alpha_k \rho_k {v_k}^2)}{\partial x} = -\alpha_k \frac{\partial p_k}{\partial x} + (R_{ki} + R_{kW}) + (S_{ki} + S_{kW}) + (v_{ki}\Gamma_{ki} + v_{kW}\Gamma_{kW}) - \alpha_k \rho_k g \sin\theta \quad (2.3.17)$$

2.3.2 Pressure differences between phases due to elevation differences

Equation 2.3.17 on the form it stands here uses separate pressures for all phases. It seems reasonable to assume that in our one-dimensional model we could adopt the same pressure in all phases, and therefore set $p_k = p$ for all k. It turns out that this is not always a good idea, and we sometimes introduce a *pressure correction term* to describe this pressure difference between phases. The term itself is discussed in greater detail in chapters 3.4 (for two-phase flow) and 15.3 (for three-phase flow).

To conceptualize why, consider the case of stratified flow shown on figure 2.1.1, with liquid at the bottom and gas on top. The liquid will experience a slightly higher pressure than the gas since it is at a lower elevation (it has more fluid on top of it). This elevation difference is often a very small one compared to the axial elevation variations resulting from the pipe not being horizontal, and it is tempting to think – as did developers of early multi-phase models - it can be neglected.

The problem is that surface waves on the liquid, like those on a lake, can only be modeled adequately if we take into account the gravitational pressure differences under a wave top compared to a wave bottom. If we neglect the pressure correction term, we cannot expect the model to reproduce surface waves accurately, and they are crucial in the mechanisms at work when stratified flow switches to slug flow.

The biggest problem with neglecting the pressure correction term, though, is that it can cause our model to lose its hyperbolicity, and that can in turn lead to numerical

problems. Interestingly, choosing spatial discretization grids with Δx exceeding the surface wavelength, something which also makes the model lose its ability to reproduce surface waves, does not lead to similar numerical problems.

As we will see later, there are also ways of simplifying these general momentum equations which avoid the loss-of-hyperbolicity problem. It is even possible to regard the pressure correction term as a minor correction introduced for the sole purpose of making the equations hyperbolic whether or not the term corresponds to physical reality (Evje & Flatten, 2005). The subject of whether multi-phase flow equations are hyperbolic, as they should be, has been investigated by a numerous authors, for instance Bonizzi & Issa (2003), Bouchut et al. (2000), and Cortes et al. (1998). As a general rule of thumb, the model tends to end up with the required hyperbolicity if those phenomena it describes have been modeled adequately. Otherwise the model tends to become *ill posed*.

A model referred to as the *drift-flux model* does also indirectly incorporate some dynamics for the surface area, although it does so in a less dynamic way (one of the momentum equations is replaced by a static equation), and that turns out to make the model robust even if the pressure correction terms are omitted. We can therefore not reverse the argument and claim the model necessarily loses its hyperbolicity if any details are approximated in a physically incorrect way. Any model rests on various simplifications, making it difficult to utilize the rule of thumb in practice – we typically do not know how well each phenomenon needs to be included to avoid problems. Other techniques - eigenvalue analysis on a linearized version of the system, say - are required to investigate a model more thoroughly, though as a mental reference, this rule of thumb can be useful.

As a general rule of thumb the conservation equations tend to end up with the required hyperbolicity when the phenomena described have been modeled accurately.

Some implicit numerical methods are robust enough to churn along even if the hyperbolicity is lost, and it took some time to recognize the problem initially. In fact this is one of the dangers of implicit integration algorithms: They may have so much numerical damping built-in they are stable even when the physical systems they simulate are not, and real, physical instabilities as well as ill-posed model formulation

can remain undetected. As a general rule, though, we cannot set all p_k equal unless we know the numerical consequences of doing so.

Assuming the pressure to be identical in all phases can lead to numerical problems in some models.

If we choose focusing solely on the model's steady-state solution, on the other hand, we neglect all time derivatives, and such a model obviously cannot replicate surface waves (or any other sorts of transient phenomena for that matter), and including the pressure correction terms serves no purpose.

Notice that introducing a pressure correction term which expresses radial pressure differences does actually make our model quasi *2D*, since we take into account only one (not all) of the multidimensional phenomena.

2.3.3 Summarizing the forces between phases

Equation 2.2.5 expresses that the sum of mass flows from phase to phase have to be zero: Mass added to one phase must disappear from another. A similar correlation must apply to forces: Any force acting on phase *k* from other phases must have an opposite counterforce on those other phases. The sum of all forces between different phases must therefore be zero. In our model, there are only three such forces: The momentum exchange, the surface tension, and the friction forces. Summarizing for all *N* phases, we get:

$$\sum_{k=1}^{N} R_{ki} + S_{ki} + v_k \Gamma_{ki} = 0 \tag{2.3.17}$$

This momentum conservation equation must therefore be satisfied in addition to equation and 2.3.16.

2.3.4 Comparing single- and multi-phase momentum conservation

For single-phase flow, $\alpha_k = 1$, and no mass transfer or forces can exist between phases. That means $\Gamma_{ki} = 0$, $R_{ki} = 0$ and $S_{ki} = 0$. If nothing flows in through the pipe wall, we can also set $\Gamma_{kW} = 0$. Neglecting surface tension forces between the fluid and the pipe wall means $S_{kW} = 0$. The friction force per unit volume of fluid can be expressed as:

$$R_{kW} = -\frac{A\rho\frac{fdx}{2d}v|v|}{Adx} \tag{2.3.18}$$

We can drop the k-index when we only have one phase. Inserting all this into equation 2.3.17, we get:

$$\frac{\partial(\rho v)}{\partial t} + \frac{\partial(\rho v^2)}{\partial x} = -\frac{\partial p}{\partial x} - \frac{f\rho}{2d}v|v| - \rho_k g\sin\theta \tag{2.3.19}$$

As expected, this result is identical to the momentum equation previously found for single-phase flow (equation 6.2.12 in *Pipe Flow 1*).

2.4 Energy conservation

As for single-phase flow, each phase's accumulated energy must equal the net sum of what that phase brings in minus what it lets out, plus any heat and work added from the outside. In addition, it is possible for the phase to receive heat and work, and also material (containing energy) from other phases. With an eye to equation 6.3.12 in *Pipe Flow 1*, we can directly write:

$$\begin{aligned}\frac{\partial}{\partial t}\left[\alpha_k\rho_k\left(u_k + \frac{v_k^2}{2} + gz_k\right)\right] \\ = -\frac{\partial}{\partial x}\left[\alpha_k\rho_k v_k\left(h_k + \frac{v_k^2}{2} + gz_k\right)\right] + q_{ki} + q_{kW} + w_{ki} + w_{kW} \\ + \Gamma_{ki}h_{ki} + \Gamma_{kW}h_{kW}\end{aligned} \tag{2.4.1}$$

q_{ki} is specific heat from other phases to phase k, q_{kW} is specific heat from the wall to phase k, w_{ki} is specific work from other phases on phase k, w_{kW} is specific work from the outside on phase k, Γ_{ki} is specific mass flow from other phases into phase k, Γ_{kW} is

specific mass flow from other sources into phase k (such as via perforations in the pipe), and h_{ki} and h_{kW} are the relevant specific enthalpies.

This can be brought over to a slightly more compact form by defining the fluid's internal energy per unit volume as:

$$E \stackrel{\text{def}}{=} \rho\left(u + \frac{v^2}{2} + gz\right) \tag{2.4.2}$$

and specific enthalpy:

$$h \stackrel{\text{def}}{=} u + \frac{p}{\rho} \tag{2.4.3}$$

We then get:

$$\frac{\partial}{\partial t}(\alpha_k E_k) = -\frac{\partial}{\partial x}[\alpha_k v_k (E_k + p_k)] + q_{ki} + q_{kW} + w_{ki} + w_{kW} + \Gamma_{ki} h_{ki} + \Gamma_{kW} h_{kW} \tag{2.4.4}$$

The sum of all specific heat from other phases to phase k must obviously summarize to zero, since heat transferred from other phases by definition must be heat lost for those other phases:

$$\sum_{k=1}^{N} q_{ki} = 0 \tag{2.4.5}$$

The sum of all specific heat being received from the wall must also summarize to the total amount of heat flowing through the wall from the environment:

$$\sum_{k=1}^{N} q_{kW} = q \tag{2.4.6}$$

Similar for specific work from phase to phase:

$$\sum_{k=1}^{N} w_{ki} = 0 \tag{2.4.7}$$

The sum of all specific work received from the outside by each phase must equal the total work added from the outside:

$$\sum_{k=1}^{N} w_{kW} = w \tag{2.4.8}$$

The sum of specific enthalpy transferred in the mass flow from phase to phase must equal zero:

$$\sum_{k=1}^{N} \Gamma_{ki} h_{ki} = 0 \tag{2.4.9}$$

2.4.1 Comparing single-phase and multi-phase energy conservation

Just as we did for the mass and momentum conservation equations, we may compare the general multi-phase energy equation 2.4.4 with the one for single-phase flow. Introducing the same modifications as explained in chapter 2.3.1, in addition to setting $q_{ki} = 0$, we get:

$$\frac{\partial E}{\partial t} = -\frac{\partial}{\partial x}[v(E+p)] + q + w \tag{2.4.10}$$

As expected, this is the same as equation 6.3.12 in *Pipe Flow 1* when the definition of *E*, equation 2.4.2, and *h*, equation 2.4.3, is inserted.

2.5 Mass transfer between phases with equal pressures

We have demonstrated that mass transfer between phases takes part in all the three conservation equations. The terms appear with different notations in various literature, but we have chosen to use Γ_{ki}, which is mass transfer per unit volume and time into phase k from all other phases combined. The phase change causing this mass transfer needs to be quantified. How can that be done?

We begin by assuming phase transfer takes place instantly according to the fluid's properties as the pressure or temperature changes, neglecting any delays in the phase change itself. The *flash calculation* – the chemical calculation to determine the new equilibrium after the pressure and/or temperature has changed determines liquid density, gas density, gas and liquid fractions, the resulting composition in each phase, and various other properties. For the purpose of the flash calculations (but not necessarily for the flow calculations) we usually neglect the pressure difference between phases since it has minimal effect on the chemical equilibrium.

For the volume-specific mass of phase k, m_k, mass increase can come from other phases or from inflowing fluid:

$$\frac{dm_k}{dt} = \dot{m}_{ki} + \dot{m}_{kW} \tag{2.5.1}$$

We define the mass fraction for phase k as:

$$\alpha_{m\,k} = \frac{m_k}{m_{total}} = \frac{m_k}{\sum_{i=1}^{N} m_i} = \frac{m_k}{\sum_{i=1}^{N} \alpha_i \rho_i} \tag{2.5.2}$$

If nothing flows into the control volume through the pipe's wall, we can set $\dot{m}_{kW} = 0$, and we get:

$$\Gamma_{ki} = \frac{dm_k}{dt} \tag{2.5.3}$$

Inserting equation 2.5.2 into 2.5.3:

$$\Gamma_{ki} = \frac{d\alpha_{m\,k}}{dt} \sum_{i=1}^{N} \alpha_i \rho_i \tag{2.5.4}$$

If the mass fraction is a function of pressure and temperature:

$$\alpha_{m\,k} = \alpha_{m\,k}(p, T) \tag{2.5.5}$$

Note that single-component fluids (for instance pure water) do not fit well into equation 2.5.5, since it boils at a particular temperature for a given pressure (approximately *100 ^0C* at *1 atmosphere ≈ 10^5 Pa in case of water*), regardless of the mass fraction of gas and liquid, meaning pressure and temperature alone cannot determine fractions. The equation developed below is therefore not applicable to single-component fluids, but this is not a serious limitation since we rarely come across those in flow assurance.

We can set:

$$d\alpha_{m\,k} = \left(\frac{\partial \alpha_{m\,k}}{\partial p}\right)_T dp + \left(\frac{\partial \alpha_{m\,k}}{\partial T}\right)_p dT \tag{2.5.6}$$

And hence:

$$\frac{d\alpha_{m\,k}}{dt} = \left(\frac{\partial \alpha_{m\,k}}{\partial p}\right)_T \frac{dp}{dt} + \left(\frac{\partial \alpha_{m\,k}}{\partial T}\right)_p \frac{dT}{dt} \tag{2.5.7}$$

Similarly we can easily show:

$$\frac{dp}{dt} = \left(\frac{\partial p}{\partial t}\right)_x + \left(\frac{\partial p}{\partial x}\right)_t \frac{dx}{dt} \tag{2.5.8}$$

And:

$$\frac{dT}{dt} = \left(\frac{\partial T}{\partial t}\right)_x + \left(\frac{\partial T}{\partial x}\right)_t \frac{dx}{dt} \tag{2.5.9}$$

The term dx/dt is the definition of velocity, and it applies to phase k:

$$v_k = \frac{dx}{dt} \tag{2.5.10}$$

By inserting equations 2.5.7-2.5.10 into 2.5.4, we finally get:

$$\Gamma_{ki} = \left\{\left(\frac{\partial \alpha_{m\,k}}{\partial p}\right)_T \left[\left(\frac{\partial p}{\partial t}\right)_x + \left(\frac{\partial p}{\partial x}\right)_t v_k\right] + \left(\frac{\partial \alpha_{m\,k}}{\partial T}\right)_p \left[\left(\frac{\partial T}{\partial t}\right)_x + \left(\frac{\partial T}{\partial x}\right)_t v_k\right]\right\} \sum_{i=1}^{N} \alpha_i \rho_i \tag{2.5.11}$$

The two partial derivatives in front of each of the square brackets in equation 2.5.11 are fluid properties, so they can be looked up from tables or calculated indirectly from such well-know correlations as the *Peng-Robinson* or the *Redlich-Kwong* equations of state, in combination with *mixing rules*. They are then fed into equation 2.5.11 as numbers, so it is only the other partial derivatives which take part in the discretization to solve the equation.

When calculating the mass transfer for each phase this way we should end up with something which satisfies equation 2.2.5. If we don't, it means we have inaccuracies in our calculations, and it is best to modify the result to make it fit equation 2.2.5 perfectly so that mass conservation is not violated.

2.6 Comments on the conservation equations

2.6.1 Averaging

When developing the equations in this chapter, we have imagined all phases are continuous. For many of the flow regimes described in *chapter 1,* that assumption does clearly not hold. Droplets and bubbles, for instance, can be very small, and when one of them passes a control volume boundary, we have a different situation compared to when they are completely inside the boundary. The flow can therefore contain discontinuities, and strictly speaking, the derivatives may at times not be defined. This

problem is usually solved by doing some sort of averaging, and numerous papers and books deal with this subject, including Ishii (1975), Yadigaroglu & Lahey (1976), Mathers et al. (1978), Nigmatulin (1979), Drew (1983), Lahey & Drew (1988), Daniels et al. (2003), Ishii & Hibiki (2006), Prosperetti & Tryggvason (2007), and Jacobsen (2008).

The most common forms of averaging are:

1. Spatial (volume or area) averaging, with no averaging in time.
2. Time averaging, with no spatial averaging.
3. Ensemble averaging, which is a statistical way to average. It can be regarded as a measure related to the repeatability of experiments (Jacobsen, 2008).
4. A combination of several of the above, such as ensemble/space averaging or time/space averaging.

The averaging process acts as a filter removing information occurring below certain length and time scales, and it smoothens out discontinuities. The averaged equations will only be able to resolve flow features down to the limits defined by the averaging process. This is not a serious problem when simulating long pipelines or wellbores, but with an exception for intermittent flow, since a slug can stretch over several grid-points or cells. Rather than going into details on all the various averaging literature, for our purpose it is sufficient to point out that the equations developed in this chapter are valid for most situations. Later we will discuss modifications for slug or churn flow.

Since multiphase flow contains discontinuous phenomena, in reality the equations used are based on some sort of averaging in time and/or space. Of the models shown here, averaging issues require attention solely for intermittent flow.

2.6.2 Closure relationships

So far we have not brought in any fluid-specific properties, such as how viscosity, density, surface tension, or specific enthalpy varies with pressure and temperature. In that sense both the mass conservation and the momentum equations are general in the form they are shown here and they are valid for any fluids, but at the cost of being incomplete. We realize that other correlations must also be added, to describe friction or heat, for instance. Those extra correlations are often referred to as *closure relationships*,

since they are required to close the equation set so the number of unknowns equals the number of equations.

We also need to establish flow regime criteria and find ways to solve the equations. As we will discover in following chapters, both tasks offer many interesting challenges. We end up with very different models depending on how we deal with those challenges, even though all models rest on the conservation principles shown here in chapter 2.

"If I have seen further it is by standing on the shoulders of giants."
Isaac Newton, 1675

3 Two-Fluid Model

Simple isothermal two-fluid two-phase models for stratified flow:

- Mass and momentum conservation
- Friction and pressure loss
- Simplifications and solution for steady-state incompressible flow
- Simplifications and solution for steady-state compressible flow
- Fully transient solution
- Simplifying by introducing the drift-flux model
- Further simplification by ignoring inertia in the drift-flux model

3.1 Problem definition

Let us now look at an example of how to utilize the very general multi-phase model from chapter 2. To avoid getting lost in details, we study a relatively simple situation:

- We have only two fluids, one gas and one liquid, and pressures and temperatures are such that evaporation or condensation does not occur. We also assume no gas can be dissolved in the liquid (even though this is never quite true, as liquids do take up some gas in the same way oxygen is taken up by water, enabling fish to breathe).
- The pipe has no perforations, so neither liquid nor gas can flow through the pipe wall.
- The flow is stratified – we simply neglect all other flow regimes for now.

- The flow is isothermal, so we do not need the energy equation to keep track of the temperature.

With these simplifications, let us try to establish all necessary conservation equations. Also, we will develop closure relationships, which in this highly simplified case are reduced to describing the frictions between the gas and the pipe wall, between the liquid and the pipe wall, and between the gas and the liquid, in addition to some fluid properties. To make the equation system hyperbolic, we also need to describe the pressure difference between the gas and the liquid.

3.2 Mass conservation

If we use index G for gas and L for liquid, we can write two mass conservation equations based on equation 2.2.4. For the gas phase, we get:

$$\frac{\partial(\alpha_G \rho_G)}{\partial t} = -\frac{\partial(\alpha_G \rho_G v_G)}{\partial x} + \Gamma_{LG} + \Gamma_{GW} \tag{3.2.1}$$

Since we have no phase change, $\Gamma_{LG} = 0$. Also, no gas is going to be added through the wall, and we therefore set $\Gamma_{GW} = 0$. Equation 3.2.1 simplifies to:

$$\frac{\partial(\alpha_G \rho_G)}{\partial t} + \frac{\partial(\alpha_G \rho_G v_G)}{\partial x} = 0 \tag{3.2.2}$$

Similarly, mass conservation for the liquid becomes:

$$\frac{\partial(\alpha_L \rho_L)}{\partial t} + \frac{\partial(\alpha_L \rho_L v_L)}{\partial x} = 0 \tag{3.2.3}$$

Equation 2.2.6 is very simple in this case:

$$\alpha_G + \alpha_L = 1 \tag{3.2.4}$$

3.3 Momentum conservation

Equation 2.3.17 applied to the gas-phase leads to:

$$\frac{\partial(\alpha_G \rho_G v_G)}{\partial t} = -\frac{\partial(\alpha_G \rho_G {v_G}^2)}{\partial x} - \alpha_G \frac{\partial p_G}{\partial x} + R_{LG} + R_{GW} + S_{LG} + S_{GW} - \alpha_G \rho_G g \sin\theta \tag{3.3.1}$$

R_{LG} is friction force pr. unit pipe volume from liquid on the gas, and R_{GW} is similarly volume-specific friction force from the wall on the gas.

Assuming all surface tension forces acting directly on the gas flow are negligible, a good approximation for stratified flow, we can set $S_{LG} = S_{Gw} = 0$. In addition, we define the pressure on the interface (the liquid surface) between the gas and liquid as p, while Δp_G is the extra pressure felt by the gas due to its average elevation being different from that of the interface (Δp_G is obviously going to be negative, given that the gas is on top of the interface).

$$\frac{\partial(\alpha_G \rho_G v_G)}{\partial t} + \frac{\partial(\alpha_G \rho_G {v_G}^2)}{\partial x} = -\alpha_G \frac{\partial(p + \Delta p_G)}{\partial x} - R_{GL} + R_{Gw} \; - \alpha_G \rho_G g \sin\theta \tag{3.3.2}$$

For the liquid, we similarly get:

$$\frac{\partial(\alpha_L \rho_L v_L)}{\partial t} + \frac{\partial(\alpha_L \rho_L {v_L}^2)}{\partial x} = -\alpha_L \frac{\partial(p + \Delta p_L)}{\partial x} + R_{GL} + R_{Lw} \; - \alpha_L \rho_L g \sin\theta \qquad (3.3.3)$$

We notice that equations 3.3.2 and 3.3.3 also satisfy the requirement that the sum of all forces between phases must be zero (equation 2.3.17), since R_{GL} occurs with opposite sign in equation 3.3.2 and 3.3.3.

3.4 Gas and liquid pressure difference in stratified flow

In this simple model, it would be tempting to neglect the pressure correction terms (setting $\Delta p_G = \Delta p_L = 0$), meaning all pressures in a cross-section would be equal so $p_G = p_L = p$. As explained in chapter 2.3.2, however, this would neglect the mechanisms creating surface waves while creating an un-physical system description which in turn can cause loss of hyperbolicity and numerical problems.

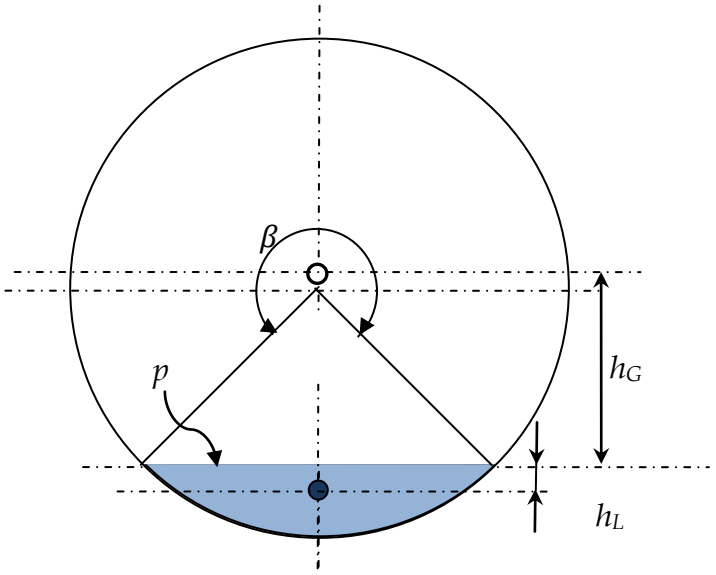

Figure 3.4.1. Stratified flow. Center of gravity for the gas is above the pipe center, while for the liquid, it is of course somewhere below the interface surface.

A pipe's circular cross-section leads to somewhat different wave conditions compared to the surface of a lake. If a wave-top rises above the pipe's center line, it does so in a diminishing cross-section. Therefore it closes the remaining cross-section relatively fast

when approaching the upper side of the pipe. That affects the wave pattern significantly, and it is clearly worthwhile implementing a relatively accurate description of the circular geometry to get this right.

For stratified flow we assume the interface in each cross-section to be a straight, horizontal line. That is a good approximation for low gas velocities, but measurements have shown that increasing velocities make the surface bend until the liquid covers the whole wall for fully annular flow.

One can calculate the pressure at a point h_L below the interface in alternative ways. Some writers propose that the pressure difference is a function only of the difference in static head between interface and liquid area center of gravity (Taitel & Duckler 1976, Watson 1990, Barnea & Taitel 1993, 1996), while others propose taking into account the Bernoulli-effect resulting from the fact that different phases have different average velocities (Tuomi 1996, Coquel et al.1997, Bestion 1990). The former approach seems to be the most correct, since pressure by definition must be the same in all directions – every point in space and time must necessarily comply with this, including points at the interface (at least in our case, where we have decided to neglect surface tension). The conservation equations describe the correlation between pressure and velocity, so the Bernoulli-effect is already built into them as they stand.

Each phase is modeled separately in stratified flow - they are only connected via friction, total cross-sectional area, and pressure. Therefore the pressure correction terms' mission is not to describe a (non-existent) pressure difference at the surface between the two, but the pressure difference between the two phases (at some average point for each phase). If the phases are distributed as shown in figure 3.4.1, the task comes down to describing the average elevation difference and resulting static pressure head between the phases. It is not self evident exactly what should be taken as average elevation for each phase, since the velocities vary across the cross-section (it is generally lower near the wall than it is elsewhere). For simplicity we use the *area center of gravity* for each phase as our elevation point.

It is worth noting that different authors use different reference levels as a basis for their pressure modification terms, some use the pipe bottom pressure as reference instead of the interface. That is not expected to affect the results, but some of the terms in the equations do of course appear to be somewhat different.

At first glance we would expect the required geometrical correlations to describe areas and elevations for a circular cross-section to be very simple, but on closer inspection they turn out to be relatively complicated. De Henau et al. (1995) have shown that:

$$h_G = \left[\frac{1}{2}\cos\left(\pi - \frac{\beta}{2}\right) + \frac{1}{3\pi\alpha_G}\sin^3\left(\pi - \frac{\beta}{2}\right)\right] d\cos\theta \tag{3.4.1}$$

$$h_L = \left[-\frac{1}{2}\cos\left(\pi - \frac{\beta}{2}\right) + \frac{1}{3\pi\alpha_L}\sin^3\left(\pi - \frac{\beta}{2}\right)\right] d\cos\theta \tag{3.4.2}$$

The pressure differences can then easily be calculated as:

$$\Delta p_G = p_G - p = -\rho_G g h_G \tag{3.4.3}$$

$$\Delta p_L = p_L - p = \rho_L g h_L \tag{3.4.4}$$

The angle β, as defined on figure 3.4.1, must be estimated from how full the pipe is, meaning from α_G and α_L. That angle is also useful when determining the various surfaces involved in the friction calculations. An accurate explicit description of the function $\beta(\alpha_G\ , \alpha_L)$ is not known, but it is possible to express an equation which can be solved to any required accuracy using Newton-iteration. Given the inaccuracies introduced on various points when developing this model, a more direct but not completely accurate approximation proposed by Biberg (1999) should suffice, it is claimed to be accurate to within $\pm\, 0.002\ rad$:

$$\beta = 2\pi - 2\left\{\pi\alpha_L + \left(\frac{3\pi}{2}\right)^{1/3}\left[1 - 2\alpha_L + {\alpha_L}^{1/3} - (1-\alpha_L)^{1/3}\right]\right\} \tag{3.4.5}$$

When $\theta = \pi/2$ (vertical pipe), $\Delta p_G = \Delta p_L = 0$, which can lead to loss of hyperbolicity. We cannot expect this model to describe surface waves in nearly vertical pipes accurately anyway (such waves are affected by surface tension more than gravity), and

we may as well limit $cos\,\theta$ in the pressure correction terms in equations 3.4.1 and 3.4.2 (though not elsewhere) so we use $max[(cos\,\theta)_{min}, cos\,\theta)]$ instead of $\cos\theta$. That way, $\cos\theta$ never falls below a certain value, for instance by setting $(\cos\theta)_{min} = 0.1$.

For our simulations to represent surface waves realistically, we have to use a very dense grid. Surface waves are quite short compared to long pipelines, and they obviously cannot be described by grid points which are further apart than half the wave length. It is not convenient to use such a dense grid in most flow assurance simulations, but, as we will discover in chapter 9, very fine grid simulations may become a practical way to describe surface waves and the onset of slugging in future models.

3.5 Friction in stratified flow

The friction between gas and pipe wall, R_{GW}, is difficult to express accurately. We remember from *Pipe Flow 1* chapter 2 and 3 that the Darcy-Weissbach friction factor can be relatively inaccurate even for circular pipes with single-phase flow. For the friction between gas and liquid, an additional difficulty comes from the fact that we do not know the surface roughness on the interface. Friction errors will also lead to incorrect volume fractions, which again affect the friction calculations. We must therefore expect estimates of the interface friction to be considerably less accurate than previous friction calculations for single-phase flow, where we encountered errors as high as 20%. Keeping these limitations in mind, we will try to develop reasonably accurate estimates for the Darcy-Weisbach friction factors.

Hydraulic diameter can be defined from the wetted perimeter of the cross-section, O, and the cross-sectional area, A, as:

$$d_h \stackrel{\text{def}}{=} \frac{4A}{O} \tag{3.5.1}$$

We may also recall that for non-circular cross-sections, it is generally necessary to include a geometric correction factor in friction calculations for non-circular cross-sections, but we are going to presume that factor to be *1* in our simple model. That is probably not a bad approximation compared to the other simplifications we are using here.

By studying figure 3.4.1, we see that wetted perimeter relevant to the friction between gas and pipe wall is:

$$O_{GW} = \beta \frac{d}{2} \tag{3.5.2}$$

Between liquid and pipe wall:

$$O_{LW} = (2\pi - \beta) \frac{d}{2} \tag{3.5.3}$$

Interface between gas and liquid:

$$O_{GL} = d \sin\left(\frac{\beta}{2}\right) \tag{3.5.4}$$

Gas cross-sectional area:

$$A_G = \alpha_G \frac{\pi d^2}{4} \tag{3.5.5}$$

Liquid cross-sectional area:

$$A_L = \alpha_L \frac{\pi d^2}{4} \tag{3.5.6}$$

From this, we define the three relevant hydraulic diameters. For calculating the gas-wall Reynolds number, we use the following hydraulic diameter:

$$d_{h\,GW} \stackrel{\text{def}}{=} \frac{4A_G}{O_{GW}} \tag{3.5.7}$$

For calculating the liquid-wall hydraulic diameter:

$$d_{h\,LW} \stackrel{\text{def}}{=} \frac{4A_L}{O_{LW}} \tag{3.5.8}$$

The Reynolds numbers can then be defined accordingly as:

$$Re_{h\,GW} \stackrel{\text{def}}{=} \frac{v_G d_{h\,GW} \rho_G}{\mu_G} \tag{3.5.9}$$

$$Re_{h\,LW} \stackrel{\text{def}}{=} \frac{v_L d_{h\,LW} \rho_L}{\mu_L} \tag{3.5.10}$$

Which area to select when defining the hydraulic diameter for the interface between liquid and gas is less obvious, since both the gas and liquid area seem to be involved. Also, keep in mind that the interface friction factor in reality is not entirely independent of the wall friction factors, since each affect both turbulence and velocity profiles and thereby also the friction mechanism. The most used empirical correlation to estimate the interfacial friction factor is probably the one proposed by Petalas & Aziz (1997):

$$f_{GL} = (0.004 + 0.5\ 10^{-6} Re_{SL}) {Fr_L}^{1.335} \frac{\rho_L d\ g}{\rho_G {v_G}^2} \tag{3.5.11}$$

Where Re_{SL} is the liquid phase Reynolds number based on superficial velocity ($= \alpha_L v_L$). The liquid's Froude number is defined by the liquid height h_L as:

$$Fr_L = \frac{v_L}{\sqrt{g h_L}} \tag{3.5.12}$$

The gas-wall friction shear τ_{Gw} becomes:

$$\tau_{Gw} = -\frac{f_{Gw} \rho_G}{8} v_G |v_G| \tag{3.5.13}$$

R_{Gw} is defined as friction force ($= \tau_{Gw} O_{GW} \Delta x$) pr. unit volume ($= A_G \Delta x$). We get:

$$R_{Gw} = -\frac{f_{Gw}\rho_G}{8}\frac{O_{GW}}{A}v_G|v_G| \tag{3.5.14}$$

Similar for the liquid-wall friction :

$$R_{Lw} = -\frac{f_{Lw}\rho_L}{8}\frac{O_{LW}}{A}v_L|v_L| \tag{3.5.15}$$

If we estimate the relevant gas-liquid velocity difference as $v_G - v_L$, the interfacial friction is estimated as:

$$R_{GL} = \frac{f_{GL}\rho_G}{8}\frac{O_{GL}}{A}(v_G - v_L)|v_G - v_L| \tag{3.5.16}$$

We can then estimate all three frictions easily as follows:

1. Use equation 3.4.5 to calculate β.
2. Use equations 3.5.2 – 3.5.10 to define the Reynolds numbers $Re_{h\,GW}$ and $Re_{h\,LW}$.
3. Use the Modified Moody Diagram (or its numerical representation, as outlined in table 2.13.3 in *Pipe Flow 1*) to estimate the Darcy-Weisbach friction factors f_{GW} and f_{LW}. For the interface friction factor f_{GL}, use equations 3.5.12 and 3.5.11.
4. Calculate R_{Gw}, R_{Lw} and R_{GL} according to equations 3.5.14 – 3.5.16.

3.6 Steady-state incompressible flow solution

3.6.1 The model

As a first approach to solving the equations, let us introduce the following simplifications (in addition to the ones already listed in chapter 3.1):

1. The flow is steady-state. That means nothing changes over time, and so the time derivatives in the conservation equations 3.2.2, 3.2.3, 3.3.2, and 3.3.3 are all going to be zero.
2. All gas and liquid properties are independent of the pressure. This means both fluids are considered incompressible with constant viscosity. That is usually not a good approximation for the gas in pipelines and is only done for convenience at this step in the process of familiarizing ourselves with the equations.
3. The pipe's elevation angle θ is constant.

As boundary conditions we impose constant mass flows for both gas and liquid at the inlet and a constant pressure at the outlet. We can use constants $k_{G\,in}$ and $k_{L\,in}$ for defining the inlet boundary conditions:

$$\alpha_G \rho_G v_G = k_{G\,in} \tag{3.6.1}$$

$$\alpha_L \rho_L v_L = k_{L\,in} \tag{3.6.2}$$

Since the flow is steady-state with no phase change and no fluid flows in through perforations, the mass flow must be constant along the entire pipeline. Equations 3.6.1 and 3.6.2 are therefore not restricted to the inlet – they are valid everywhere.

When the mass conservation equation 3.2.2 is stripped of the time derivative, it becomes:

$$\frac{\partial(\alpha_G \rho_G v_G)}{\partial x} = 0 \tag{3.6.3}$$

This can be written as:

$$\alpha_G \rho_G \frac{\partial v_G}{\partial x} + \rho_G v_G \frac{\partial \alpha_G}{\partial x} + \alpha_G v_G \frac{\partial \rho_G}{\partial x} = 0 \tag{3.6.4}$$

Since the density is constant, the last term on the left-hand side is zero, and we end up with

$$\alpha_G \frac{\partial v_G}{\partial x} + v_G \frac{\partial \alpha_G}{\partial x} = 0 \tag{3.6.5}$$

This means any change in gas fraction must always be offset by a similar change in gas velocity to satisfy the mass balance. But since no property changes with pressure, the absolute pressure cannot affect the flow at any point in the pipe, only the pressure loss per unit length can. The same goes for all other parameters affecting the flow, such as the frictions and the elevations: They all affect each point along the pipe in a constant way, and therefore there is nothing which can favor an increase or decrease in α_G (and a corresponding variation in v_G) along the pipeline. This implies that α_G and v_G must be constant from inlet to outlet. Only the pressure changes along the pipe, and all spatial derivatives not containing the pressure vanish. The continuity equations only express $0 = 0$, and we are left with the momentum equations.

Since this very simplified model cannot describe surface waves on the liquid's surface anyway and has no hyperbolicity to maintain, we neglect the pressure difference between phases by setting $\Delta p_G = \Delta p_L = 0$, and the momentum equations 3.3.2 and 3.3.3 are reduced to:

$$0 = -\alpha_G \frac{\partial p}{\partial x} - R_{GL} + R_{GW} \; - \alpha_G \rho_G g \sin\theta \tag{3.6.6}$$

$$0 = -\alpha_L \frac{\partial p}{\partial x} + R_{GL} + R_{GW} \; - \alpha_L \rho_L g \sin\theta \tag{3.6.7}$$

We can use these two equations to eliminate $\partial p/\partial x$:

$$-\frac{R_{GL}}{\alpha_G} + \frac{R_{GW}}{\alpha_G} \; - \rho_G g \sin\theta = \frac{R_{GL}}{\alpha_L} + \frac{R_{LW}}{\alpha_L} \; - \rho_L g \sin\theta \tag{3.6.8}$$

If we look at equations 3.5.14 – 3.5.16 and the relatively simple correlations they rely on, equations 3.4.5 and 3.5.2 – 3.5.12, we see that they can be solved relatively easily by inserting all underlying equations into equation 3.6.8.

We define a matrix based on equations 3.6.1, 3.6.2, 3.6.8, and 3.2.4:

$$F = \begin{bmatrix} f_1 \\ f_2 \\ f_3 \\ f_4 \end{bmatrix} = \begin{bmatrix} \alpha_G \rho_G v_G - k_{G\,in} \\ \alpha_L \rho_L v_L - k_{L\,in} \\ \frac{R_{GLi}}{\alpha_G} - \frac{R_{GW}}{\alpha_G} + \rho_G g \sin\theta + \frac{R_{GLi}}{\alpha_L} + \frac{R_{LW}}{\alpha_L} - \rho_L g \sin\theta \\ \alpha_G + \alpha_L - 1 \end{bmatrix} = \begin{bmatrix} 0 \\ 0 \\ 0 \\ 0 \end{bmatrix} \tag{3.6.9}$$

The input variables are:

$$Y = \begin{bmatrix} y_1 \\ y_2 \\ y_3 \\ y_4 \end{bmatrix} = \begin{bmatrix} \alpha_G \\ \alpha_L \\ v_G \\ v_L \end{bmatrix} \tag{3.6.10}$$

3.6.2 Solution method

Newton-iteration on equation 3.6.9 and 3.6.10 is straight forward:

$$Y_{n+1} = Y_n - J^{-1} F_n(Y_n) \tag{3.6.11}$$

We start by guessing a likely value for α_G, and we set $\alpha_L = 1 - \alpha_G$. This is used to determine starting values for v_G and v_L in such a way that they satisfy the inlet boundary conditions in equations 3.6.1 and 3.6.2. Then it becomes possible to calculate starting values for the frictions by setting $R_{GL} = R_{GL}(\alpha_G, \alpha_L, v_G, v_L)$, $R_{GW} = R_{GW}(\alpha_G, \alpha_L, v_G, v_L)$, and $R_{LW} = R_{Lw}(\alpha_G, \alpha_L, v_G, v_L)$. These values are used to estimate the *Y* and *F*-vectors.

The Jacobi-matrix $J = \partial F / \partial Y$ can be estimated by varying each argument slightly and then investigating how that affects *F*. We start by calculating *F* and then give α_G a slightly larger value, say $\alpha_G + \Delta\alpha_G$, where $\Delta\alpha_G$ may be in the order of 10^{-7}. All other arguments remain as they are, and a new *F*-matrix is calculated, let us call it $F_{\Delta\alpha_G}$. This enables us to estimate the first row in the Jacobi-matrix:

$$J_{11} = \frac{\partial f_1}{\partial y_1} \approx \frac{f_{1\,\Delta\alpha_G} - f_1}{\Delta\alpha_G}, J_{21} = \frac{\partial f_2}{\partial y_1} \approx \frac{f_{2\,\Delta\alpha_G} - f_2}{\Delta\alpha_G}, \ldots \quad (3.6.12)$$

The same process is repeated for each of the arguments so that the whole Jacobi-matrix is estimated, and equation 3.6.11 is used to iterate. Careful programming is necessary to make the algorithm robust. The usual potential problems due to division by zero or attempting to take roots of negative numbers can otherwise occur.

The iteration process is repeated until convergence, typically less than 10 times. Since (according to equation 3.6.9) the *F*-vector should end up having zero length, some norm of *F* can be used as convergence criterion, for instance the absolute norm:

$$\sqrt{\sum_{i=1}^{4} {f_i}^2} \leq \; e_F \quad (3.6.13)$$

where e_F is the maximum accepted error.

After convergence is achieved, we may want to know the pipe's pressure profile. Since all velocities, fractions and fluid properties are constant, the pressure loss is going to be a linear function of x, and we can accurately set:

$$\frac{\partial p}{\partial x} = \frac{\Delta p}{\Delta x} \quad (3.6.14)$$

This can be used to calculate the pressure difference Δp compared to the outlet pressure (or the inlet pressure, if that had been one of the known boundary conditions) at any distance Δx from the outlet by inserting equation 3.6.14 into 3.6.6 or 3.6.7.

3.7 Steady-state compressible flow solution

Our model becomes more useful if we abandon the requirement from chapter 3.6 that both fluids have to be incompressible. The spatial derivatives can no longer be neglected, but the flow is still steady-state, and all time derivatives continue to be zero. We see that the mass conservation equations 3.2.2 and 3.2.3 stripped of the time

derivative terms simply state that the mass flows are the same everywhere, which means that the boundary equations 3.6.1 and 3.6.2 still will be valid throughout the pipe. The momentum conservation equations 3.3.2 and 3.3.3 are somewhat simplified, and, as explained in chapter 3.4, the pressure correction terms Δp_G and Δp_L serve no useful purpose in a steady-state solution and can be removed. To close the equation system, we obviously need to correlate density, pressure and temperature. Such correlations on general form can be expressed as:

$$\rho_G = \rho_G(p, T) \tag{3.7.1}$$

$$\rho_L = \rho_L(p, T) \tag{3.7.2}$$

When choosing discretization method for the spatial derivatives, it is worth noting that if we knew all boundary conditions in one end of the pipe, we would easily be able to construct a simple recursive, explicit solution scheme. In our example, the gas and liquid mass flows at the inlet are known, and so is the pressure at the outlet. But in a steady-state model, the outlet mass flows are going to be the same as the inlet flows, so we do in fact know both the mass flows and the pressure at the outlet. We do, however, initially not know the pressure at the inlet. It is therefore natural to start the calculations at the outlet, and then compute backwards towards the inlet.

We may use a first order approximation for the spatial derivatives:

$$\frac{\partial(\alpha_G \rho_G {v_G}^2)}{\partial x} \approx \frac{(\alpha_G \rho_G {v_G}^2)_i - (\alpha_G \rho_G {v_G}^2)_{i+1}}{\Delta x} \tag{3.7.3}$$

This leads to the following recursive algorithm:

$$F_{i+1} = \begin{bmatrix} f_1 \\ f_2 \\ f_3 \\ f_4 \\ f_5 \\ f_6 \\ f_7 \end{bmatrix}_{i+1} = \begin{bmatrix} (\alpha_G \rho_G v_G)_i - k_{G\,in} \\ (\alpha_L \rho_L v_L)_i - k_{L\,in} \\ (\alpha_G \rho_G {v_G}^2)_{i+1} - (\alpha_G \rho_G {v_G}^2)_i + \alpha_{G,i}(p_{i+1} - p_i) - \Delta x F_{G,i+1} \\ (\alpha_L \rho_L {v_L}^2)_{i+1} - (\alpha_L \rho_L {v_L}^2)_i + \alpha_{L,i}(p_{i+1} - p_i) - \Delta x F_{L,i+1} \\ \rho_{G,i} - \rho_G(p, T)_i \\ \rho_{L,i} - \rho_L(p, T)_i \\ \alpha_G + \alpha_L - 1 \end{bmatrix} = \begin{bmatrix} 0 \\ 0 \\ 0 \\ 0 \\ 0 \\ 0 \\ 0 \end{bmatrix} \tag{3.7.4}$$

The friction and elevation terms have been written as:

$$F_{G,i+1} = -R_{GLi,i+1} + R_{GW,i+1} \; - \alpha_{G,i+1}\rho_G g \sin\theta_{i+1}$$
$$F_{L,i+1} = R_{GLi,i+1} + R_{LW,i+1} \; - \alpha_{L,i+1}\rho_L g \sin\theta_{i+1} \quad (3.7.5)$$

The variables we seek to determine are:

$$Y = \begin{bmatrix} y_1 \\ y_2 \\ y_3 \\ y_4 \\ y_5 \\ y_6 \\ y_7 \end{bmatrix} = \begin{bmatrix} \alpha_G \\ \alpha_L \\ v_G \\ v_L \\ \rho_G \\ \rho_L \\ p \end{bmatrix} \quad (3.7.6)$$

We start by inserting everything we know at the outlet into vector Y. The pressure is directly inserted as p_{out}. We need to guess a value for α_G, for instance $\alpha_G = 0.5$. That also determines $\alpha_L = 1 - \alpha_G = 0.5$. The densities follow from the fluid properties for the gas and liquid in question according to equations 3.7.1 and 3.7.2.

Next, velocities are determined by equations 3.6.1 and 3.6.2, and all values in Y are thereby known. We index the Y-vector at the outlet Y_{i+1} so that Y_i becomes the nearest upstream grid-point. Using equations 3.4.2, 3.4.5, 3.5.2 – 3.5.12, 3.5.14 – 3.5.16, and 3.7.5, it is straight forward to calculate everything indexed *i+1* in equation 3.7.4 after we have chosen a discretization length Δx. Y_i can then be determined by Newton-iteration on equation 3.7.4 in the same way as it was described for equation 3.6.9.

The process is repeated throughout the pipe until we reach the inlet end. As starting values in grid point *i* we may use those from grid point *i+1*, or we may extrapolate from several already calculated grid points.

If we made a poor guess regarding outlet value for α_G, we are still going to approach the correct values some way into the pipe. The inaccurate outlet value will appear as a relatively abrupt change in the fraction. Since values some distance into the pipe are

going to be more accurate, we can use those to extrapolate to the outlet, get better starting values, and do a re-run of the calculations. That procedure can be repeated several times to improve accuracy further.

3.8 Fully transient simulation model

In a fully transient model the time derivatives will obviously no longer be zero, so we need both some sort of spatial discretization as well as discretization in time. Numerical solution methods are discussed in chapter 18, but at this stage, we are only focusing on stratified flow. Without worrying about the complications other situations may bring, we simply conclude that the two-fluid model shown here can be simulated in ways which solve the primary variables (those occurring as time derivatives in the conservation equations, meaning $\alpha_G\rho_G$, $\alpha_L\rho_L$, $\alpha_G\rho_G{v_G}^2$, and $\alpha_L\rho_L{v_L}^2$) at every cell for each time-step.

Once the primary variables are determined, we must calculate the secondary variables (those in Y in equation 3.7.6) by some iteration procedure, for instance Newton-iteration. That iteration can be based on equation 3.8.1:

$$F = \begin{bmatrix} f_1 \\ f_2 \\ f_3 \\ f_4 \\ f_5 \\ f_6 \\ f_7 \end{bmatrix} = \begin{bmatrix} \alpha_G\rho_G - (\alpha_G\rho_G) \\ \alpha_L\rho_L - (\alpha_L\rho_L) \\ \alpha_G\rho_G v_G - (\alpha_G\rho_G v_G) \\ \alpha_L\rho_L v_L - (\alpha_L\rho_L v_L) \\ \rho_{G,i} - \rho_G(p,T) \\ \rho_{L,i} - \rho_L(p,T) \\ \alpha_G + \alpha_L - 1 \end{bmatrix} = \begin{bmatrix} 0 \\ 0 \\ 0 \\ 0 \\ 0 \\ 0 \\ 0 \end{bmatrix} \tag{3.8.1}$$

$(\alpha_G\rho_G)$ is the value coming out of the time integration (kept constant during the iteration), while $\alpha_G\rho_G$ are updated for each iteration as α_G and ρ_G converges towards their new values. For the densities, $\rho_G(p,T)$ is the density value calculated by inserting the pressure and (constant) temperature into the gas property equation, while ρ_G is the density as it stands (as it was calculated in the previous iteration). The iterations can be carried out in the same way as described for equation 3.6.11. Initial values can be those from the previous time-step or some extrapolation from several time-steps, or they can be based on values from neighboring grid points or cells.

Equation 3.8.1 is not optimized in any way, and we could for instance insert $\alpha_L = 1 - \alpha_G$ everywhere and eliminate one equation to reduce the work involved in inverting the Jacobi matrix. As explained in chapter 12.8, it is also possible that other iteration methods could converge at a lower cost than Newton-iteration. The purpose here, though, is to show a simple algorithm. Ways of optimizing and generalizing the method are discussed later.

3.9 The drift-flux model

The drift-flux model goes one step on the way to simplifying the full two-fluid model described thus far. Both models are widely used and very similar, but in some ways the drift-flux model is simpler to deal with numerically. In addition, it can be shown that we do not need to include the pressure correction terms Δp_G and Δp_L to maintain hyperbolicity for the drift-flux model.

The drift-flux model combines the two dynamic momentum equations by summarizing them. To maintain closure, the 'lost' momentum equation is replaced by an extra algebraic equation.

The mass conservation equations remain equations 3.2.2 – 3.2.4. The dynamic momentum conservation equation is created by neglecting the pressure correction terms and summarizing equations 3.3.2 and 3.3.3:

$$\frac{\partial(\alpha_G\rho_G v_G + \alpha_L\rho_L v_L)}{\partial t} + \frac{\partial(\alpha_G\rho_G {v_G}^2 + \alpha_L\rho_L {v_L}^2 + p)}{\partial x} = R_{GW} + R_{LW} - (\alpha_G\rho_G + \alpha_L\rho_L)g\sin\theta \quad (3.9.1)$$

Since this equation contains no information about individual forces on each phase, we realize that it cannot fully describe how the velocity difference between the two phases is going to develop. We therefore create an algebraic equation by eliminating $\partial p/\partial x$ between equations 3.3.2 and 3.3.3 (after again having neglected the pressure correction terms). We then take the steady-state, incompressible version of the result, as we also did in equation 3.6.8. That leads to:

$$\frac{R_{GL}}{\alpha_G \alpha_L} - \frac{R_{GW}}{\alpha_G} + \frac{R_{LW}}{\alpha_L} - (\rho_L - \rho_G) g \sin\theta = 0 \qquad (3.9.2)$$

This static equation replaces the second dynamic mass conservation equation.

In the two-fluid drift-flux model, one dynamic momentum equation is replaced by an algebraic equation.

By studying the eigenvalues of a linearized version of these system equations it is possible to show that two of them are associated with acoustic waves while the third is associated with a much slower surface wave (though not of the true gravitational sort, since they are not included in the model).

Unlike the model based directly on equations 3.3.2 and 3.3.3, no part of the spatial derivative in equation 3.9.1 has a factor in front of it (in equations 3.3.2 and 3.3.3, the spatial pressure derivatives have α_G and α_L in front of them), so this model is on the same form as the equations we became familiar with in single-phase flow. We can therefore use the Kurganov-Tadmore order 3-scheme (KT3) for spatial discretization directly here, too, just as we could in *Pipe Flow 1*. We will later see that we do not necessarily choose that method, but it offers a simple, explicit solution alternative.

3.10 Ignoring inertia in the momentum equations

We saw in chapter 15.5 in *Pipe Flow 1* that the inertia terms in the momentum equations often can be of little significance in pipelines, it is most often the frictions which dominate. A simplified model based on ignoring inertia obviously cannot describe pressure waves, and it has therefore sometimes been referred to as the *no-pressure-wave model*.

If we neglect everything to do with inertia in equation 3.9.1, we get:

$$\frac{\partial p}{\partial x} = R_{Gw} + R_{LW} - (\alpha_G \rho_G + \alpha_L \rho_L) g \sin\theta \qquad (3.10.1)$$

We now have 2 dynamic equations, namely 3.2.2, 3.2.3, in addition to the algebraic equation 3.9.2 and equation 3.10.1, which contains a spatial derivative, though no time derivative.

Simulating these equations is not straight forward, but Patault & Tran (1996) has developed a workable implicit method for doing so. As shown by Viviand (1996) and Masella et al. (1998), the model gives similar results to the full two-fluid model as well as to the drift-flux model for many pipeline situations. Masella et al. (1998) have pointed out, though, that solving these equations seems no more efficient than the (more accurate) drift-flux model, so the no-pressure-wave model appears to be less attractive. Therefore we are not going to go into further details regarding Patault & Tran's (1996) model.

We could in principle go on developing equations to get something similar to what we did for single-phase flow (equation 15.5.11, *Pipe Flow 1*), but we end up with very many terms in the two-phase case. It is unclear whether this procedure would lead to a faster algorithm, and the time it might save is likely to be marginal.

3.11 Incompressible transient model

If we consider both fluids to be incompressible, we avoid having to determine any of the densities, and we can combine the mass conservation equations in the same way as the momentum equations were combined for the drift-flux model. We will see that the pressure term can be eliminated from the main equations, and this model is therefore sometimes called the *pressure-free-model*.

The mass conservation equations 3.2.2 and 3.2.3 can be summarized:

$$\frac{\partial(\rho_G \alpha_G + \rho_L \alpha_L)}{\partial t} + \frac{\partial(\alpha_G \rho_G v_G + \alpha_L \rho_L v_L)}{\partial x} = 0 \qquad (3.11.1)$$

The momentum equations 3.3.2 and 3.3.3 are written without the pressure correction terms, and then combined in such a way that the pressure is eliminated:

$$\frac{1}{\alpha_G}\left[\frac{\partial(\alpha_G\rho_G v_G)}{\partial t}+\frac{\partial(\alpha_G\rho_G {v_G}^2)}{\partial x}\right]+\frac{R_{GLi}}{\alpha_G}-\frac{R_{GW}}{\alpha_G}+\rho_G g\sin\theta$$

$$=\frac{1}{\alpha_L}\left[\frac{\partial(\alpha_L\rho_L v_L)}{\partial t}+\frac{\partial(\alpha_L\rho_L {v_L}^2)}{\partial x}\right]-\frac{R_{GLi}}{\alpha_L}-\frac{R_{LW}}{\alpha_L}+\rho_L g\sin\theta \tag{3.11.2}$$

The terms inside the first bracket can be written as:

$$\left[\frac{\partial(\alpha_G\rho_G)}{\partial t}v_G+\alpha_G\rho_G\frac{\partial v_G}{\partial t}+\frac{\partial(\alpha_G\rho_G v_G)}{\partial x}v_G+\alpha_G\rho_G v_G\frac{\partial v_G}{\partial x}\right] \tag{3.11.3}$$

From the continuity equation, it follows that:

$$\left[\frac{\partial(\alpha_G\rho_G)}{\partial t}+\frac{\partial(\alpha_G\rho_G v_G)}{\partial x}\right]v_G=0 \tag{3.11.4}$$

Notice also that:

$$\frac{\partial(\rho_G v_G)}{\partial x}=\rho_G\frac{\partial(v_G)}{\partial x}+v_G\frac{\partial(\rho_G)}{\partial x} \tag{3.11.5}$$

But since the density is constant, we also have $\partial\rho_G/\partial x=0$. Therefore:

$$\frac{\partial(\rho_G v_G)}{\partial x}=\rho_G\frac{\partial(v_G)}{\partial x} \tag{3.11.6}$$

This could have been used to eliminate the densities from the two mass conservation equations before we summarized them to become equation 3.11.1. Had we done so, equation 3.11.1 would have taken an alternative form without any of the densities.

Equation 3.11.6 also means:

$$\frac{\partial(\rho_G {v_G}^2)}{\partial x} = \rho_G v_G \frac{\partial(v_G)}{\partial x} + v_G \frac{\partial(\rho_G v_G)}{\partial x} = 2\rho_G v_G \frac{\partial(v_G)}{\partial x} \tag{3.11.7}$$

If we combine equations 3.11.3, 3.1.4, and 3.11.7, we see that:

$$\frac{1}{\alpha_G}\left[\frac{\partial(\alpha_G \rho_G v_G)}{\partial t} + \frac{\partial(\alpha_G \rho_G {v_G}^2)}{\partial x}\right] = \left[\frac{\partial(\rho_G v_G)}{\partial t} + \frac{\partial\left(\frac{1}{2}\rho_G {v_G}^2\right)}{\partial x}\right] \tag{3.11.8}$$

Inserting this into equation 3.11.2, and doing a similar transformation for the terms inside the brackets at the right-hand side, we get:

$$\frac{\partial(\rho_L v_L - \rho_G v_G)}{\partial t} + \frac{\partial \frac{1}{2}(\rho_L {v_L}^2 - \rho_G {v_G}^2)}{\partial x} = \frac{R_{GL}}{\alpha_L} + \frac{R_{GL}}{\alpha_G} + \frac{R_{LW}}{\alpha_L} - \frac{R_{GW}}{\alpha_G} - (\rho_L - \rho_G) g \sin\theta \tag{3.11.9}$$

With no compressibility at all in the system, the total volumetric flow at any point in the pipe must constantly equal the total flow injected into the pipe, so:

$$\dot{m}_{G\,in} + \dot{m}_{L\,in} = \alpha_G \rho_G v_G + \alpha_L \rho_L v_L \tag{3.11.10}$$

Our unknowns are the velocities v_G and v_L, and the fractions α_G and α_L. Those 4 unknowns can be solved using equations 3.11.1 and 3.11.9, together with the saturation constraint 3.2.4 and the boundary conditions 3.11.10.

"An expert is a person who has made all the mistakes that can be made in a very narrow field."
Niels Bohr

4 Three-fluid model

Three-fluid two-phase model without evaporation or condensation:

- Mass conservation
- Momentum conservation
- Energy conservation
- Pressure equation
- Fluid properties on a general form

4.1 General

Let us now go one step further than the previous chapter in adding complexity. We still have only two fluids, but in annular flow, liquid can occur both as a film around the pipe wall and as droplets carried by the gas core. The one gas and two liquid forms can be described by three different mass, momentum, and energy conservation equations and we refer to such a formulation as a *three-fluid model*.

Annular flow is one of the most common flow patterns encountered in natural gas well-bores and pipelines. It occurs at high gas and low to medium liquid flow-rate and at all pipe elevation angles.

Droplets can be torn from liquid film (droplet entrainment), and droplets can also settle and become part of the film again (liquid film deposition). Depending on the entrainment and deposition rates, it is known that in the most extreme cases, all the liquid can flow as liquid film or (nearly all) as droplets.

In this model, we do not assume the flow to necessarily be isothermal. Apart from that, we keep the main simplifications from chapter 3 (no boiling or condensation, the pipe does not have perforations, the flow regime does not change).

As in chapter 3, we denote quantities referring to the gas with a G-subscript. Continuous liquid is given L as a subscript, and liquid in droplet form has subscript D. We will show how to establish all necessary conservation equations, correlations for friction, droplet entrainment and liquid film deposition for such a three-fluid model.

The model in this chapter is general and would be valid for other flow regimes than annular if we set the droplet fraction $\alpha_D = 0$, but we are not going to focus on anything other than annular flow.

4.2 Mass conservation

We can now write 3 continuity equations based on equation 2.2.4. For the gas phase, we get:

$$\frac{\partial(\alpha_G \rho_G)}{\partial t} = -\frac{\partial(\alpha_G \rho_G v_G)}{\partial x} + \Gamma_{LG} + \Gamma_{DG} + \Gamma_{GW} \tag{4.2.1}$$

Since we are dealing with two different fluids which do not change phase, $\Gamma_{LG} = \Gamma_{DG} = 0$. Also, no gas is going to be added through perforations in the pipe wall, and therefore $\Gamma_{GW} = 0$. Equation 4.2.1 becomes:

$$\boxed{\frac{\partial(\alpha_G \rho_G)}{\partial t} + \frac{\partial(\alpha_G \rho_G v_G)}{\partial x} = 0} \tag{4.2.2}$$

Liquid can jump between liquid film and droplets, though, in a process called liquid entrainment and droplet deposition. For the liquid film we get:

$$\frac{\partial(\alpha_L \rho_L)}{\partial t} + \frac{\partial(\alpha_L \rho_L v_L)}{\partial x} = -\Gamma_{LDi} + \Gamma_{DLi} \tag{4.2.3}$$

The droplets are assumed to have the same density as the liquid film. Using equation 2.2.4 and 2.2.5, we get:

$$\frac{\partial(\alpha_D \rho_D)}{\partial t} + \frac{\partial(\alpha_D \rho_L v_D)}{\partial x} = +\Gamma_{LDi} - \Gamma_{DLi} \tag{4.2.4}$$

Equation 2.2.6 becomes:

$$\alpha_G + \alpha_L + \alpha_D = 1 \tag{4.2.5}$$

4.3 Momentum conservation

Equation 2.3.16 for the gas yields:

$$\frac{\partial(\alpha_G \rho_G v_G)}{\partial t} = -\frac{\partial(\alpha_G \rho_G {v_G}^2)}{\partial x} - \alpha_G \frac{\partial p_G}{\partial x} + R_{LGi} + R_{DG} + R_{Gw} + S_{LG} + S_{DG} + S_{Gw} - \alpha_G \rho_G g \sin\theta \tag{4.3.1}$$

R_{LG} represents friction force from liquid film on the gas, R_{DG} is friction force pr. unit pipe volume from the droplets on the gas, and R_{GW} is similarly volume-specific friction force from the wall on the gas. In our model we presume the film covers the entire wall's surface. Therefore, there is no direct contact between gas and pipe wall, and $R_{GW} = 0$.

If all surface tension forces acting directly on the gas flow are negligible, we can set $S_{LGi} = S_{DGi} = S_{Gw} = 0$. For simplicity, we also assume the pressure to be constant across all phases in each cross-section so $p = p_G = p_L = p_D$ (even though we know that can lead to the equations not being hyperbolic):

$$\frac{\partial(\alpha_G \rho_G v_G)}{\partial t} + \frac{\partial(\alpha_G \rho_G {v_G}^2)}{\partial x} = -\alpha_G \frac{\partial p}{\partial x} - R_{GL} - R_{GD} \quad - \alpha_G \rho_G g \sin\theta \tag{4.3.2}$$

Similar momentum equation for the liquid film:

$$\frac{\partial(\alpha_L \rho_L v_L)}{\partial t} + \frac{\partial(\alpha_L \rho_L {v_L}^2)}{\partial x} = -\alpha_L \frac{\partial p}{\partial x} - v_{L(D)} \Gamma_{LD} + v_{D(L)} \Gamma_{DL} + R_{GL} + R_{DL} - R_{Lw} \quad - \alpha_L \rho_L g \sin\theta \tag{4.3.3}$$

We have adopted the notation $v_{L(D)}$ for the average velocity of liquid becoming entrained as droplets. This can be approximated as the average liquid film velocity v_L (as we will do in the example in chapter 5). But the absolute velocity $v_{L(D)}$ should not be confused with v_{LD}, a notation used for velocity difference between liquid film and droplets – a parameter relevant to some of the friction calculations.

For the droplets:

$$\frac{\partial(\alpha_D \rho_L v_D)}{\partial t} + \frac{\partial(\alpha_D \rho_L {v_D}^2)}{\partial x} = -\alpha_D \frac{\partial p}{\partial x} + v_{L(D)}\Gamma_{LD} - v_{D(L)}\Gamma_{DL} - R_{DL} + R_{GD} - \alpha_D \rho_L g \sin\theta \quad (4.3.4)$$

4.4 Energy equation

By summarizing equation 2.4.4 for all phases, and applying equations 2.4.5 - 2.4.9, we get:

$$\frac{\partial}{\partial t}(\alpha_G E_G + \alpha_L E_L + \alpha_D E_D) + \frac{\partial}{\partial x}[\alpha_G v_G (E_G + p) + \alpha_L v_L (E_L + p) + \alpha_D v_D (E_D + p)] = \Gamma_{Gw} h_{Gw} + \Gamma_{Lw} h_{Lw} + \Gamma_{Dw} h_{Dw} + q + w \quad (4.4.1)$$

Enthalpy from mass sources (contained in any fluid flowing in through the pipe wall) is assumed to come in the form of gas, liquid film, or droplets. q is volume-specific heat from the environment through the pipe wall into the fluid, and w is work carried out on the fluid (in pumps or compressors, or negative work in a turbine).

4.5 Fluid properties

Since this model presumes no gas will become liquid or vice versa, gas and liquid properties can be considered independent of each other. The main properties are simply the state equations correlating pressure, temperature and density for the gas and liquid separately, as they were shown in equations 3.7.1 and 3.7.2.

The viscosities are of course involved in the friction calculations, and like the densities, they generally depend both on pressure and temperature:

$$\mu_G = \mu_G(p, T) \tag{4.5.1}$$

$$\mu_L = \mu_L(p, T) \tag{4.5.2}$$

The liquid's surface tension when in contact with the particular gas is also involved, so we also need:

$$\sigma_{LG} = \sigma_{LG}(p, T) \tag{4.5.3}$$

"A good decision is based on knowledge and not on numbers."
Plato, 400 BC

5 Friction, deposition and entrainment

How to close the three-fluid two-phase model in chapter 4 for annular flow in vertical pipes:

- Friction between phases and against the wall
- Liquid film entrainment (droplets being torn from the liquid film)
- Droplet deposition (droplets colliding into the liquid film and being absorbed)
- Droplet size estimation

5.1 Friction between gas core and liquid film

5.1.1 General about friction

Our momentum equations rely on determining the friction between the gas and the liquid film, R_{LG}, between the gas and the droplets, R_{DG}, between the liquid and the droplets, R_{DL}, as well as between the liquid film and the pipe wall, R_{DL}. We remember from *Pipe Flow 1* that even in straight pipes with single-phase flow, it is quite common to end up with errors of up to 20% when determining the friction factor. Multi-phase

flow is much more complex, and we realize that any multi-phase model is likely to be more inaccurate than what we can achieve for single-phase flow.

A number of researchers have presented empirical correlations for the friction factors needed. Some of them ignore the pipe surface's roughness and how that influences friction, perhaps due to (in some situations considerably larger) inaccuracies in the other approximations we need to rely on, while others try to account for roughness in various ways.

5.1.2 The friction model

The friction between gas and liquid film, R_{LG}, is similar to the friction experienced by single-phase gas flowing in a normal pipe, the difference being the 'pipe wall' surrounding the gas is a moving liquid film. In addition, the imaginary 'liquid pipe wall' has quite a complicated sort of surface roughness which changes when ripples and surface waves are generated. We must therefore expect the roughness to be a function of all parameters capable of affecting the surface, including film thickness, surface tension, and even pipe inclination (since the liquid film tends to be somewhat thicker near the pipe's lower side in horizontal pipes).

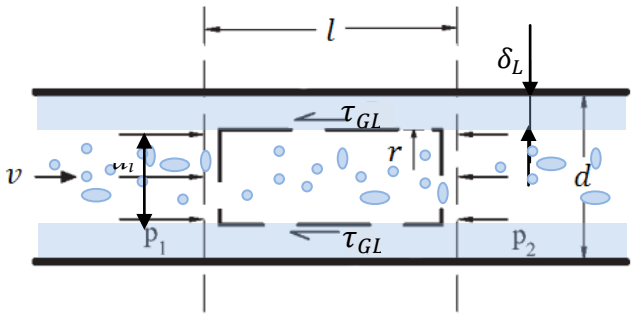

Figure 5.1.1. Shear forces between liquid film at the pipe wall and gas in the pipe core.

If we neglect forces from the droplets and presume the flow to be axis-symmetrical, we can write the following steady-state force balance for the gas:

$$shear\ force\ along\ interface = \ pressure\ force\ at\ end\ surfaces$$

$$\tau_{GL} \cdot \pi d_i \cdot l = \Delta p \cdot \frac{\pi {d_i}^2}{4} \frac{\alpha_G}{(\alpha_G + \alpha_D)} \qquad (5.1.1)$$

d_i is the diameter of the inner gas core (gas including the droplets it may be carrying).

The factor $\alpha_G/(\alpha_G + \alpha_D)$ accounts for part of the effective area at the end surfaces of the control volume being displaced by droplets. A similar factor to modify the shear stress along the interface has not been introduced, which means our friction model relies on the area displacement being less significant there. Since droplets tend to occupy a relatively small part of the volume, the difference is not expected to be significant.

Equation 5.1.1 leads to:

$$\tau_{GL} = \frac{\alpha_G}{(\alpha_G + \alpha_D)} \frac{\Delta p d_i}{4l} \tag{5.1.2}$$

The pressure drop along a pipe with single-phase flow was discussed in great detail in *Pipe Flow 1*, chapter 2:

$$\Delta p = \frac{f_{GL} l \rho_G}{2 d_i} v_{GL} |v_{GL}| \tag{5.1.3}$$

Exactly which velocity difference between gas and liquid to use as v_{GL} is not self evident. It is most common to presume the interface between the gas and liquid to move at the average liquid velocity, v_L, so the gas experiences friction as if it moves at velocity $v_G - v_L$ through the pipe. However, since the gas in most situations moves much faster than the liquid, the liquid's surface is typically dragged along by the gas. If the liquid film is laminar, it can easily be shown that Newton's law of viscosity leads to the liquid film velocity profile being close to triangular, which means the interface velocity becomes close to twice the average liquid film velocity. In turbulent flow, the velocity profile is a bit more complicated, but at least for thin films, setting the surface velocity double the average velocity should be quite a good approximation. For higher gas velocities, the film's surface can become very irregular, and it is hard to define any meaningful surface velocity at all. As long as the average gas velocity is much higher than the average liquid velocity, Δp is not going to be affected significantly by whether we set $v_{GL} = v_G - v_L$ or $v_{GL} = v_G - 2v_L$, though, and it happens to be the first alternative which has been chosen by most researchers, including those who have attempted to

establish correlations for the friction factor f_{GL}. We therefore choose to set $v_{GL} = v_G - v_L$ in this model.

Inserting equation 5.1.3 into 5.1.2, we get:

$$\tau_{GL} = \frac{\alpha_G}{(\alpha_G + \alpha_D)} \frac{f_{GL}\rho_G}{8} v_{GL}|v_{GL}| \tag{5.1.4}$$

The friction force pr. unit pipe volume, R_{LG}, can now be expressed by multiplying the shear stress τ_{LG} by circumference area pr. unit pipe volume:

$$R_{GL} = \frac{\tau_{LG}\pi d_i l}{\frac{\pi d^2}{4} l} \tag{5.1.5}$$

This leads to:

$$R_{GL} = \frac{d_i}{d^2} \frac{\alpha_G}{(\alpha_G + \alpha_D)} \frac{f_{GL}\rho_G}{2} v_{GL}|v_{GL}| \tag{5.1.6}$$

5.1.3 The Darcy-Weisbach friction factor for the liquid film-gas interface

Many researchers have attempted to come up with a reliable Darcy-Weisbach friction factor f_{LG}. Probably the best known and possibly oldest correlation is the one by Wallis (1969). Later work by Hentstock & Hanratty (1976), Asali et al. (1985), Ambrosini et al. (1991), Nigmatulin (1991), Fukano & Furukawa (1998), Fore et al. (2000), in addition to several others has produced generally inconclusive results. Fossa et al. (1998) and Fore et al. (2000) are skeptical regarding whether any of the proposed modifications to Wallis' equation actually improve the estimates.

Wallis' correlation states that the friction factor for the gas-liquid film interface is:

$$f_{GL} = 0.02\left(1 + 300\frac{\delta_L}{d}\right) \tag{5.1.7}$$

Here, $\delta_L = (d - d_i)/2$ is the liquid film's thickness. We see that equation 5.1.7 is going to result in $f_{LG} \to 0.02$ as $d_i \to d$, meaning f_{LG} is always approaching the same value if the liquid film thickness approaches zero (corresponding to single-phase flow), irrespective of Reynolds number or pipe surface relative roughness. We know from single-phase flow theory that this is an inaccurate approximation.

Another remarkable property of equation 5.1.7 is that for $\delta_L/d > 0.001$, it results in friction factors much higher than those corresponding to a sand grain roughness of a similar size. If we use the modified Moody-diagram in figure 2.9.1 in *Pipe Flow 1*, we see that $f = 0.02$ matches smooth pipe flow for $Re = 6 \cdot 10^4$. We would think that if we smeared a liquid film on the surface of such a pipe, that film could not possibly deform in a way that creates higher equivalent sand grain roughness than the thickness of the film itself. Therefore, we would intuitively expect that if $\delta_L/d = 0.01$ (which according to equation 5.1.7 leads to $f_{GL} = 0.08$), it cannot possibly result in a friction factor higher than if we had $k_s/d = 0.01$ (which according to the most conservative of the modified Moody diagrams leads to $f = 0.038$). Even if the liquid surface became so wavy that its peaks and valleys corresponded to $k_s/d = 0.02$, the Moody diagram would only lead to $f = 0.05$, which also is considerably less than equation 5.1.7 predicts. This seemingly logical reasoning is not quite correct, however.

If we look back to figure 2.8.11 in *Pipe Flow 1*, we see that corrugated pipes, which may have greater similarity with the sort of roughness created by surface waves on a liquid film, can produce considerably higher friction than would be expected from measurements on other types of pipes, and this lends credibility to Wallis' results for relatively thick liquid films. Also, Geraci et al. (2007) has found that the surface roughness can in fact be much higher than the average liquid film thickness, something which further supports Wallis' surprisingly high friction factors.

Nigmatulin (1991) and several others have attempted to modify Wallis' equation in a way which takes the actual single-phase smooth-pipe friction factor into account while continuing to ignore the pipe's roughness. Alipchenkov et al.'s version (2004) of Nigmatulin's modifications is:

$$f_{GL} = f\left(Re_{GL}, \frac{k_s = 0}{d}\right) + 6\frac{\delta_L}{d} \tag{5.1.8}$$

This equation is identical to 5.1.7 when it comes to what the liquid film adds to the friction factor. It differs in the value it starts at when $\delta_L = 0$. That value is set to the smooth-pipe friction factor, but as it would have been if we had single-phase gas flow in the pipe (based on the gas Reynolds number Re_G). We can immediately spot one weakness in equation 4.2.8 in that it fails to converge towards the correct roughness-dependent friction factor when the film thickness approaches zero.

It is worth mentioning that according to Gaard & Isaksen (2003), a very moderate fluid layer on the pipe's surface can in fact reduce the friction compared to a dry pipe. With very thin layers, the liquid's main effect can be reducing the surface roughness. It may therefore be a fair approximation to use smooth pipe as basis once the liquid layer is thick enough to smoothen the pipe surface's imperfections, as equation 5.1.7 does, but it clearly looses it validity for very thin liquid layers. What seems apparent, however, is that pipes which are not hydraulically smooth for the given gas Reynolds number may actually have its friction reduced if a very thin liquid layer is formed, but that friction starts to increase again once a certain layer thickness is reached. One important question nobody has yet attempted answering is: Which liquid layer thickness gives the lowest friction? Even if we do not know the exact answer to that question, we are going to propose one simple modification to equation 5.1.8 that enables it to capture the main tendencies:

$$f_{GL} = f\left(Re_{GL}, \frac{\max(0, k_s - \delta_L)}{d}\right) + 6\frac{\delta_L}{d} \tag{5.1.9}$$

The first term in equation 5.1.9 is calculated as for single-phase flow, but with a surface roughness reduced by the liquid layer's thickness δ_L. The last term comes directly from equation 5.1.8. This equation produces the actual surface roughness-dependent single-phase friction factor when $\delta_L = 0$, meaning it converges towards the correct value when we approach single-phase flow. That is an improvement both physically and numerically. If δ_L increases, it is assumed to gradually cover the pipe surface imperfections more and more until $\delta_L = k_s$, in which case no surface imperfections affect the gas flow directly. The roughness can of course not take negative values, that is why we must use $\max(0, k_s - \delta_L)$ rather than $k_s - \delta_L$. Equation 5.1.9 uses the Darcy-Weisbach friction factor from chapter 2 in *Pipe Flow 1*, though with a surface smoothened by the liquid film in case the liquid layer is very thin, and simply adds a term originating from Wallis' results.

The friction factor for the interface between gas and liquid film in annular flow must approach the roughness-dependent Darcy-Weisbach friction factor when the film thickness approaches zero. Ideally, the friction factor correlation should also take into account the film's ability to reduce the apparent surface roughness for very thin films.

The gas Reynolds number is defined relative to the moving liquid. If we (for this purpose only) neglect the droplets' effect on the gas, we define:

$$Re_{GL} = \frac{v_{GL} d_i \rho_G}{\mu_G} \tag{5.1.10}$$

Note that various authors use different definitions for the gas Reynolds number, such as defining it from the gas velocity v_G rather than the relative velocity v_{GL}. As long as the gas velocity is much larger than the liquid velocity, all those definitions lead to relatively similar results.

5.1.4 Friction between the liquid film and the wall

The friction between the gas and the pipe wall, R_{Gw}, and between the gas and the liquid film, R_{LG}, is difficult to express accurately. We remember from *Pipe Flow 1*, chapter 2 and 3 that the Darcy-Weisbach friction factor can be relatively inaccurate even for circular pipes with single-phase flow. When we have stratified or annular flow, we do not even know the exact liquid distribution in all situations. With that in mind, let us try to come up with a reasonably accurate friction model.

Using the definition of hydraulic diameter in equation 3.5.1, we set the liquid film area $A_L = \alpha_L \pi d^2/4$ and wetted perimeter $O_{LW} = \pi d$. The liquid film Reynolds number then becomes:

$$Re_{LW} = \frac{\alpha_L |v_L| d \rho_L}{\mu_L} \tag{5.1.11}$$

For laminar flow in a full pipe (single-phase flow), we recall that the Darcy-Weisbach friction factor could be calculated as:

$$f = \frac{64}{Re} \tag{5.1.12}$$

Basing the friction factor directly on inserting Re_{LW} into equation 5.1.12 does not produce an accurate friction factor for annular flow because gravity tends to make the liquid film thicker at the lower section of the pipe (unless the pipe is vertical). In Alipchenkov et al.'s model (2004), this is accounted for by defining a gravity parameter:

$$G \stackrel{\text{def}}{=} (\rho_L - \alpha_G \rho_G - \alpha_D \rho_L) \frac{\delta_L}{\tau_{GL} + \tau_{DL}} g |\sin\theta| \tag{5.1.13}$$

The shear stresses τ_{GL} and τ_{DL} are calculated using equations 5.1.4 and 5.3.10. From this, they defined a correction parameter which takes care of the deformation in the laminar annular liquid cross-section:

$$k_f = \frac{1 + G}{1 + \frac{2}{3} G} \tag{5.1.14}$$

In case of laminar flow, the *f*-value coming out of equation 5.1.12 is multiplied with k_f to get the final Darcy-Weisbach friction factor. The profile deformation is assumed insignificant for turbulent flow, so the factor is only used for relatively low laminar Reynolds numbers. Pipe roughness is not accounted for when the liquid film becomes turbulent, and as for the gas-liquid friction factor, it converges towards very inaccurate values when the pipe approaches single-phase liquid flow. In this book this part of their model is therefore also modified and we calculate the liquid film friction factor in the same way as in chapter 2 in *Pipe Flow 1* (corresponding to the last parenthesis in equation 5.1.15), but modified by taking into account the liquid film being thickest at the lower section of the pipe for laminar flow (the term in brackets in equation 5.1.15):

$$f_{LW} = \left[k_d k_f + (1 - k_d)\right] \cdot f\left(Re_{LW}, \frac{k_s}{d}\right) \tag{5.1.15}$$

The k_d-factor is simply a factor modeled to vary smoothly from 1 for low Reynolds numbers (meaning the gravity parameter is taken into account for laminar flow) and gradually becoming 0 when we approach turbulent flow (neglecting the gravity parameter for turbulent flow). The *sigmoid* function is well known to have such properties, and we get a smooth transfer by setting:

$$k_d = \left\{1 + exp\left[\frac{(Re_{LW} - 1600)}{100}\right]\right\}^{-1} \tag{5.1.16}$$

The friction pr. unit pipe volume becomes:

$$R_{LW} = \frac{f_{LW}\rho_L}{2d} v_L|v_L| \tag{5.1.17}$$

Note that although we have included annular friction modifications to account for inclination in case the pipe is not vertical, we are not going to do so for all parts of the theory, and the deposition and entrainment models shown in chapters 5.2 – 5.6 are therefore best suited to vertical pipes.

5.2 Droplet gas friction and dynamic response time

When droplets are ripped from the annular liquid film, they are likely to start out with a velocity similar to the interface between liquid film and gas. Once surrounded by gas, they accelerate towards the gas' velocity. During that acceleration phase, the difference in gas and droplet velocity is going to result in a drag force on the droplets. This drag force is what creates the friction between the droplets and the gas. We need to find an expression for those friction forces per unit pipe volume (let us call them R_{DG}) in the same way as we did for the friction between liquid and pipe wall in equation 5.1.15.

Yuen & Chen (1976) and numerous others have found that a (small) droplet's drag coefficient is close to that of a solid sphere. In the turbulent motion inside a pipe we must expect droplets to move around quite violently and to take various shapes, some of which may deviate considerably from spherical. Still, we assume the sphere drag coefficient to be sufficiently accurate to model the droplet drag for our purpose.

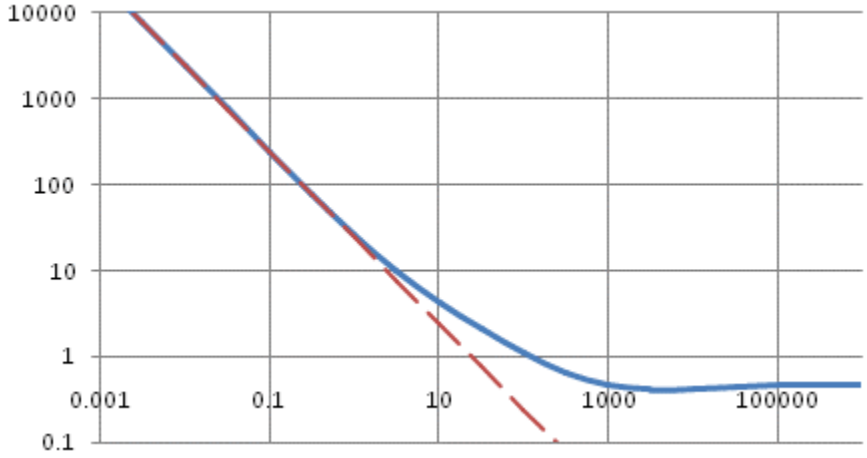

Figure 5.2.1. Drag coefficient C_D as a function of Re_{DG} according to equation 5.2.1. The broken line indicates how C_D would be if we approximated C_D as $24/Re_{DG}$, something which turns out to be quite accurate for $Re_{DG} < 0.2$.

Cheng (2008) has shown that a sphere's drag coefficient can be modeled as:

$$C_D = \frac{24}{Re_{DG}}(1 + 0.27Re_{DG})^{0.43} + 0.47[1 - exp(-0.04Re^{0.38})] \qquad (5.2.1)$$

Cheng's empirical model describes a sphere in turbulence-free flow (except turbulence created by the sphere itself), for instance a sphere moving through still air. In pipe flow, where the gas itself flows and therefore contains turbulent eddies, it is known that C_D tends to be larger than equation 5.2.1 predicts, see for instance Bagchi & Balachandar (2003). Bicyclists may notice the same effect. If the air contains a lot of turbulence, pedaling gets heavier. On a quiet night after the turbulence has had time to die down, it can be a thrill to discover that pedaling is considerably lighter than in the daytime, even if the daytime turbulence was not driven by headwind. The lack of turbulence eddies is usually much more significant in explaining the difference than the higher evening temperature and/or humidity causing reduced air density.

For the sake of simplicity, we are going to neglect the turbulence's influence on the drag in our droplet model and use equation 5.2.1 directly when we calculate average droplet friction. We are also going to neglect it in some bubble models (in later chapters).

The droplet Reynolds number is defined as:

$$Re_{DG} = \frac{|v_{GD}| d_D \rho_G}{\mu_G} \tag{5.2.2}$$

The drag force on a liquid sphere moving relative to a gas becomes:

$$F_{1\,Drop} = \frac{C_D \rho_G}{2} \frac{\pi {d_D}^2}{4} v_{GD} |v_{GD}| \tag{5.2.3}$$

The number of droplets n_D fitting into a pipe section of length Δx can be calculated by applying the definition of the droplet volume fraction α_D:

$$\alpha_D = \frac{n_D \cdot \frac{4\pi}{3} \left(\frac{d_D}{2}\right)^3}{\frac{\pi d^2}{4} \cdot \Delta x} \tag{5.2.4}$$

This leads to:

$$n_D = \alpha_D \frac{3d^2}{2{d_D}^3} \Delta x \tag{5.2.5}$$

Droplet drag force per unit volume pipe can now we found by summarizing for all droplets:

$$R_{GD} = \frac{n_D \cdot F_{1\,Drop}}{\frac{\pi d^2}{4} \cdot \Delta x} \tag{5.2.6}$$

By simple algebra we then get:

$$R_{GD} = \frac{3\alpha_D \rho_G C_D}{4 d_D} v_{GD}|v_{GD}| \tag{5.2.7}$$

In addition to the friction between gas and droplets, as described by equation 5.2.7, we also need to know to which extent the droplets tend to come into contact with the liquid film as they travel in the turbulent gas eddies. We will later see that this can be estimated using Stokes number, which again relies on something called the droplet's dynamic response time.

We start by observing that a sphere-shaped droplet's mass can be expressed as:

$$m_{1\,Drop} = \frac{1}{6}\pi {d_D}^3 (\rho_L + C_{D\,m}\rho_G) \tag{5.2.8}$$

The term $C_{D\,m}\rho_G$ takes into account that the gas closest to the droplet tends to follow the droplet and in effect increases its inertia, thereby making the droplet act as if it had an added mass. That added volume tends to be relatively well estimated by setting $C_{D\,m} = 0.5$.

Newton's second law applied to a droplet during its acceleration phase can be expressed as:

$$\frac{dv_{GD}}{dt} = \frac{\frac{C_D \rho_G}{2}\frac{\pi {d_D}^2}{4}}{\frac{1}{6}\pi {d_D}^3 (\rho_L + C_{D\,m}\rho_G)} v_{GD}|v_{GD}| = \frac{3C_D\rho_G}{4d_D(\rho_L + C_{D\,m}\rho_G)} v_{GD}|v_{GD}| \tag{5.2.9}$$

For high Re_{DG}, C_D varies little as a function of Re_{DG} and can be considered constant. If so, the differential equation 5.2.9 is separable and can easily be solved as:

$$v_{GD} = \frac{4}{3}\frac{(\rho_L + C_{D\,m}\rho_G)d_D}{\rho_G C_D}\frac{1}{t_{D\,R}} \tag{5.2.10}$$

$t_{D\,R}$ is the time from the droplet started, presuming its starting velocity was negligible compared to the gas velocity, until it has reached the speed $v_{GD} = v_G - v_D$. Equation 5.2.10 can be re-formulated as:

$$t_{D\,R} = \frac{4(\rho_L + C_{D\,m}\rho_G)d_D}{3\rho_G C_D |v_{GD}|} \tag{5.2.11}$$

We define $t_{D\,R}$ as *the droplet's dynamic response time* – referred to by some authors as *particle relaxation time* - a measure of how fast it can come up to speed if accelerated by the fluid (in our case gas) flowing past it.

When we study figure 5.2.1, we see the assumption that C_D is constant only holds for fully turbulent flow ($Re_{DG} > 10^3$), which is sometimes not the case for droplets. For very low Reynolds numbers, namely $Re_{DG} < 0.2$ we can set $C_D = 24/Re_{GD}$. Inserting that and equation 5.2.7 into equation 5.2.9 yields:

$$\frac{dv_{GD}}{dt} = \frac{18\,\mu_G}{{d_D}^2(\rho_L + C_{D\,m}\rho_G)} v_{GD} \tag{5.2.12}$$

For simplicity, we will not define a different $t_{D\,R}$ for low or intermediate Reynolds numbers. Instead, we'll just keep in mind that equation 5.2.11 can be expected to give most accurate results for $Re_{DG} > 10^3$.

5.3 Droplet liquid friction forces

5.3.1 Introduction

At first it may not seem meaningful to define such a thing as friction between droplets and the liquid film. One could instead model each droplet as if it would either remained in the gas flow (in the studied control volume) and have no contact with the liquid film, or it would touch the film and 'explode' or merge with the film nearly instantly. That

would be similar to rain drops splashing onto the ground or along a wall. All forces between droplets and the liquid film would be transferred in the form of the momentum carried by droplets becoming part of the liquid film or vice versa, as modeled in the form of mass transfer terms in the momentum equations.

An alternative way of modeling these forces is to consider the droplet phase as a continuum and use approximations for droplet-film interaction like those for gas-film interaction. When a droplet touches the wall, measurements have shown that some of it splashes back into the gas flow instead of becoming part of the liquid film, and a continuum-based model can more easily incorporate this. Alipchenkov at al. (2004) achieved remarkable results using such a model, and the equations below are for the most part based on their paper in addition to conversations during 2007 and 2009 with one of the authors, Prof. Leonid Zaichik. Numerous errors in the original paper were identified during those conversations, and they have been corrected here. Zaichik et al. (2008) have now also published a book where parts of the underlying theory for the model have been included.

Alipchenkov at al.'s 2004-model rests on a model for the eddy-droplet interaction time, and was developed by Zaichik (1998) and Zaichik & Alipchenkov (1999). First we will have a closer look at their model.

5.3.2 Zaichik and Alipchenkov's eddy-droplet interaction time model

Zaichik (1998) and Zaichik and Alipchenkov (1999) used definitions of *Eulerian time microscale*, t_E, and *Lagrangian time scale*, t_{Lag}, and several others, taken from turbulence theory. The definitions are listed below:

$$t_E = 0.1 \frac{d_i}{\left(\frac{|\tau_{GL}|}{\rho_G}\right)^{1/2}} \tag{5.3.1}$$

τ_{GL} can be computed using equation 5.1.4. Time scale of turbulence averaged over the pipe cross-section, the Lagrangian time-scale, is:

$$t_{Lag} = 0.04 \frac{d_i}{\left(\frac{|\tau_{GL}|}{\rho_G}\right)^{1/2}} = 0.4 t_E \tag{5.3.2}$$

Stokes number, which is a measure of to which extent particles (or droplets) tend to follow the gas if it changes direction, is defined as:

$$St = \frac{t_{D\,R}}{t_E} \tag{5.3.3}$$

A dimensionless so-called *drift parameter*:

$$v_{GD}{}^{*} = \frac{|v_{GD}|}{\left(\frac{|\tau_{GL}|}{\rho_G}\right)^{1/2}} \tag{5.3.4}$$

Eddy droplet interaction time at zero droplet dynamic response time, describing how long a droplet would stay in a turbulence eddy if the droplet had no mass:

$$t_{D\,i0} = t_{Lag}\frac{12C_\alpha + 6C_\alpha{}^2 + 2}{5C_\alpha(1+C_\alpha)^2} \tag{5.3.5}$$

The factor C_α is defined as:

$$C_\alpha = \left(1 + v_{GD}{}^{*2} + \frac{2v_{GD}{}^{*}}{\sqrt{3}}\right)^{1/2} \tag{5.3.6}$$

Eddy droplet interaction time at infinite droplet dynamic response time, describing how long a droplet would stay in a turbulence eddy if the droplet had infinite mass:

$$t_{D\,i\infty} = t_{Lag}\frac{6(2 + v_{GD}{}^{*})}{5(1 + v_{GD}{}^{*})^2} \tag{5.3.7}$$

An *interpolation function* dependent on Stokes number:

$$f_{St} = \frac{St}{1+St} - \frac{5St^2}{4(1+St)^2(2+St)} \tag{5.3.8}$$

This finally makes it possible to estimate *the eddy droplet interaction time* $t_{D\,i}$, a measure of how long it takes a droplet to emerge from a turbulence eddy once it has entered it, as:

$$t_{D\,i} = t_{D\,i0} + (t_{D\,i\infty} - t_{D\,i0}) f_{St} \tag{5.3.9}$$

5.3.3 Droplet-liquid film friction modeled as if the droplets were a continuum

If we look back at equation 5.1.4, we see that the shear stress caused by friction between the gas core and the liquid film, τ_{GL}, is proportional to the gas' density and to the square of the velocity difference between the gas and liquid. By analogy, the continuous droplet 'cloud' should have similar properties. The idea is to start out by calculating τ_{GL}, then simply dividing it by everything to do with the gas (gas fraction, gas density and gas velocity square), and finally replacing it with everything to do with the droplets in order to find a similar shear stress for the droplets moving relative to the liquid film:

$$\tau_{DL} = \frac{\alpha_D \rho_L {v_{DL}}^2}{\alpha_G \rho_G {v_{GL}}^2} C_{G\,R} \tau_{GL} \tag{5.3.10}$$

We see that the correlation also includes a factor $C_{G\,R}$, which is a *particle response coefficient* defined by Hinze (1975). It has to do with the turbulent fluctuations in the gas phase and is defined as:

$$C_{G\,R} = \frac{1 + C_0 \frac{t_{D\,R}}{t_{D\,i}}}{1 + \frac{t_{D\,R}}{t_{D\,i}}} \tag{5.3.11}$$

The droplets' dynamic response time $t_{D\,R}$ is calculated with equation 5.2.11, and the eddy droplet interaction time $t_{D\,i}$ is calculated according to equation 5.3.9. The factor C_0 is defined as:

$$C_0 = \frac{(1 + C_{D\,m})\frac{\rho_G}{\rho_L}}{1 + C_{D\,m}\frac{\rho_G}{\rho_L}} \tag{5.3.12}$$

The shear stress between the liquid film and the 'continuous' droplets can now be estimated as:

The volume-specific friction force can then be calculated by multiplying the shear stress with the interface area pr. volume pipe ($= (\pi d_i l)/(\pi d^2/4)$):

$$R_{DLi} = \frac{4d_i}{d^2}\tau_{DL} \tag{5.3.13}$$

5.4 Droplet deposition

There are several models for deposition of droplets, but the most convincing seems to be the one developed by Zaichik (1998), Zaichik et al. (1998), and Zaichik & Alipchenkov (2001). They created an analytical model for predicting the rate of deposition in a vertical tube, and later improved and simplified it (Alipchenkov et al., 2004). They showed that the radial intensity of the gas velocity fluctuations could be expressed as:

$$\langle {v'_{G\,r}}^2 \rangle = \frac{\frac{t_{D\,i}}{t_{Lag}}\left(\frac{|\tau_{GL}|}{\rho_G}\right)^{1/2}\frac{C_r d_i}{2t_{D\,R}}}{1 + \left[\frac{t_{D\,i}}{t_{Lag}}\left(\frac{|\tau_{GL}|}{\rho_G}\right)^{1/2}\frac{16C_r d_i t_{D\,R}}{\pi}\left(\frac{\alpha_D}{5d_D} + \frac{1}{d_i}\right)^2\right]^{1/3}} \tag{5.4.1}$$

The constant $C_r = 5/81$. The Liquid film Weber number is defined as:

$$We_{LGD} = \frac{(\tau_{GL} + \tau_{DL})\delta_L}{\sigma_{LG}} \tag{5.4.2}$$

Alipchenkov et al. (2004) defined a reflection coefficient X, which expresses how large part of a droplet splashes back into the gas flow again after it comes in contact with the liquid film. The two most extreme situations are dry surface and infinite Weber number (infinite liquid film thickness or zero surface tension). For dry surfaces, almost nothing splashes back, making X = 0, while nothing is absorbed by the liquid film in case the Weber number is zero. This can be modeled by a simple *Sigmoid* function as:

$$X = 1 - exp(-3We_{LGD}) \tag{5.4.3}$$

The droplet deposition can then be estimated as:

$$\Gamma_{DLi} = \frac{\frac{32\alpha_D \rho_L t_{D\,R} \langle v'_{G\,r}{}^2 \rangle}{d^2}}{1 + \left(\frac{1-X}{1+X}\sqrt{\frac{2}{\pi}} + 4\frac{1+X}{1-X}\sqrt{\frac{\pi}{2}}\right)\frac{2t_{D\,R}\sqrt{\langle v'_{G\,r}{}^2 \rangle}}{d_i}} \tag{5.4.4}$$

Note that Alipchenkov et al.'s paper from 2004 contains two serious misprints in the equation for calculating Γ_{DL}, so it should be replaced by equation 5.4.4.

5.5 Liquid film entrainment

For very low gas velocities, we realize that no droplets are going to be ripped from the liquid film. Also, we realize that thick liquid films are more likely to lead to entrainment than thin films, while no film at all ($\delta_L = 0$) obviously never leads to entrainment. Several authors have found it possible to define a critical Reynolds number (using equation 5.1.11) below which no entrainment takes place. Ishii and Grolmes (1975) concluded that the critical Reynolds number is $Re_{LW}{}^* = 160$, and that is also close to Nigmatulin et al.'s results (1982), who recommended $Re_{LW}{}^* = 180$.

Alipchenkov et al. (2004) developed the theory further and defined a critical Weber number, to be used as criterion instead of a critical Reynolds number. Their correlation is based on the critical Weber number:

$$We_{LGD}{}^{*} = [7 \cdot 10^{-6} + 4 \cdot 10^{-4}(Re_{LW} - Re_{LW}{}^{*})^{-0.8}]Re_{LW} \tag{5.5.1}$$

Many researchers have attempted to establish analytical or empirical correlations for the liquid film entrainment rate, and they have generally tried to do so by either using the critical Reynolds number or the critical Weber number. Convincing correlations have been presented by Hewitt and Govan (1990), Nimatulin et al. (1996), and de Bertodano and Assad (1998). We are going to use the correlation proposed by Zaichik (1999), which is based on the Kelvin-Helmholz instability theory. It has been shown to fit the experimental data reported by Hanratty and Daykhno (1997). Zaichik's correlation states:

$$\Gamma_{LD} = 0.023 \frac{4d_i}{d^2} \sqrt{\rho_L(\tau_{GL} + \tau_{DL})}(We_{LGD} - We_{LGD}{}^{*}) \; for \; We_{LGD} > We_{LGD}{}^{*}$$

$$\Gamma_{LD} = 0 \qquad for \; We_{LGD} \leq We_{LGD}{}^{*} \tag{5.5.2}$$

This results in the following procedure to estimate Γ_{DL}:

1. Calculate the liquid film Reynolds number Re_{LW} according to equation 5.1.11.
2. Calculate the critical Weber number $We_{LGD}{}^{*}$ according to equation 5.5.1.
3. Calculate τ_{GL} and τ_{DL} according to equations 5.1.4 and 5.3.10.
4. Calculate the Weber number We_{LGD} according to equation 5.4.2.
5. Calculate the liquid film entrainment volume-specific mass flow using equation 5.5.2.

5.6 Droplet size

We saw that the droplet deposition rate calculations in chapter 5.5 rely on knowing the droplet size. We obviously cannot expect all droplets to have the same size, and we need to utilize some sort of average in our calculations. The approach we are going to use here is to first estimate the maximum droplet size which can survive under the

prevailing gas flow conditions, and then set the average droplet size at some percentage of that maximum.

There are two mechanisms which may limit the maximum droplet size. The first is the drag force due to the droplets and the gas moving at different average velocities. That drag force can overcome the droplet's surface tension and lead to breakup. The second mechanism is a result of turbulent eddies in the gas. A droplet passing through an eddy will experience different gas velocities at different points on the droplet, since the different points will be at different distances from the eddy's center. This can create forces large enough to overcome the droplet's surface tension. This mechanism is most often the dominating one, though not always. We therefore need to estimate both and define the maximum droplet diameter according to the most limiting mechanism. We will now have a closer look at how to calculate the maximum stable droplet diameter according to these two limits.

5.6.1 Maximum stable droplet diameter due to average velocity difference

Hinze (1955), Katoka et al. (1983), and Nigmatulin (1991) have presented experimental data which shows that the critical droplet Weber number, above which the droplets start to break up, $We_{DG}{}^{*}$, can be described by the following equation:

$$We_{DG}{}^{*} = 12 + 18\left(\frac{\rho_L \sigma_{LG} d_D}{{\mu_L}^2}\right)^{-0.37} \tag{5.6.1}$$

It is thought that $We_{DG}{}^{*}$ is linked to the droplet's natural frequency for droplet oscillation. Such oscillations can be observed by filling a balloon with water and tapping on its surface. If we tap with the right frequency, we can build up large oscillations with very moderate efforts.

The definition of the Weber number for droplets in a gas can be written as:

$$We_{DG} = \frac{d_D \rho_G {\Delta v_{GD}}^2}{\sigma_{LG}} \tag{5.6.2}$$

The critical (meaning maximum stable) droplet diameter follows from this definition and the critical Weber number as determined by equation 5.6.1. This means:

$$d_{D\,\Delta v}{}^{*} = \frac{We_{DG}{}^{*}\sigma_{LG}}{\rho_G \Delta v_{GD}{}^{2}} \tag{5.6.3}$$

We need an estimate of the velocity difference between gas and liquid v_{GD} in order to use equation 5.6.3. The largest velocity difference between gas and droplet must be expected immediately after the liquid has been torn off the liquid film, and before the droplet has had time to accelerate up to the gas velocity. That velocity difference can be much higher than what it becomes when the droplets have had time to accelerate and reach velocities close to that of the gas. It is difficult to know exactly how far into the gas stream they get before they break up, and therefore we do not know where at the gas' radial velocity profile we should pick a typical gas velocity experienced by most droplets. For simplicity we set $v_{GD} = v_G - v_L$, which probably is quite conservative (meaning a high velocity difference, leading to small droplet diameters). It results in:

$$d_{D\,\Delta v}{}^{*} = \frac{We_{DG}{}^{*}\sigma_{LG}}{\rho_G (v_G - v_L)^2} \tag{5.6.4}$$

By setting the droplet diameter in equation 5.6.1 equal to the critical droplet diameter, $d_D = d_{D\,\Delta v}{}^{*}$, we can combine equation 5.6.1 and 5.6.4 and solve $d_{D\,\Delta v}{}^{*}$. Analytical solution seems impossible, but the equations are easily solved by Newton- or fixedpoint-iteration. Fixedpoint-iteration typically converges after 3 iterations by first guessing an initial diameter, $d_{D\,\Delta v}{}^{*} = 10^{-4}\,m$ for instance, inserting that in equation 5.6.1 to calculate $We_{DG}{}^{*}$, then calculating an improved diameter using equation 5.6.4 and so on.

5.6.2 Maximum stable droplet diameter due to turbulence

The Kolmogorov-Hinze droplet breakup hypothesis (Hinze, 1975) is based on the assumption that droplet breakup is controlled by turbulent eddies, the sizes of which are close to the droplet diameter, since eddies of that size must be expected to create the largest velocity differences. If a droplet happens to pass through the center of such an eddy, this theory presumes, it would experience maximum gas velocity going in opposite directions at opposite sides, leading to maximum forces on its surface. If those forces are larger than the surface tension, breakup occurs.

Alipchenkov et al. (2004) has shown that the critical droplet Weber number due to turbulence eddies in the gas is:

$$We_{DG\ turb}{}^{*} = \frac{3}{C_{G\ R2}\left(1 + 2\frac{\rho_L}{\rho_G}\right)} \tag{5.6.5}$$

The coefficient of response, which we also discussed in equation 5.3.11, is in this case going to be:

$$C_{G\ R2} = \frac{1 + C_0 \frac{t_{D\ R}}{t_{\Delta D\ i}}}{1 + \frac{t_{D\ R}}{t_{\Delta D\ i}}} \tag{5.6.6}$$

C_0 is calculated from equations 5.3.12, and $t_{\Delta D\ i}$ is the time scale that specifies the fluctuating velocity increment at two points separated by the droplet diameter. $t_{D\ R}$ is the dynamic response time, as calculated by equation 5.2.11. The theory is explained in greater detail by Sevik and Park (1973) and Zaichik & Alipchenkov (2003).

Based on the Kolmogorov-Prandtl constant C_μ=0.09, the kinetic turbulence energy k_G is calculated as:

$$k_G = \frac{\frac{\tau_{GL}}{\rho_G}}{\sqrt{C_\mu}} \tag{5.6.7}$$

and the gas energy dissipation per unit mass ε_G:

$$\varepsilon_G = 25\frac{\left(\frac{\tau_{GL}}{\rho_G}\right)^{3/2}}{d_i} \tag{5.6.8}$$

Zaichik et al. (2003) used these two equations as basis to define something they called the *gas velocity structure function*, a function which characterizes how the turbulence interacts with the droplets:

$$S_G(d_D) = \left[\left(\frac{15\mu_G}{\varepsilon_G {d_D}^2 \rho_G}\right)^n + \left(\frac{1}{2{\varepsilon_G}^{2/3}{d_D}^{2/3}}\right)^n + \left(\frac{3}{4k_G}\right)^n\right]^{-1/n} \quad (5.6.9)$$

They also defined the time scale for the velocity difference between a droplet's two sides:

$$t_{\Delta D\,i} = \left[\frac{1}{\left(\frac{5\mu_G}{\varepsilon_G \rho_G}\right)^{n/2} + \left(\frac{0.3{d_D}^{2/3}}{{\varepsilon_G}^{1/3}}\right)^n} + \left(\frac{1}{t_{D\,i}}\right)^n\right]^{-1/n} \quad (5.6.10)$$

n is called the *interpolation exponent*, and it is set to $n = 20$.

The largest stable droplet diameter can then be calculated according to:

$${d_{D\,turb}}^* = \frac{{We_{d\,turb}}^* \sigma_{LG}}{\rho_G S_G} \quad (5.6.11)$$

The calculation procedure calls for iteration. As for the calculations in chapter 5.6.1, we can use fixed-point iteration to achieve convergence after 10 iterations or so:

1. Guess a diameter, for instance ${d_{D\,turb}}^* = 10^{-4}\,m$ and insert that into equation 5.2.12 to get the droplet's dynamic response time $t_{D\,R}$.
2. Calculate the kinetic turbulence energy k_G and the energy dissipation ε_G using equations 5.6.7 and 5.6.8.
3. Calculate the eddy droplet interaction time $t_{D\,i}$ according to equations 5.3.9 and the other relevant equations in chapter 5.3.
4. Calculate S_G and $t_{\Delta D\,i}$ using equation 5.6.9 and 5.6.10.
5. Use equation 5.6.6 to calculate $C_{G\,R2}$.
6. Find an improved estimate for ${d_{D\,turb}}^*$ using equation 5.6.11.
7. Go back to 2. and iterate until convergence.

5.6.3 Average droplet diameter

Once a droplet has coagulated with other droplets and grown to either the maximum size allowed by the average velocity difference ($d_{D\,\Delta v}{}^{*}$, as outlined in chapter 5.6.1) or the maximum allowed by the turbulent eddies ($d_{D\,turb}{}^{*}$, as outlined in chapter 5.6.2), additional growth will result in the droplet breaking up. Whichever limit is reached first is going to be restrictive, so the maximum droplet diameter becomes:

$$d_D{}^{*} = min(d_{D\,\Delta v}{}^{*},\, d_{D\,turb}{}^{*}) \tag{5.6.12}$$

The droplets are not all going be of identical size, but it is impractical making calculations for a lot of different sizes likely to occur in the flow, so we need to use some representative average of the actual diameter distribution. Azzopardi (1997), and Alipchenkov et al. (2003) showed that the so-called *Sauter mean diameter*, which is 25% of the maximum diameter, can be used as a reasonably representative average in the deposition and entrainment calculations:

$$d_D = 0.25 d_D{}^{*} \tag{5.6.13}$$

"Experience teaches slowly and at the cost of mistakes."
James A. Froude, 1880

6 Solving the two-phase three-fluid equations

How to solve the dispersed-flow model from the two previous chapters:

- Steady-state isothermal incompressible flow solution
- Comparison with measurements
- Steady-state isothermal compressible flow
- Transient isothermal annular flow

6.1 Steady-state incompressible isothermal flow

When testing out a fully transient model like the one we have outlined in the two previous chapters, it is convenient to start by simulating something as simple as possible: Steady-state, incompressible isothermal flow with no boiling or condensation. Unlike most steady-state models in use, the one shown here is simply a special case of the fully transient model where the time derivative is set to zero. Our simplified model can therefore be regarded as one step on the way to testing the fully transient model and not a separate model in itself.

As long as we choose to study a short section of the pipe with very moderate pressure loss, we can consider both densities to be constant. We also neglect inertia due to the volume expansion as the pressure falls towards the pipe outlet – in this case that makes no difference since acceleration cannot occur in steady-state incompressible flow anyway. Therefore we consider all spatial derivates to be zero as well. With these simplifications, equation 4.2.2 is eliminated (it simply states *0 = 0*). Equation 4.2.3 becomes identical to 4.2.4:

$$\Gamma_{LD} - \Gamma_{DL} = 0 \tag{6.1.1}$$

The momentum equations 4.3.2 – 4.3.4 are reduced to:

$$-\alpha_G \frac{\partial p}{\partial x} - R_{GL} - R_{GD} \ - \alpha_G \rho_G g \sin\theta = 0 \tag{6.1.2}$$

$$-\alpha_L \frac{\partial p}{\partial x} - v_{LD}\Gamma_{LD} + v_{DL}\Gamma_{DL} + R_{GL} + R_{DL} - R_{Lw} \ - \alpha_L \rho_L g \sin\theta = 0 \tag{6.1.3}$$

$$-\alpha_D \frac{\partial p}{\partial x} + v_{LD}\Gamma_{LD} - v_{DL}\Gamma_{DL} - R_{DL} + R_{GD} \ - \alpha_D \rho_L g \sin\theta = 0 \tag{6.1.4}$$

To keep the equations from becoming very long, we define the sum of all friction, gravity and mass transfer forces on the gas, liquid film and droplets as:

$$F_G = -R_{GL} - R_{GDi} \ - \alpha_G \rho_G g \sin\theta \tag{6.1.5}$$

$$F_L = -v_{LD}\Gamma_{LD} + v_{DL}\Gamma_{DL} + R_{GLi} + R_{DL} - R_{Lw} \ - \alpha_L \rho_L g \sin\theta \tag{6.1.6}$$

$$F_D = v_{LD}\Gamma_{LD} - v_{DL}\Gamma_{DL} - R_{DL} + R_{GD} \ - \alpha_D \rho_L g \sin\theta \tag{6.1.7}$$

With this notation we eliminate $\partial p/\partial x$ between equations 6.1.2 and 6.1.3 as well as between 6.1.2 and 6.1.4 and get:

$$\frac{F_G}{\alpha_G} = \frac{F_L}{\alpha_L} \tag{6.1.8}$$

$$\frac{F_G}{\alpha_G} = \frac{F_D}{\alpha_D} \tag{6.1.9}$$

We don't need the energy equations to determine temperatures when the flow is isothermal, so equation 4.4.1 is unnecessary.

The pipe inlet is supplied with constant gas and liquid superficial velocities. That happens to be the boundary conditions used in some measurements we will compare the results to in the next chapter. It can also be fairly similar to the situation in petroleum wells producing two-phase flow. We define the inlet constants accordingly:

$$\alpha_G v_G = k_{G\,in} \tag{6.1.10}$$

$$(\alpha_L v_L + \alpha_D v_D)\rho_G = k_{L\,in} \tag{6.1.11}$$

Equations 6.1.1 and 6.1.8 – 6.1.11 can now be used as the main equations. Closure relationships for all the terms in equations 6.1.8 and 6.1.9 are calculated with equations 6.1.5 – 6.1.7, which are again based on friction calculations outlined in chapter 5.

We can use Newton-iteration to solve the equations. To do so, it is convenient to re-formulate them to:

$$F = \begin{bmatrix} f_1 \\ f_2 \\ f_3 \\ f_4 \\ f_5 \\ f_6 \end{bmatrix} = \begin{bmatrix} \alpha_G v_G - k_{G\,in} \\ (\alpha_L v_L + \alpha_D v_D)\rho_G - k_{L\,in} \\ \alpha_G + \alpha_L + \alpha_D - 1 \\ \Gamma_{LD} - \Gamma_{DL} \\ \frac{F_G}{\alpha_G} - \frac{F_L}{\alpha_L} \\ \frac{F_G}{\alpha_G} - \frac{F_D}{\alpha_D} \end{bmatrix} = \begin{bmatrix} 0 \\ 0 \\ 0 \\ 0 \\ 0 \\ 0 \end{bmatrix} \tag{6.1.11}$$

We define the input variables as:

$$Y = \begin{bmatrix} y_1 \\ y_2 \\ y_3 \\ y_4 \\ y_5 \\ y_6 \end{bmatrix} = \begin{bmatrix} \alpha_G \\ \alpha_L \\ \alpha_D \\ v_G \\ v_L \\ v_D \end{bmatrix} \tag{6.1.12}$$

Solving the equations is then straight forward as it was explained in chapter 3.6.

6.2 Comparing with measurements

In figure 6.2.1 we have used the method described in chapter 6.1 to simulate a vertical pipe with diameter $d = 0.032\,m$. Water and air flows upwards through it at room temperature. The pressure $p = 1.5 \cdot 10^5\,Pa$. Water at a constant rate of $(\alpha_L v_L + \alpha_D v_D)\rho_L = 80\ kg/(m^2 s)$ is inserted at the pipe inlet. The gas flow is varied in steps and plotted along the horizontal axis in the form of superficial velocity $\alpha_G v_G$. The flow is allowed to become steady-state for every step so no transients caused by the altered gas flow remain at the time of measurement. The air density is assumed to be $\rho_L = 1.725\ kg/m^3$, and the water density $\rho_L = 998\ kg/m^3$. The dynamic viscosities are $\mu_G = 1.78 \cdot 10^{-5}\ kg/(ms)$ and $\mu_G = 9.98 \cdot 10^{-4}\ kg/(ms)$, the surface tension between water and air is $\sigma_{LG} = 0.073\ N/m$.

Measurements are only available for the droplets, so we are only able to compare with entrained liquid mass flux on the form $\alpha_D v_D \rho_L$, not the droplet size or any other parameter. When carrying out simulations, the whole equation set must be solved, and we are of course able to plot all the parameters produced by the model. The results turn out to be similar, but not identical to Alipchenkov et al.'s (2004) results.

Figure 6.2.1 a) shows the available measurements plotted together with the simulations. Both simulations and measurements show that the droplet superficial mass flow rate reaches a minimum for a particular superficial gas flow rate. The measured droplet mass flows are lower than the simulated ones for low gas velocities, while the opposite is true for high gas velocities. Other models for estimating the droplet size and also for estimating entrainment and deposition do exist - see for instance Kolev's second book (2002, 2005) - and they may achieve better agreement for this particular example, though they are more empirical and not very scalable. Since most measurements have been done on much smaller diameter pipes than the ones we normally encounter in pipelines, most models have severe limitations. The model used here does not rest on

any assumptions known to be sensitive to the pipe diameter, so this model is expected to be equally valid for large and small diameter pipes.

Comparisons with measurements other than the ones shown here, for instance comparisons with Jepson et al.'s (1988) measurements, seem to indicate that Zaichik's model generally estimates somewhat too large droplet sizes, particularly for low gas flow rates. This is an area where there is a potential for improving the model.

The fractions, figure c), turn out to be separated by more than an order of magnitude, and the liquid film and droplet fractions go up when the gas velocity is reduced. That is expected when the total liquid mass flow (liquid film + droplet) is constant, as it is here. Lower velocities mean the fluid uses longer time to travel through the pipe, and hence the liquid fraction increases.

Figure d) shows that the liquid film's velocity approaches zero at around $\alpha_G v_G = 7\ m/s$, indicating that below this value, the gas does not manage to overcome gravity for the liquid film. The droplets, on the other hand, seem to travel at around $4\ m/s$ lower speed than the gas, the difference being nearly independent on v_G. Droplet transport can therefore continue even when the liquid film flows slowly downwards. But for very low gas velocities we will obviously get very low or even negative transport capacity for liquid, and high liquid accumulation will sooner or later lead to flow regime change. This can also be seen from the superficial mass flow rates plotted in figure e).

Since this example presumes steady-state flow, liquid film entrainment and droplet deposition must be identical, and that is why those two parameters overlap in figure f).

Keeping in mind that the vertical axis in figure 6.2.2 is logarithmic, we see that the friction forces between gas and liquid film, as illustrated by R_{GL}, are an order of magnitude higher than the forces caused by the momentum transfer due to droplet deposition ($v_D \Gamma_{DL}$), and two orders of magnitude larger than momentum transfer due to liquid film entrainment ($v_L \Gamma_{LD}$). Therefore, the most critical parameter when attempting to estimate the pressure loss accurately is the friction factor f_{GL} (see equations 5.1.6 and 5.1.9). The friction is less sensitive to potential errors in Γ_{DL} and Γ_{LD}. That is fortunate, since those parameters must be expected to be associated with relatively large uncertainty and are directly affected by any inaccuracies in droplet diameter and fraction. Note, though, that the droplet fraction still affects the liquid transport speed significantly, since droplets travel much faster than the liquid film.

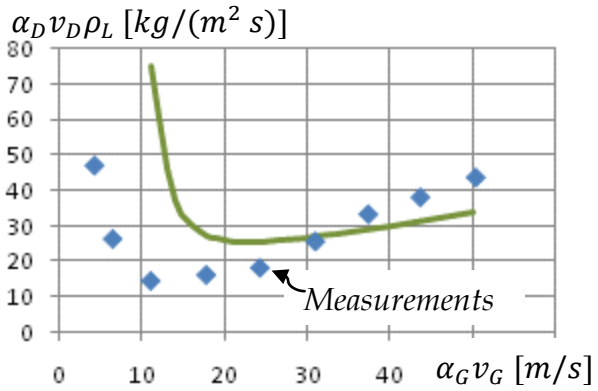

a) *Droplet superficial mass flow rate*

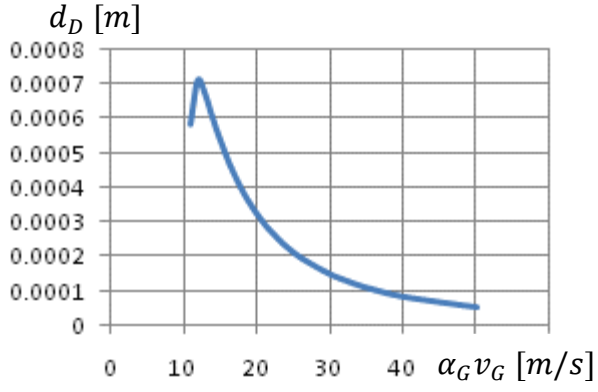

b) *Mean droplet (Sauter) diameter*

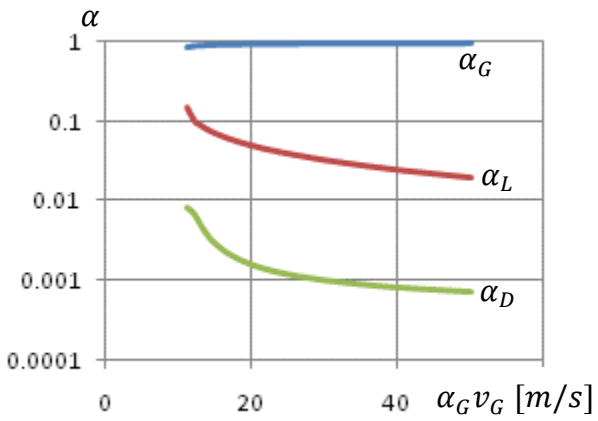

c) *Gas, liquid film and droplet fractions*

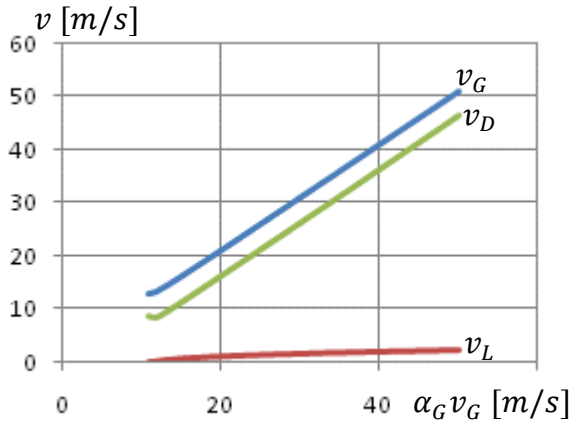

d) *Gas, liquid film and droplet velocities*

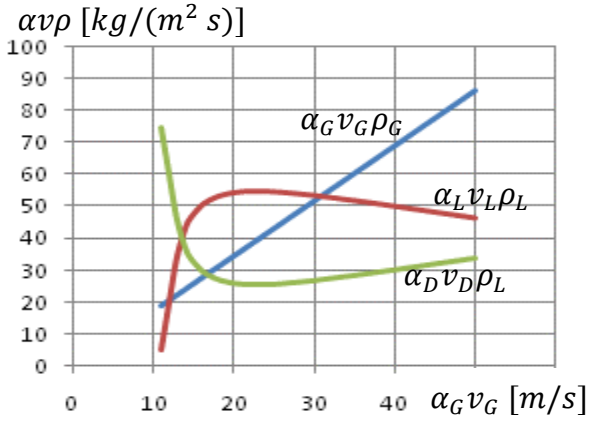

e) *Gas, liquid film and droplet superficial mass flow rates*

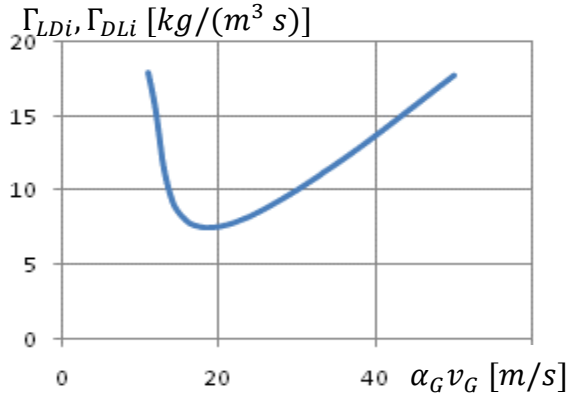

f) Liquid film entrainment and droplet deposition (overlapping curves)

Figure 6.2.1. Simulations of flow in a vertical pipe with diameter d = 0.032 m. Both the gas and the liquid flow upwards. In figure a), measurements from Azzopardi and Zaidi (2000) are also shown. All data are plotted as a function of superficial gas velocity $\alpha_G v_G$, while the superficial liquid mass flow has been kept constant at $(\alpha_L v_L + \alpha_D v_D)\rho_L = 80\ kg/(m^2 s)$.

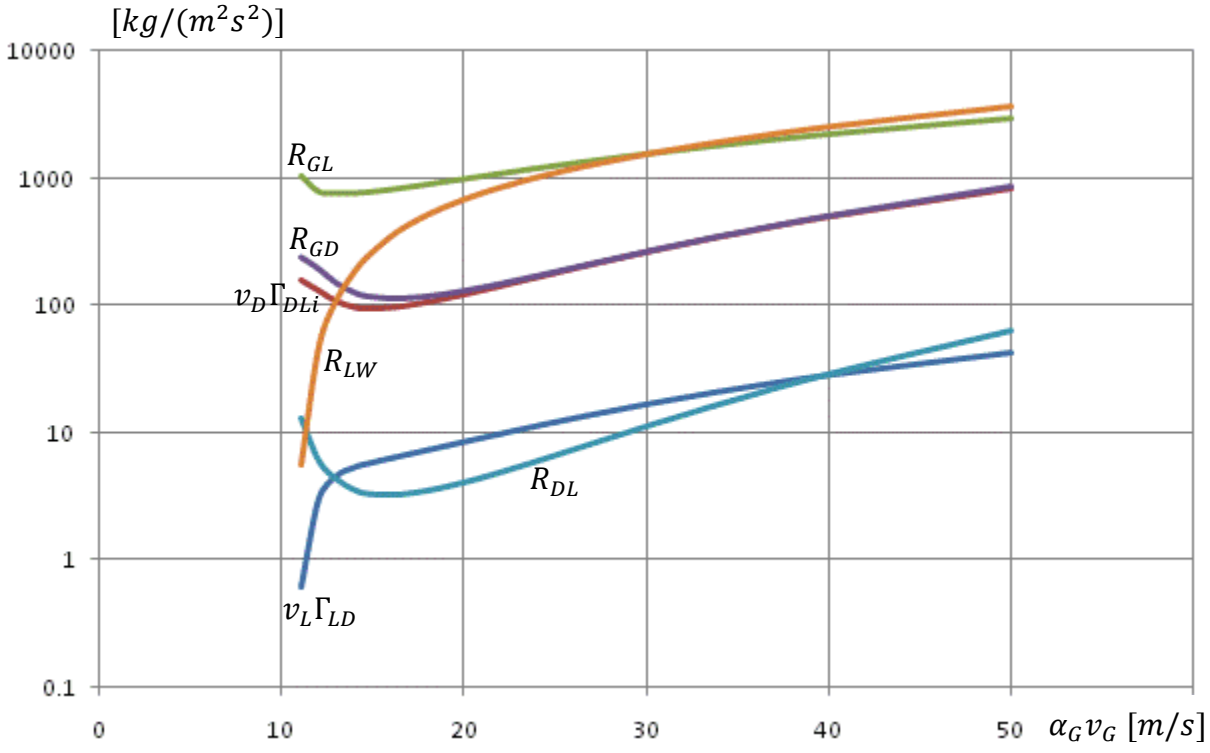

Figure 6.2.2. The different volume-specific forces taking part in the momentum equations 6.1.2-6.1.4.

We see that the friction forces between the liquid film and the wall, as illustrated by R_{LW}, is also dominant, particularly for superficial gas velocities of more than *20 m/s*. That friction factor is based on the relatively well established single-phase flow theory, so we expect the expression for calculating R_{LW} to be considerably more accurate than the one used to calculate R_{GL}, see equation 5.1.15 and 5.1.17. In sum, that makes R_{GL} the main parameter to watch and try to improve when devising better models for two-phase dispersed annular flow, at least for data similar to this example.

Also, it is comforting to see that R_{DL} is very low, so the somewhat uncertain simplifications it builds on, as outlined in chapter 5.3, do not seem to be reason for concern regarding the final result.

6.3 Steady-state compressible flow

We will now go one step further into the real world compared to the incompressible model in chapter 6.1. This time, the time derivatives in the conservation equations from

chapter 3 are the only ones set to zero. The mass conservation equations 4.2.2 – 4.2.4 become:

$$\frac{\partial(\alpha_G \rho_G v_G)}{\partial x} = 0 \tag{6.3.1}$$

$$\frac{\partial(\alpha_L \rho_L v_L)}{\partial x} = -\Gamma_{LD} + \Gamma_{DL} \tag{6.3.2}$$

$$\frac{\partial(\alpha_D \rho_L v_D)}{\partial x} = +\Gamma_{LD} - \Gamma_{DL} \tag{6.3.3}$$

Using the definitions in equations 6.1.5 – 6.1.7, the momentum equations 4.3.2 – 4.3.4 become:

$$\frac{\partial(\alpha_G \rho_G {v_G}^2)}{\partial x} = -\alpha_G \frac{\partial p}{\partial x} + F_G \tag{6.3.4}$$

$$\frac{\partial(\alpha_L \rho_L {v_L}^2)}{\partial x} = -\alpha_L \frac{\partial p}{\partial x} + F_L \tag{6.3.5}$$

$$\frac{\partial(\alpha_D \rho_L {v_D}^2)}{\partial x} = -\alpha_D \frac{\partial p}{\partial x} + F_D \tag{6.3.6}$$

In addition, we must use equations 4.2.5, 3.7.1 and 3.7.2. We then have 9 equations. The independent variables are all the fractions (3), the velocities (3), the densities (2) and the pressure (1), 9 in total.

We may use the same first order approximation for the spatial derivatives as in chapter 3.7, namely equation 3.7.3. The incompressible flow equation set, equation 3.7.4, can now be extended and becomes:

$$F_i = \begin{bmatrix} f_{1,i} \\ f_{2,i} \\ f_{3,i} \\ f_{4,i} \\ f_{5,i} \\ f_{6},i \\ f_{7,i} \\ f_{8,i} \\ f_{9,i} \end{bmatrix} = \begin{bmatrix} (\alpha_G \rho_G v_G)_{i+1} - (\alpha_G \rho_G v_G)_i \\ (\alpha_L \rho_L v_L)_{i+1} - (\alpha_L \rho_L v_L)_i + \Delta x\left(\Gamma_{LD,i} - \Gamma_{DL,i}\right) \\ (\alpha_D \rho_L v_D)_{i+1} - (\alpha_D \rho_L v_L)_i - \Delta x\left(\Gamma_{LD,i} - \Gamma_{DL,i}\right) \\ (\alpha_G \rho_G {v_G}^2)_{i+1} - (\alpha_G \rho_G {v_G}^2)_i + \alpha_{G,i}(p_{i+1} - p_i) - \Delta x F_{G,i} \\ (\alpha_L \rho_L {v_L}^2)_{i+1} - (\alpha_L \rho_L {v_L}^2)_i + \alpha_{L,i}(p_{i+1} - p_i) - \Delta x F_{L,i} \\ (\alpha_D \rho_L D^2)_{i+1} - (\alpha_D \rho_L {v_D}^2)_i + \alpha_{D,i}(p_{i+1} - p_i) - \Delta x F_{D,i} \\ \alpha_{G,i} + \alpha_{L,i} + \alpha_{D,i} - 1 \\ \rho_{G\,i+1} - \rho_G(p,T)_{i+1} \\ \rho_{L\,i+1} - \rho_L(p,T)_{i+1} \end{bmatrix} = \begin{bmatrix} 0 \\ 0 \\ 0 \\ 0 \\ 0 \\ 0 \\ 0 \\ 0 \\ 0 \end{bmatrix} \quad (6.3.7)$$

And:

$$Y = [\alpha_G, \alpha_L, \alpha_D, v_G, v_L, v_D, \rho_G, \rho_L, p]^T \quad (6.2.8)$$

Solution follows the procedure outlined in chapter 3.7.

6.4 Transient three-fluid two-phase annular flow model

In the transient case, we can of course no longer neglect the time derivatives. We see directly, though, that the number of equations needed is the same as for the steady-state example: 9 equations and 9 unknowns, the only difference being that we must include the time derivatives.

When solving those equations, there are at least two important problems to consider: First, most explicit algorithms are ineffective if the equations describe both fast and slow phenomena at the same time, they typically require very small time-steps in order to avoid instability. In multi-phase flow, it is known that the highest naturally occurring system eigenfrequencies have to do with boiling and condensation, for instance steam becoming water or vice versa. Since we have no boiling or condensation in this example, those problems should not arise. The slowest phenomenon is convective

transport, but that, too, does not cause any concern here. Since the flow is isothermal, we are not going to use very long simulation times to see how hot or cold liquid propagates through the pipe.

There is one remaining problem, however: If any of the droplet fractions approaches zero, we intuitively understand that its response time also approaches zero. In chapter 6.2, figure 6.2.1, we saw an example of droplet fractions in the order of 0.1%, at the same time as forces acting on the droplets, figure 6.2.2, were considerable. We expect explicit methods for the most part to work satisfactorily in our simplified, boiling-free model, though not if any fractions approach zero. To get robust code, we therefore need to define limits for how low each fraction is allowed to fall, or set the fraction to zero and remove it from the equations if it falls below a predefined threshold.

More efficient implicit integration methods are outlined in chapter 12.

"Do not worry about your difficulties in Mathematics.
I can assure you mine are still greater."
Albert Einstein

7 Gas-liquid slug flow

What slugs are and how to model them for steady-state incompressible flow:

- Slug mechanisms
- Empirical slug period and length correlations
- Slug profile calculation
- Slug flow friction calculations
- Transient slug modeling

7.1 Slug mechanisms

As indicated in figure 7.1.1, slug flow is characterized by an alternating flow of gas pockets (Taylor-bubbles) and liquid slugs. Most of the gas phase is concentrated in the Taylor-bubbles. They are bullet-shaped and symmetrical for vertical flow, but in inclined and horizontal pipes, they flow in the upper part of the pipe with a liquid film below them. There are also some bubbles dissolved in the liquid.

Hydrodynamic slugs in horizontal and near horizontal pipes of the sort illustrated on figure 1.2.1 iii) are formed by waves growing on the liquid surface to a height sufficient to completely fill the pipe. Terrain slugging, illustrated in figure 1.2.2, is typically

created near a dip in a flow-line, well, or riser. Understanding and controlling the phenomena might prevent shutdowns and lost production.

Initially, hydrodynamic slugs are relatively short, but they typically grow to form longer slugs. Terrain slugs can be many hundreds of meters long, and in multi-phase production gathering networks and flow-lines, slugging periods can be hours long. It is not uncommon for hydrodynamic slugs and terrain slugs to occur at different times during the lifespan of a flow-line riser system.

Other types of slugging are initiated by pipeline operations. Pigging of a pipeline causes most of the liquid to be pushed from the line as a liquid slug ahead of the pig. Line shut-down will drain the liquid remaining in the line down to the low points, and during restart the accumulated liquid can exit the pipeline as a slug. Also, increasing or decreasing the flow rate of either gas or liquid leads to a change in liquid fraction. Depending on flow-rate and various other factors, this can create a slug.

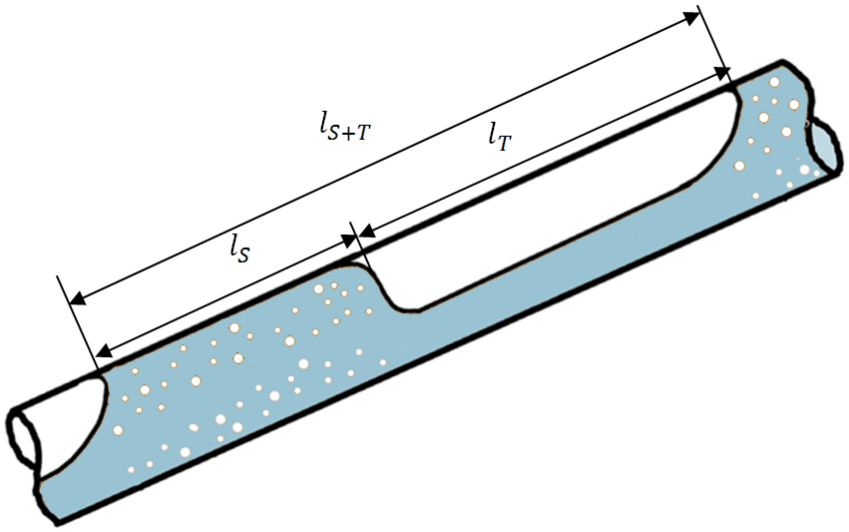

Figure 7.1.1 Simplified schematic model of slug train in inclined pipe. The liquid slug's length is l_S, while the Taylor-bubbles length is l_T. The total slug unit's length is called l_{S+T}.

Slugs are by their very nature transient: Any point along the pipeline will experience alternating high and low gas fractions in case of slugging. One may therefore strictly speaking claim that there is no such thing as steady-state slug flow, but we use the term to describe constant average mass flows and stable slug lengths.

We will establish empirical correlations for average slug length, frequency, liquid fraction and some others. Based on those correlations, we will show that liquid slug and Taylor-bubble friction can be estimated, and those friction estimates can also be used in transient models.

Dukler & Hubbard (1975) simplified by suggesting that the liquid slug covers the whole cross-section in the part termed l_S on figure 7.1.1. As a result, the liquid slug must move at a velocity close to the mixture velocity. We realize that this must be so if we compare the slug to a plug (such as a cleaning pig) moving with the flow. On average, it has to move as fast as the sum of everything else moving through the pipe (liquid and gas) to satisfy mass balance. For the slug, this analogy is somewhat compromised by the fact that it sheds some liquid (along with the small bubbles in that liquid) from its tail end and is also fed liquid (containing small bubbles) at its front. Still, the 'pig-analogy' may be helpful as a mental reference.

The liquid film under the Taylor-bubble moves more slowly, and the relatively fast-moving slug overruns the film in front of it, picks it up, and accelerates it to the slug velocity. If the slug keeps its length constant (a common presumption, even though it is known not to be completely correct), it means the mass flow shedding at its end and the mass flow pickup at its front must be equal. Several authors have tried to describe the shedding and pickup mechanism separately to create a model which reproduces a realistic slug length distribution, including individual slug's length variations. Later we will discuss such models further, but in this chapter we stick to the simpler, but also potentially less general empirical correlations for slug lengths.

7.2 Empirical slug period correlations

7.2.1 Slug frequency and slug length

Zabaras (2000) has given a useful overview over various slug frequency prediction methods. One of the most well-know methods is the one by Hill & Wood (1994), which is based on extensive laboratory and field data. They defined two dimensionless groups:

$$\pi_{fS} = \frac{f_S d}{\alpha_G v_G + \alpha_L v_L}(1 - 0.05\alpha_G v_G)d^{0.3} \tag{7.2.1}$$

$$\pi_{h_{LS}} = \frac{h_{LS}}{d}\left(1 - \frac{0.068}{\alpha_L v_L}\right) \tag{7.2.2}$$

f_S is the slug frequency, and h_{LS} is the equilibrium stratified-flow liquid level, as it would have been if the flow had not switched from stratified to slug. Note that h_{LS} is defined differently from h_L in figure 3.4.1, as h_{LS} is measured from the bottom of the pipe to the liquid's surface. h_{LS} can be determined by inserting stratified-flow friction factors into a steady-state incompressible version of the two momentum equations. Stratified-flow friction factors are described in chapter 3.

α_G and α_L are now volume fractions averaged over a whole slug train and do not correspond to gas fraction in the slug, α_{GS}, or the Taylor-bubble fraction, α_{GT}.

Hill & Wood (1994) proposed the following empirical correlation for the two groups in equations 7.2.1 and 7.2.2 (converted here to SI-units):

$$3600\pi_{f_S} = -24.729 + 0.00766 \cdot exp\left(9.91209\pi_{h_{LS}}\right) + 24.721 \cdot exp\left(0.20524\pi_{h_{LS}}\right) \tag{7.2.3}$$

Zabaras (2000) proposed the following alternative slug frequency correlation based on 399 data for pipe diameters $0.0254m \le d \le 0.20m$ and elevation angles $0^0 \le \theta \le 11^0$. His correlation may be the most accurate empirical one for horizontal and slightly inclined pipes. Converted to SI-units it becomes:

(7.2.4)

$$f_S = 0.0226\left(\frac{\alpha_L v_L}{gd}\right)^{1.2}\left[\frac{64.8}{\alpha_G v_G + \alpha_L v_L} + 3.281(\alpha_G v_G + \alpha_L v_L)\right]^{1.2}[0.836 + 2.75(\sin\theta)^{0.25}]$$

The slug length is of course correlated to the slug frequency via the slug velocity:

$$l_S = \frac{v_S}{f_S} \tag{7.2.5}$$

If the slug velocity is unknown, we can estimate the slug length directly by the empirical Scott et al. (1989) correlation based on data from the Prudhoe Bay field. Converted to SI-unites and adapted to take into account that there exists a minimum,

below which the slug length is thought not to fall even for very low diameters, Scott's equation can be written as:

$$l_s = \max\left\{30d, exp\left\{-26.8 + 28.5\left[ln\left(\frac{d}{0.0254}\right)\right]^{0.1}\right\}\right\} \quad (7.2.6)$$

This can be plotted as follows:

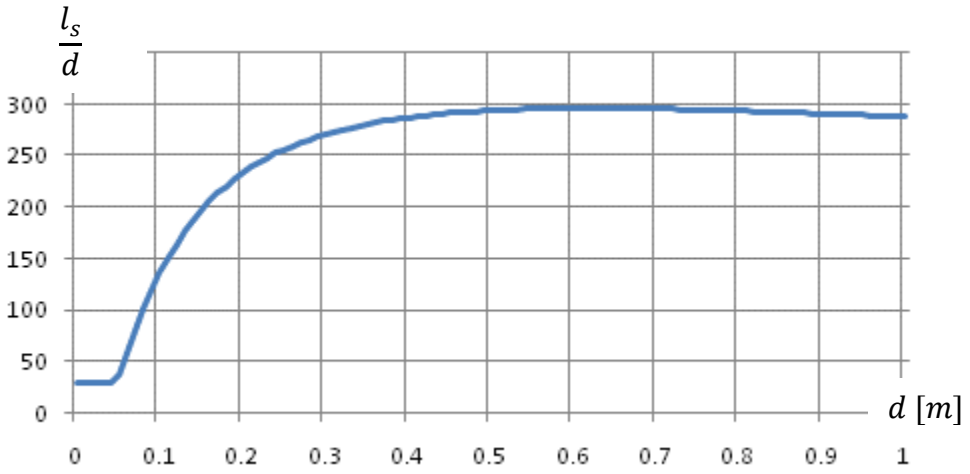

Figure 7.2.1. l_s/d as a function of d according to Scott's equation, equation 7.2.6.Note that the figure has been plotted to a diameter above what was available in the underlying empirical data, so we must use the results with care.

We see that for pipe diameters above *0.5 m*, Scott's equation indicates that the average slug length is somewhere in the order of $300d$.

Remember that this is for hydrodynamic slugs, terrain generated slugs can be much longer. Hydrodynamic slugs also have a random distribution around this average, so the largest slugs will be considerably longer, possibly up to twice the average.

Other, more recent slug length prediction models exist. Shea et al. (2004) developed a slug frequency correlation as a function of pipe length measured from pipe inlet, l_{in}:

$$f_S = \frac{0.47(\alpha_L v_L)^{0.75}}{d^{1.2} l_{in}^{\ 0.55}} \quad (7.2.7)$$

This correlation has no theoretical basis and is a pure curve fitting. Still, it has shown fair agreement with a large base of laboratory and field data. We notice that the input parameters in equations 7.2.7 and 7.2.4 (or 7.2.6) are not identical, reflecting the fact that slugging is a complicated phenomenon which is still not completely understood.

Al-Safran (2009) has developed an empirical correlation which also accounts for stochastic variation in slug lengths. It is relatively complex and not shown here.

7.2.2 Slug fractions

As illustrated on figures 7.1.1 and 9.4.1, the 'liquid' part of the slug train contains some small bubbles. Therefore, we generally have a slug liquid fraction $\alpha_{LS} < 1$, and hence $\alpha_{GS} = 1 - \alpha_{LS} > 0$. Several different empirical correlations for estimating α_{LS} have been proposed, including by Gregory et al. (1978) and Barnea & Brauner (1985). The most general correlation appears to be the one proposed by Gomez et al. (2000), which covers all inclinations from horizontal to upward vertical flow:

$$\alpha_{LS} = exp[-(7.85 \cdot 10^{-3}\theta + 2.48 \cdot 10^{-6} Re_{LS})] \, , 0^0 \leq \theta \leq 90^0 \tag{7.2.8}$$

θ is measured in degrees ($\theta = 0^0$ is as before defined as horizontal pipe, $\theta = 90^0$ means vertical upwards). The liquid slug Reynolds number is defined according to the average volume fractions for the whole slug train:

$$Re_{LS} = \frac{d\rho_L(\alpha_G v_G + \alpha_L v_L)}{\mu_L} \tag{7.2.9}$$

7.2.3 Taylor-bubble and slug bubble velocities

Shoham (2005) has shown how empirical results from Davis & Taylor (1950), Dumitrescu (1943), Benjamin (1968), and Bendiksen (1984) can be combined to form the following correlation for a Taylor bubble's velocity (which under steady-state conditions is the same as the whole slug unit's velocity):

$$v_T = c_{0T}(\alpha_G v_G + \alpha_L v_L) + 0.54\sqrt{gd}\cos\theta + 0.35\sqrt{gd}\sin\theta \, , 0^0 \leq \theta \leq 90^0 \tag{7.2.10}$$

The so-called *flow distribution coefficient* for the Taylor-bubbles $c_{0T} = 1.2$ for turbulent and $c_{0T} = 2$ for laminar flow.

If we have no net flow so that $\alpha_G v_G + \alpha_L v_L = 0$, v_{GT} becomes the bubble rise velocity in a pipe with no net average flow (when neglecting compressibility). Interestingly, the terms $0.54\sqrt{gd}\cos\theta + 0.35\sqrt{gd}\sin\theta$ do not reach a maximum for the pipe being vertical. As we can see from figure 7.2.2, the bubble's rise velocity is largest for inclinations of around 30^0. This appears to be because even though the Taylor-bubble's axial buoyancy is largest for vertical pipes, the bubble blocks the liquid more efficiently and the liquid drainage around the bubble is restricted when the inclination is steep. This is a bit like trying to empty a bottle: Holding it vertically upside-down is not optimal, it empties faster if care is taken not to obstruct the air being sucked into it. Similarly, the asymmetric bubble in less steeply inclined pipes allows the liquid to escape past it more easily, and the optimum angle turns out to be quite low at only around 30^0.

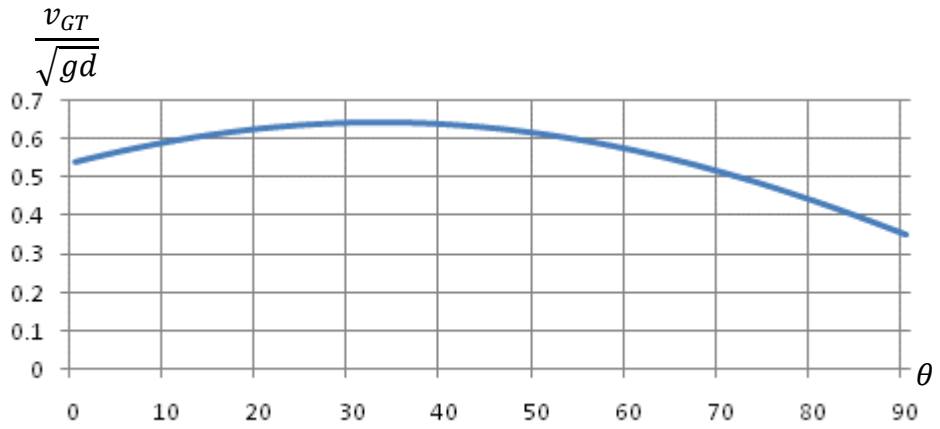

Figure 7.2.2. Non-dimensional Taylor-bubble rise velocity for $(\alpha_G v_G + \alpha_L v_L) = 0$ *as a function of pipe inclination angle according to equation 7.2.10.*

Gas bubbles in the slug move in a similar manner, and the bubbles tend to rise in the liquid. At the same time the liquid itself moves, and we get the total velocity by summarizing the two:

$$v_{GS} = c_{0B}(\alpha_G v_G + \alpha_L v_L) + 1.53\left[\frac{g\sigma_{GL}(\rho_L - \rho_G)}{{\rho_L}^2}\right]^{0.25} {\alpha_{LS}}^{0.5}\sin\theta\,, 0^0 \le \theta \le 90^0 \quad (7.2.11)$$

The slug bubble distribution coefficient c_{0B} is according to Wallis (1969) between *1* and *1.5*, with the most probable value being $c_{0B} = 1.2$ for steep inclinations, but $c_{0B} = 1$ for horizontal or nearly horizontal pipes where the bubbles tend to accumulate near the top of the pipe. α_{LS} is calculated according to equation 7.2.8 and 7.2.9.

7.3 Slug train friction

Taitel & Barnea (1990) proposed methods for calculating the friction in slug flow. For the most part this chapter is based on their theory, inspired by the presentation of it in Shoham's book (Shoham, 2005).

In slug flow, the different fractions are of course going to vary a lot at different locations in a slug train. By relatively simple steady-state analysis, it is possible to show that the average fraction must be:

$$\alpha_L = \frac{\alpha_{LS}(v_T - v_{LS}) + (\alpha_L v_L)}{v_T} \tag{7.3.1}$$

α_{LS} is the liquid fraction in the slug, while v_T is Taylor-bubble's velocity, as given by equations 7.2.7 and 7.2.9. $(\alpha_L v_L)$ is the average superficial velocity, which in a steady-state incompressible model follows from the constant mass flow, given as a boundary condition. A similar analysis for the gas leads to an alternative way to calculate α_L:

$$\alpha_L = \frac{\alpha_{LS} v_T + (1 - \alpha_{LS}) v_{GS} - (\alpha_G v_G)}{v_T} \tag{7.3.2}$$

The Taylor-bubble and the slug follow each other, so they must move at the same speed. The liquid in the slug moves slower due to the liquid it receives via the film under the Taylor bubble, and the difference between them will be $(v_T - v_{LS})$. The volumetric flow rate coming via the film must be large enough to fill the volumetric difference $\alpha_{LS}(v_T - v_{LS})$, and we get:

$$\alpha_{LT}(v_T - v_{LT}) = \alpha_{LS}(v_T - v_{LS}) \tag{7.3.3}$$

By re-arranging:

$$v_{LT} = v_T - \frac{\alpha_{LS}}{\alpha_{LT}}(v_T - v_{LS}) \tag{7.3.4}$$

The Taylor-bubble sheds smaller gas bubbles from its tail and also receives a similar amount of bubbles at its tip. The gas in the bubble therefore moves slower than the Tailor-bubble itself. The total area-specific flow, $(\alpha_G v_G + \alpha_L v_L)$ must equal the sum of the gas- and the liquid part:

$$(\alpha_G v_G + \alpha_L v_L) = (1 - \alpha_{GT})v_{GT} + \alpha_{LT} v_{LT} \tag{7.3.5}$$

From this, the velocity for the gas in the Taylor-bubble can be determined as:

$$v_{GT} = \frac{(\alpha_G v_G + \alpha_L v_L) - \alpha_{LT} v_{LT}}{(1 - \alpha_{GT})} \tag{7.3.6}$$

Since the flow is assumed to be steady-state and incompressible, a continuity balance on both liquid and gas phases results in constant volumetric flow rate through any cross section. In the slug, the volumetric flow rate consists of the liquid and the bubbles in the section of length l_S in figure 7.1.1:

$$\alpha_G v_G + \alpha_L v_L = \alpha_{LS} v_{LS} + (1 - \alpha_{LS})v_{GS} \tag{7.3.7}$$

It then becomes possible to solve the velocity of the liquid in the slug, v_{LS}. Just remember that v_{LS} is not the same as the slug's velocity, since liquid is constantly fed into the slug at its front and drained from it at its tail:

$$v_{LS} = \frac{\alpha_G v_G + \alpha_L v_L - (1 - \alpha_{LS}) v_{GS}}{\alpha_{LS}} \tag{7.3.8}$$

Since the Taylor-bubble moves faster than the liquid, the liquid in front of it must pass it via the liquid film below it. Continuity for this process can be expressed as:

$$\alpha_{LS}(v_T - v_{LS}) = \alpha_{LT}(v_T - v_{LT}) \tag{7.3.9}$$

From this we can solve:

$$v_{LT} = v_T - \frac{\alpha_{LS}(v_T - v_{LS})}{\alpha_{LT}} \tag{7.3.10}$$

For the liquid film under the Taylor bubble, we can approximate the friction by assuming stratified flow. For long Taylor-bubbles, which create the most interesting type of slug flow for pipelines, we have a nearly constant film thickness under most of the Taylor bubble's length. The situation is therefore similar to stratified flow. To describe this, we use the momentum equations 3.3.2 and 3.3.3 and consider steady-state, incompressible flow, and we neglect the pressure correction terms. This was also what we did in chapter 3.6 (see equations 3.6.6 and 3.6.7). In this case that leads to:

$$-\alpha_{GT}\frac{\partial p}{\partial x} - R_{GL} + R_{Gw} \; - \alpha_G \rho_G g \sin\theta = 0 \tag{7.3.11}$$

And:

$$-\alpha_{LT}\frac{\partial p}{\partial x} + R_{GL} + R_{Lw} \; - \alpha_L \rho_L g \sin\theta = 0 \tag{7.3.12}$$

$\partial p/\partial x$ must be the same in both equations, which means:

$$\boxed{\frac{R_{GL}}{\alpha_{LT}} + \frac{R_{GLi}}{\alpha_{GT}} + \frac{R_{Lw}}{\alpha_{LT}} - \frac{R_{Gw}}{\alpha_{GT}} - (\rho_L - \rho_G) g \sin\theta = 0} \tag{7.3.13}$$

The friction factors R_{GL}, R_{Lw}, and R_{Gw} depend on α_{LT}. We therefore need to start by guessing a value for α_{LT} (or some other parameter, such as h_{LT}). Geometrical considerations then determine everything required in equation 7.3.13. If the results fail to agree with equation 7.3.11, we have to try a new guess for α_{LT} and iterate until we get agreement. In practice we use some clever method to speed up convergence, for instance Newton-iteration.

Once we have convergence, α_{LT} and $\alpha_{GT} = (1 - \alpha_{LT})$ are known. Then, the slug train length can be determined as:

$$\boxed{l_{S+T} = \frac{l_S(\alpha_{LS} v_{LS} - \alpha_{LT} v_{LT})}{v_S - \alpha_{LT} v_{LT}}} \tag{7.3.14}$$

And of course:

$$l_T = l_{S+T} - l_S \tag{7.3.15}$$

By inserting the now known parameters into equations 7.3.11 and 7.3.12, we can show that:

$$\Delta p_S = \rho_S g \sin\theta \, l_S + \frac{4\tau_S}{d} l_S \tag{7.3.16}$$

$$\Delta p_T = \rho_T g \sin\theta \, l_T + \frac{4\tau_{GW} S_G}{\pi d^2} l_T \tag{7.3.17}$$

Where:

$$\rho_S = \alpha_{LS}\rho_L + (1 - \alpha_{LS})\rho_G \tag{7.3.18}$$

$$\rho_T = \alpha_{LT}\rho_L + (1 - \alpha_{LT})\rho_G \tag{7.3.19}$$

These pressure loss calculations can be used in both transient and steady-state simulations models.

The terms $\rho_S g \sin\theta \, l_S$ and $\rho_T g \sin\theta \, l_T$ in equations 7.3.16 and 7.3.17 are the ones accounting for the pipe elevation, while the rest describe the frictions needed in the transient model.

7.4 Dynamic slug simulation

Although it is not the only possible way to simulate multi-phase transient pipe flow, we will at first focus on the simplest way to do so – by using an Eulerian formulation based on a fixed grid. This raises some problems unique to slug flow in that stationary grids have a strong tendency to diffuse the slug fronts. As we will discover in chapter 9, this can be countered by using an extremely dense grid. Alternatively, two other strategies are possible: the *slug unit* approach and the *slug tracking* approach.

In the slug unit approach, the flow is considered to be a succession of identical slug units composed of a slug and a gas bubble in the way we have done when developing the steady-state model in chapters 7.1 – 7.2 (see figure 7.1.1). Normal slug flow is regarded as an averaged flow, where information on individual slugs is replaced by average pressure drop and liquid fractions of the sorts developed in the steady-state model. We can determine how far each slug has moved by integrating the slug unit

velocity v_T as described by equation 7.2.9. This, together with the correlations for slug frequency and length, as well as the slug unit length, enables us to estimate the time-dependent oscillating liquid and gas fraction at critical points in the pipe. This method is relatively easy to implement, see Bendiksen et al. (1996), but it has been found that large slugs travelling long distances are smoothened out by numerical diffusion. That means the results will be inaccurate, since numerical diffusion obviously does not correspond to any real phenomenon in the pipeline.

The slug tracking schemes were developed to reduce the diffusion problem. The position of each slug front and bubble nose is calculated from conservation laws or experimental closures. Examples of such slug tracking schemes have been described by Nydal & Banerjee (1996) and Zheng et al. (1994). The OLGA code (*Pipe Flow 1,* chapter 1) has incorporated a slug tracking option that superimposes a moving *Lagrangian* front tracking model on the stationary Eulerian grid. With this strategy the developers have succeeded in improving the prediction of terrain slugging, including slug lengths and frequencies, but the results depend to some extent on the fixed grid being manually specified by the user. Larsen et al. (1997) has shown that these disadvantages can be overcome by introducing an adaptive (rather than fixed mesh-size), moving grid together with a fully integrated slug tracking model.

Further details on how to implement this has been discussed by Renault (2007).

"An invasion of armies can be resisted,
but not an idea whose time has come."
Victor Hugo, 1852

8 Including boiling and condensation

Extending the three-fluid two-phase model from chapters 4 - 6 to include phase change and energy conservation for all flow regimes:

- Including boiling and condensation terms in the conservation equations
- Accounting for surface waves
- Avoiding mass terms approaching zero
- An alternative way to model the pressure
- Simplified deposition correlations
- Bubble flow correlations
- Slug flow correlations

8.1 Extending the three-fluid two-phase model

Now we are going to go one step further in the three-fluid two-phase model developed in chapters 4 – 6 and allow boiling, condensation and inflow/outflow through the pipe wall, too. We will also allow for flow regimes other than the ones discussed so far. Since phase change is closely linked to temperature change, we will include the energy equation and calculate temperatures, too.

In addition, we are going to show two modifications presented by Bendiksen et al. (1991) in their description of the model for the commercial simulator OLGA. It is a drift-flux-type combination of the momentum conservation equations for gas and droplets (though not for gas and liquid film) for annular flow, as well as an alternative way to calculate the pressure by including a separate differential equation for it. In some cases that can make the simulations computationally faster than the way we previously have included the pressure-density-temperature properties.

The model covers all flow regimes, and certain fractions may of course become zero for certain flow regimes (no droplets in slow stratified flow, for instance, corresponds to zero droplet fraction). We will also discuss some new closure relationships.

8.2 Mass conservation

Conservation of mass, equation 2.2.4, is now going to be somewhat more complicated than in the other models we have discussed. For the gas we get:

$$\frac{\partial(\alpha_G \rho_G)}{\partial t} = -\frac{\partial(\alpha_G \rho_G v_G)}{\partial x} + \Gamma_{Gi} + \Gamma_{GW} \tag{8.2.1}$$

Conservation of mass for the continuous liquid film at the wall:

$$\frac{\partial(\alpha_L \rho_L)}{\partial t} = -\frac{\partial(\alpha_L \rho_L v_L)}{\partial x} + \Gamma_{Li} + \Gamma_{LW} \tag{8.2.2}$$

Conservation of mass for the droplet phase:

$$\frac{\partial(\alpha_D \rho_L)}{\partial t} = -\frac{\partial(\alpha_D \rho_L v_D)}{\partial x} + \Gamma_{Di} + \Gamma_{DW} \tag{8.2.3}$$

As before, the liquid film and the droplets have the same density, so we have already replaced ρ_D with ρ_L in equation 8.2.3.

Equation 2.2.5 tells us that the sum of all mass transfers between phases must be zero. All gas can come from or become liquid, and so:

$$\Gamma_{Gi} = -\Gamma_{LG} - \Gamma_{DG} \tag{8.2.4}$$

Γ_{Gi} is the sum of all mass transfer pr. unit pipe volume and time from other phases into the gas. Γ_{LG} is the contribution from the liquid film (*from* Liquid *to* Gas), and Γ_{DG} is the contribution from the droplets. We have not established any way to determine how large an amount of the gas condensing (or the liquid evaporating) goes to (or comes from) the liquid at the wall, as opposed to how large a part goes to (or comes from) the droplets. Bendiksenet al. (1991) proposed that it is proportional to the amount of liquid already in each of those different states, so:

$$\frac{\Gamma_{LG}}{\alpha_L} = \frac{\Gamma_{DG}}{\alpha_D} \tag{8.2.5}$$

Equations 8.2.4 and 8.2.5 lead to:

$$\Gamma_{LGi} = -\Gamma_{Gi}\frac{\alpha_L}{\alpha_L + \alpha_D} \tag{8.2.6}$$

And:

$$\Gamma_{DGi} = -\Gamma_{Gi}\frac{\alpha_D}{\alpha_L + \alpha_D} \tag{8.2.7}$$

We saw in chapter 4 that it is also possible for droplets to be ripped from the surface of the liquid at the pipe wall, leading to mass transfer from the wall liquid to droplets,

meaning $\Gamma_{LD} \neq 0$. Similarly, droplets can be deposited at the liquid film, leading to $\Gamma_{DL} \neq 0$. Inserting that and equation 8.2.6 into equation 8.2.2 gives:

$$\frac{\partial(\alpha_L \rho_L)}{\partial t} = -\frac{\partial(\alpha_L \rho_L v_L)}{\partial x} - \Gamma_{Gi}\frac{\alpha_L}{\alpha_L + \alpha_D} - \Gamma_{LD} + \Gamma_{DL} + \Gamma_{LW} \tag{8.2.8}$$

Inserting equation 8.2.7 into 8.2.3 leads to:

$$\frac{\partial(\alpha_D \rho_L)}{\partial t} = -\frac{\partial(\alpha_D \rho_L v_D)}{\partial x} - \Gamma_{Gi}\frac{\alpha_D}{\alpha_L + \alpha_D} + \Gamma_{LDi} - \Gamma_{DL} + \Gamma_{DW} \tag{8.2.9}$$

The general mass conservation equations 2.2.4 - 2.2.5 have thereby been adapted to our two-phase three-fluid model by converting them to equations 8.2.1, 8.2.8 and 8.2.9.

8.3 Momentum conservation

8.3.1 Main equations

Applying equation 2.3.16 on the gas phase, we get:

$$\begin{aligned}\frac{\partial(\alpha_G \rho_G v_G)}{\partial t} = &-\frac{\partial(\alpha_G \rho_G {v_G}^2)}{\partial x} - \alpha_G \frac{\partial p_G}{\partial x} + R_{LGi} + R_{DGi} + R_{GW} \\ &+ S_{LGi} + S_{DGi} + S_{Gw} + (v_{Gi}\Gamma_{Gi} + v_{GW}\Gamma_{GW}) - \alpha_G \rho_G g \sin\theta\end{aligned} \tag{8.3.1}$$

Assuming all surface tension forces are negligible, we can set $S_{LGi} = S_{DGi} = S_{Gw} = 0$. If any gas flowing in through perforations in the wall flows perpendicular to the pipe axis, it does not bring any momentum with it, and the axial component of the velocity $v_{GW} = 0$. This would be different if gas was flowing out through the perforations, but that is a more unusual situation and for simplicity we neglect that here.

v_{Gi} is the velocity of the fluids transferring mass between the gas and the liquid. In case of gas condensing, that must be the gas velocity at the locations where condensation takes place. We know that the gas typically flows more slowly near the pipe wall (or liquid film in our case) than it does near the center, but we neglect such variations and simply use the average gas velocity by setting $v_{Gi} = v_G$. When we have evaporation, the gas receives momentum both from the liquid film and the droplets. By averaging according to equation 8.2.5, we get the following velocity:

$$v_{Gi} = v_L \frac{\alpha_L}{\alpha_L + \alpha_D} + v_D \frac{\alpha_D}{\alpha_L + \alpha_D} \tag{8.3.2}$$

We use pressure correction terms Δp_G and Δp_L from chapter 3.4. Those equations were defined only for stratified flow, but we may also include them for annular flow to maintain hyperbolicity.

From equation 2.3.17 it follows that in case we have evaporation, gas momentum conservation becomes:

$$\begin{aligned} \frac{\partial(\alpha_G \rho_G v_G)}{\partial t} = &- \frac{\partial(\alpha_G \rho_G {v_G}^2)}{\partial x} - \alpha_G \frac{\partial(p + \Delta p_G)}{\partial x} + R_{LGi} + R_{DGi} + R_{GW} \\ &+ \Gamma_{Gi}\left(v_{L(G)} \frac{\alpha_L}{\alpha_L + \alpha_D} + v_{D(G)} \frac{\alpha_D}{\alpha_L + \alpha_D}\right) - \alpha_G \rho_G g \sin\theta \end{aligned} \tag{8.3.3}$$

$v_{L(G)}$ is the liquid's velocity as it boils and becomes gas, while $v_{D(G)}$ is the droplet's velocity as it becomes gas. If we have condensation, gas momentum conservation becomes:

$$\begin{aligned} \frac{\partial(\alpha_G \rho_G v_G)}{\partial t} = &- \frac{\partial(\alpha_G \rho_G {v_G}^2)}{\partial x} - \alpha_G \frac{\partial(p + \Delta p_G)}{\partial x} + R_{LG} + R_{DG} + R_{GW} \\ &+ v_{G(L,D)} \Gamma_{Gi} - \alpha_G \rho_G g \sin\theta \end{aligned} \tag{8.3.4}$$

$v_{G(L,D)}$ is the gas' velocity as it condenses into liquid film and droplets.

The average gas velocity does not have to be exactly the same when it condenses into a droplet (which in some situations tends to happen relatively close to the center of the pipe where the gas velocity is high) and onto the liquid film (which happens near the wall, where the gas velocity is lower). We are not attempting to distinguish these two averages in equation 8.3.4 and simply call them both $v_{G(L,D)}$. We simplify further by setting $v_{G(L,D)} = v_G$. Similarly, we set $v_{L(G)} = v_L$and $v_{D(G)} = v_D$.

The droplet pressure is assumed to be as for the gas. As before, we neglect all surface tension forces in the momentum equations, and we get similar formulations for evaporation and condensation:

In case of evaporation:

$$\frac{\partial(\alpha_D \rho_L v_D)}{\partial t} = -\frac{\partial(\alpha_D \rho_L {v_D}^2)}{\partial x} - \alpha_G \frac{\partial(p + \Delta p_G)}{\partial x} - R_{DG} - v_{D(L)}\Gamma_{Gi}\frac{\alpha_D}{\alpha_L + \alpha_D} + v_{L(D)}\Gamma_{LD} - v_{D(L)}\Gamma_{DL} - \alpha_D \rho_D g \sin\theta$$

In case of condensation: (8.3.5)

$$\frac{\partial(\alpha_D \rho_L v_D)}{\partial t} = -\frac{\partial(\alpha_D \rho_L {v_D}^2)}{\partial x} - \alpha_G \frac{\partial(p + \Delta p_G)}{\partial x} - R_{DG} - v_{G(D)}\Gamma_{Gi}\frac{\alpha_D}{\alpha_L + \alpha_D} + v_{L(D)}\Gamma_{LD} - v_{D(L)}\Gamma_{DL} - \alpha_D \rho_D g \sin\theta$$

If we summarize equations 8.3.3/8.3.4 and 8.3.5, the friction force (or, more appropriately referred to as the drag force) between gas and droplets, R_{DG}, cancel each other out, and we end up with:

$$\frac{\partial(\alpha_G\rho_G v_G + \alpha_D\rho_L v_D)}{\partial t} = -\frac{\partial(\alpha_G\rho_G {v_G}^2 + \alpha_D\rho_L {v_D}^2)}{\partial x} - (\alpha_G + \alpha_D)\frac{\partial(p + \Delta p_G)}{\partial x}$$
$$+ R_{LG} + R_{Gw} + v_{EC}\Gamma_{Gi}\frac{\alpha_L}{\alpha_L + \alpha_D}$$
$$+ v_{L(D)}\Gamma_{LD} - v_{D(L)}\Gamma_{DL} - (\alpha_G\rho_G + \alpha_D\rho_L)g\sin\theta \quad (8.3.6)$$

Where:

$$v_{EC} = v_{L(G)}\ in\ case\ of\ evaproation$$

$$v_{EC} = v_{G(L)}\ in\ case\ of\ condensation$$

The equations for evaporation and condensation are very similar. Since equation 8.3.6 treats momentum conservation for gas and droplets together, it is only the liquid film – the only phase not included in equation 8.3.6 – which can add momentum when it boils and becomes part of the gas. It is therefore no surprise that v_L is the only velocity of relevance in the $v_L\Gamma_{Gi}\frac{\alpha_L}{\alpha_L+\alpha_D}$-term.

For condensation, it is only the gas which condensates and it is the gas' velocity which determines how much momentum that mass carries when it becomes liquid.

The liquid film momentum equation is similar to equation 8.3.6, and here we also introduce the same simplifications by neglecting surface tension and assuming any inflowing liquid through perforations in the pipe carries no axial momentum:

$$\frac{\partial(\alpha_L \rho_L v_L)}{\partial t} = -\frac{\partial(\alpha_L \rho_L {v_L}^2)}{\partial x} - \alpha_L \frac{\partial(p + \Delta p_L)}{\partial x} - R_{LGi} + R_{Lw}$$
$$- v_{EC}\Gamma_{Gi}\frac{\alpha_L}{\alpha_L + \alpha_D} - v_{L(D)}\Gamma_{LDi} + v_{D(L)}\Gamma_{DLi} - \alpha_L \rho_L g \sin\theta \quad (8.3.9)$$

Where:

$$v_{EC} = v_{L(G)}\ in\ case\ of\ evaproation$$

$$v_{EC} = v_{G(L)}\ in\ case\ of\ condensation$$

8.3.2 Some comments on interface velocity

In chapter 5.1.2, we pointed out that in annular flow, we usually use an interface velocity between the gas core and the liquid film $v_{GL} = v_G - v_L$, as Bendiksen et al. (1991) proposed, but it is difficult to determine it accurately, and the reality may well be closer to $v_{GL} = v_G - 2v_L$.

A similar problem exists for the droplets: Turbulence eddies are going to give them some radial movement as they travel axially with the gas, so they will be affected by various parts for the gas' velocity profile. The ones coming into contact with the liquid film may already have had their velocity reduced somewhat by the time they hit the film (since the gas is also slower near its boundary). Therefore it is not obvious that average velocity for all droplets, v_D, is the best estimate for the average of those droplets which hit the liquid film.

The velocities to insert into the mass transfer terms in equation 8.3.6 partly follow from the definition of the friction forces between phases used in the same equation. Both mass transfer and friction create forces attempting to even out velocity differences. In *Pipe Flow 1*, chapter 2, we saw that friction between single-phase flow and the pipe wall is caused by turbulence eddies moving radially, occasionally coming into contact with the laminar surface layer (and in some cases being affected by surface roughness). When examined this way, any turbulence eddy coming into contact with the pipe wall (or into contact with the surface of another phase in the case of annular or stratified flow) would have its speed reduced to that surface's velocity (either zero if that surface

is the pipe wall, or the interface velocity if it is another surface) if the eddy is small enough. The force necessary for that retardation is *defined* as the friction force. Equations 3.5.14 and 3.5.15 are in fact designed according to that definition (though only valid for continuous phases, not droplets). The interface velocity is used in the definition of the friction factor. The rest of the forces interacting between phases should therefore also be defined according to the same interface velocity. For the continuous phases, it would probably be most accurate to set $v_G = v_L = v_{interface}$ in all mass transfer terms in equation 8.3.6, both for evaporation and condensation.

Gravity and liquid surface waves also play a part, and this complicates any estimate of the interface velocity. We will allow equation 8.3.6 to stand, but it is worth remembering that since both the gas, the liquid film, and the droplets have different average velocities at different locations across each cross section, it is unclear exactly which velocity one should use to get the most accurate results.

8.4 Energy equation

By summarizing equation 2.4.4 for all phases, and applying equations 2.4.5 - 2.4.9, we get:

$$\begin{aligned}&\frac{\partial}{\partial t}(\alpha_G E_G + \alpha_L E_L + \alpha_D E_D)\\ &\qquad = -\frac{\partial}{\partial x}[\alpha_G v_G(E_G + p) + \alpha_L v_L(E_L + p) + \alpha_D v_D(E_D + p)]\\ &\qquad + \Gamma_{Gw} h_{Gw} + \Gamma_{Lw} h_{Lw} + \Gamma_{Dw} h_{Dw} + q + w\end{aligned} \tag{8.4.1}$$

We have not included the pressure difference corrections in the energy equation as it has no significance there, and it is only in the momentum equations it influences the equations' hyperbolicity.

Enthalpy from mass sources (contained in any fluid flowing in through the pipe wall) is assumed to come in the form of gas, liquid film or droplets. q is volume-specific heat

from the environment through the pipe wall into the fluid, and w is work carried out on the fluid (in pumps or compressors, or negative work in a turbine).

In addition, we need some of the equations from *Pipe Flow 1*. We defined the fluid's energy pr. unit volume as:

$$E = \rho\left(u + \frac{v^2}{2} + gz\right) \tag{8.4.2}$$

The specific internal energy is a fluid property and can either be tabulated directly as a function of pressure and temperature, or it can be tabulated in the form of the fluid property specific enthalpy h:

$$h = u + \frac{p}{\rho} \tag{8.4.3}$$

In multi-phase flow we split these equations into each phase so in our case, we have:

$$E_G = \rho_G\left(h_G - \frac{p}{\rho_G} + \frac{{v_G}^2}{2} + gz\right) \tag{8.4.4}$$

$$E_L = \rho_L\left(h_L - \frac{p}{\rho_L} + \frac{{v_L}^2}{2} + gz\right) \tag{8.4.5}$$

$$E_D = \rho_L\left(h_L - \frac{p}{\rho_L} + \frac{{v_D}^2}{2} + gz\right) \tag{8.4.6}$$

8.5 Pressure equation

In chapter 6, we showed various models based on 3 continuity and 3 momentum conservation equations, in addition to some closure equations. We discovered that this was enough to solve the equations and determine all important parameters, including

the pressure p (when we had no phase change). But the fastest and most convenient way to keep track of the pressure may be by including a separate differential equation for it so that p becomes a primary variable. We will adapt that method to our current model.

The continuity equation 8.2.1 can be modified by observing:

$$\frac{\partial(\alpha_G \rho_G)}{\partial t} = \alpha_G \frac{\partial \rho_G}{\partial t} + \rho_G \frac{\partial \alpha_G}{\partial t} \tag{8.5.1}$$

Dividing everything by α_G:

$$\frac{\alpha_G}{\rho_G}\frac{\partial \rho_G}{\partial t} + \frac{\partial \alpha_G}{\partial t} = -\frac{1}{\rho_G}\frac{\partial(\alpha_G \rho_G v_G)}{\partial x} + \frac{\Gamma_{Gi}}{\rho_G} + \frac{\Gamma_{GW}}{\rho_G} \tag{8.5.2}$$

Similar modifications of equations 8.2.8 and 8.2.9 lead to:

$$\frac{\alpha_L}{\rho_L}\frac{\partial \rho_L}{\partial t} + \frac{\partial \alpha_L}{\partial t} = -\frac{1}{\rho_L}\frac{\partial(\alpha_L \rho_L v_L)}{\partial x} - \frac{\Gamma_{Gi}}{\rho_L}\frac{\alpha_L}{\alpha_L + \alpha_D} - \frac{\Gamma_{LDi}}{\rho_L} + \frac{\Gamma_{DLi}}{\rho_L} + \frac{\Gamma_{LW}}{\rho_L} \tag{8.5.3}$$

And:

$$\frac{\alpha_D}{\rho_L}\frac{\partial \rho_L}{\partial t} + \frac{\partial \alpha_D}{\partial t} = -\frac{1}{\rho_L}\frac{\partial(\alpha_D \rho_L v_D)}{\partial x} - \frac{\Gamma_{Gi}}{\rho_L}\frac{\alpha_D}{\alpha_L + \alpha_D} + \frac{\Gamma_{LDi}}{\rho_L} - \frac{\Gamma_{DLi}}{\rho_L} + \frac{\Gamma_{DW}}{\rho_L} \tag{8.5.4}$$

If we summarize equations 8.5.2 - 8.5.4 and insert $\alpha_L + \alpha_D = 1 - \alpha_G$, we get:

$$\frac{\alpha_G}{\rho_G}\frac{\partial \rho_G}{\partial t} + (1-\alpha_G)\frac{\alpha_L}{\rho_L}\frac{\partial \rho_L}{\partial t} + \frac{\partial(\alpha_g + \alpha_L + \alpha_D)}{\partial t}$$
$$= -\frac{1}{\rho_G}\frac{\partial(\alpha_g \rho_g v_g)}{\partial x} - \frac{1}{\rho_L}\frac{\partial(\alpha_L \rho_L v_L)}{\partial x} - \frac{1}{\rho_L}\frac{\partial(\alpha_D \rho_L v_D)}{\partial x} + \Gamma_{Gi}\left(\frac{1}{\rho_G} - \frac{1}{\rho_L}\right) \quad (8.5.5)$$
$$+ \frac{\Gamma_{GW}}{\rho_G} + \frac{\Gamma_{LW}}{\rho_L} + \frac{\Gamma_{DW}}{\rho_L}$$

Since $\alpha_G + \alpha_L + \alpha_D = 1$, its time derivative is zero. We also insert:

$$\frac{\partial \rho_G}{\partial t} = \left(\frac{\partial \rho_G}{\partial p}\right)_T \frac{\partial p}{\partial t} + \left(\frac{\partial \rho_G}{\partial T}\right)_p \frac{\partial T}{\partial t} \quad (8.5.6)$$

And:

$$\frac{\partial \rho_L}{\partial t} = \left(\frac{\partial \rho_L}{\partial p}\right)_T \frac{\partial p}{\partial t} + \left(\frac{\partial \rho_L}{\partial T}\right)_p \frac{\partial T}{\partial t} \quad (8.5.7)$$

This can be inserted in both the mass conservation and energy equations to and organized to make p and T primary variables. For simplicity, we will instead progress with the assumption that we have isothermal flow, meaning $\partial T/\partial t = 0$:

$$\frac{\alpha_G}{\rho_G}\left(\frac{\partial \rho_G}{\partial p}\right)_{T,\alpha_G}\frac{\partial p}{\partial t} + \frac{(1-\alpha_G)}{\rho_L}\left(\frac{\partial \rho_L}{\partial p}\right)_{T,\alpha_G}\frac{\partial p}{\partial t}$$
$$= -\frac{1}{\rho_G}\frac{\partial(\alpha_g \rho_g v_g)}{\partial x} - \frac{1}{\rho_L}\frac{\partial(\alpha_L \rho_L v_L)}{\partial x} - \frac{1}{\rho_L}\frac{\partial(\alpha_D \rho_L v_D)}{\partial x} \quad (8.5.8)$$
$$+ \Gamma_{Gi}\left(\frac{1}{\rho_G} - \frac{1}{\rho_L}\right) + \frac{\Gamma_{GW}}{\rho_G} + \frac{\Gamma_{LW}}{\rho_L} + \frac{\Gamma_{DW}}{\rho_L}$$

By some re-arranging, this leads to:

$$\frac{\partial p}{\partial t} = \left[-\frac{1}{\rho_G}\frac{\partial(\alpha_G \rho_G v_G)}{\partial x} - \frac{1}{\rho_L}\frac{\partial(\alpha_L \rho_L v_L)}{\partial x} - \frac{1}{\rho_L}\frac{\partial(\alpha_D \rho_L v_D)}{\partial x} + \Gamma_{Gi}\left(\frac{1}{\rho_G} - \frac{1}{\rho_L}\right) + \frac{\Gamma_{GW}}{\rho_G} + \frac{\Gamma_{Lw}}{\rho_L} + \frac{\Gamma_{DW}}{\rho_L} \right] / \left[\frac{\alpha_G}{\rho_G}\left(\frac{\partial \rho_G}{\partial p}\right)_{T,\alpha_G} + \frac{(1-\alpha_G)}{\rho_L}\left(\frac{\partial \rho_L}{\partial p}\right)_{T,\alpha_G} \right] \tag{8.5.9}$$

We see that equation 8.5.9 makes p a primary variable and directly produces a value for it as we integrate in time without having to do any indirect transformation from the primary variables (as we did in *Pipe Flow 1*, equation 10.6.5). In order to use it, we must calculate Γ_{Gi}. In the next chapter, we will examine how to do that. Remember, though, that equation 8.5.9 is only valid for isothermal flow.

8.6 Mass transfer from liquid (film and droplets) to gas

The general volume-specific mass transfer equation 2.5.11 applied to two-phase flow gives us the gas mass transfer directly:

$$\Gamma_{Gi} = \left\{ \left(\frac{\partial \alpha_{m\,G}}{\partial p}\right)_T \left[\left(\frac{\partial p}{\partial t}\right)_x + \left(\frac{\partial p}{\partial x}\right)_t v_G \right] + \left(\frac{\partial \alpha_{m\,G}}{\partial T}\right)_p \left[\left(\frac{\partial T}{\partial t}\right)_x + \left(\frac{\partial T}{\partial x}\right)_t v_G \right] \right\} \cdot \left[\alpha_G \rho_G + (1-\alpha_G)\rho_L\right] \tag{8.6.1}$$

When attempting to use equation 8.6.1, we need to remember that it does not work well for fluids with constant boiling temperature at constant pressure, such as water or other single-component fluids (see chapter 2.5).

8.7 Slip between gas and droplets in annular flow

When we discussed the drift-flux model in chapter 3.9, it was pointed out that combining two momentum equations reduces the number of differential equations by one while requiring some static correlation between the two phases instead. In the three-fluid model discussed now, we recall that for annular flow, the gas and droplet momentum equations were merged into one by summarizing them (equation 8.3.6), and therefore we need some way to describe their velocity difference.

Droplets are partly slowed down by interacting with the liquid film on the wall, and partly by gravity (if the pipe slopes upwards). If we neglect the first part, we are left with the contribution from gravity:

$$v_G - v_D = v_{GD0} \sin\theta \tag{8.7.1}$$

v_{GD0} is the droplets' average velocity as it would have been if allowed to fall in gas at rest. To quantify v_{GD0}, we can use a simple static momentum balance for a droplet and require the droplet drag balances its gravity force minus its buoyancy in the gas. If the droplets are spherical with a diameter d_D, we get:

$$F_{1\,Drop} = \frac{\pi {d_D}^3}{6}(\rho_L - \rho_G)g \tag{8.7.2}$$

If we insert equation 5.2.3 for drag force on a sphere, we get:

$$v_{GD0} = \sqrt{\frac{4}{3}\frac{d_D(\rho_L - \rho_G)g}{C_D \rho_G}} \tag{8.7.3}$$

We recall that the drag coefficient C_D can be estimated by equation 5.2.1. One obvious problem with equation 8.7.3 is that it relies on knowing the droplet diameter. The

challenge is identical to the one we were faced with in the somewhat more advanced model outlined in chapter 5. We cannot determine the droplet forces without knowing the average droplet diameter. In this case we are going to fall back on a relatively well-known semi-empirical method for estimating the Sauter mean droplet diameter, specifically the one proposed by Azzopardi (1985):

$$d_D = \lambda_T \left[\frac{15.4}{\left(\frac{\alpha_L}{\alpha_G} We_{\lambda_T}\right)^{0.58}} + 3.5 \frac{\alpha_L v_L}{\alpha_G v_G} \right] \tag{8.7.4}$$

The length scale defined in these calculations, λ_T, is defined as:

$$\lambda_T = \sqrt{\frac{\sigma_{LG}}{\rho_L g}} \tag{8.7.5}$$

The Weber number We_{λ_T} for this length scale is:

$$We_{\lambda_T} = \frac{\rho_G (\alpha_G v_G)^2 \lambda_T}{\sigma_{LG}} \tag{8.7.6}$$

We see that 8.7.4 – 8.7.6 can be used to determine d_D. Equations 8.7.3 and 5.2.1 enable us to determine the droplet fall velocity in still gas, and $v_G - v_D$ is thereafter easily calculated using equation 8.7.1.

8.8 Droplet deposition in annular flow

We already showed a model for droplet deposition in chapter 5.5. It was primarily developed for flow in vertical pipes, and it is not well documented. Other models exist, but they are more empirical. We must therefore expect them to be less general, they are

probably most reliable for data close to the ones used to develop them (the diameter often being an order or even two smaller than what we encounter in pipelines, and the pressure being relatively low, resulting in the gas density often being an order of magnitude lower than in most pipelines.) Increasing the pressure leads to higher gas density and thereby higher friction between the phases. Higher pressure also leads to lower surface tension, and that has significant impact on both droplet deposition and liquid film entrainment.

No general correlation for all inclination angles, pipe diameters, velocities, and gas/liquid properties exists. What we are certain of, though, is that all of these parameters play a part, and any model neglecting them must have limited validity. The liquid and gas properties thought to be important are viscosity, density, and surface tension. Since those properties also depend on pressure and temperature, both pressure and temperature play an indirect part, too. To further complicate matters, any boiling at the pipe wall's surface is known to contribute to tearing out parts of the liquid film at the pipe wall and cause added liquid film entrainment.

Droplet deposition and liquid film entrainment takes part in both the continuity and momentum equations, reflecting that it affects both the pipeline's mass transport capacity directly (the larger the part of the liquid which is in the form of droplets carried by the gas, the faster the liquid travels through the pipeline) and friction (the more the liquid alternates between the pipe wall and the gas flow, the more the liquid is accelerated and decelerated, creating more resistance). In long pipelines, where things generally happen slowly, getting fast and very accurate equilibrium conditions when deposition and entrainment take place is not the primary consideration. It is more important to have reasonably accurate droplet fraction α_D, deposition-, and entrainment rates Γ_{LD} and Γ_{DL} most of the time. If we know Γ_{LD} and Γ_{DL}, α_D follows from the simulation model. But we also have another alternative - seemingly overlooked by most authors: If we know α_D and either Γ_{LD} or Γ_{DL} from empirical correlations, we can estimate the remaining one indirectly.

Empirical droplet entrainment fraction correlations are simpler to deal with than droplet entrainment correlations. The droplet entrainment fraction – the α_D we end up with when achieving equilibrium between entrainment and deposition – is easier to estimate than the droplet deposition, at least if we simply accept one of the many empirical correlations for it. Entrainment and deposition must cancel each other out when equilibrium is reached, meaning $\Gamma_{DL} = \Gamma_{LD}$ when α_D has stabilized at a constant value, we will refer to it as α_{D0}. Such a process can be modeled as an exponential correlation:

$$\Gamma_{DLi} = max(\Gamma_{DL\,Min}, \Gamma_{LD})\exp[t_0(\alpha_{D0} - \alpha_D)] \tag{8.8.1}$$

Here, t_0 is a time constant which determines how closely Γ_{DL} is going to follow Γ_{LD}. Since we must assume some deposition takes place as long as there are droplets in the gas (whether Γ_{LD} is zero or not), we have included a minimum value $\Gamma_{DLi\,Min}$ below which the factor in front of $\exp[t_0(\alpha_{D0} - \alpha_D)]$ never falls. Several authors have shown that α_D stabilizes in a matter of seconds (Alipchenkov et al., 2004, Sawant et al., 2007). To replicate this, we could set t_0 to a few seconds, but there should be nothing wrong with setting it much higher when desired for numerical stability purposes (fast phenomena tend to lead to short time-steps for explicit integration methods), as long as it is much shorter than the time the fluid travels through the pipeline (typically hours or days).

The liquid film entrainment Γ_{LD} can be estimated as described in chapter 5.5, though one may use any of the other empirical correlations available (for instance one of those presented in chapter 5 of Kolev's second book from 2005).

The most well known empirical entrainment fractions are probably the ones of Wallis (1969), Oliemans et al. (1986), Ishii & Mishima (1989), and the later one by Sawant et al. (2008). All are based on vertical upward flow.

8.8.1 The Wallis-correlation

The Wallis (1969)-correlation states:

$$\frac{\alpha_{D0}v_D}{\alpha_L v_L + \alpha_{D0}v_D} = 1 - exp[-0.125(\Phi - 1.5)] \tag{8.8.2}$$

where the dimensionless factor is:

$$\Phi = 10^4 \frac{\alpha_G v_G \mu_G}{\sigma_{LG}} \left(\frac{\rho_G}{\rho_L}\right)^{0.5} \tag{8.8.3}$$

From this, the steady-state equilibrium α_{D0} can be solved.

8.8.2 The Oliemans, Pots, and Trope-correlation

The Oliemans et al. (1986)-correlation has been developed using regression-analysis on a large database. They proposed the following correlation and factors:

$$\frac{\alpha_{D0} v_D}{\alpha_L v_L} = 10^{\beta_0} \rho_L{}^{\beta_1} \rho_G{}^{\beta_2} \mu_L{}^{\beta_3} \mu_G{}^{\beta_4} \sigma_{LG}{}^{\beta_5} d^{\beta_6} (\alpha_L v_L)^{\beta_7} (\alpha_G v_G)^{\beta_8} g^{\beta_9} \tag{8.8.4}$$

β_0	β_1	β_2	β_3	β_4	β_5	β_6	β_7	β_8	β_9
-2.52	1.08	0.18	0.27	0.28	-1.8	1.72	0.70	1.44	0.46

Table 3.8.1. β-factors for the Oliemans et al.-correlation.

8.8.3 The Ishii and Mishima-correlation

The Ishii & Mishima (1989)-correlation is based on a modified Weber-number defined as:

$$We_{Ishii} = We \cdot \left(\frac{\rho_L - \rho_G}{\rho_G}\right)^{1/3} = \frac{\rho_G v_G{}^2 d_{h\,L}}{\sigma_{LG}} \left(\frac{\rho_L - \rho_G}{\rho_G}\right)^{1/3} \tag{8.8.5}$$

To define the hydraulic diameter for the annular liquid film, $d_{h\,L}$, we use the annular liquid ring's area as A and the liquid surface in contact with the pipe wall as the part of relevance to the wetted circumference O. This leads to:

$$d_{h\,L} = \frac{4\alpha_L \frac{\pi d^2}{4}}{\pi d} = \alpha_L d \tag{8.8.6}$$

Inserting equation 8.8.6 into 8.8.5 we get:

$$We_{Ishii} = \frac{\rho_G {v_G}^2 \alpha_L d}{\sigma_{LG}} \left(\frac{\rho_L - \rho_G}{\rho_G} \right)^{1/3} \tag{8.8.7}$$

With this definition, Ishii and Mishima found that the entrainment fraction is going to stabilize according to:

$$\frac{\alpha_{D0} v_D}{\alpha_L v_L + \alpha_D v_D} = tanh\left[7.25 \cdot 10^{-7} {We_{Ishii}}^{1.25} {Re_L}^{0.25} \right] \tag{8.8.8}$$

The liquid film's Reynolds number is defined by the hydraulic diameter and becomes:

$$Re_L = \frac{\alpha_L v_L \rho_L d}{\mu_L} \tag{8.8.9}$$

8.8.4 The Sawant, Ishii, and Mori-correlation

In 2007, Sawant et al. improved their correlation for vertical upward flow. Based on a lot of experimental data, they managed to come up with a simple-to-use, explicit equation set:

$$\alpha_{D0} = E_m \tanh(aWe^{1.25}) \tag{8.8.10}$$

The Weber number is defined as:

$$We = \frac{\alpha_G \rho_G v_G d}{\sigma_{LG}} \left(\frac{\rho_L - \rho_G}{\rho_G} \right)^{1/3} \tag{8.8.11}$$

and the factors:

$$E_m = 1 - \frac{{Re_{LW}}^*}{Re_{LW}} \tag{8.8.12}$$

$$a = 2.31 \cdot 10^{-4} {Re_{LW}}^{-0.35} \tag{8.8.13}$$

The Reynolds number for the annular film on the wall, Re_{LW}, is as before determined according to equation 5.1.11. The critical Reynolds number ${Re_{LW}}^*$, below which no entrainment occurs, was not set to be constant (as we did in chapter 5.6), but as:

$${Re_{LW}}^* = 250 ln(Re_{LW}) - 1265 \tag{8.8.14}$$

According to Patruno et al. (2008), this correlation (and probably all the other correlations presented here) are valid only for situations of relatively high surface tension, which tend to be at relatively low pressures. So even though the Sawant et al. (2007) correlations may be the best available, they probably work well only for vertical upward flow with moderate pressures, which obviously is not always what we have in pipelines.

8.9 Dispersed bubble flow

Bubbles carried by the liquid are somewhat similar to droplets carried by the gas, the difference being there is no annular film around the pipe wall. In bubbly flow it is the liquid phase which is continuous while the gas phase is not. Bubbly flow occurs in the form of bubbles in the liquid at high liquid flow rates. The bubble drift can be modeled in a way similar to droplets in equation 8.7.1, but v_{GD0} needs to be replaced by v_{LB0} (gas bubble rise velocity in still liquid).

Malnes (1982) proposed the following:

$$v_{LB0} = 1.18 \left[\frac{g \sigma_{LG} (\rho_L - \rho_G)}{{\rho_L}^2} \right]^{0.25} \tag{8.9.1}$$

We need 2 mass conservation equations: One for the gas bubbles and one for the liquid. The two momentum conservation equations can be combined by summarizing them, making this a drift-flux model, and using equation 8.9.1 to calculate the drift velocity.

Alternatively, we may keep two momentum equations and combine them with other available correlations for estimating the different friction factors for bubbly flow. If we prefer this method, we keep equations 8.2.1, 8.2.8, 8.3.3/8.3.4, 8.3.5, 8.3.6, 8.4.1, and 8.5.9, while removing all terms to do with droplets.

Friction between pipe wall and gas must be modified, and we simply make it proportional to the amount of gas in the flow:

$$R_{Gw} = -\alpha_G \frac{f_{Gw}\rho_G}{2d} v_G|v_G| \tag{8.9.2}$$

Similarly for the liquid:

$$R_{Lw} = -\alpha_L \frac{f_{Lw}\rho_L}{2d} v_L|v_L| \tag{8.9.3}$$

The Reynolds number used to determine the Darcy-Weisbach friction factor for each phase is simply defined as:

$$Re_k = \frac{v_k d \rho_k}{\mu_k}, \quad _{k=G,L} \tag{8.9.4}$$

These Reynolds numbers are used to determine the friction factors as described in *Pipe Flow 1*. It was shown by Stosic & Stevanovic (2001) that the resulting fractions are not very sensitive to variations in f_{Gw} and f_{Lw}, but the overall friction, and therefore the pipeline's capacity, is of course affected. The interfacial friction between the bubbles and the liquid turns out to have great impact on the fractions. We use the Ishii-Zuber correlation (Ishii & Zuber, 1979), modified by Stosic & Stevanovic (2001), to model this friction:

$$R_{GL} = -\frac{3}{4}\alpha_G \rho_L \frac{C_D}{d_B} C_S (v_G - v_L)|v_G - v_L| \tag{8.9.5}$$

d_B is the bubble diameter, C_D is the local interfacial drag coefficient, and C_S is an empirical factor defined by Stosic and Stevanovic as:

$$C_S = \begin{cases} 10^3, & Re_L \le 21{,}000 \; and \; \alpha_G \ge \dfrac{\alpha_G v_G}{\alpha_G v_G + \alpha_L v_L} \\ 2.5 \cdot 10^5 exp(-2.629 \cdot 10^{-4} Re_L), & 21{,}000 < Re_L \le 42{,}000 \; and \; \alpha_G \ge \dfrac{\alpha_G v_G}{\alpha_G v_G + \alpha_L v_L} \\ 22.97 exp(-4.161 \cdot 10^{-5} Re_L), & Re_L > 42{,}000 \end{cases} \tag{8.9.6}$$

The drag coefficient:

$$C_D = \frac{2}{3} d_B \left[\frac{(\rho_L - \rho_G)g}{\sigma_{LG}}\right]^{1/2} \left(\frac{1 + 17.67{\alpha_L}^{9/7}}{{\alpha_L}^{1.5}}\right)^2 \tag{8.9.7}$$

We notice this model does not rely on estimating the bubble diameter as an intermediate step while estimating the interfacial friction.

8.10 Slug flow

For intermittent flow (elongated bubble, slug, or churn flow), our simulation model has some extra problems to deal with: We need to know where the slugs are, and we need to know how long they are. We also encounter a problem when slugs cross control cell boundaries in that the gas and liquid fractions will obviously change rapidly when that happens. In chapter 7.4, we saw that various ways to deal with these problems have been proposed, including Lagrangian methods, where the free surface is located at one boundary of the mesh, and the mesh deforms as the free surface moves (Mao & Dukler, 1990, and Clark & Issa, 1997, Renault 2007). Another method is to keep the grid fixed, as we have done for all other flow regimes in our previous models, while tracking the surface as a sharp interface moving through the computational grid (Kawaji et. Al, 1997,

and Anglart & Podowski, 2002). Issa & Kempf (2003) have presented an advanced model for describing slug growth in horizontal and nearly horizontal pipes, but that model requires very dense grid, typically several orders of magnitude denser than what is acceptable for relatively fast, commercial simulation of long pipelines.

Probably the simplest way to simulate slugs is to consider the slug train as a continuum of average fractions, and to model the friction as described by the steady-state equations in chapter 7. Notice that $\alpha_D = 0$ since we do not involve any droplets. Also, notice that equations 7.3.16 and 7.3.17 give us information about the total friction for the Taylor-bubble and the liquid slug while not giving us separate forces for the liquid and the gas. Therefore, we must summarize the momentum equations for gas and liquid to get an expression for $\alpha_G \rho_G v_G + \alpha_L \rho_L v_L$. That means the slug momentum equations are solved using the drift-flux method, and we need an additional equation to describe the velocity difference (slip) between gas and liquid.

Using Bendiksen's Taylor-bubble equation 7.2.9 and equation 7.3.1, we get an additional correlation, expressing α_L from known quantities. We then have an equation set which is going to produce values for $\alpha_G v_G$ and $\alpha_L v_L$ (mass conservation), $\alpha_G \rho_G v_G + \alpha_L \rho_L v_L$ (momentum conservation), $\alpha_G E_G + \alpha_L E_L$ (energy conservation) and p (equation 8.5.9). , in addition to α_L from equation 7.3.1. From that, we can caluclate T and determine α_G, α_L, v_G, v_L, ρ_G, and ρ_L. Following the methods outlined in chapter 7, we quantify the friction between gas and pipe wall by equations 7.3.16 and 7.3.17.

"There is no harm in doubt and skepticism, for it is through these that new discoveries are made."
Richard Feynman, 1985

9 Improved slug flow modeling

Slug formation in horizontal and nearly horizontal pipes:

- Model philosophy and governing equations
- Friction model
- Gas entrainment into the slugs
- Model validity and results

9.1 Introduction

We have already studied a steady-state slug model in chapter 7, and we have also explained how to incorporate some of the correlations from that model into a fully transient simulation model in chapter 8.10. We have yet to discuss how to determine whether we have slug flow or another flow regime (we will have a closer look in chapter 11), but for now we simply state that it is traditionally done by using stability theory and some semi-empirical correlations. Issa & Kempf (2003), Bonizzi & Issa (2003), and Issa et al. (2006) have recently shown that at least for horizontal flow, the main mechanisms leading to slug flow can be incorporated directly into the mathematical model without adding any separate slugging criteria. The model takes advantage of some empirical results for friction and gas bubble entrainment into the

liquid slug, but it is still more analytical than most other models. It does have serious limitations, though, the most important being:

- The flow needs to be horizontal or nearly horizontal.
- The grid resolution must be very fine, in the order of half the pipe diameter. Also, it is necessary to simulate with different grid resolutions to check that the chosen resolution is fine enough.
- The model is not well-posed for all possible flow conditions (at least not the version which has been most thoroughly investigated, a model which neglects liquid compressibility), so it can become unstable and unusable in some situations.

These problems currently limit the model's usefulness for commercial pipeline simulations, but better computer capacity and further refinement is likely to change that in the future. Besides, the model is already useful when investigating the physics of slugs, and it can also produce reference cases with which commercial software can be compared.

9.2 Governing equations

Bonizzi & Issa (2003) started out with two mass conservation and two momentum conservation equations, and later added yet another mass conservation equation:

$$\frac{\partial(\alpha_G \rho_G)}{\partial t} + \frac{\partial(\alpha_G \rho_G v_G)}{\partial x} = -\Gamma_{GM} \tag{9.2.1}$$

$$\frac{\partial(\alpha_M \rho_M)}{\partial t} + \frac{\partial(\alpha_M \rho_M v_M)}{\partial x} = \Gamma_{GM} \tag{9.2.2}$$

$$\frac{\partial(\alpha_G \rho_G v_G)}{\partial t} + \frac{\partial(\alpha_G \rho_G {v_G}^2)}{\partial x} = -\alpha_G \frac{\partial p}{\partial x} - R_{GL} + R_{GW} \; - \alpha_G \rho_G g \sin\theta \tag{9.2.3}$$

$$\frac{\partial(\alpha_M \rho_M v_M)}{\partial t} + \frac{\partial(\alpha_M \rho_M {v_M}^2)}{\partial x} = -\alpha_M \frac{\partial p}{\partial x} - \alpha_M \rho_M g \frac{\partial h_{LS}}{\partial x} \cos\theta - R_{GM} + R_{MW} \quad - \alpha_M \rho_M g \sin\theta \tag{9.2.4}$$

We use one mass and one momentum conservation equation to model the gas, while the liquid is modeled as a mixture of liquid with small bubbles in it and indexed M. The G-index is actually used to identify the separated part of the gas (the Taylor-bubbles in case of developed slugs, or the gas layer in case of stratified flow). We notice that in case no gas bubble entrainment into the liquid slug (or liquid film) is accounted for (which is how Issa & Kempf, 2003, initially modeled the slug flow), the 'mixture' would become pure liquid, and the M-index could be replaced by an L-index. That is also the situation we have when the flow is stratified.

Γ_{GM} is gas mass pr. unit volume and time going into the gasified liquid slug. If we do not have any phase change, Γ_{GM} symbolizes the small bubbles being shed from the Taylor-bubble and getting mixed into the slug (or, if negative, the gas being released from the slug and going into the Taylor bubble). In the Bonizzi & Issa model (2003), only mass exchange occurring at the front and end of each slug was considered, even though in reality some bubbles also probably escape from the liquid film under the Taylor-bubbles.

We remember that Γ_{GM} should show up in the momentum equations, too, since mass transfer brings its momentum with it. For simplicity, we neglect that here (that is thought to be a good approximation if the gas density is much lower than the liquid density), but of course there would not have been anything wrong with including it. Also, notice that the model neglects the pressure correction term for the gas, while there is such a term for the liquid. That is likely to be a good approximation, since the pressure varies far less with elevation in gas than it does in liquid. In this model, as in the one we described in chapter 2, p is defined as the pressure at the liquid's surface (or, in case of the gasified slug, the liquid-gas bubble mixture surface), and since we neglect the pressure correction term for the gas, it is also the pressure across the whole cross section for the separated gas. The liquid pressure correction term $-\alpha_M \partial \Delta p_L / \partial x$ in equation 3.3.3 has been converted to the equivalent form $-\alpha_M \rho_M g \partial h / \partial x \cos\theta$ by inserting $\partial \Delta p_L / \partial x = \rho_M g \cos\theta \, \partial h / \partial x$.

Bonizzi & Issa (2003) modeled the gas as compressible (they used ideal gas properties, but real gas properties should work just as well), while the liquid was modeled as incompressible. Since the liquid is much less compressible than the gas, it should not make much of a physical difference whether the liquid's compressibility is included or not as long as the gas fraction is significant (but its effect on numerical stability may not have been investigated properly, so it can potentially affect the complete model).

We assume isothermal flow and omit the energy equation. This is done for convenience only, and including the energy equation would not alter the model's basic slug capturing capabilities. A transport equation for the conservation of mass for the gas bubbles entrained in the liquid slugs can be formulated as:

$$\frac{\partial(\alpha_{GS}\rho_G)}{\partial t} + \frac{\partial(\alpha_{GS}\rho_G v_{GS})}{\partial x} = \Gamma_{GM} \tag{9.2.5}$$

Equation 9.2.5 serves to determine α_{GS}, which is the gas bubble fraction in the slug (meaning α_G for those points in time and space where we have a slug).

9.3 Friction model

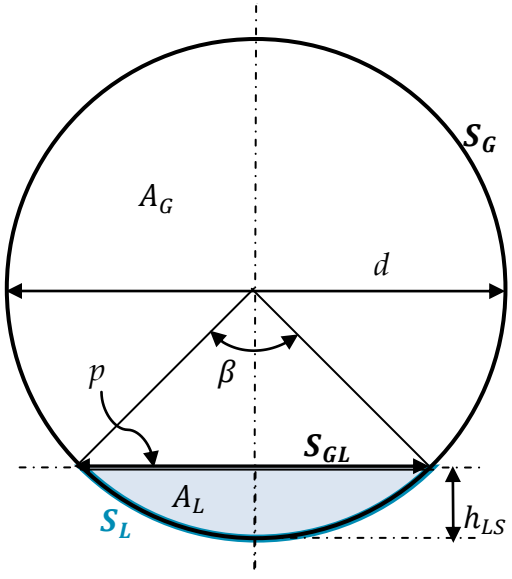

Issa & Kempf (2003) used Taitel & Dukler's simplified friction factor correlations for gas-wall and gas-liquid friction:

$$f_{GW} = \begin{cases} \dfrac{64}{Re_G} & for\ laminar\ flow \\ 0.184 {Re_G}^{-0.2} & for\ turbulent\ flow \end{cases} \tag{9.3.1}$$

$$f_{GL} = \begin{cases} \dfrac{64}{Re_{GL}} & for\ laminar\ flow \\ 0.184 {Re_{GL}}^{-0.2} & for\ turbulent\ flow \end{cases} \tag{9.3.2}$$

Figure 9.3.1. Stratified flow cross-section.

For the liquid phase shear stress, they obtained best agreement with measurements by using Spedding & Hand's correlation (1997):

$$f_{LW} = \begin{cases} \dfrac{96}{Re_L} & for\ laminar\ flow \\ 0.1048(\alpha_L Re_L)^{-0.139} & for\ turbulent\ flow \end{cases} \tag{9.3.3}$$

In a later paper (Issa et al., 2006), they recommended using a modified correlation for the interface between gas and liquid in case the interface had become wavy, namely the one proposed by Andritsos & Hanratty (1987). They observed that the ratio f_{GL}/f_{GW} remained roughly equal to unity until a certain value of the superficial gas velocity ($\alpha_G v_G$) corresponding to the transition from smooth interface to a regime where large, irregular waves are created. That velocity was found to be (other criteria are later explained in chapter 11.2):

$$v_G{}^* = 5\sqrt{\frac{\rho_{G\ atm}}{\rho_G}} \tag{9.3.4}$$

They then proposed the following relation for determining f_{GL}, replacing equation 9.3.2:

$$f_{GL} = \begin{cases} f_{GW}\left[1 + 15\sqrt{\dfrac{h_{LS}}{d}}\left(\dfrac{v_G}{5}\sqrt{\dfrac{\rho_G}{\rho_{G\ atm}}} - 1\right)\right] & for\ v_G \geq v_G{}^* \\ f_{GW} & for\ v_G < v_G{}^* \end{cases} \tag{9.3.5}$$

For a slug containing gas bubbles, Malnes (1982) noticed an increase in the friction. He concluded that the friction factor for dispersed gas-liquid flow must be modified compared to the one relevant to pure liquid flow:

$$f_{LW\,B} = \Phi_{LW\,B} f_{LW} \tag{9.3.6}$$

where:

$$\Phi_{LW\,B} = \begin{cases} 1 & for\ pure\ liquid \\ \dfrac{1}{1-\alpha_B}\left(1 + 15.3\dfrac{\alpha_B}{\sqrt{1-\alpha_B}}\dfrac{v_{LB0}}{v_M}\right) & for\ liquid\ with\ bubbles \end{cases} \quad (9.3.7)$$

And:

$$v_{LB0} = 1.18\left[\frac{g\sigma_{LG}(\rho_L - \rho_G)}{{\rho_L}^2}\right]^{0.25} \quad (9.3.8)$$

The bubble rise velocity in still water v_{LB0} can be estimated with equation 8.9.1. For the slugs, we use $f_{LW\,B}$ rather than f_{LW} when calculating the friction.

The different Reynolds numbers are defined from wetted circumference and fluid filled cross-section in the same way as we did in chapter 3.5. We can write this as:

$$Re_G = \frac{4A_G v_G \rho_G}{(S_G + S_{GL})\mu_G} \quad (9.3.9)$$

$$Re_{GL} = \frac{4A_G (v_G - v_L)\rho_G}{(S_G + S_{GL})\mu_G} \quad (9.3.10)$$

$$Re_L = \frac{d\alpha_L v_L \rho_L}{\mu_L}\ (for\ slug) \quad (9.3.11)$$

Equation 9.3.11 is valid only for the gasified slug. For stratified flow, we follow the calculation procedure outlined in chapter 3.5.

The friction factors, defined as friction force pr. unit volume of pipe, become similar to equations 3.5.14 - 3.5.15, though with a modification for the one relevant to liquid pipe wall friction:

$$R_{GW} = -\frac{f_{Gw}\rho_G}{8}\frac{O_{GW}}{A_G}v_G|v_G| \tag{9.3.12}$$

$$R_{GL} = -\frac{f_{GL}\rho_G}{2}\frac{O_{GW}}{A_G}(v_G - v_L)|v_G - v_L| \tag{9.3.13}$$

$$R_{MW} = -\Phi_{LW\,B}f_{LW}\frac{\beta\rho_L}{\pi d\alpha_M}v_M|v_M|, \beta\ in\ radians \tag{9.3.14}$$

9.4 Slug bubble entrainment and release

9.4.1 Slug bubble velocity

Each bubble in the slug must obviously comply with momentum conservation. Since the gas typically has much lower density than the liquid, it is reasonable to neglect the time derivative, and thereby in effect presume that the bubble has zero response time. We also neglect compressibility (for this specific purpose only). Since the model we are now developing is restricted to horizontal or nearly horizontal pipes, we may also neglect the bubble gravity's influence on the bubble. The bubble's momentum equation can then be expressed as:

$$-\frac{\pi}{6}{d_B}^3\frac{\partial p}{\partial x} = \frac{C_D\rho_L}{2}\frac{\pi{d_B}^2}{4}v_{GBS}|v_{GBS}| \tag{9.4.1}$$

That leads to the following expression for the bubble slip velocity in the slug:

$$v_{GBS} = -\sqrt{-\frac{4d_B}{3C_D\rho_L}\frac{\partial p}{\partial x}} \tag{9.4.2}$$

The slip velocity is defined as the difference between the bubble and the liquid velocity in the 'liquid' slug:

$$v_{GBS} \stackrel{\text{def}}{=} v_{BS} - v_{LS} \tag{9.4.3}$$

Since there is much more liquid than bubbles in the slug, we approximate by setting $v_L \approx v_M$. From this and equations 9.4.2 and 9.4.3 if follows that the bubble velocity can be expressed as:

$$v_{BS} = v_{MS} - \sqrt{-\frac{4d_B}{3C_D\rho_L}\frac{\partial p}{\partial x}} \tag{9.4.4}$$

This very simple equation shows that due to the pressure gradient $\partial p/\partial x$, the bubbles in the slugs are going to travel slower than the liquid. This also happens to be precisely what experimental observations show.

To quantify the terms in equation 9.4.4, we need to know the average bubble diameter d_B. Bonizzi & Issa (2003) used experimental findings of Andreussi et al. (1993), where the entrained bubbles turned out to have a nearly constant diameter of around *1 mm*. Recognizing that this is not going to be the correct diameter for all surface tensions, viscosities, densities, and pipe diameters, it seems more reasonable to use the estimates by Kuznecov (1989), who recommend the maximum bubble diameter be estimated as:

$$d_{B\,Max} = 31.68 d^{2/5}\left(\frac{\sigma_{LG}}{\rho_L}\right)^{3/5}\left(\frac{\rho_L}{\rho_G}\right)^{1/5} {v_{MS}}^{6/5} \tag{9.4.5}$$

The mean bubble diameter is for this purpose calculated as:

$$d_B = 0.0615 d_{B\,Max} \tag{9.4.6}$$

Since bubbles affect each other, we cannot use the single-sphere equation 5.2.1 directly to estimate the bubble drag coefficient C_D. Instead, we use the correlation for the bubble 'swarm' as proposed by Tomiyama et al. (1995), which takes the bubble interaction into account:

$$C_D = \frac{C_{DS}}{\sqrt{\alpha_{LS}}} \tag{9.4.7}$$

Where:

$$C_{DS} = max\left[\frac{24}{Re_B}\left(1 + 0.15{Re_B}^{0.687}\right), \frac{8}{3}\frac{E_{0B}}{E_{0B}+4}\right] \tag{9.4.8}$$

Re_B and E_{0B} represent the bubble Reynolds and Eötvös numbers:

$$Re_B = \frac{\rho_L d_B |v_{MS} - v_{BS}|}{\mu_L} \tag{9.4.9}$$

$$E_{0B} = \frac{g(\rho_L - \rho_G){d_B}^2}{\sigma_{LG}} \tag{9.4.10}$$

We see that the Eötvös number is proportional to the bubble's buoyancy and inversely proportional to its surface tension. It is a way to characterize the bubble's shape when submerged in a surrounding fluid.

9.4.2 Bubbles entering and leaving the liquid slug

The shedding rate of dispersed bubbles at the slug tail is obtained by assuming all the bubbles arriving at the tail leave the slug and enter the Taylor-bubble behind it immediately:

$$\dot{M}_B = \rho_G \frac{\pi d^2}{4}(v_{S\,Tail} - v_{BS})\alpha_{BS} \tag{9.4.11}$$

$v_{S\,Tail}$ represents the local velocity at which the tail of the slug propagates.

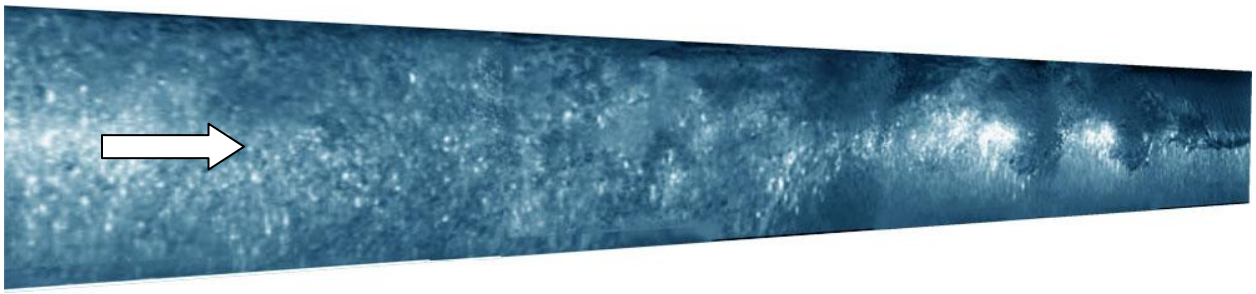

Figure 9.4.1. Slug front mixing zone in a horizontal pipe carrying air and water. The slug front can be several diameters long, and we can see how the bubbles are mixed into the liquid: At the far right, the air is on top of the water, forming the tail of the Taylor-bubble, while the liquid fraction increases into the slug to the left. In the current 1D model it is necessary to simplify to come up with manageable estimation methods, and we do not attempt to describe the mixing zone accurately. Instead, the focus is on the font's velocity.

The entrainment rate at the front of the slug can be estimated by the correlation proposed by Nydal & Andreussi (1991):

$$\dot{M_{GM}} = \rho_G \frac{\pi d^2}{4}\left[0.076\frac{S_{GL}}{d}(v_{SF} - v_{LT}) - 0.15\right] \tag{9.4.12}$$

v_{SF} represents the propagation velocity at the front of the slug (which is also the Taylor bubble's tail velocity, since they follow each other). Notice that now, unlike in the steady-state model we developed in chapter 7, the slugs do not have constant length, so there is no such thing as slug velocity v_S. We need to distinguish between front and tail velocities, since they no longer are the same. v_{LT} is the liquid film velocity (for the liquid film under the Taylor bubble), and S_{GL} is the interfacial distance indicated on figure 9.3.1. Equation 9.4.12 was based on air-water measurements at atmospheric conditions, so it cannot be expected to give accurate results for petroleum flow-lines.

Bonizzi & Issa (2003) achieved better agreement using one of the many published correlations for air intrusion in a hydraulic jump, and they chose the one recommended by Chanson (1996):

$$\dot{M_{BM}} = \rho_G A_{Lf}[(v_{SF} - v_{LT})\zeta(Fr - 1)^{\varepsilon}] \tag{9.4.13}$$

The Froude number is based on the relative velocity between slug front and liquid film, which corresponds to the relative velocity of the liquid 'jet' (the liquid film under the Taylor bubble) entering the slug front:

$$Fr = \frac{v_{SF} - v_{LT}}{\sqrt{\frac{gA_{LF}}{S_{GL}}}} \tag{9.4.14}$$

A_{LF} is the cross-sectional area occupied by the liquid film under the Taylor bubble. The coefficients ζ and ε are functions of the Froude number (Rajaratnam, 1967, Wisner, 1965):

$$\begin{aligned} Fr = 0.018, \varepsilon = 1.245 \; if \; 2.5 < Fr < 7 \\ Fr = 0.014, \varepsilon = 1.400 \; if \; 7 < Fr < 30 \end{aligned} \tag{9.4.15}$$

Whether bubble entrainment into the slug occurs or not depends on the slug front's velocity v_{SF} as well as the liquid film velocity v_{LT} (Andreussi & Bendiksen, 1989, Nydal & Andreussi, 1991, Manolis, 1995). If we use equation 9.4.12, we see that bubble entrainment is predicted for $v_{SF} - v_{LT} > 2\ [m/s]$. If we use equation 9.4.14 instead, the criterion for bubble entrainment becomes:

$$v_{SF} - v_{LT} > \sqrt{\frac{gA_{LF}}{S_{GL}}} \tag{9.4.16}$$

Once the bubble mass flow $\dot{M}_B$ has been estimated, mass flow pr. unit pipe volume, Γ_{GM}, can easily be calculated and inserted into equation 9.2.5.

Even though fluid properties such as surface tension and density are known to be important for the formation of bubbles, they are not included in any of the models shown above, and that indicates these models have limited validity. Issa et al. (2006) have pointed out that some later publications have improved the bubble entrainment models. One was proposed by Brauner & Ullmann (2004):

$$\dot{M_{GM}} = \frac{\rho_G \pi d^2}{16{,}000 C_j} d_{crit}(We - We_{cr})\alpha_{LT}(v_{SF} - v_{LT}) \tag{9.4.17}$$

C_j is a coefficient in the order of 1. The critical bubble diameter is:

$$d_{crit} = \sqrt{\frac{0.4\sigma_{LG}}{g(\rho_L - \rho_G)}} \tag{9.4.18}$$

The Weber numbers We and We_{cr} are defined by:

$$We = \frac{\rho_L (v_{SF} - v_{LT})^2 d}{\sigma_{LG}} \tag{9.4.19}$$

And:

$$We_{cr} = \frac{100C'}{\frac{d_{crit}}{d}} \tag{9.4.20}$$

It was proposed to use $C' = 0.5$ for the constant.

9.4.3 Film and slug front/tail velocities

In chapter 9.4.2, we discovered that we must know the slug front and tail velocities, v_{SF} and $v_{S\,Tail}$. Bonizzi & Issa (2003) tested two different ways of estimating them, and both methods gave similar results. The first method was based on a correlation by Bendiksen (1984) which is somewhat similar to equation 7.2.10:

$$v_{SF} = C_{0T} v_{MS} + v_{dS} \tag{9.4.21}$$

$$v_{S\,Tail} = C_{0T} v_{MS} + v_{dS} \tag{9.4.22}$$

Equations 9.4.21 and 9.4.22 look identical, but since v_{MS} varies in space, the similarity does not necessarily mean the slug's front and tail end up with the same velocity. C_{0T} and the drift velocity v_{dS} between bubbles and liquid was set to:

$$\begin{aligned} C_{0T} &= 1.2, \qquad v_{dS} = 0 \qquad for\ Fr_M \geq 3.5 \\ C_{0T} &= 1.05, \quad v_{dS} = 0.54\sqrt{gd} \quad for\ Fr_M < 3.5 \end{aligned} \tag{9.4.23}$$

The Froude number was here defined as:

$$Fr_M = 0.54\frac{v_{MS}}{\sqrt{gd}} \tag{9.4.24}$$

The other alternative method is to simply track the front and tail of the slugs as they develop from time-step to time-step, and then calculate v_{SF} and $v_{S\,Tail}$ from that. This procedure is in principle relatively straight forward, but it makes the computer code significantly more complex.

For both methods, the location of the slug and Taylor-bubble is determined by looking at the fractions ($\alpha_G = 0\ and\ \alpha_M = 1$ means we have a slug).

9.5 Model validity and results

As pointed out before, it can be difficult to ensure the model is well-posed in all flow situations. There are several ways to investigate well-posedness, but here we are only going to give the results from an eigenvalue-analysis presented by Bonizzi & Issa (2003). They showed that the model becomes hyperbolic and thereby well posed if and only if:

$$(v_G - v_M)^2 \leq \left(\frac{\alpha_M}{\rho_M} + \frac{\alpha_G}{\rho_G}\right)\frac{\pi d}{4\sin\left(\frac{\beta}{2}\right)} g\rho_M \tag{9.5.1}$$

We see from this that when $\beta \to 0$ or $\beta \to 360^0$ (nearly only gas or nearly only liquid in the pipe), we have no problems satisfying this criterion. Close to $\beta = 180^0$ (meaning

$\alpha_M \approx \alpha_G \approx 0.5$; half-full pipe), on the other hand, hyperbolicity can be threatened if the gas velocity is very high and/or the gas density is high. As previously pointed out, the numerical damping in implicit integration methods may be so strong that even ill-posed models run and produce results, so in most cases this model will run and produce (reasonable, it turns out) results.

Bonizzi & Issa (2003) and Issa & Kempf (2003) have compared results produced by this model both for slugs with and without gas bubble entrainment (by neglecting everything to do with bubble entrainment shown above) on 3 different pipes, all of length $l = 37m$ and diameter $d = 0.078m$ containing air-water. The first pipe was horizontal, the second -1.5^0 (slightly downward inclined), the third V-shaped with first section -1.5^0 and the last section 1.5^0 inclined. They achieved remarkably good agreements with measurements both for fractions, statistical slug length distributions and friction. Even though the limitations explained in chapter 9.1 apply, it seems likely that this model can have a great potential for slug flow simulations, including for steeply inclined pipes (it would require bubble entrainment correlations developed for that purpose, and possibly also other modifications).

"It is no good to try to stop knowledge from going forward.
Ignorance is never better than knowledge."
Enrico Fermi

10 Multi-phase flow heat exchange

Heat exchange between fluid and environment:

- Relevant single-phase heat flow correlations
- Simplified multi-phase heat exchange correlations
- Stratified flow heat transfer
- Dispersed bubble and bubble flow heat transfer
- Slug flow heat transfer

10.1 Introduction

Knowing the temperature inside a pipeline can be critical in some cases, for instance when investigating temperature-sensitive phenomena like hydrate or wax deposition. The energy conservation equation 2.4.4 is used for that purpose. It contains the terms q_{ki}, the specific heat flow between different fluid phases, and q_{kW}, specific heat flow between each phase and the pipe wall. To calculate the temperatures as a function of time and space, both terms must be estimated. In *Pipe Flow 1* (chapter 8), we learned how to do so for single-phase flow. In that case, the only specific heat involved was the one flowing between the pipe wall and the fluid, and we called it q. We may also recall that relatively well established empirical correlations were available to calculate q for single-phase flow. The challenges facing us are more complex when dealing with multi-

phase flow: Not only are more heat flows involved, but the correlations necessary to estimate them are generally less well proven.

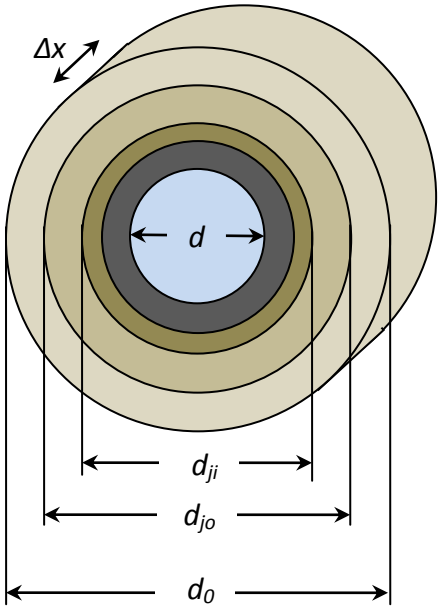

Figure 10.1.1. Pipe layers.

Let us start by repeating some key correlations for single-phase flow.

The overall heat transfer coefficient U_o *[W/(m²K)]* can be correlated to the outer diameter d_o as:

$$U_o d_o = \frac{1}{\frac{1}{U_1 d_1} + \frac{1}{U_2 d_2} + \frac{1}{U_3 d_3} + \cdots + \frac{1}{U_n d_n}} \qquad (10.1.1)$$

The term q *[J/m³]* representing heat added to the fluid from the environment should be taken pr. unit volume of fluid and can then be calculated as:

$$q = \frac{4U_o d_o}{d^2}\left(T_o - T_f\right) \qquad (10.1.2)$$

Determining q comes down to determining $U_o d_o$ with adequate accuracy. The different terms to do with the pipe wall and insulation layers are relatively easy to estimate if we know each layer's thermal conductivity. At the outside of the outermost layer, we may typically have air or water, or the pipe may be buried in various types of soil. For the innermost layer, we saw that the heat transfer coefficient could be estimated by correlating the Reynolds number, the *Nusselt number* and the *Prandtl number*. The last two were defined as:

$$Nu \stackrel{\text{def}}{=} \frac{Ud}{k_f} \qquad (10.1.3)$$

U is the convective heat transfer coefficient we are seeking, and k_f is the fluid's thermal conductivity *[W/(m·K)]*. *Pr* is defined as:

$$Pr \overset{\text{def}}{=} \frac{\nu}{\alpha} = \frac{c_p \mu}{k_f} \tag{10.1.4}$$

ν is kinematic viscosity *[m²/s]*, μ is dynamic viscosity *[kg/(m·s)]*, α is thermal diffusivity *[m²/s]* (not to be confused with fraction), and c_p is specific heat at constant pressure *[J/(kg·K)]*. *Pr* is a pure fluid property, so it can be expressed as a function of temperature and pressure in tables, or in the form of curve-fits.

Sieder & Tate's correlation (1936) still seems to be the most widely accepted for single-phase laminar flow. For long pipelines, it reduces to:

$$Nu = 3.66 \tag{10.1.5}$$

For turbulent flow and long pipelines, it can be written as

$$U_{ST} = 0.027 Re^{4/5} Pr^{1/3} \left(\frac{k_f}{d}\right)\left(\frac{\mu}{\mu_W}\right)^{0.14} \tag{10.1.6}$$

$\mu\ [kg/(m \cdot s)]$ is the fluid's average dynamic viscosity, and μ_W is the fluid's viscosity at the wall. Note that we have added $_{ST}$ in the index to distinguish it from other alternative ways of determining the convective heat transfer coefficient. In later chapters, this particular correlation is used as a reference to calculate multi-phase heat transfer coefficients. It is valid only under the following stated limitations:

$$\begin{gathered} 13 \leq Re \leq 2300 \\ 0.48 \leq \mathrm{Pr} \leq 16{,}700 \\ 0.0044 \leq \frac{\mu}{\mu_w} \leq 9.75 \end{gathered} \tag{10.1.7}$$

For turbulent single-phase flow, the Gnielinski-correlation (1976, 1983) is probably the best available at present:

$$Nu = \frac{\frac{f}{8}(Re - 1{,}000)Pr}{1.07 + 12.7\left(\frac{f}{8}\right)^{1/2}(Pr^{2/3} - 1)} \tag{10.1.8}$$

The stated validity of equation 10.1.7 is:

$$2300 \leq Re \leq 5 \cdot 10^6$$
$$0.5 \leq \mathrm{Pr} \leq 2{,}000 \tag{10.1.9}$$

10.2 Classical, simplified mixture correlations

DeGance & Atherthon (1970) proposed the following flow-regime independent correlation for two-phase flow:

$$Nu = 0.023 Re^{0.8} Pr^{1/3} \tag{10.2.1}$$

This equation is based on averaging all properties, and the fractions α_G and α_L are calculated as if there was no slip, so $v_G = v_L$. It means that the average density $\rho_M = \alpha_G \rho_G + \alpha_L \rho_L$ and so on for viscosity, thermal conductivity, and Prandtl number. For this to work, we also need to assume the temperature to be the same in all phases – an approximation which most often is acceptable for pipelines and wellbores and used in most models shown in this book. Equation 10.2.1 works best for well mixed phases, which basically is dispersed bubble flow only.

In cases where the pipe is so well insulated that the pipe wall temperature stays close to the fluid temperature, the fluid-pipe convective heat transfer coefficient is not important to the overall result (its insulating effect is much smaller than the outside insulation). In those cases equation 10.2.1 may be adequate for non-dispersed flow regimes, too (the pipe wall's temperature will be very close to the fluid's temperature).

An alternative approach goes via definitions of the quality x and a parameter we simply choose to call X:

$$x = \frac{\alpha_G \rho_G v_G}{\alpha_G \rho_G v_G + \alpha_L \rho_L v_L} \tag{10.2.2}$$

$$X = \left(\frac{1-x}{x}\right)^{0.9} \left(\frac{\rho_G}{\rho_L}\right)^{0.5} \left(\frac{\mu_L}{\mu_G}\right)^{0.1} \tag{10.2.3}$$

We notice that x is the ratio of the gas mass flow rate to the total mass flow rate. For steady-state calculations, this is known from the boundary conditions, so this method was developed to be particularly convenient for steady-state analysis.

For separated, turbulent flow (both gas and liquid being turbulent), it has been suggested calculating the overall two-phase heat transfer coefficient U as:

$$U = U_L C_q \left(\frac{1}{X}\right)^{n_q} \tag{10.2.4}$$

Where U_L is the heat coefficient we would have had for single-phase liquid flow. Dengler & Addoms (1956) proposed setting the coefficients $C_q = 3.5$ and $n_q = 0.5$, while Collier & Pulling (1962) used $C_q = 2.5$ and $n_q = 0.7$.

For vertical flow, a type of flow obviously very relevant to wells and risers, Rezkallah & Sims (1987) proposed the following correlations, thought to be somewhat more accurate for vertical flow than the other simplified methods presented here:

$$U = \begin{cases} U_L \left[1 + 4 \left(\frac{\alpha_G v_G}{\alpha_L v_L} \right)^{0.25} Pr_L{}^{-0.23} \right] & for\ Re_{\alpha_L v_L} \leq 2{,}000 \\ U_L \left(\frac{1}{1-\alpha_G} \right)^{0.9} & for\ Re_{\alpha_L v_L} > 2{,}000 \end{cases} \quad (10.2.5)$$

$Re_{\alpha_L v_L}$ is the Reynolds number based on the liquid superficial velocity $\alpha_L v_L$.

None of these simplified correlations distinguish between different flow regimes, and they are relatively inaccurate compared to those correlations which have been adapted to each flow regime separately.

10.3 Improved correlations for all flow regimes in horizontal two-phase gas-liquid flow

Kim et al. (1999) and Ghajar (2005) have published an extensive overview over different correlations (both those shown here and numerous others), and they have also tested them out on various flow regimes. As one would expect, it turns out that none of the 'general' correlations are accurate for all flow regimes, nor are any of them accurate for all other combinations of fluid properties or pipe inclinations and diameters, so they decided to try to fit results for horizontal pipes into the following correlation:

$$U = U_{L\,ST} F_p \left\{ 1 + C \left[\left(\frac{x}{1-x} \right)^m \left(\frac{1-F_p}{F_p} \right)^n \left(\frac{Pr_G}{Pr_L} \right)^p \left(\frac{\mu_G}{\mu_L} \right)^q \right] \right\} \quad (10.3.1)$$

x is defined as in equation 10.2.2, and *C, m, n, p,* and *q* are the empirical constants Ghajar et al. (2006) used to fit equation 10.3.1 to their empirical data (see table 10.3.1). F_p is the effective wetted perimeter defined as:

$$F_p = \alpha_{L\,C} + \alpha_{G\,C} F_S{}^2 \quad (10.3.2)$$

$\alpha_{G\,C}$ and $\alpha_{L\,C}$ are given by equation 10.3.6. The shape factor F_S is defined as:

$$F_S = \frac{2}{\pi}\tan^{-1}\left[\sqrt{\frac{\rho_G(v_G - v_L)^2}{gd(\rho_L - \rho_G)}}\right] \; if \; v_G \geq v_L \tag{10.3.3}$$

Any well-known single-phase turbulent heat transfer correlation such as the Gnielinski-correlation, equation 10.1.8, could in principle have been used to calculate the heat coefficient we would have had for single-phase liquid flow, $U_{L\,ST}$. However, Ghajar et al. (2006) chose to consistently use the Sieder & Tate (1936) correlation to calculate $U_{L\,ST}$, and that is why we have added $_{ST}$ to the index. Had a different correlation been used as basis, slightly different values for C, m, n, p, and q would probably have resulted, but the end result for the overall U would have been nearly the same. For consistency, we therefore need to use the Sieder & Tate (1936) correlation 10.1.6, not 10.1.8, which for the liquid becomes:

$$U_{L\,ST} = 0.027 {Re_L}^{4/5} {Pr_L}^{1/3} \left(\frac{k_L}{d}\right)\left(\frac{\mu_L}{\mu_{LW}}\right)^{0.14} \tag{10.3.4}$$

The Reynold's number to be used in equation 10.3.4 can be defined from the liquid mass flow $\dot{m}_L$ as:

$$Re_L = \left(\frac{\rho v d}{\mu}\right)_L = \frac{4\dot{m}_L}{\pi\sqrt{\alpha_{L\,C}}\mu_L d} \tag{10.3.5}$$

In Ghajar et al.'s study (2006), a complete dynamic model producing values for α_G and α_L (like the one shown in chapter 2) was not used, so they relied on estimating α_G and α_L in another way, manemly the Chisholm (1973)-correlation, which states:

$$\alpha_{G\,C} = (1 - \alpha_{L\,C}) = \left[1 + \left(\frac{\rho_L}{\rho_M}\right)^{0.5}\left(\frac{1-x}{x}\right)\left(\frac{\rho_G}{\rho_L}\right)\right]^{-1} \tag{10.3.6}$$

where the mixture density:

$$\rho_M = \left(\frac{1-x}{\rho_L} + \frac{x}{\rho_G}\right)^{-1} \tag{10.3.7}$$

Ghajar et al. (2006) tried out equation 10.3.1 over a wide range of Reynolds numbers for horizontal pipe flow. Using the empirical values in table 10.3.1, they achieved remarkably good agreement with measurements for plug/slug flow, slug flow, slug/bubbly flow, slug/bubbly/annular flow, slug/wavy flow, wavy/annular flow, annular flow, and wavy flow. Less good agreement was achieved for plug and stratified flows.

C	m	n	p	q
0.7	0.08	0.06	0.03	-0.14

Table 10.3.1. Empirical factors for equation 10.3.1.

That seems to make equation 10.3.1 the most general flow regime-independent heat transfer coefficient correlation for horizontal pipe flow currently available.

10.4 Flow regime-dependent approximation for horizontal flow

When the flow regimes are known (something they have to be to calculate friction and other parameters in our overall simulation model), we may use that information when determining U. In an earlier publication (preceding the one used as basis for chapter 10.3), Ghajar (also repeated in his later, 2005-publication) defined:

$$U = U_{L\,ST}\alpha_{L\,C}\left\{1 + C\left[\left(\frac{x}{1-x}\right)^{m}\left(\frac{\alpha_{G\,C}}{\alpha_{L\,C}}\right)^{n}\left(\frac{Pr_G}{Pr_L}\right)^{p}\left(\frac{\mu_G}{\mu_L}\right)^{q}\right]\right\} \qquad (10.4.1)$$

This was fitted to results by using the constants given in table 10.4.1.

	C	m	n	p	q
Slug, bubbly/slug, bubbly/slug/annular	2.86	0.42	0.35	0.66	-0.72
Wavy-annular	1.58	1.40	0.54	-1.93	-0.09
Wavy	27.89	3.10	-4.44	-9.65	1.56

Table 10.4.1. Empirical factors for equation 10.4.1.

Both the mean and standard deviation was smaller when using equation 10.4.1 compared to 10.3.1, but equation 10.4.1 covers fewer flow regimes. For those who insist on using very simple heat correlations, the best alternative therefore seems to be to use equation 10.4.1 for those flow regimes it covers, while using equation 10.3.1 for other horizontal flow situations.

10.5 Flow-regime dependent two-phase correlations for inclined pipes

The most accurate correlation, but also the one covering least flow regimes (only slug and annular flow), was published by Ghajar (2005):

$$U = U_{L\,ST}\alpha_{L\,C}\left\{1 + C\left[\left(\frac{x}{1-x}\right)^{m}\left(\frac{\alpha_{G\,C}}{\alpha_{L\,C}}\right)^{n}\left(\frac{Pr_G}{Pr_L}\right)^{p}\left(\frac{\mu_G}{\mu_L}\right)^{q}\left(1+\frac{gd\sin\theta}{(\alpha_{L\,C}v_L)^2}\right)^{r}\right]\right\} \quad (10.5.1)$$

The empirical factors turned out to be the ones given in table 10.5.1.

	C	m	n	p	q	r
Slug	0.86	0.35	-0.8	0.33	-0.67	1.75
Annular	1.4	0.35	0.045	0.33	-0.67	0.26

Table 10.5.1. Empirical factors for equation 10.5.1.

10.6 Dispersed bubble flow

A liquid slug has relatively low gas fraction and can therefore for this purpose be regarded as single-phase flow, so we may use equation 10.1.8 for it, but with all physical properties averaged according to the gas/liquid fractions. The mixture density is calculated as defined in equation 1.5.3, which for two-phase gas-liquid flow becomes:

$$\rho_M = \alpha_G\rho_G + \alpha_L\rho_L \quad (10.6.1)$$

We define mixture quantities similarly for all other data relevant to calculating *Re, Pr* and *Nu,* and this enables us to calculate the mixture convective heat transfer coefficient. The bubble flow heat calculations are expected to be equally valid for all pipe inclinations, just as they are for single-phase flow.

10.7 Stratified flow

Stratified flow can be regarded as two different, nearly independent phases, with heat flowing between the gas and the pipe wall, between the liquid and the pipe wall, and between the gas and the liquid. The liquid typically has at least an order of magnitude higher heat capacity than the gas compared to its volume, and U_{LW} is also larger than U_{GW}. If the purpose of our calculations is to find the total heat interaction with the environment, we may not even have to consider the gas in the energy equation if the liquid fraction is high. Due to its lower heat capacity, the gas' temperature tends to follow the environment's temperature more closely than the liquid does. When hot gas and oil emerges from a well, this means the gas often cools faster than the liquid, and we may want to consider it separately in stratified flow.

If we look back to figure 9.3.1 and the definitions of hydraulic diameter in equation 3.5.1, we are able to come up with the Reynolds numbers for gas-wall, liquid-wall and the gas-liquid interface, just as we did in equations 9.3.9 - 9.3.11. Those Reynolds numbers allow us to calculate all 3 relevant Nusselt numbers by using equation 10.1.3 for each of them in a similar way. We can use the full equation 10.1.1 and 10.1.2 for each of the insulation layers, while reducing the final values according to how large a part of the pipe wall comes in contact with gas and liquid. The interface heat flow can be estimated by considering the interface circumference to be a straight line (single-layer, 'constant' diameter in equations 10.1.1 and 10.1.2).

10.8 Slug flow

The overall two-phase heat transfer coefficient U for slug flow can be calculated according to equation 10.5.1. If we choose that approach, we are calculating an average U for the slug unit at any point in space for a given time, even though U in reality depends on whether we have a liquid slug (with bubbles in it), a Taylor-bubble with a liquid film zone below it, or a mixing zone at the front of the liquid slug at the point we are studying. Using equation 10.5.1 therefore cannot be expected to produce realistic temperature variations as liquid slugs and Taylor-bubbles pass by it. If the slugs are

short at the same time as the temperature difference between the fluids and the pipe's surroundings are moderate, or if the pipe is well insulated, the difference may be insignificant. It situations where we have strong cooling or heating, we may want to go into further details to get better estimates of the temperature reduction during periods of high gas content.

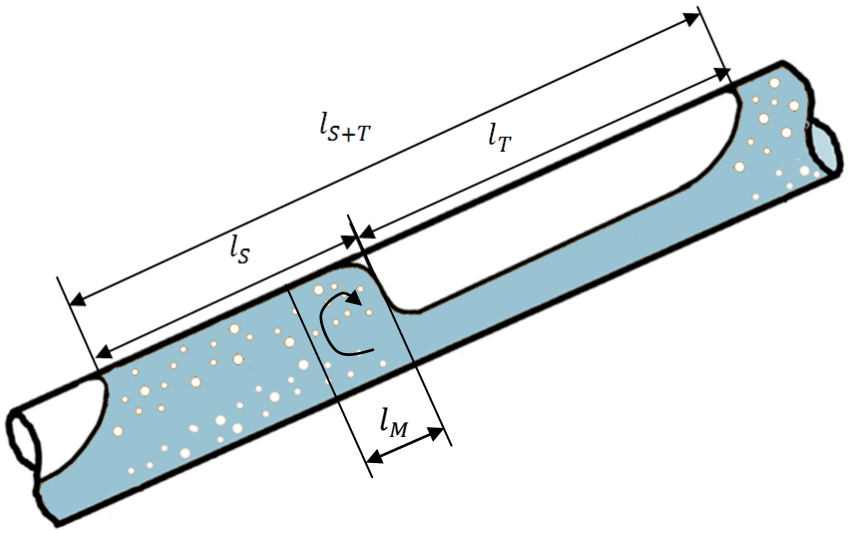

Figure 10.8.1. Slug unit with liquid slug of length l_S, Taylor-bubble with liquid film under it of length l_T, and a mixing zone of length l_M.

For long Taylor-bubbles, which are of most interest when we focus on temperature pulsations, the Taylor-bubble thickness is relatively constant, and we can calculate U as if the flow were stratified, see chapter 10.7. The liquid slug can be modeled as dispersed bubble flow the way it was outlined in chapter 10.6. The mixing eddy at the front of the slug has a higher U-value than the main part, but in measurements carried out by Shoham et al. (1982) the extra contribution is less than 100%. Although the mixing zone can be longer than it appears in figure 10.8.1 (figure 9.4.1 is more realistic in that respect), it is much shorter than the rest of the slug in most situations of interest. For long slugs, such as $l_S > 100d$, the extra heat exchange in the slug front can safely be neglected compared to other inaccuracies.

"All truths are easy to understand once they are discovered; the point is to discover them."
Galileo Galilei, ca. 1600

11 Flow regime determination

Various models for determining flow regime in two-phase flow:

- Beggs & Brill's model
- Taitel & Dukler's model
- Flow regime maps for horizontal and vertical pipes
- Flow regime transition mechanisms
- The OLGA minimum-slip flow regime criterion

11.1 The Beggs & Brill flow regime map

All the most accurate models we have discussed so far rely on knowing the flow regime. Stratified flow is modeled quite differently compared to annular or slug flow and the results will obviously suffer if we use the wrong sort of flow regime. Determining the flow regime is important, but unfortunately it is also one of the least accurate parts of the flow models. In cases where the flow happens to be near the border between two or even three different flow regimes, the uncertainties are generally most significant. We may also experience situations where minor changes in fluid properties or inclination angle is likely to change the flow regime, and the simulations may require more accurate pipe elevation profiles or fluid composition data than are available. We can investigate such uncertainties by simulating several times with

slightly different input-data and see how the results compare, but it also helps to know the philosophy behind the simulation program's flow regime detection module. This chapter deals with such flow regime detection.

The Beggs & Brill (1973)-correlation for horizontal flow is based on the mixture Froude-number, Fr_M, and the no-slip liquid fraction $\alpha_{L\,noslip}$ (this would be the same as the liquid fraction α_L if the gas and liquid velocities were identical. Beggs & Brill chose to call this *no-slip liquid holdup*):

$$Fr_M = \frac{\alpha_G v_G + \alpha_L v_L}{\sqrt{gd}} \tag{11.1.1}$$

And:

$$\alpha_{L\,noslip} = \frac{\alpha_L v_L}{\alpha_G v_G + \alpha_L v_L} \tag{11.1.2}$$

Based on empirical results, they concluded that for horizontal flow, one may determine the flow patterns from 4 critical Froude numbers defined as:

$$Fr_1 = \sqrt{316\alpha_{L\,noslip}{}^{0.302}} \tag{11.1.3}$$

$$Fr_2 = \sqrt{0.0009252\alpha_{L\,noslip}{}^{2.4684}} \tag{11.1.4}$$

$$Fr_3 = \sqrt{0.10\alpha_{L\,noslip}{}^{-1.4516}} \tag{11.1.5}$$

$$Fr_4 = \sqrt{0.5\alpha_{L\,noslip}{}^{-6.738}} \tag{11.1.6}$$

Using these definitions they concluded that the flow pattern may be determined as:

Segregated if:
$\alpha_{L\,noslip} < 0.01$ and $Fr_M < Fr_1$, or
$\alpha_{L\,noslip} \geq 0.01$ and $Fr_M < Fr_2$

Transition if:
$\alpha_{L\,noslip} \geq 0.01$ and $Fr_2 \leq Fr_M \leq Fr_3$

Intermittent if:
$0.01 \leq \alpha_{L\,noslip} < 0.4$ and $Fr_3 \leq Fr_M \leq Fr_1$, or
$\alpha_{L\,noslip} \geq 0.4$ and $Fr_3 \leq Fr_M \leq Fr_4$

Distributed if:
$\alpha_{L\,noslip} < 0.4$ and $Fr_M \geq Fr_1$, or
$\alpha_{L\,noslip} \geq 0.4$ and $Fr_M > Fr_4$

This is shown in the form of a diagram in figure 11.1.1.

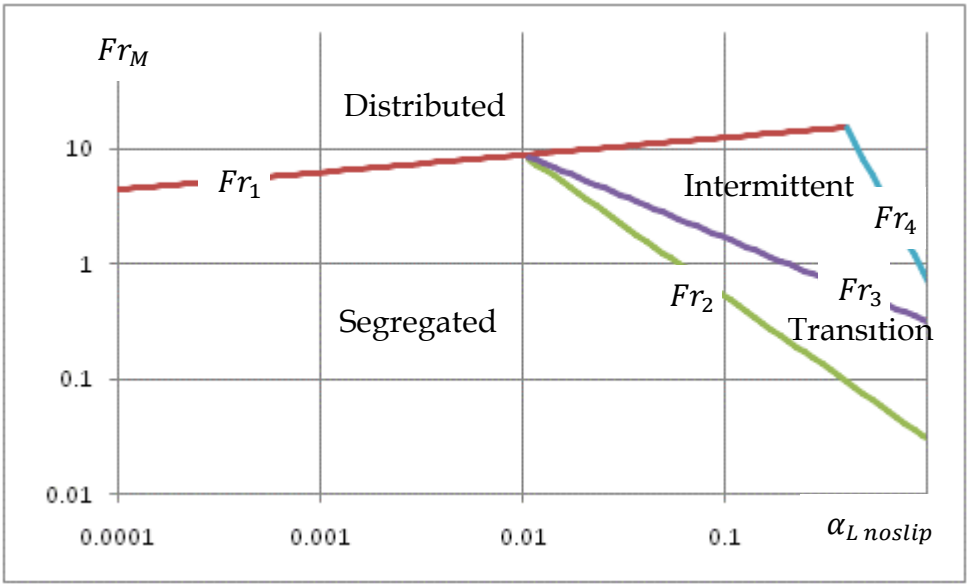

Figure 11.1.1. Two-phase gas-liquid flow pattern map for horizontal pipes according to Beggs & Brill (1973).

The Beggs & Brill correlations were developed with steady-state calculations in mind, but we can use them together with transient calculations as well. In the transition-zone, they recommended using a weighted average between the conditions in the neighboring regions (segregated and intermittent flow).

One obvious problem with this diagram is its limited validity, since most practical flows are not completely horizontal. Beggs & Brill recognized this and proposed correction factors for inclined flow, and they also developed methods for estimating the fractions and steady-state pressure gradient. Their calculation procedure for fractions and friction is very simple to use but also considered relatively inaccurate, particularly for upward inclination, and the complete model has therefore not been included here. Further details can be found in the original paper. A clear presentation of the model can also be found in Shoham (2006).

11.2 The Taitel & Duckler horizontal flow model

Like Beggs & Brill (1973), Taitel & Duckler (1976) developed a model for steady-state two-phase flow and for (nearly) horizontal pipes. It is considered valid for up to $\pm 10^0$ inclination (Shoham, 2006), and it is based on a somewhat more physical understanding on what causes the flow regime shifts.

The Taitel & Dukler model starts out by considering stratified flow. A stability analysis is carried out to determine if the stratified flow regime will be stable under the prevailing conditions. If it is not, a change to one of the other flow regimes occurs.

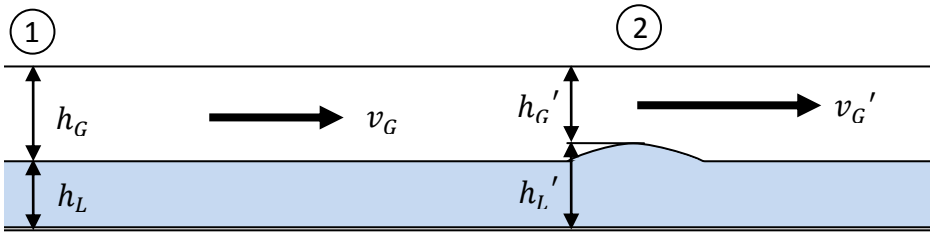

Figure 11.2.1. Stratified two-phase flow just before switching to another flow regime.

The main mechanism at work is thought to be the Bernoulli effect, which reduces the pressure if the gas' velocity is increased. Suppose, for instance, that the liquid's level is somewhat higher at a point *2* than in the rest of the pipe, as illustrated in figure 11.2.1. By simply writing Bernoulli's energy equation for the gas flow from a point *1* in front of

it to point 2, neglecting friction and the slight average gas altitude difference for those two points, the pressure difference can be expressed as:

$$p - p' = \frac{\rho_G}{2}\left({v_G}'^2 - {v_G}^2\right) \tag{11.2.1}$$

If the flow can be considered incompressible for the purpose of this stability analysis, steady-state mass conservation becomes a simple continuity equation:

$$v_G A_G = {v_G}' {A_G}' \tag{11.2.2}$$

Let us first assume the pipe cross-section to be rectangular so that the areas $A_{G\,1}$ and $A_{G\,2}$ are proportional to $h_{G\,1}$ and $h_{G\,2}$. Then equation 12.2.2 can be expressed as:

$$v_G h_G = {v_G}' {h_G}' \tag{11.2.3}$$

For a wave of the sort shown in figure 12.2.1 to develop, the pressure difference $p - p'$ must be large enough to 'carry' the wave, meaning large enough to counter the wave's static pressure head. Since the liquid is 'submerged' in gas, we have to correct for the liquid's buoyancy in the gas, and the effective density becomes $\rho_L - \rho_G$:

$$p - p' > (\rho_L - \rho_G) g (h_G - {h_G}') \tag{11.2.4}$$

Combining equations 11.2.1 – 11.2.4, we can develop an expression for how large the gas velocity v_G must be in a rectangular pipe before the Bernoulli effect can cause instabilities like this:

$$v_G > C_1 \left[\frac{(\rho_L - \rho_G) g h_G}{\rho_G}\right]^{0.5} \tag{11.2.5}$$

Equation 11.2.5 is valid if we define C_1 as:

$$C_1 = \left[\frac{2}{\frac{h_G}{h_G'}\left(\frac{h_G}{h_G'}+1\right)}\right]^{0.5} \tag{11.2.6}$$

For an infinitesimal wave, $h_G' \to h_G$, and so $C_1 \to 1$. Equation 12.2.5 reduces to the so-called *Kelvin-Helmholz Inviscid Wave Growth Criterion*.

The analysis can be extended to circular pipes and also to account for inclination. In that more general case, we get:

$$v_G > \left[\frac{2(\rho_L - \rho_G) g \cos\theta \, (h_L' - h_L)}{\rho_G} \frac{A_G'^2}{A_G^2 - A_G'^2}\right]^{0.5} \tag{11.2.7}$$

We can use Taylor series to expand A_G' around A_G and show that instability (the onset of a small wave) occurs if:

$$v_G > C_2 \left[\frac{(\rho_L - \rho_G) g \cos\theta \, A_G}{\rho_G S_{GL}}\right]^{0.5} \tag{11.2.8}$$

S_{GL} is defined in figure 9.3.1, and:

$$C_2 = \left[\frac{2\left(\frac{A_G}{A_G'}\right)^2}{\left(\frac{A_G'}{A_G}+1\right)}\right]^{0.5} \tag{11.2.9}$$

It is common to linearize C_2. We see that if $A_G' \to A_G$, $C_2 \to 1$, and if $A_G' \to 0$, $C_2 \to 0$. As discussed in chapter 9.3, A_G, (and thereby also A_G') are in reality relatively complicated functions of the circular geometry. It has been found, though, that reasonable results can be achieved by simply setting:

$$C_2 = \left(1 - \frac{h_L}{d}\right) \tag{11.2.10}$$

This leads to the final criterion for the transition boundary as:

$$v_{G\,B}{}^{*} = \left(1 - \frac{h_L}{d}\right)\left[\frac{(\rho_L - \rho_G) g \cos\theta\, A_G}{\rho_G S_{GL}}\right]^{0.5} \tag{11.2.11}$$

The flow remains stratified if $v_G < v_{G\,B}{}^{*}$. Notice that many parameters other v_G are involved in determining whether we have stratified flow or not. h_L, for instance, is going to be affected both by the gas and liquid velocities, and that also affects A_G and S_{GL}. In addition, the absolute pressure is going to influence the gas' density significantly.

There is actually one more mechanism which may create surface waves other than the Bernoulli-effect already described, namely the same effect which creates surface waves on the ocean. This happens at a lower gas velocity than the one described by equation 11.2.11, and it was shown by Jeffrey (1926) that the criterion for wave initiation is:

$$(v_G - c_w)^2 c_w > \frac{4\mu_L(\rho_L - \rho_G) g \cos\theta}{s\rho_L\rho_G} \tag{11.2.12}$$

Where c_w is the waves' propagation velocity, s is the so-called *sheltering coefficient* determined by Sverdrup & Munk (1947) to be 0.01. If the liquid's velocity is considerably higher than the waves' propagation velocity in still liquid, we may approximate the wave velocity on moving liquid as $c_w \approx v_L$. If the gas velocity is also much larger than the waves' propagation velocity ($v_G \gg c_w \approx v_L$), as is the most typical situation in pipelines, equation 11.2.12 can be modified to:

$$v_{G\,w}{}^{*} = \left[\frac{4\mu_L(\rho_L - \rho_G) g \cos\theta}{s\rho_L\rho_G v_L}\right]^{0.5} \tag{11.2.13}$$

This means the surface between the gas and the liquid is going to be smooth as long as $v_G \leq v_{G\,w}{}^*$, while it becomes wavy for $v_{G\,w}{}^* < v_G \leq v_{G\,B}{}^*$. For $v_G > v_{G\,B}{}^*$, the flow is no longer going to be stratified.

If we conclude that the flow is not going to be stratified, it remains to be determined which of the several other possible alternatives flow regimes we end up with. For low gas and high liquid flow rates, the liquid level is high. If surface waves form, they may reach the top of the pipe and block the entire cross-section, in which case a slug forms. At high gas and low liquid flow rates, on the other hand, the liquid level in the pipe is going to be low, and the lowest part of the wave is going to reach the bottom of the pipe before the uppermost part reaches the top. The result is that the liquid is swept around the inside of the pipe to create annular flow instead of slugs. Therefore, the liquid level determines whether we end up with slug of annular flow. As a first assumption, is was thought that if $h_L > d/2$, we would get slug flow, otherwise annular flow. Barnea et al. (1980) modified this assumption to account for the fact that slugs do not consist of liquid only. Barnea et al. suggested it is better to set:

Annular flow if $v_G > v_{G\,B}{}^*$ and $h_L < 0.35d$
Slug flow if $v_G > v_{G\,B}{}^*$ and $h_L > 0.35d$ (11.2.14)

If we have slug flow and continue to increase the turbulence in the pipe, the Taylor-bubbles will at some point be shattered into small bubbles which disperse in the liquid. Therefore, the transition to dispersed bubble flow occurs when the turbulent fluctuations in the liquid-phase are strong enough to overcome the bubble buoyancy forces. The buoyancy forces per unit length are obviously:

$$F_B = A_G(\rho_L - \rho_G)g\cos\theta \tag{11.2.15}$$

The turbulence forces acting on a Taylor-bubble from the liquid are:

$$F_T = \frac{1}{2}\rho_L \langle {v'_L}_r^2 \rangle S_{GL} \tag{11.2.16}$$

S_{GL} is defined in figure 9.3.1, and $\langle {v'_L}_r^2 \rangle$ is the radial intensity of the liquid fluctuations, similar to what we calculated in equation 5.4.1 for the gas phase. Here we determine $\langle {v'_L}_r^2 \rangle$ by first approximating the Reynolds stress as:

$$\tau_R = \rho_L \langle {v'_L}_r^2 \rangle \tag{11.2.17}$$

As we have seen before, the wall shear stress can be expressed in terms of the friction at the wall, as determined by the liquid Darcy-Weisbach friction factor, f_L, as:

$$\tau_W = \frac{1}{2} f_L \rho_L {v_L}^2 \tag{11.2.18}$$

By setting $\tau_R = \tau_W$, we get an expression for $\langle {v'_L}_r^2 \rangle$, which we insert into equation 11.2.16. Setting $F_B = F_T$, we then get the criterion for when bubble breakup will happen:

$$v_{L\,D}{}^* = \left[\frac{4A_G}{S_{GL}} \frac{g \cos\theta}{f}\left(1 - \frac{\rho_G}{\rho_L}\right)\right]^{0.5} \tag{11.2.19}$$

This means that we get dispersed bubble flow if $v_L > v_{L\,D}{}^*$, otherwise we get intermittent (slug) flow.

The results here are easily integrated into the transient flow models, which is our main purpose. If we want to plot the results from this chapter in a diagram, we have to choose some of the parameters (such as the pipe inclination) in order to be able to use the equations, and the diagram is going to be valid only for the choices we make – it will not be general. Alternatively, we can order our variables into dimensionless groups and concentrate all information in one diagram (Shoham, 2006). That makes it possible to present the results in a very compact form, but that also makes them somewhat more

abstract. We will therefore choose to plot the results along a diagram with the superficial gas velocity $\alpha_G v_G$ along the horizontal axis, and the superficial liquid velocity $\alpha_L v_L$ along the vertical axis.

When we study the relevant equations (12.2.11, 12.2.13, 12.2.14, and 12.2.19), we see that we also need to know the fractions (or its equivalent, h_L) to be able to plot the flow regime diagram. The fractions would follow from the complete transient simulation model when we carry out simulations, but when plotting a steady-state diagram of a similar sort as figure 11.1.1, we require a steady-state solution for the fractions, too. For stratified flow, such a correlation can be created by setting the pressure, and therefore also the pressure loss along the pipe, equal for both the gas and the liquid.

If we use the steady-state, incompressible version of equations 3.3.2 without the pressure correction term, in addition to equations 3.5.14 and 3.5.16 for the gas flow, we get:

$$\frac{\partial p}{\partial x} = -\frac{f_{GL}\rho_G}{2\alpha_G}\frac{O_{GL}}{A_G}(v_G - v_L)|v_G - v_L| - \frac{f_{Gw}\rho_G}{8\alpha_G}\frac{O_{GW}}{A_G}v_G|v_G| \; - \rho_G g \sin\theta \tag{11.2.20}$$

Similarly, for the liquid flow, we get:

$$\frac{\partial p}{\partial x} = \frac{f_{GL}\rho_G}{2\alpha_L}\frac{O_{GL}}{A_G}(v_G - v_L)|v_G - v_L| - \frac{f_{Lw}\rho_L}{8\alpha_L}\frac{O_{LW}}{A_L}v_L|v_L| \; - \rho_L g \sin\theta \tag{11.2.21}$$

Combining equations 11.2.20 and 11.2.21, and for simplicity assuming all velocities to be positive, leads to:

$$\left(\frac{1}{\alpha_G} + \frac{1}{\alpha_L}\right)\frac{f_{GL}\rho_G}{2}\frac{O_{GL}}{A_G}(v_G - v_L)^2 + \frac{f_{Gw}\rho_G}{8\alpha_G}\frac{O_{GW}}{A_G}{v_G}^2 - \frac{f_{Lw}\rho_L}{8\alpha_L}\frac{O_{LW}}{A_L}{v_L}^2 \; - (\rho_G - \rho_L)g\sin\theta = 0 \tag{11.2.22}$$

Equation 11.2.22 cannot be solved analytically. Instead, we must use the steady-state boundary conditions (such as gas and liquid mass flow into the pipe, together with a known pressure for the section we are studying), and guess on a fraction (for instance $\alpha_G = 0.5$). From that, we calculate all other geometrical data, such as A_G, O_{GL}

and so on, together with velocities and densities. If the result does not agree with equation 11.2.22, we need to make another guess, and continue to do so until we get convergence. In order to get the fastest convergence possible, we use one of the known techniques, typically Newton-iteration.

Once convergence is achieved and the equilibrium liquid level has been established (so fractions and velocities are known), we must use equation 11.2.11 to determine whether the stratified flow-assumption equation 11.2.22 was built on was valid. If we have stratified flow, we can also use equation 11.2.13 to determine whether the surface is smooth or wavy. In case the flow is not stratified, we need to try another flow regime. If we try slug flow, equation 11.2.22 is invalid, and we need instead to determine the geometrical quantities in the way is was described in chapter 7. Afterwards, we must check the result with equations 12.2.19, 12.2.14, and 12.2.11 to see if the slug flow assumption was correct. If not, we must calculate fractions for another flow regime using the relevant friction calculations until we achieve a valid result.

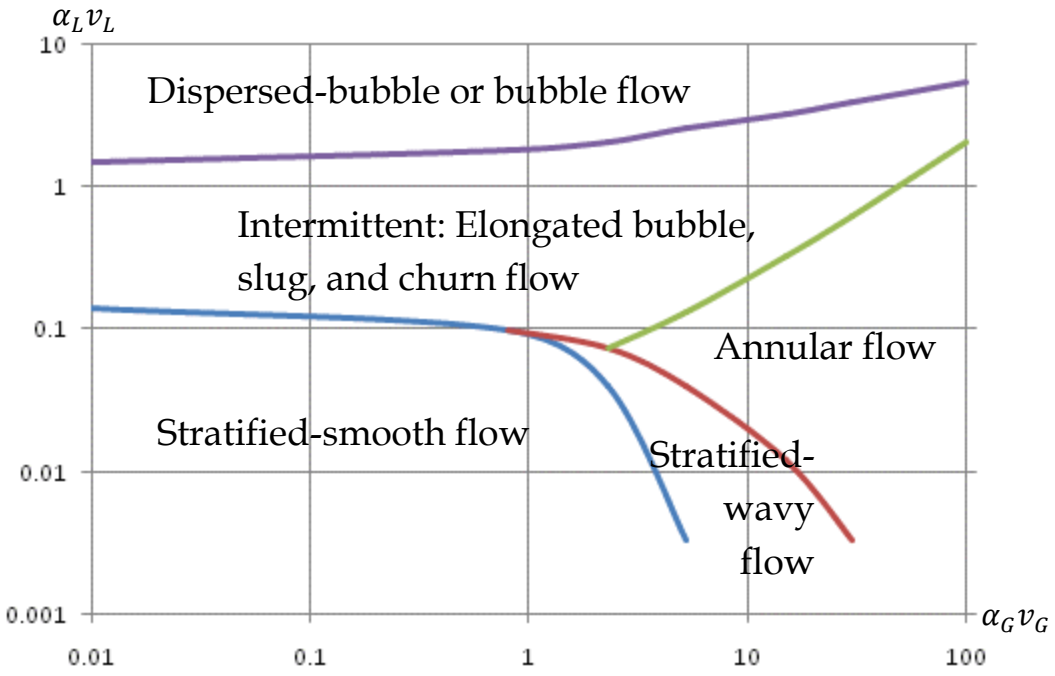

Figure 11.2.1. Example of flow regime plot for horizontal pipe according to Taitel & Dukler (1976). The different flow regimes are also illustrated in figures 1.2.1 and 1.2.4.

Notice that these methods work equally well for transient flow models, and we can establish the flow regime according to Taitel & Duckler's recommendations for each

point in the space-time grid. We also realize that some trial and error is involved. In most cases, though, the flow regime in the next time-step is going to be the same as it was in the previous step, and in practice trial and error is restricted to relatively few cases.

The Taitel & Duckler-model has proven to agree quite well with measurements in small-diameter two-phase flow for horizontal and slightly inclined pipes. If we make similar plots within the model's validity range ($\pm 10^0$ inclination), we will see that even small inclination changes have dramatic consequences for the flow regimes, reflecting the fact that knowing and also implementing the pipeline's elevation profile accurately is essential to the results.

In addition to the limitations in the inclination range, we see other weaknesses when we look at the diagram: We have not established any criteria to differentiate between the different sorts of intermittent or annular flow. Intermittent flow can be separated into elongated bubble, slug, and churn flow, while annular flow can be with or without droplets in the gas stream, and with a smooth or wavy surface for the liquid film on the pipe wall. We recall that liquid film entrainment and droplet deposition for annular flow was discussed in chapter 4.

11.3 Flow regimes in vertical flow

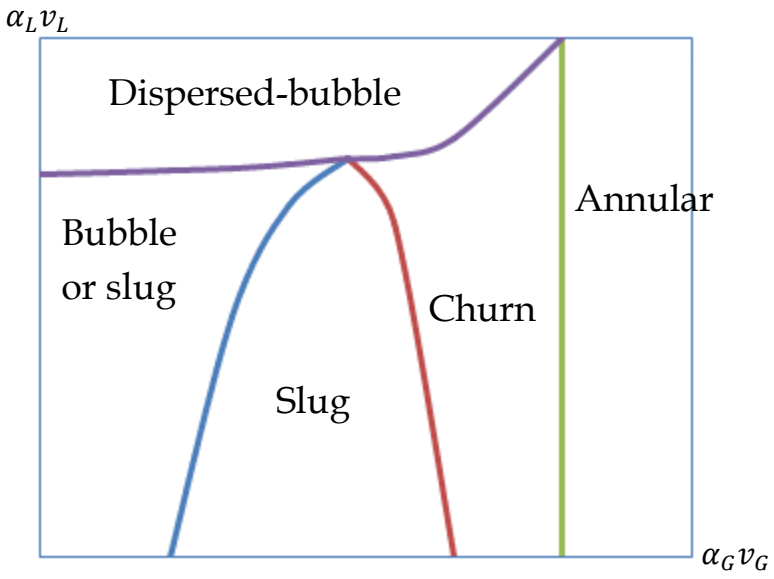

Figure 11.3.1. Typical vertical flow regime map. Each flow regime is illustrated in figures 1.2.3.

Two-phase vertical flow is somewhat more chaotic than horizontal flow, and it is more difficult to determine the flow regime by visually inspecting the flow in the laboratory. There is not even a universally agreed-upon list of which flow regimes actually exist. Unsurprisingly, this has lead to even larger spreads in flow regime models for vertical flow compared to horizontal flow.

Of the many different models proposed by various authors, the one by Taitel et al. (1980) is one of the most utilized. The flow patterns considered in their model are bubble flow, slug flow, churn flow, annular flow and dispersed-bubble flow. We will have a closer look at how their model predicts the flow regime in vertical flow.

11.3.1 Bubble to slug transition

Before discussing what makes bubble flow become slug flow, it is interesting to observe that bubble flow cannot exist in vertical two-phase flow for small diameter pipes. The reason for this can best be seen by comparing the rise speed for small and large bubbles. In a small bubble, the surface tension tends to be large compared to the bubble's buoyancy. The surface tension tries to make the surface as small as possible, and that leads to small bubbles being spherical. The drag force on spheres was discussed regarding droplets in chapter 5.3, and the same theory is directly applicable for bubbles. The drag force can be described similar to equation 5.2.3, and that force can be set equal to the buoyancy so we get:

$$F_{1\,Bubble} = \frac{C_D \rho_L}{2} \frac{\pi {d_B}^2}{4} {v_{0\infty}}^2 = \frac{\pi {d_B}^3}{6} (\rho_L - \rho_G) g \tag{11.3.1}$$

This leads to the following rise velocity for (small) spherical bubbles:

$$v_{s\infty} = \left[\frac{4 d_B (\rho_L - \rho_G) g}{3 C_D \rho_L} \right]^{0.5} \tag{11.3.2}$$

For somewhat larger bubbles, the shape is no longer spherical, and Harmathy (1960) found that the steady-state rise velocity is:

$$v_{max\infty} = 1.53\left[\frac{(\rho_L - \rho_G)g\sigma_{LG}}{{\rho_L}^2}\right]^{0.25} \tag{11.3.3}$$

The bubble rise velocity for large bubbles is – somewhat counter-intuitively, perhaps – independent of the bubble's size. It indicates that there is a certain maximum bubble rise velocity, above which the velocity never rises even if we keep increasing the bubble size. The reason is that larger bubbles deform, and this deformation happens in such a way as to make the velocity remarkably independent of size.

If we set $v_{s\infty} = v_{max\infty}$, we can determine the critical diameter, defined as the smallest diameter which can achieve the maximum rise velocity:

$${d_B}_{min}^{\ *} = 1.76C_D\left[\frac{\sigma_{LG}}{(\rho_L - \rho_G)g}\right]^{0.5} \tag{11.3.4}$$

As an example, consider air bubbles in water at atmospheric pressure. If we set $\rho_G = 1.2\ kg/m^3$, $\rho_L = 998\ kg/m^3$ and $\sigma_{LG} = 0.073\ N/m$, equation 1.3.3 leads to $v_{max\infty} = 0.25\ m/s$. If the water's kinematic viscosity is $\nu = 10^{-6}\ m^2/s$ and we at first guess ${d_B}^*$ to be in the order of $3 \cdot 10^{-3} m$, the Reynolds number becomes 750. The drag coefficient C_D can then be found from figure 5.2.1 or equation 5.2.1, and it is in the order of *0.5*. From equation 1.3.4 it follows that $d_{B\,crit} = 2.4\ mm$. This corresponds to what many of us have observed when a diver's bubbles rise at amazingly similar velocity even if they vary a lot in size (at least those bubbles which are larger than *2.4 mm* in diameter).

Taylor-bubbles, on the other hand, have another rise velocity than the one described by equations 1.3.2 or 1.3.3. Dumitrescu (1943), Davis & Taylor (1950), and Nicklin et al. (1962) found that the rise velocity for Taylor-bubbles in vertical pipes is:

$$v_{G\,T} = 0.35\sqrt{gd} \tag{11.3.5}$$

We see that the larger the diameter, the faster a Taylor-bubble rises. If a Taylor-bubble starts to form, it is going to rise faster than other bubbles (as described by equation 1.3.3) only if the pipe diameter is above a certain size. It turns out that when such a forming Taylor-bubble reaches smaller, slower bubbles, the smaller bubbles simply pass

around the Taylor-bubble and do not contribute to Taylor-bubble growth. In case the smaller bubbles move fastest, they rise in under the Taylor bubble's tail and merge with it. This means that for slow-moving Taylor-bubbles, which occur in small-diameter pipes, Taylor-bubbles 'swallow' all smaller bubbles, and bubbly flow will always become slug (for moderate liquid rates, otherwise we get dispersed bubble flow, see figure 11.3.1). That is why bubble flow does not occur in small diameter pipes.

If we use equations 11.3.3 and 11.3.5 to set $v_{max\infty} = v_{G\,T}$, we can calculate the diameter which corresponds to Taylor-bubbles and smaller bubbles rising at the same velocity, and hence the critical pipe diameter which the pipe diameter must be above for bubble flow to be able to occur is:

$$d_B{}^* = 19\left[\frac{(\rho_L - \rho_G)\sigma_{LG}}{\rho_L{}^2 g}\right]^{0.5} \tag{11.3.6}$$

If we insert the same air-water data as in the example below equation 11.3.4, we see that bubble flow can occur if the pipe diameter $d \geq 5.2\ cm$.

For pipes with a large enough diameter for bubble flow to occur at relatively low superficial gas velocities (see figure 11.3.1), it is assumed that if we continue to increase the gas fraction, the bubble fraction will eventually become so high that neighboring bubbles start merging with each other. It turns out that the bubble fraction does not have to be so high that the bubbles actually touch each other before this starts to occur. Measurements have shown that Taylor-bubble growth takes place if $\alpha_G \geq 0.25$.

The bubble rise velocity calculated with equation 11.3.3 does of course correspond to the difference between gas bubbles and liquid velocity, so that:

$$v_{max\infty} = v_G - v_L \tag{11.3.7}$$

If we insert equation 11.3.3 into equation 11.3.7, as well as $\alpha_L = 1 - \alpha_G = 0.75$, the line separating bubble and slug flow in figure 11.3.1 is described by:

$$\alpha_L v_L = 3\alpha_G v_G - 1.15\left[\frac{(\rho_L - \rho_G) g \sigma_{LG}}{{\rho_L}^2}\right]^{0.25} \quad (11.3.8)$$

11.3.2 Transition to dispersed-bubble flow

Dispersed bubble flow occurs at high liquid flow rates. The driving mechanism is that the liquid turbulence becomes strong enough to mix the bubbles into the liquid with a force large enough to overcome the bubble's buoyancy. The turbulence also contributes to breaking up the bubbles so that they are relatively small. The surface tension tries to keep the bubbles together, while the turbulence tries to rip them apart. Hinze (1955) proposed that the maximum bubble diameter of the dispersed phase can be described as:

$$d_{B\,max} = k_\varepsilon \frac{\left(\frac{\sigma_{LG}}{\rho_L}\right)^{0.6}}{\varepsilon^{0.4}} \quad (11.3.9)$$

The energy dissipation pr. unit mass, ε, can for pipe flow be estimated from the friction as:

$$\varepsilon = \left|\frac{dp_f}{dx}\right| \frac{v_M}{\rho_M} \quad (11.3.10)$$

The index M stands for mixture, indicating that gas bubbles and liquid flow at the same velocity v_M, and that the average density ρ_M can be used in equation 11.3.10 (see equation 1.5.3 for definition of ρ_M).

The friction pressure loss can be determined by the Darcy-Weisbach correlation:

$$\left|\frac{dp_f}{dx}\right| = \frac{f \rho_M {v_M}^2}{2d} \quad (11.3.11)$$

For the purpose of calculating the Darcy-Weisbach friction factor, the Blasius smooth pipe correlation is often considered accurate enough (see *Pipe Flow 1*, table 2.13.2. It can

easily be replaced by one of the more advanced correlations, though). The Reynolds number is based on the liquid data:

$$f = \frac{0.3164}{\left(\frac{v_M d \rho_L}{\mu_L}\right)^{0.25}} \tag{11.3.12}$$

Hinze (1955) suggested a constant value for $k_\varepsilon = 0.725$. Barnea et al. (1985) modified this value to account for the bubbles affecting the turbulence. Shoham (2006) reported that these results can be used to modify equation 1.3.8 to:

$$d_{B\,max} = \left(0.725 + 4.15\sqrt{\frac{\alpha_G v_G}{\alpha_G v_G + \alpha_L v_L}}\right)\frac{\left(\frac{\sigma_{LG}}{\rho_L}\right)^{0.6}}{\varepsilon^{0.4}} \tag{11.3.13}$$

If $d_{B\,max}$ is small enough, the theory states, the bubbles will keep a nearly spherical shape, and will not agglomerate to form any other than dispersed bubble flow. Brodkey (1967) suggested a correlation for what this critical size is, a correlation later modified by Barnea et al. (1982) into:

$$d_{B\,disp} = 2\left[\frac{0.4\sigma_{LG}}{(\rho_L - \rho_G)g}\right]^{0.5} \tag{11.3.14}$$

Dispersed-bubble flow occurs if:

$$d_{B\,max} \leq d_{B\,disp} \tag{11.3.15}$$

The boundary for dispersed-bubble flow in figure 11.3.1 is then determined by equations 11.3.13 and 11.3.14 as:

$$\left(0.725 + 4.15\sqrt{\frac{\alpha_G v_G}{\alpha_G v_G + \alpha_L v_L}}\right)\frac{\left(\frac{\sigma_{LG}}{\rho_L}\right)^{0.6}}{\varepsilon^{0.4}} = 2\left[\frac{0.4\sigma_{LG}}{(\rho_L - \rho_G)g}\right]^{0.5} \quad (11.3.16)$$

ε is calculated using equations 11.3.10 and 11.3.11. According to this theory, slug flow cannot exist for higher $\alpha_L v_L$ than what is given by this equation.

There is also another limitation in when dispersed-bubble flow can exist. If the gas content is very high, the bubbles touch or even cut into each other so that long, continuous bubbles form. This leads to churn flow, or for even higher gas fractions, annular flow. For the highest gas contents, the boundary between dispersed-bubble and churn flow is therefore found to be described by (see the right-side bend of the uppermost line in figure 13.3.1):

$$\frac{\alpha_G v_G}{\alpha_G v_G + \alpha_L v_L} = 0.52 \quad (11.3.17)$$

11.3.3 Slug to churn transition

If we have slug flow and start increasing the gas content, the bubble concentration increases more and more, and the coalescence between bubbles increases, too. The slugs become shorter and frothy, and the Taylor-bubbles increase in length. Eventually, the liquid slugs' length become zero, and transition to churn flow occurs. Churn flow is in some ways more chaotic than slug flow, since the interface between gas and liquid is not well defined, even though a strong fluctuation in gas and liquid fractions remain. Shoham (2006) suggested that in vertical pipes where slug flow occurs some distance inside the pipe, the flow is always churn at the pipe inlet. The entry region – the length of pipe required for the flow to switch from churn to slug – is according to this theory described by:

$$\frac{L_e}{d} = 40.6\left(\frac{v_M}{\sqrt{gd}} + 0.22\right) \tag{11.3.18}$$

For a given length inside the pipe, equation 11.3.18 results in a value for the mixture velocity $v_M = \alpha_G v_G + \alpha_L v_L$, and that enables us to plot a curve for $\alpha_L v_L(\alpha_G v_G)$, which forms the boundary between slug and churn flow in figure 11.3.1.

11.3.4 Transition to annular flow

For very high gas flow rates, annular flow occurs. As already described, the liquid forms a film on the pipe wall, and part of that film is torn off to form droplets. In upward vertical flow, the gas must flow fast enough for these droplets to be transported with the gas. Otherwise the gravity will make the droplets fall and accumulate, and churn or slug flow will form. The so-called droplet model, proposed by Turner et al. (1969), simply suggests that transition to annular flow occurs when the velocity in the core is high enough to lift the droplets. As with spherical bubbles, we can easily establish the steady-state spherical droplet momentum balance by looking back to chapter 5.3:

$$F_{1\,Drop} = \frac{C_D \rho_G}{2} \frac{\pi {d_D}^2}{4} {v_G}^2 = \frac{\pi {d_D}^3}{6}(\rho_L - \rho_G)g \tag{11.3.19}$$

We can re-formulate this as:

$$v_G = \sqrt{\frac{4(\rho_L - \rho_G)g d_D}{3 C_D \rho_G}} \tag{11.3.20}$$

For equation 11.3.20 to be useful, the droplet diameter must be known (how to determine maximum stable droplet diameter was outlined in chapter 5.6). For the purpose of determining the flow regime, it has been found that droplet diameter can be described by a critical Weber number ${We_{DG}}^*$ between 20 or 30. We also assume $v_L \ll v_G$

so that we can set $v_L = 0$. Using this, the droplet diameter follows from equation 5.6.4, which we insert into equation 11.3.2 to get:

$$v_G{}^* = \left[\frac{4We_{DG}{}^*\sigma_{LG}g(\rho_L - \rho_G)}{3C_D\rho_G{}^2}\right]^{0.25} \tag{11.3.21}$$

If we want to plot a diagram like the one in figure 11.3.1 for data specific to a certain pipe (the criteria described here are normally used directly in the simulation program - not primarily to plot flow regime diagrams), we may take advantage of the fact that the gas fraction α_G is close to *1* for annular flow, so that $\alpha_G v_G \approx v_G$. The line separating churn and annular flow then becomes a vertical line directly described by equation 1.3.21.

11.4 Flow regimes in inclined pipes

Most measurements on multi-phase flow have been carried out on horizontal and vertical pipes, so the models in chapter 11.2 and 11.3 are generally more reliable than models for any other inclinations. Still, pipes and wellbores can occur at any inclination, and we need to deal with those as well. It has been shown that a slight upward inclination causes the intermittent flow area in figure 11.2.1 to expand and take place for a wider range of flow conditions. The stratified to intermittent transition is very sensitive to the pipe's angle. This has been illustrated in figure 11.4.1, where a gas of density $\rho_G = 2$ kg/m^3 flows through the same pipeline as liquid of density $\rho_L = 1000$ kg/m^3. Assuming steady-state incompressible flow, pipe diameter $d = 0.5m$ and gas mass flow $\alpha_G\rho_G v_G = 2.51\ kg/s$, while the liquid mass flow is $\alpha_L\rho_L v_L = 35.3\ kg/s$, calculations according to equation 3.9.2 leads to $\alpha_L = 0.36$ in the entire pipe, which is what is illustrated in the uppermost pipe in figure 11.4.1. Bending the pipe very slightly to a U-shape, from -1^0 to +1^0, reduces α_L to only half that of the steepest downhill inclination, while it grows to around 0.68 at the slight uphill inclination. That would probably have been enough for slugs to form, something these simple calculations did not check.

As already mentioned, the Taital & Dukler model in chapter 11.2 can be used for up to 10^0 inclination. For higher inclinations, the methods below are recommended.

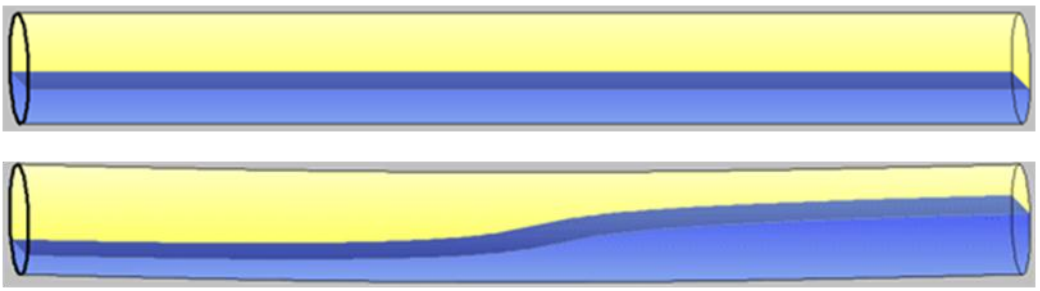

Figure 11.4.1. Stratified flow in straight pipe (top), slightly U-shaped pipe (so slight that it can hardly be seen on the figure) from -1⁰ inclination downwards to +1⁰ inclination upwards (bottom). The computer program used to create these plots is freely available at this book's internet site.

11.4.1 Bubble to slug transition

The bubble to slug transition discussed in chapter 11.3.1, equation 11.3.8, is now modified to take into account the bubble rise velocity along the pipe axis:

$$\alpha_L v_L = 3\alpha_G v_G - 1.15\left[\frac{(\rho_L - \rho_G) g \sigma_{LG}}{{\rho_L}^2}\right]^{0.25} \sin\theta \qquad (11.4.1)$$

As for vertical flow, equation 11.3.6 can be used to determine whether the pipe can experience bubble flow. It has been suggested, though, that in addition to that criterion we must also have pipe inclination angles higher than 60⁰ before bubble flow can occur. For lower inclinations, the bubbles tend to aggregate along the pipe's upper surface and create large bubbles and therefore slug flow (Shoham, 2006).

11.4.2 Transition to dispersed-bubble flow

This mechanism is thought to be independent of pipe inclination, and the results from chapter 11.3.2 are considered directly applicable.

11.4.3 Intermittent to annular transition

Here we simply use the same principle as for vertical pipes in chapter 11.3.4, but we use the gravity component along the pipe's axis to determine whether the gas manages to carry the liquid uphill:

$$v_G = \left[\frac{4We_{DG}{}^{*}\sigma_{LG}g\sin\theta\,(\rho_L-\rho_G)}{3C_D\rho_G{}^{2}}\right]^{0.25} \tag{11.4.2}$$

We realize that this criterion no longer makes sense when we approach horizontal pipes, since that would push the churn-annular line to the far right in the flow regime map, making all flow annular. It should therefore only be used down to 10^0 inclination, where the Taitel & Dukler-model is allowed to take over.

11.4.4 Slug to churn transition

The region of churn flow shrinks considerably once the pipe is no longer vertical, and it disappears completely for inclinations below 70^0. It is common to model this in the same way as intermittent flow, even though strictly speaking it is not. Agreement has still been found to be reasonable (Shoham, 2006).

11.4.5 Downward inclination

For moderate downward inclination, from 0 to -10^0, the flow regime can be quite well predicted with the Taitel & Dukler (1976) model. Steeper downward inclinations than that are relatively rare in pipelines, wellbores and risers. Also, slug flow, the flow regime generally causing us most trouble, is less common for downhill inclinations than for horizontal and uphill flow. Therefore we are not going to outline flow regime change in steep downward inclinations with the same degree of detail as in other inclinations, but we will discuss it briefly. A more thorough discussion of it can be found in Shoham (2006).

As illustrated in figure 11.4.1, even very slight downward inclination has large impact on stratified flow. When gravity assists in driving the liquid forward, less liquid builds up in the pipe, and the stratified flow regime is considerably expanded. This change

primarily takes place for angles from 0 to -10^0, which happens to be within the range covered by the already discussed Taitel & Dukler (1976) model. At inclinations below -10^0, the flow regime switches directly from stratified to dispersed bubble flow according to equation 11.3.16. At around -70^0, increasing the inclination angle further results in a gradual change from stratified to annular flow. The annular region is expanded, while the stratified region shrinks until it disappears completely at vertical downward flow.

Intermittent to annular transition occurs when stratified flow is unstable at the same time as not enough liquid is available to form slugs. The modified Barnea et al. (1980)-criterion (equation 11.2.14) can be used to predict this transition boundary. At inclinations steeper than -70^0, the flow can stay annular down to very low gas flow rates. Transition to dispersed-bubble flow is independent of inclination angle and can be determined as outlined in chapter 11.3.2.

Transition from stratified-smooth to stratified-wavy flow can be predicted using equation 11.2.13. But in downward flow, the liquid surface can also become wavy due to instability on the interface (not caused by the interfacial shear between phases described by equation 11.2.13), and Barnea et al. (1982) suggested this happens if the Froude number becomes higher than 1.5:

$$Fr = \frac{v_L}{\sqrt{g h_L}} > 1.5 \tag{11.4.3}$$

v_L and h_L are calculated as in the Taitel & Dukler (1976) model. We therefore need to use equation 11.4.3 for low gas flow rates, and equation 11.2.13 for high gas rates.

Transition from stratified to annular flow at low gas flow rates and steep downward inclinations happens because liquid is torn off from the surface and entrained into the gas flow, and further deposited at the top of the pipe, forming a continuous liquid film on the pipe wall. The energy for this process originates in the liquid flow, not the gas, and happens if the liquid velocity:

$${v_L}^2 > \frac{g d \cos\theta \left(1 - \frac{h_L}{d}\right)}{f_{LW}} \tag{11.4.4}$$

In downwards vertical flow, the dominant flow regime is annular flow. Experiments with air-water two-phase flow have shown transition from annular to slug flow happens at around $\alpha_L v_L = 0.6$, and transition to dispersed bubble flow happens at around 2.

11.5 The minimum-slip flow regime criterion

We have seen that the Tatel & Dukler model is based on starting out by assuming stratified flow, and then switching to other flow regimes if certain criteria are met. Wallis (1969) proposed an alternative way to describe the transition from annular to slug flow: He simply calculated the flow as if it were annular, then as if it were slug flow, and then chose the one which turned out to lead to least average velocity difference between gas and liquid. Wallis showed that this method usually agreed well with measurements, even though the physics underpinning *the minimum slip criterion* are unclear. Bendiksen et al. (1991) went further in their model: They used the same criterion to determine transition from stratified to bubble flow, from stratified to slug flow, from annular to slug flow, and from annular to bubble flow.

Bendiksen et al. used some other criteria, too. In distributed flow, bubble flow is obtained continuously when all gas is carried by the liquid slugs, leaving no gas for the Taylor-bubbles. This occurs when the gas fraction in the liquid slug, α_{GS}, becomes larger than the average gas fraction, α_G. Stratified to annular flow transition happens when the wave height reaches the top of the pipe. To determine wave height, they used the following correlation:

$$h_w = \frac{1}{2}\left\{\frac{\rho_G(v_G - v_L)^2}{2(\rho_L - \rho_G)g\cos\theta} + \sqrt{\left[\frac{\rho_G(v_G - v_L)^2}{2(\rho_L - \rho_G)g\cos\theta}\right]^2 - \frac{4\sigma_{LG}}{(\rho_L - \rho_G)g\cos\theta}}\right\} \qquad (11.5.1)$$

The much-used commercial computer code OLGA is according to Bendiksen et al. (1991) based on these criteria. It is difficult claiming that their validity is well documented in open publications, even though OLGA has been shown to perform well for some simulations. Details on exactly how the criteria have been implemented remain unpublished, and it is known that modifications to OLGA have been done in numerous projects after Bendiksen et al.'s publication. It is possible that those modifications may have included adjusting the flow regime criteria.

We notice that the minimum slip criterion has the advantage of being applicable to any pipe inclination as well as to both normal pipes and perforated pipes with inflowing fluid (typically wellbores), and it can also in principle be applied to any number of phases. This flexibility is very attractive, but the lack of any published, solid theoretical foundation for the theory behind it is not.

"Mathematics may be defined as the subject in which we never know what we are talking about, nor whether what we are saying is true."
Bertrand Russell, 1917

12 Numerical solution methods

Which numerical solution methods to use, and which potential problems to look out for while using them:

- Essential properties of numerical integration methods
- Essentials about hyperbolic equations
- Solving systems of hyperbolic equations
- How to account for source terms in the hyperbolic equations
- How to select appropriate discretization methods
- The TR-BDF2 method as an example of an implicit method
- Liles and Reed's semi-implicit method
- Solving nonlinear equation systems with Newton and Newton-Krylov iteration

12.1 Some essentials about numerical methods

12.1.1 Some problems with higher order methods

We recall from *Pipe Flow 1* that for single-phase flow, we used the Kurganov-Tadmor spatial discretization scheme of order 3 (*KT3*), and we simulated the discrete pipe model in time by a variable-step explicit Runge-Kutta order 4-5 algorithm (*RK4-5*). That worked well: The KT3-scheme's high order made it possible to use a relatively course

grid and still get reasonable accuracy, and it also had very favorable numerical dissipation and dispersion properties. For that reason the moderate time-steps imposed by RK4-5's stability properties turned out to be acceptable and we could simulate even very long pipelines much faster than real time.

That approach is not necessarily applicable to multi-phase flow, since the equations no longer are on the form $\partial Y/\partial t + \partial F/\partial x = D$. Some models, for instance the drift-flux model, allow us to bring the equations over to this form, but when dealing with multi-phase flow, we are not in the situation that any model formulation fits into the KT3-scheme. Besides, if we have phase change (boiling or condensation), eigenvalue studies have shown that the fastest phenomena involved are not the pressure wave propagation , but the phase change itself, as illustrated by Masella et al. (1998) and Omgba-Essama, (2004). We therefore end up with a much stiffer set of equations in multi-phase flow, and the necessity for implicit schemes increases.

There is also another reason why it is more difficult to take advantage of higher order schemes in multi-phase flow. Some multi-phase flow phenomena are very sensitive to the pipe's local elevation angle. If the pipe has frequent elevation angle changes – a common situation for most pipelines – our grid needs to be dense enough to represent the elevation profile accurately. That (sometimes in addition to other phenomena) leads to a need for very fine grid even when numerical accuracy would otherwise not require it. When the fine grid results in numerical accuracy exceeding the model's accuracy, there is no further gain to be made by increasing the numerical method's order.

Although high order is a desirable property for any numerical method, discontinuities and the need to represent the elevation profile accurately make high order methods less advantageous in multi-phase than single-phase pipe flow.

12.1.2 Using Taylor-expansion to approximate

Some of the most important properties of even complex numerical integration methods can be well illustrated by using them on the very simple, one-dimensional equation 12.1.1:

$$\frac{dy(t)}{dy} + ay(t) = 0 \qquad (12.1.1)$$

As we saw in chapter 9 in *Pipe Flow 1*, we may approximate a derivative by looking at a Taylor-expansion from time level *j* to level *j+1*:

$$y_{i,j+1} = y_{i,j} + \Delta t \left(\frac{\partial y}{\partial t}\right)_{i,j} + \frac{1}{2}\Delta t^2 \left(\frac{\partial^2 y}{\partial t^2}\right)_{i,j} + \cdots, \tag{12.1.2}$$

Since equation 12.1.1 does not have any spatial derivatives, we drop the *i*-index. Equation 12.1.2 can then be solved for $\partial y/\partial t$ (which is the same as dy/dt in equation 12.1.1 since only one sort of derivative occurs there), and we get:

$$\left(\frac{\partial y}{\partial t}\right)_j = \frac{y_{j+1} - y_j}{\Delta t} - \frac{1}{2}\Delta t \left(\frac{\partial^2 y}{\partial t^2}\right)_j + \cdots, \tag{12.1.3}$$

Inserting 12.1.3 into 12.1.1 leads to:

$$\frac{y_{j+1} - y_j}{\Delta t} - \frac{1}{2}\Delta t \left(\frac{\partial^2 y}{\partial t^2}\right)_j + \cdots, + a y_j = 0 \tag{12.1.4}$$

And finally:

$$y_{j+1} = (1 - a\Delta t) y_j + \frac{1}{2}\Delta t^2 \left(\frac{\partial^2 y}{\partial t^2}\right)_j + \cdots, \tag{12.1.6}$$

12.1.3 Truncation error, order, stability, consistency, and convergence

If we had included all terms in the Taylor-expansion, equation 12.1.6 would have been exact. Since there is an infinite amount of terms, that is clearly impossible in practice. But for smooth functions, the first term in the Taylor-expansion is generally the largest, with each subsequent term being smaller than the previous. If we do not include the term containing Δt^2, the *truncation error* – the error resulting from not including all Taylor-expansion terms – is dominated by the term containing Δt^2. The *local truncation error* – the truncation error resulting from a single time-step - is therefore going to be

(nearly) proportional to Δt^2. If we reduce the time-step, for instance by halving it, we can expect the local truncation error to be reduced to $1/2^2 = 1/4$. That is a very nice result, because it indicates we gain more than a proportional amount of accuracy if we reduce the step length Δt.

Since we need more steps to reach a certain point in time if we reduce the step length, it leads to error contributions from a larger number of steps, and this accuracy reduction is proportional to the number of time-steps required. The overall consequence of reducing the step length – the *global truncation error* - is therefore one order less favorable than the local truncation error. The *Explicit Euler Integration Method*, as this is referred to, is therefore said to be of order *1*, meaning the global truncation error is proportional to the step length in power *1*. Had we included one more of the terms in the Taylor-expansion (and managed to find an estimate for it), we would have ended up with an integration method of order 2.

This leads us to one important conclusion: The explicit Euler-method can achieve any required global accuracy, as long as we choose a short enough time-step. Put another way, the error approaches zero if the time-step approaches zero. That property is called *consistency*, and it is one of the conditions required for the method to be usable.

If we start the integration at the starting value $y_j = y_0$ for $j = 0$ and ignore all higher order Taylor terms, we see that after $j + 1$ integrations, equation 12.1.6 leads to:

$$y_{j+1} = (1 - a\Delta t)^{j+1} y_0 \tag{12.1.7}$$

If $1 - a\Delta t > 1$, or $1 - a\Delta t < -1$, we see that as we integrate and j becomes larger and larger, the factor in front of y_0 is also going to increase accordingly. In the latter case, the solution is obviously also going to oscillate, since a negative number in power j, where $j = 1, 2, 3, \ldots$ shifts between positive and negative as j shifts between even and odd. Either way, the contribution from the initial value is going to grow forever. If the initial value was partly incorrect, the error would also grow infinitely. In addition, any errors coming into the equation at a later stage (such as the *computer round-off error*, due to the computer's inability to represent real numbers with infinite accuracy), are also going to grow progressively for each time-step. To avoid this, stability generally requires:

$$|1 - a\Delta t| \leq 1 \tag{12.1.8}$$

Since the time-step must be larger than *0*, we see that the real part of a has to be positive: $a \geq 0$. That is in fact a physical stability requirement which would also arise in an analytical solution of equation 12.1.1, so the numerical method produces stability in the same situation as the physical system. It is comforting to see that the numerical solution and the analytical one agree with each other in that respect, that is not the case for all numerical solution methods. But equation 12.1.8 also requires $\Delta t \leq 2a$. That is a very characteristic type of restriction for explicit integration methods: There is a maximum time-step beyond which the integration method becomes unstable. That requirement has no analogy in the physical system equation 12.1.1 describes, it is a purely numerical phenomenon. But at least we see that as long as we keep the time-step small enough, the explicit Euler method is *stable*.

The *Lax Equivalence Theorem* states that when a method is both *stable* and *consistent*, the method is also *convergent*. For small enough time-steps, (namely those satisfying equation 12.1.8), the explicit Euler method is convergent, meaning it produces an ever improved approximation for the real solution of equation 12.1.1 the smaller time-steps we use. If the required time-step is very small, we run into trouble because it takes very long time to simulate the required time-span into the future.

We can also get problems due to the machine round-off error becoming significant, particularly for small time-steps. That can for instance lead to the result from the last time step being so similar to that of the previous that they are rounded off to the same number. But as seen from a purely mathematical point of view, stability and consistency are the two required properties for an integration method to work.

A numerical integration method *must* be stable and consistent.

It is *desirable* that a numerical integration method, if it were possible, has:

1. **The same stability area as the physical system it simulates,**
   - **reproducing physical instabilities when they occur in the physical system,**
   - **not becoming unstable for purely numerical reasons**
2. **A high order, making the method relatively accurate even for long time steps.**

12.1.4 Implicit integration methods

If we had approximated the value $ay(t)$ in equation 12.1.1 with ay_{j+1} rather than ay_j, equation 12.1.4 would have become:

$$\frac{y_{j+1}-y_j}{\Delta t}-\frac{1}{2}\Delta t\left(\frac{\partial^2 y}{\partial t^2}\right)_j+\cdots,+ay_{j+1}=0 \tag{12.1.9}$$

Ignoring higher order terms leads to:

$$(1+a\Delta t)y_{j+1}=y_j \tag{12.1.10}$$

And hence:

$$y_{j+1}=\frac{1}{1+a\Delta t}y_j=\left(\frac{1}{1+a\Delta t}\right)^{j+1}y_0 \tag{12.1.11}$$

This way of integrating is called *implicit Euler integration*. It is implicit in the sense that it uses the derivate for the time-step it has yet to calculate the argument for. In this very simple case with only one linear equation, basic algebra results in a direct way to calculate each 'implicit' time-step. That is not possible for more complicated nonlinear systems of equations, and we need to iterate to find the solution for each time-step.

For the same reason as described for explicit Euler integration, implicit Euler integration is stable and therefore also convergent (since consistency is satisfied for the same reason as for explicit Euler integration) if:

$$\left(\frac{1}{1+a\Delta t}\right)\leq 1 \tag{12.1.12}$$

For a physically stable system, where $a>0$, any step length Δt is going to satisfy equation 12.1.12. In this case, as is often the case for implicit integration methods used on linear systems, we do not run into stability problems as long as the physical system itself is stable. Long time-steps can of course lead to poor accuracy, since the truncation

error increases, but at least we are not going to experience instability (which typically materializes itself as a program crash with the simulations stopping).

Equation 12.1.12 also reveals something less desirable: Even unstable physical systems ($a < 0$) can lead to stable integration if Δt is large enough. It indicates the simulations may run smoothly and tell us that the system works well even when it does not! Implicit methods have built-in numerical damping, and that makes them somewhat insensitive to many physical problems we would want them to expose. It means conservation equations which are not well posed, for instance the ones we end up with if we neglect the pressure correction terms for stratified flow (setting $\partial \Delta p_G / \partial x = 0$ and $\partial \Delta p_L / \partial x = 0$ in equations 3.3.2 and 3.3.3, say), may still lead to seemingly sensible results. Also, most programming or input data errors tend to lead to instabilities when we use explicit integration methods, and that has the desirable effect of making us aware of them.

Implicit integration methods are blunt tools in the sense that they tend to hide rather than expose physical instabilities and various errors. Still, they normally represent the best alternative and are much used since they allow long time steps without becoming numerically unstable.

12.1.5 Combining explicit and implicit methods

We would expect that if we took some sort of average of the (too stable) implicit and (not sufficiently stable) explicit method, we would end up with a numerical method having a stability area closer to that of the physical system. Let us try to use the mean average by setting:

$$ay = a\frac{y_{j+1} + y_j}{2} \tag{12.1.13}$$

This transforms equation 12.1.4 (or 12.1.9) into:

$$\frac{y_{j+1} - y_j}{\Delta t} - \frac{1}{2}\Delta t\left(\frac{\partial^2 y}{\partial t^2}\right)_j + \cdots, + a\frac{y_{j+1} + y_j}{2} = 0 \tag{12.1.14}$$

Ignoring higher order Taylor terms and expressing this by the initial value y_0, we get:

$$y_{j+1} - y_j = \left(\frac{2 - a\Delta t}{2 + a\Delta t}\right)^{j+1} y_0 \tag{12.1.15}$$

This method, called the *trapezoidal method*, turns out to be stable for any Δt as long as a's real part is positive, while it will be unstable if a's real part is negative. That means the trapezoidal method has the same stability area as the physical system – a rare, but for the most part desirable property. But it is not always a good thing. This method has much lower damping, and it allows numerical noise to live longer than implicit Euler-integration does. Also, if our model briefly becomes ill-posed, something it can be difficult to avoid for some of our multi-phase flow models, a more highly dampened method could be able to work its way through the (slightly) erroneous part and sometimes produce reasonable overall results, while the trapezoidal method would more easily result in the integration 'exploding' almost immediately. We will therefore later show a method which combines the trapezoidal method with some added damping, referred to as the *TR-BDF2* method.

It can be shown that the trapezoidal method is of global order *2*, which is much better than the two previous methods which were only of order *1*. Also, notice that the method uses information from the next time-step when estimating the derivative (in addition to information from the current step), so it is implicit. Our conservation equations are nonlinear, and the system of nonlinear equations we have to solve for each time step when we use an implicit method are typically fed less accurate starting values if the time-step is long. The overall integration method may therefore not be stable for very long time-steps even if we use an unconditionally stable (implicit) integration method. Long time steps can cause the solution of the algebraic equations to fail instead of the implicit integration method as such. Still, implicit integration is normally the fastest and most robust way available when we want to simulate multiphase pipe flow.

12.2 Some essentials about hyperbolic equations

Our conservation equations are hyperbolic, at least if they are well posed. For the purpose of understanding some fundamentals of hyperbolic equations, let us look at a very simple linear equation:

$$\frac{\partial u}{\partial t} + a\frac{\partial u}{\partial x} = 0 \qquad (12.2.1)$$

This is quite similar to the heat equation shown in the simplified model in chapter 9.1. in *Pipe Flow 1*, but in this case without any of the terms to do with heat or work exchange with the environment. We showed that it had a single characteristic, corresponding to the heat transport in the pipe flow (such as hot water travelling downstream with the current).

We have seen how easy it is to replace a derivative with a simple numerical approximation. Could we just replace each of the two derivatives in equation 12.2.1 with such an approximation and produce a solution that way? What if we use first order Taylor-expansion on the time derivative as in 12.1.3 (indicated as thick, vertical line in the grid in figure 12.2.1) and a second order central approximation of the spatial derivative (thick horizontal line), so that:

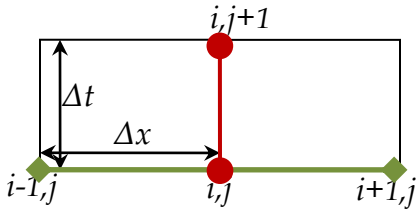

Figure 12.2.1. Graphical illustration of equation in the space-time grid.

$$\frac{du}{dt} \approx \frac{u_{i,j+1} - u_{i,j}}{\Delta t} \qquad (12.2.2)$$

$$\frac{du}{dx} \approx \frac{u_{i+1,j} - u_{i-1,j}}{2\Delta x} \qquad (12.2.3)$$

That would lead to:

$$u_{i,j+1} = u_{i,j} - \frac{a\Delta t}{2\Delta x}\left(u_{i+1,j} - u_{i-1,j}\right) \qquad (12.2.4)$$

Equation 12.2.4 is symmetrical and at first glance it seems perfectly OK. It is also consistent since the truncation error falls monotonously when we reduce Δt. But it can relatively easily be shown (using for instance von Neumann stability analysis, see Colella & Puckett, 1994) that it is unstable no matter which choice we make for Δt, it is *unconditionally unstable* and therefore not convergent. It means this method is useless!

If we replace equation 12.2.3 with a first-order *downwind* approximation so that:

$$\frac{du}{dx} \approx \frac{u_{i+1,j} - u_{i,j}}{\Delta x} \tag{12.2.5}$$

Equation 12.2.4 becomes:

$$u_{i,j+1} = \left(1 + \frac{a\Delta t}{\Delta x}\right) u_{i,j} - \frac{a\Delta t}{\Delta x} u_{i+1,j} \tag{12.2.6}$$

This, unfortunately, goes equally badly in that this method is also unstable for any choice of Δt if $a < 0$. It is possible to spot an intuitive reason why this method cannot possibly work: If we compare with the thermodynamic characteristic for equation 9.2.4 in *Pipe Flow 1*, a stands for the fluid's velocity, and it expresses that the temperature at a point in the pipe depends on the temperature upstream of it. Using equation 12.2.5 is similar to attempting to estimate the temperature in a point one time-step into the future by looking at the temperature of fluid which has already passed it. We must instead focus on the fluid which is going to arrive at the point of interest one time-step into the future, and that fluid comes from upstream. Therefore, we have to replace the *downwind* approximation of equation 12.2.3 with an *upwind* approximation, so that:

$$u_{i,j+1} = \frac{a\Delta t}{\Delta x} u_{i-1,j} + \left(1 - \frac{a\Delta t}{\Delta x}\right) u_{i,j} \tag{12.2.7}$$

This method turns out to be stable if:

$$0 < \frac{a\Delta t}{\Delta x} \leq 1 \; and \; a > 0 \tag{12.2.8}$$

So, finally we have something we can use. Notice that if the flow direction changes (as symbolized by the factor a), we need to switch from equation 12.2.7 to equation 12.2.6 so that we always use upwind differencing for the spatial derivative. This method is sometimes called the *first-order upwind method*.

If our hyperbolic equation is nonlinear, so that equation 12.2.1 can be considered a linearized version of the main equation, we need to keep track of which way the

characteristic goes to be able to decide what should be considered upwind. It becomes even more complicated if we have a system of many equations. When we used the characteristics method for pressure wave propagation in *Pipe Flow 1*, we learned that pressure waves travel both ways simultaneously. It then becomes less obvious which side is 'upwind'. We will have a closer look at that in the next chapter.

12.3 Solving systems of hyperbolic equations

12.3.1 Flux-vector splitting

Suppose that equation 2.2.1 is replaced by a system of linear equations of the form:

$$\frac{\partial U}{\partial t} + A\frac{\partial U}{\partial x} = 0 \tag{12.3.1}$$

$U = [u_1, u_1, \dots, u_N]^T$, and A is a N *x* N matrix. Solving hyperbolic equations on this form is sometimes called the *Riemann-problem,* and research regarding how best to do it is still ongoing. Having seen that the upwind method requires us to use upwind differences, the question becomes how to decide what is upwind when we have more than one equation.

The answer lies in decoupling equation 12.3.1 by using A's eigenvalues and eigenvectors. We may recall from mathematics that A can be expressed as:

$$A = K\Lambda K^{-1} \tag{12.3.2}$$

Where Λ is the diagonal matrix formed by the eigenvalues of A, and K is the matrix whose columns are the right eigenvectors of A. Remembering that hyperbolic equations have real eigenvalues, it seems intuitive that we can decide the 'upstream-problem' by looking at their signs. That is in fact a good idea, and we can split the eigenvalue matrix Λ by putting all positive eigenvalues in one, Λ^+, while all the negative ones are in the other, Λ^-, so:

$$\Lambda = \Lambda^+ + \Lambda^- \tag{12.3.3}$$

We can then ensure upwind-only differencing by setting:

$$U_{i,j+1} = U_{i,j} - \frac{\Delta t}{\Delta x} K \Lambda^{+} K^{-1} \left[U_{i,j} - U_{i-1,j} \right] - \frac{\Delta t}{\Delta x} K \Lambda^{-} K^{-1} \left[U_{i+1,j} - U_{i,j} \right] \tag{12.3.4}$$

The method is quite straight forward, but we see that it takes some effort to satisfy the upwind-requirement if we have a set of equations. If our equations are nonlinear, we have to linearize first by calculating the *local Jacobian* (not to be confused with the *global Jacobian* involved in the Newton-iteration in implicit integration methods) in each grid point first, and then calculate the local eigenvalues and eigenvectors.

As an example, recall that in chapter 7 in *Pipe Flow 1*, we introduced something called Allieiv's simplification for transient pipe flow (only reasonable for liquids, not gases) and got:

$$\frac{\partial p}{\partial t} = -\rho {a_s}^2 \frac{\partial v}{\partial x} \tag{12.3.5}$$

$$\frac{\partial v}{\partial t} = -\frac{1}{\rho}\frac{\partial p}{\partial x} - \frac{f}{2d} v|v| - g sin\theta \tag{12.3.6}$$

We recall that a_s is the speed of sound. If we neglect the so-called source terms (the ones to do with friction and elevation), this can be written as:

$$\frac{\partial}{\partial t}\begin{bmatrix} p \\ v \end{bmatrix} + \begin{bmatrix} 0 & \rho {a_s}^2 \\ \frac{1}{\rho} & 0 \end{bmatrix} \frac{\partial}{\partial x}\begin{bmatrix} p \\ v \end{bmatrix} = 0 \tag{12.3.7}$$

This system is linear, and we can determine the matrix's eigenvalues directly by setting $|A - \lambda I| = 0$. They are easily found to be $\lambda_1 = a_s,\ \lambda_{12} = -a_s$. The eigenvectors can then be found as $AK^{(1)} = \lambda_1 K^{(1)}$ and $AK^{(2)} = \lambda_2 K^{(2)}$, where the first eigenvector $K^{(1)} = [k_1, k_2]^T$ and similarly for the second. It turns out that solving $AK^{(1)} = \lambda_1 K^{(1)}$ in this particular case produces two linearly dependent equations, so we have in effect two unknowns and one equation. We can therefore choose one of them. One possible result becomes:

$$\Lambda = \begin{bmatrix} a_s & 0 \\ 0 & -a_s \end{bmatrix}, \Lambda^+ = \begin{bmatrix} a_s & 0 \\ 0 & 0 \end{bmatrix}, \Lambda^- = \begin{bmatrix} 0 & 0 \\ 0 & -a_s \end{bmatrix} \tag{12.3.8}$$

And

$$K = \begin{bmatrix} 1 & -1 \\ \frac{1}{a_s\rho} & \frac{1}{a_s\rho} \end{bmatrix}, leading\ to\ K^{-1} = \begin{bmatrix} \frac{1}{2} & \frac{a_s\rho}{2} \\ -\frac{1}{2} & \frac{a_s\rho}{2} \end{bmatrix} \tag{12.3.9}$$

By multiplying out $K\Lambda^+K^{-1}$ and $K\Lambda^-K^{-1}$ and insert into equation 12.3.4, we get:

$$\begin{bmatrix} p \\ v \end{bmatrix}_{i,j+1} = \begin{bmatrix} p \\ v \end{bmatrix}_{i,j} - \frac{\Delta t}{\Delta x} \begin{bmatrix} \frac{a_s}{2} & \frac{{a_s}^2\rho}{2} \\ \frac{1}{2\rho} & \frac{a_s}{2} \end{bmatrix} \left[\begin{bmatrix} p \\ v \end{bmatrix}_{i,j} - \begin{bmatrix} p \\ v \end{bmatrix}_{i-1,j} \right] - \frac{\Delta t}{\Delta x} \begin{bmatrix} \frac{a_s}{2} & -\frac{{a_s}^2\rho}{2} \\ -\frac{1}{2\rho} & \frac{a_s}{2} \end{bmatrix} \left[\begin{bmatrix} p \\ v \end{bmatrix}_{i+1,j} - \begin{bmatrix} p \\ v \end{bmatrix} U_{i,j} \right] \tag{12.3.10}$$

This method of solving the equations is called *flux-vector splitting*.

The stability restriction is as for the one-dimensional case, equation 12.2.6, but with a replaced with the largest eigenvalue, which is a_s.

Even though the explicit method shown in equations 12.2.5 and 12.2.4 can be used, it is not a natural choice in most commercial simulation software: The method only has order 1, and the stability properties are quite poor, leading to very short time-steps for multi-phase applications. But for small exercises or for performing simple checks, it may be a feasible alternative for simulating multi-phase flow. For the particular example the method was applied to here - liquid transient pipe flow - the method offers no apparent advantages over the familiar method of characteristics.

12.3.2 Lax-Friedrich's method

The Lax-Friedrich's method is another example of a simple first order method which can be used to solve linear equations on the form shown in equation 12.3.1. It can also more easily be used to solve nonlinear equations on the form:

$$\frac{\partial U}{\partial t} + \frac{\partial F(U)}{\partial x} = 0 \tag{12.3.11}$$

Lax-Friedrich's method is based on replacing $u_{i,j}$ in equation 12.2.2 with the average of its two spatial neighbors so that $u_{i,j} = \left(u_{i+1,j} + u_{i-1,j}\right)/2$. It turns out to be even more dissipative than the upwind method, so it is incapable of reproducing discontinuities accurately. Fast transients, such as the ones we get in case of fast pump startup or stoppage or fast valve operations are therefore not realistically simulated with this method. Doing the simulations is easy enough, but the transient will appear as if they are smoothened out much faster than they would have been in a real system. The method does, however, have the advantage of being fully explicit (like the upwind method), and in this simple example, it does not require us to perform any linearization to determine the Jacobian even if the equations are nonlinear (unlike the upwind method). Lax-Friedrich's method is very robust, though, and its simplicity is attractive. When applied to equation 12.3.11, the method becomes:

$$U_{i,j+1} = \frac{1}{2}\left(U_{i+1,j} + U_{i-1,j}\right) - \frac{\Delta t}{2\Delta x}\left[F\left(U_{i+1,j}\right) - F\left(U_{i-1,j}\right)\right] \tag{12.3.12}$$

There are several other desirable qualities we would like our numerical integration scheme to have other than the ones already discussed so far, including that they satisfy the precise entropy decay dictated by thermodynamics. When we do not study very abrupt transients, something we rarely do in multiphase pipelines, the entropy inequality is generally not something we have to worry about. If we are interested in accurate simulation of pipe rupture, the speed may reach the speed of sound, this subject can become important and sets some requirements for our integration method (see for instance Thomas, 1995, Toro, 1999, Zhong, 2007). Some discretization schemes, such as the Nessyahu Tadmor spatial discretization method mentioned in chapter 12.5, satisfy the entropy constraints and also work well for sharp discontinuities. Another desirable property of that method is the fact that it is a *central* scheme, so we do not have to keep track of what is upwind or downwind.

12.4 Hyperbolic equations with source terms

Unlike equation 12.2.1, our hyperbolic equations are nonlinear, and the sum of the time- and spatial derivatives are not zero. We can write them as:

$$\frac{\partial U}{\partial t} + \frac{\partial F(U)}{\partial x} = S(U) \tag{12.4.1}$$

We choose to call the right-hand side of equation 12.4.1 the source term (corresponding to phase change in the mass conservation equations, phase change, friction, elevation change, and possibly surface tension in the momentum conservation equations, as well as interfacial heat, work, energy, and phase change in the energy conservation equations). How do we deal with the source terms in our solution methods?

It turns out that phase change can happen much faster than pressure wave propagation. For an explicit method, that means $S(U)$ can pose the greatest restrictions on the time-step. We can in principle slow down phase change artificially (pretending it happens slowly even if in reality it does not), but this poses its own modeling problems and may also affect the model's validity. Since implicit methods tend to be much more stable than explicit methods, the presence of fast phase change terms makes implicit methods more desirable.

Many of the published methods for solving nonlinear hyperbolic equations are dealing with equations without source terms, meaning equations on the form 12.3.11. But how do we use those methods to solve equation 12.4.1?

One alternative is to split equation 12.4.1 into two problems. First, we solve:

$$\frac{\partial U}{\partial t} = S(U) \tag{12.4.2}$$

After having taken one time-step with equation 12.4.3 we use the result from that time-step as initial value for a second step according to equation 12.3.11.

We notice that equation 12.4.2 is a system of ordinary differential equations, since the time derivative is the only derivative involved.

We may want to change which of the two methods we solve first for each time-step in order to counter possible bias (for time-step *j*, we may start solving equation 12.4.2, then 12.3.11, while in time-step *j+1*, we may start solving 12.3.11, then 12.4.2 and so on). We can also use shorter time-steps for one of the methods than for the other (as long as they both reach the same point in time before we continue with next step).

To get an intuitive understanding for why this might work, let us look at a far simpler problem, namely the momentum equation for a mass m influenced by an external force F_e and a linear damper with damping coefficient C_d so:

$$m\frac{dv}{dt} = -C_d v + F_e \tag{12.4.3}$$

Or, if we re-formulate it:

$$\frac{dv}{dt} + \frac{C_d}{m}v = \frac{F_e}{m} \tag{12.4.4}$$

Equation 12.4.4 is not hyperbolical, but we can investigate what happens if we use a numerical method in the same way as explained for equations 12.4.2 and 12.3.11. If we use explicit Newton-iteration on the first part, we can set:

$$v^1{}_{j+1} = v_j + \Delta t \frac{F_e}{m} \tag{12.4.5}$$

The next step becomes:

$$v_{j+1} = v^1{}_{j+1} - \Delta t \frac{C_d}{m} v^1{}_j = v_j + \Delta t \left(-\frac{C_d}{m} v_j + \frac{C_d}{m} \right) - \Delta t^2 \frac{C_d C_d}{m^2} \tag{12.4.6}$$

If we had done the two integration steps in equation 12.4.5 and 12.4.6 in the opposite order, it is easy to show that result would still become the same.

If we apply explicit Euler-integration on equation 12.4.4 directly, we get:

$$v_{j+1} = v_j + \Delta t \left(-\frac{C_d}{m} v_j + \frac{C_d}{m} \right) \tag{12.4.7}$$

This is very similar to what we came up with in equation 12.4.6, the difference being the last term in equation 12.4.6. That term, *the splitting error*, is of as high order as explicit Euler-integration (the factor Δt^2 is of *local order 2*, and therefore *global order 1*, which happens to be the same as the order for explicit Euler-integration). If we switch to using higher order methods, we are generally going to end up with a splitting error of order 2, so the splitting described here only works well for 1. order methods (although in principle, it is possible to craft the methods such that the splitting order becomes higher, it is difficult to achieve that in practice). But even though the splitting error formally is of global order 1, it turns out that it often is quite small anyway, so it makes sense to combine two 2. order methods for both steps (LeVeque, 2002). As explained by Toro (1999), there is also a better way to formally achieve 2. order accuracy for the splitting by adding one step pr. integration:

1. Integrate equation 12.3.11 for time-step $\Delta t/2$.
2. Use the result as starting value for equation 12.4.2 and integrate a full time-step Δt.
3. Use the result as starting value and integrate equation 12.3.11 with half a time-step $\Delta t/2$. The result from this is the final result for the whole time-step.

Even when the equations are multidimensional, nonlinear, and hyperbolical, the same thing generally holds: Dividing the integration into the three steps indicated above leads to a usable method of order 2. We can even combine an implicit method in one step with an explicit method in the next. That can be attractive if the stiffest part of the physical phenomena involved (the fastest part) is related to the source term, as it often the case when we have phase change. Doing so, we could for instance use the *Trapezoidal Rule – Backward Differentiation method of order 2 (TR-BDF2)* to ensure stability for the steps corresponding to the PDE, equation 12.4.2. In the step corresponding to the ordinary differential equations 12.4.3, we could even get away with using an explicit method, even though an implicit or semi-implicit method for that step, too, is most often more appropriate.

A hyperbolic differential equation with source terms can be solved as if it had no such terms, and the source terms are solved separately. By doing this in three separate steps of order two or better and combining the results appropriately, the overall method maintains order 2.

It is worth noting that although this two- or three-step method offers flexibility in the way it deals with stiff terms, the partly decoupling of sources from the flux may lead to inaccuracies of a sort which may be confusing if we are unaware of the method's peculiarities (Stewart & Wendroff, 1984). This becomes particularly apparent when we approach steady-state conditions, since the flux and source terms need to balance each other out as the time derivative becomes zero, something they can never fully do unless solved simultaneously. This method will therefore show that the system never becomes 100% steady-state.

12.5 Selecting discretization methods

We have now seen examples of simple methods for solving hyperbolic differential equations, and we have seen how to account for source terms. It appeared that the first order upwind method was very simple when applied to a single equation, but less so for systems of equations. In that case we need to satisfy the upwind requirement, which leads to significant extra work, particularly if the equations are nonlinear.

As explained in *Pipe Flow 1*, Gudonov's theorem states that linear methods of order higher than 1 have to be oscillatory (creating false oscillations in the solution), but we

have also seen that the use of limiters (and in effect accepting lower order at certain points in time and space) makes it possible to live with this constraint without being much affected by it in practice (such as in the Nessyahu-Tadmor order *2* or the Kurganov-Tadmor order *3* method, the latter described in *Pipe Flow 1*). Those methods can be used directly to simulate the incompressible transient model or drift-flux model, but need to be modified to handle the full two- or three-fluid models. We have also seen that a relatively dense grid is necessary when simulating multiphase pipe flow, so it does not seem to make sense to put effort into achieving higher order than *order 2*. That is also the order most easily handled by the method if including the source terms the way it was outlined in chapter 12.4.

Nearly all the different commercial codes for simulating multi-phase flow use different methods. Part of the reason is that different codes were developed at different times, and both numerical methods and computers have seen exciting progress over the last years, and different codes have also had different goals (nuclear reactor codes, as opposed to flow assurance codes). Prosperetti & Tryggvason (2007) have given a good overview of the methods used by some of the commercial transient multi-phase flow codes, including TRAC, RELAP, COBRA-TF, CATHARE, and CFX, and they have also included some comments regarding OLGA. Most of these codes are intended for simulating boiling in nuclear reactors, not flow assurance in pipelines (chapter 1 in *Pipe Flow 1)*.

There are lots of good books and articles on how to solve hyperbolic equations numerically, for instance Colella & Puckett (1994), Toro (1999), Randall (2002), Evje & Flåtten (2005), and Quarteroni (2007). They describe the basics of such methods as the second order Lax-Wendrof, Warming-Beam, as well as various types of MUSCL-type higher order methods, including NT2 and KT3. We are not going to repeat all details here. Instead, we will show one example of a general implicit solution method for ordinary differential equations (which is what we need to solve after having done the spatial discretization). Afterwards, we will show an example of a semi-implicit method.

12.6 Improved TR-BDF2 method

One method which seems to work well for solving the conservation equations is the so called second order *Trapezoidal Rule – Backward Differentiation (TR-BDF2)* method. The method is also implemented in the much-used Matlab technical computing library (owned by MathWorks). As the name suggests, the *TR-BDF2*-scheme consists of two steps. The first marches our solution from time t_j to $t_{j+\gamma}$ (some way towards t_{j+1}) using

the second order trapezoidal rule, while the second step reaches t_{j+1} using backward differentiation.

Although the well-known trapezoidal method is second-order accurate and stable, it is only marginally stable in the stiff case, and this can lead to problems in the context of stiff hyperbolic equations. That is why we use the trapezoidal method only for the first part of the time-step, and then continue with a second stage that is a backward differentiation formula of order two. We can construct the method such that the same iteration matrix can be used for both stages.

With the differential equation on the form 12.3.11 and $\gamma = 1/2$, the first step becomes:

$$\frac{U_{j+1/2} - U_j}{\Delta t} = -\frac{1}{2}\left[F(U_j) + F(U_{j+1/2})\right] \tag{12.6.1}$$

The BDF2-step is then done by using a second order approximation for the time derivative:

$$\frac{U_{j+1} - U_{j+1/2}}{\Delta t} + \frac{U_{j+1} - 2U_{j+1/2} + U_j}{2\Delta t} = -F(U_{j+1}) \tag{12.6.2}$$

In the second step, U_j and $U_{j+1/2}$ are already known, so only U_{j+1} needs iteration to solve the equation. This can be formulated as an implicit, two-step Runge-Kutta method. But the two steps require equal amounts of computational work, with full estimation of the Jacobian in each step (or, alternatively, by using Jacobian-free iteration, as described in chapter 12,8).

It has been shown by Dharmaraja et al. (2008) that splitting the two steps exactly at the middle is not the optimal way to do this. It is better to modify equations 12.6.1 and 12.6.2 to:

$$U_{j+\gamma} - U_j = -\frac{\gamma \Delta t}{2}\left[F(U_j) + F(U_{j+\gamma})\right] \tag{12.6.3}$$

And:

$$(2-\gamma)U_{j+1} - \frac{1}{\gamma}U_{j+\gamma} + \frac{(1-\gamma)^2}{\gamma}U_j = -(1-\gamma)\Delta t F\left(U_{j+1}\right) \tag{12.6.4}$$

Where γ is a number chosen somewhere between 0 and 1. Dharmaraja et al. (2008) showed that setting:

$$\gamma = 2 - \sqrt{2} \tag{12.6.5}$$

is the best choice. It improves the method's stability, and it also makes it possible to estimate the two Jacobians required (one for the first step, another for the second step) proportionally so that the second-step Jacobian can be estimated from the first step. The Jacobians in equations 12.6.3 and 126.4 for $U_{j+\gamma}$ and U_{j+1} become:

$$J_{trapez} = I - \frac{\gamma\Delta t}{2}F' \; and \; J_{BDF2} = (2-\gamma)I - (1-\gamma)\Delta t F' \tag{12.6.6}$$

With the selected value for γ, this leads to:

$$J_{BDF2} = \sqrt{2}\cdot J_{trapez} \tag{12.6.7}$$

This means that if the Jacobian is constant (or fairly constant) over several time steps, we can use the same Jacobian as found in the (last iteration of) the trapezoidal step to estimate the Jacobian for the BDF2-step. Although J may vary only moderately in some situations, a general, robust multiphase program typically needs to re-calculate it for every time step.

Shampine & Hosea recommends using U_j as starting value for iterating $U_{j+\gamma}$ from equation 12.5.3, while the starting value for U_{j+1} in the BDF2-iteration is recommended to be:

$$U_{0\ j+1} = \left(1.5 + \sqrt{2}\right)U_j + \left(2.5 + 2\sqrt{2}\right)U_{j+\gamma} - \left(6 + 4.5\sqrt{2}\right)\left[F\left(U_{j+\gamma}\right) - F\left(U_j\right)\right] \qquad (12.6.8)$$

12.7 Semi-implicit methods

We have seen that when we use fully implicit integration methods, we can get very good stability. We have also seen that the price we pay for such solution methods is that we must do more work per time-step (considerable iteration required), we get high numerical dissipation (transients tend to die out faster than they would in a real system), and we reduce the possibilities of model or programming errors revealing themselves by producing obvious errors in the results (even non-hyperbolic and therefore somewhat unphysical system formulations can lead to the simulations producing seemingly logical results). Semi-implicit methods represent a compromise between the higher sensitivity, less damping and less work per time-step achieved by explicit methods and the possibility of using the longer time-steps which the fully implicit methods allow. The method below is based on the ideas of Liles & Reed (1978). It was further refined by Stewart & Wendroff (1984), Mahaffy (1993) and Prosperetti & Tryggvason (2007). A modified version of their method is presented below.

The main idea is to only make those variables which tend to create stability problems implicit. It is difficult to see exactly which parameters they are, but we can get some clues by going back to the single-phase equations 12.3.5 and 12.3.6. Those simplified equations were only good for liquid flow, but the qualitative logic relevant here applies to gas, too. The argument goes as follows:

The most important term affecting the time derivative in the continuity equation 12.3.5 is the spatial derivative of the velocity. Therefore, $\partial v/\partial x$ should not be allowed to produce the unrestricted sort of oscillations we know explicit approximations can produce, and we need to use an implicit approximation for $\partial v/\partial x$ in the mass conservation equation.

For the momentum equation, it is not completely obvious which of the terms on the right-hand side dominate, it can be either the spatial derivative of the pressure or the friction. It can vary depending on pipe diameter, viscosity and other parameters, and it is safest to make them both implicit.

With this philosophy in mind, the continuity equations are discretized as:

$$\frac{(\alpha_G\rho_G)_{i,j+1} - (\alpha_G\rho_G)_{i,j}}{\Delta t} + \frac{(\alpha_G\rho_G)_{i+ir,j}\, v_{G\, i+1/2,j+1} - (\alpha_G\rho_G)_{i-il,j}\, v_{G\, i-1/2,j+1}}{\Delta x} = 0 \qquad (12.7.1)$$

$$\frac{(\alpha_L\rho_L)_{i,j+1} - (\alpha_L\rho_L)_{i,j}}{\Delta t} + \frac{(\alpha_L\rho_L)_{i+ir,j}\, v_{L\, i+1/2,j+1} - (\alpha_L\rho_L)_{i-il,j}\, v_{L\, i-1/2,j+1}}{\Delta x} = 0 \qquad (12.7.2)$$

The indexes are as follows:

$$ir = 0\ if\ v_{G\, i+1/2,j+1} \geq 0$$

$$ir = 1\ if\ v_{G\, i+1/2,j+1} < 0$$

$$il = 0\ if\ v_{G\, i-1/2,j+1} \geq 0$$

$$il = 1\ if\ v_{G\, i-1/2,j+1} < 0$$

Notice that for simplicity we have not included any mass transfer terms due to phase shift or inflow/outflow through perforations in the pipe wall. We could easily do so directly in this model, and if so, we would choose to do it at time level *j + 1*, making those terms implicit as well.

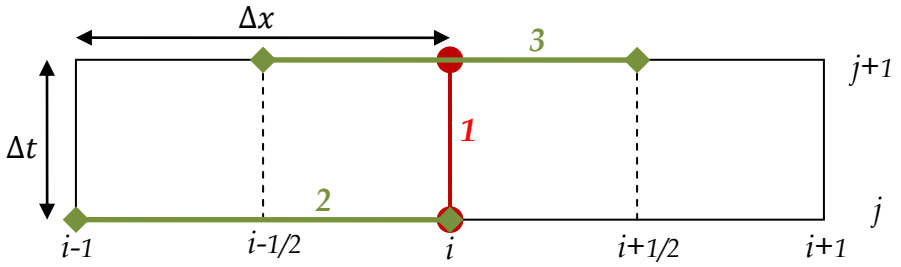

Figure 12.7.1. Graphical illustration of the grid parts involved in integrating one time-step for the mass conservation equations 12.7.1 and 12.7.2. The vertical line marked 1 shows the points in the grid involved in estimating the time derivative, corresponding to the first term in the equations. The spatial derivatives are computed using a mix of αρ from time level j, line 2, and v at time level j+1, line 3. In case the flow becomes negative, line 2 is moved Δx to the right.

Interpreting the first term in equation 12.7.1 is straight forward: It is a first order approximation of the time derivatives. The spatial derivative approximated by the second term is a bit more complicated in that it contains a mixture of parameters from the j'th time-step ($\alpha_G\rho_G$) and the j+1'th time-step (v_G). As already explained, this has been found to create a reasonable compromise between computation work pr. time-step (which generally favors explicit methods, using only information from the j'th time-step) and stability constraints on the time-step length (which favors implicit methods, using information from the j'th time-step for all spatial derivatives as well as for any source variables). Notice also that ($\alpha_G\rho_G$) is always taken from upstream of the studied grid point (the upwind rule). It is based on the fact that mass transport obviously comes from upstream, and that the downstream points cannot predict what comes drifting from upstream. This is similar to the upwind method we discussed in chapter 12.2

The momentum equations are discretized as:

$$\begin{aligned}(\alpha_G\rho_G)_{i+1/2,j}\left[\frac{v_{G\ i+1/2,j+1}-v_{G\ i+1/2,j+1}}{\Delta t}+v_{G\ i+1/2,j}\frac{v_{G\ i+1/2+i0,j}-v_{G\ i-1/2+i0,j}}{\Delta x}\right]\\ +\alpha_{G\ i+1/2,j}\frac{(p+\Delta p_G)_{i+1,j+1}-(p+\Delta p_G)_{i,j+1}}{\Delta x}\\ =-R_{GLi\ i,j+1}+R_{Gw\ i,j+1}\ -(\alpha_G\rho_G)_{i,j}g\sin\theta\end{aligned} \tag{12.7.3}$$

$$\begin{aligned}(\alpha_L\rho_L)_{i+1/2,j}\left[\frac{v_{L\ i+1/2,j+1}-v_{L\ i+1/2,j+1}}{\Delta t}+v_{G\ i+1/2,j}\frac{v_{L\ i+1/2+i0,j}-v_{L\ i-1/2+i0,j}}{\Delta x}\right]\\ +\alpha_{L\ i+1/2,j}\frac{(p+\Delta p_L)_{i+1,j+1}-(p+\Delta p_L)_{i,j+1}}{\Delta x}\\ =R_{GLi\ i,j+1}+R_{Lw\ i,j+1}\ -(\alpha_G\rho_G)_{i,j}g\sin\theta\end{aligned} \tag{12.7.4}$$

The upwind rule is satisfied by defining the indexes:

$$i0 = 0 \; if \; v_{G\,i+1/2,j} \geq 0$$

$$i0 = 1 \; if \; v_{G\,i+1/2,j} < 0$$

Again, we have for simplicity assumed no mass transfer between phases or through perforations in the pipe wall, but including such terms is straight forward, and should be done at time level $j + 1$. Where we need to find half-way values, we take the linear average of the nearest known neighbors, so that for instance for the gas equations, we set:

$$(\alpha_G \rho_G)_{i+1/2,j} = \frac{(\alpha_G \rho_{LG})_{i,j} + (\alpha_G \rho_G)_{i+1,j}}{2} \tag{12.7.5}$$

And:

$$\alpha_{G\,i+1/2,j} = \frac{\alpha_{G\,i,j} + \alpha_{G\,i+1,j}}{2} \tag{12.7.6}$$

To solve these equations, we need some initial values to get started. We can use the steady-state model in the previous chapter for that purpose.

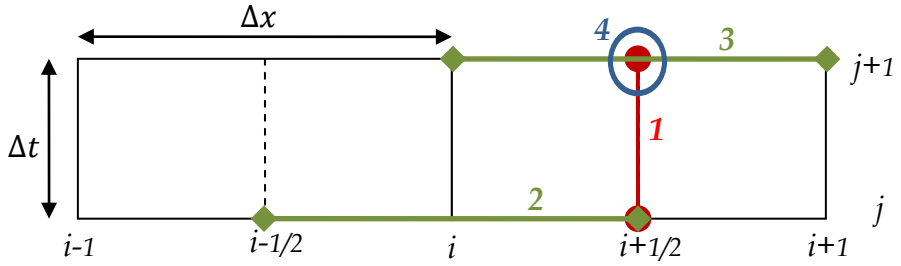

Figure 12.7.2. Graphical illustration of the grid parts involved in integrating one time-step for the momentum conservation equations 12.7.3 and 12.7.4. The vertical line marked 1 shows the points in the grid involved in estimating the time derivative, corresponding to the first term in equations 12.7.3 and 12.7.4. The first spatial derivatives are computed using velocities on time level j, line 2, and the second using p at time level j+1, line 3. In case the flow becomes negative, line 2 is moved Δx to the right. The terms at the right-hand side of the equations are calculated according to values in the grid-point marked by the circle 4.

In one rare case, namely the pipe being horizontal and the initial velocities being zero, both pressures (equal to the boundary outlet pressure), the flows (zero), and the fractions (the pipe is in effect acting like a tank, so the fractions will be constant

throughout the pipe, and any α_G and α_L satisfying $\alpha_G + \alpha_L = 1$ will be possible). This situation is therefore very easy to describe and can alternatively be used as initial condition. If we choose to do it that way, we may alter the pipe elevation and the boundary conditions gradually to the real situation corresponding to the steady-state situation for the actual system, from which we want to introduce the transients of interest.

From figures 12.7.1 and 12.7.2 we immediately see that both the mass and the momentum conservation equations use values from more than one cell. That becomes a problem at the boundaries, since cells there do not have neighboring values on both sides. This problem was discussed thoroughly when simulating single-phase flow in *Pipe Flow 1*, where a technique for utilizing ghost cells was developed. The same idea can be used here. Since the method shown here is only *order 1*, it makes no sense to go to great lengths to create sophisticated ghost values, using the nearest known value is normally sufficient.

The equations form a nonlinear set, and solving them requires iteration. In the next chapter, we will look at some of the methods most utilized.

12.8 Newton-Rapson and Newton-Krylov iteration

12.8.1 The problem with Newton-Rapson iteration for large systems

All the implicit integration methods result in a set of nonlinear equations which need to be solved for each time-step. Probably the most well-known way of doing so, *Newton-Rapson iteration* (most often simply called *Newton-iteration*), has been discussed before. We remember that if we seek the solution of a set of algebraic equations of *N* variables on the form:

$$F(U) = \begin{bmatrix} f_1(u_1, u_2, \dots, u_N) \\ f_2(u_1, u_2, \dots, u_N) \\ \vdots \\ f_N(u_1, u_2, \dots, u_N) \end{bmatrix} = \begin{bmatrix} 0 \\ 0 \\ \vdots \\ 0 \end{bmatrix} \tag{12.8.1}$$

Newton-iteration involves guessing an initial value for U, and then calculating progressively better estimates by iterating:

$$U_{n+1} = U_n - J^{-1}F_n(U_n) \tag{12.8.2}$$

The Jacobian is an *N x N* -matrix where an element in row *i*, column *j* is defined as:

$$J_{i,j} = \frac{\partial f_i(U)}{\partial u_j} \tag{12.8.3}$$

We go on iterating until the result is below some error limit e_F:

$$\|F(U)\|_2 \leq e_F \tag{12.8.4}$$

The 2-norm is defined as the length of the vector:

$$\|F(U)\|_2 \stackrel{\text{def}}{=} \sqrt{[f_1(U)]^2 + [f_2(U)]^2 +, \dots, +[f_N(U)]^2} \tag{12.8.5}$$

In realistic multi-phase pipe flow models, we are typically unable to determine J analytically by derivation due to the complex flow regime and fluid property relationships. In chapter 3.6 we saw an example of how it could be done numerically by differentiation. There, we gave each u_j a little addition Δu_j, then calculated $f_i(u_j + \Delta u_j)$ for all i, and by doing so for all u_j, we could create a first order estimate for the whole Jacobian by inserting:

$$J_{i,j} = \frac{\partial f_i(U)}{\partial u_j} \approx \frac{\Delta f_i(u_1, u_2, \dots, (u_j + \Delta u_j), \dots, u_N)}{\Delta u_j} \tag{12.8.6}$$

We see that this method requires one function call for each $(u_j + \Delta u_j)$ in addition to function call to $F(U)$, meaning $N + 1$ function calls in all. If N is large, as it may be in long pipelines or in pipe networks, this results in time-consuming calculations.

12.8.2 Creating and inverting the Jacobian

Various ways of computing the Jacobian are discussed in Averick et al. (1993).

It is important to choose appropriate values for the ΔU-vector. Its elements should be as small as possible to produce good approximations, though not so small that we go below the computer's accuracy. If it is too small, the result will be contaminated by floating-point roundoff errors. We can try out different values, and we typically end up using something like 10^{-6} of the maximum values one expects to encounter for all Δu_j for 64 bit double precision. For instance, if $\alpha_G \rho_G$ is expected to vary from 0 to10, we may choose the corresponding Δu_j as 10^{-5}.

In addition to *creating* the Jacobian, it must also be inverted, and the Jacobi elements have to be stored. For a system of conservation equations like the ones we have in transient pipe flow, J is *sparse*, meaning most of its elements are zero. Using sparse techniques for storage together with efficient inversion algorithms, it is possible to do the inversion with time consumption and storage requirement more or less proportional to N (as opposed to proportional to N^2, which direct inversion results in), but it can still be quite time and storage consuming.

12.8.3 Some problems with Newton-iteration

Even though Newton-iteration is often used, we see is has 3 obvious disadvantages:

1. It is relatively expensive to use for systems with many unknowns.
2. Since the conservation equations can contain discontinuities due to flow regime changes, shocks and various fluid properties, the Jacobian is not always defined for all situations. This can lead to numerical problems when calculating it by differentiation, but we can to some extent counter this by defining maximum or minimum values for each element (this may prevent the simulations from stopping, but it can also produce erroneous results at times).
3. Newton-iteration is known to be 'caught' in local minima or maxima if such exist between the true solution and the point where the iteration was started. When that happens, the iteration converges towards the wrong solution. It can also

start off (and continue) in the wrong direction and never converge if the starting point is unfortunate. If we are able to identify the problem when it happens, we may try new initial values or reduce the time-step length to make it easier to produce better starting values. Shorter time-steps do of course generally produce better starting values, since it makes it easier to extrapolate values from previous time-steps.

We see that point 2 and 3 can result in lack of convergence, and that is not a problem we can solve by switching to the so-called *Jacobian-Free Newton-Krylov (JFNK)* methods. The first problem, on the other hand, the one to do with computation speed and storage, can in some cases be much improved by using *JFNK*.

12.8.4 Avoiding the Jacobian using Newton-Krylov iteration

In equation 12.8.2, we saw that each step in the Newton-Rapson iteration required us to calculate the Jacobian and to invert it. The main idea behind Newton-Krylov iteration is to replace that and perform each Newton iteration step without the Jacobian. It takes significant effort to fully understand the theory behind the methods used by JFNKs (so much, in fact, that the theory still contains large 'grey' areas). It is also considerably more work to implement any of the Krylov methods as code compared to the direct methods explained in chapters 12.8.1 and 12.8.2. We are not going to describe any of the various JFNKs in great detail, but rather focus on the main principles, intending to throw light on their main advantages and potential problems.

Knoll & Keyes (2004) have created a useful overview of different JFNKs. Helpful information can also be found in Dennis & Schnabel (1996), Van der Vorst (2003), and Kelley (2003). We will try to explain its principle by looking at a system consisting of two coupled nonlinear equations on the form shown in equation 12.8.1 so that $f_1(u_1, u_2) = 0$ and $f_2(u_1, u_2) = 0$. For this system, the Jacobian is:

$$J = \begin{bmatrix} \frac{\partial f_1}{\partial u_1} & \frac{\partial f_1}{\partial u_2} \\ \frac{\partial f_{12}}{\partial u_1} & \frac{\partial f_2}{\partial u_2} \end{bmatrix} \tag{12.8.7}$$

Rather than using the Jacobian together with equation 12.8.2, let us make two observations. First, we see that if we make a function call at U and another a small

distance away, namely at $U + \epsilon V$, where ϵ is some small number, and V is some vector consisting of v_1 and v_2 so that $V = [v_1, v_2]^T$, we can calculate:

$$\frac{F(U+\epsilon V) - F(U)}{\epsilon} \stackrel{\text{def}}{=} \begin{bmatrix} \dfrac{f_1(u_1 + \epsilon v_1, u_2 + \epsilon v_2) - f_1(u_1, u_2)}{\epsilon} \\ \dfrac{f_2(u_1 + \epsilon v_1, u_2 + \epsilon v_2) - f_2(u_1, u_2)}{\epsilon} \end{bmatrix} \tag{12.8.8}$$

The clever trick is to make the following second observation: If we approximate $F(U + \epsilon V)$ using Taylor-series on the form shown in equation 12.1.2 (since F is multi-dimensional we must of course do it in vector form), we get the following first-order approximation:

(12.8.9)

$$\frac{F(U+\epsilon V) - F(U)}{\epsilon} \approx \begin{bmatrix} \dfrac{f_1(u_1, u_2) + \epsilon v_1 \dfrac{\partial f_1}{\partial u_1} + \epsilon v_2 \dfrac{\partial f_1}{\partial u_2} - f_1(u_1, u_2)}{\epsilon} \\ \dfrac{f_2(u_1, u_2) + \epsilon v_1 \dfrac{\partial f_2}{\partial u_1} + \epsilon v_2 \dfrac{\partial f_2}{\partial u_2} - f_2(u_1, u_2)}{\epsilon} \end{bmatrix} = \begin{bmatrix} v_1 \dfrac{\partial f_1}{\partial u_1} + v_2 \dfrac{\partial f_1}{\partial u_2} \\ v_1 \dfrac{\partial f_2}{\partial u_1} + v_2 \dfrac{\partial f_2}{\partial u_2} \end{bmatrix}$$

The last bracket is the Jacobian J multiplied by the vector V. This means we have found a way to estimate JV by using only two function calls:

$$JV \approx \frac{F(U+\epsilon V) - F(U)}{\epsilon} \tag{12.8.10}$$

The iteration can now be performed by moving in the JV-direction:

$$U_{n+1} = U_n + sJV \tag{12.8.11}$$

We need to guess s. We may for instance start with $s = 1$ and calculate U_{n+1} according to equation 12.8.10. We then have to check if the new value is more accurate than the old by comparing the norms. We have improved the result if:

$$\|F_{n+1}(U_{n+1})\|_2 < \|F_n(U_n)\|_2 \tag{12.8.12}$$

If it turns out the criterion in equation 12.8.11 does not hold, it is likely we have overshot the solution, and we may try a smaller s, maybe $s = 0.5$. We then see if this improves the result. We continue until we have found an s-value which satisfies:

$$\|F_{n+1}(U_{n+1})\|_2 < \gamma\|F_n(U_n)\|_2 \tag{12.8.13}$$

Where the *forcing term* γ is a number which obviously must be chosen smaller than 1, so that we go on iterating until we have achieved an improvement compared to the value we started with. Once we have satisfied equation 12.8.13, we have completed the Krylov-iteration for our first Newton iteration step. We then calculate a new JV with our improved U-vector according to equation 12.8.9, and repeat the Krylov-iterations for the next Newton-iteration and so on, until we have achieved the desired overall accuracy. Choosing a γ-value leading to high overall efficiency is one of the challenges involved in using the method.

For the JFNK-method to work well in practice, its convergence characteristics need to be improved by something called *preconditioning*, a step we will not show in detail.

We will instead summarize JFNK-methods as follows:

1. Jacobian-free Newton-Krylov methods replace the need for calculating the Jacobian in Newton-Rapson iteration by carrying out Krylov-iteration for each Newton iterations step.
2. Krylov-iteration is more laborious to implement than methods based on estimating the Jacobian and inverting it, but it can do the calculations much faster in some large systems, and it also requires less storage. These methods should therefore be considered when large pipe networks or long pipelines are simulated.
3. Krylov-iterations have their own potential problems, and JFNK also inherits all problems associated with Newton iteration. The methods can therefore be less robust than Jacobian-based iterations.

When simulating multiphase flow, it is often most convenient to use JNFK for 'inverting' the system equations' Jacobain as it occurs in the implicit ordinary differential equation solver - not for replacing the Jacobian as such. When using implicit

numerical time integration, we end up having to solve an equation on the form $Ax = b$ for each time step. A is a matrix arising from the spatially discretized system's Jacobian, and x and b are vectors. This equation is linear, and rather than solving it by inverting A, we do so by some sort of JNFK.

We may say that this way of solving the equations is a combination of normal Newton-iteration and JNFK, and it seems to be the best known method at this stage.

"Water flows humbly to the lowest level.
Nothing is weaker than water,
Yet for overcoming what is hard and strong,
Nothing surpasses it."
Lao Tzu, 600 B.C.

13 Two-phase liquid-liquid flow

How liquid-liquid two-phase flow differs from gas-liquid flow:

- Description of flow regimes
- Dispersions, emulsions, inversion and inversion prediction
- Friction models

13.1 General

Flows of two immiscible liquids such as oil and water have not been explored to the same extent as gas-liquid flows. Two-phase liquid-liquid flow is not principally different from two-phase gas-liquid flow, but the density- and viscosity ratios tend to be different, and they mix differently. That often puts liquid-liquid flow outside the validity area of some of the gas-liquid models. In case both liquids have the same density, neither has a greater tendency than the other to form the lower layer in stratified flow, and the flow regimes become similar to how they would have been without gravity. When there is no such thing as up or down, the flow regimes become independent of inclination angle, and stratified flow cannot exist. That is no longer so if the densities differ, but we realize that the more similar the densities are, the less the

flow is affected by inclination angle. The more different the densities are, on the other hand, the more the flow tends to behave like gas-liquid flow.

How close we are to 'weightlessness' in terms of how the flow behaves can be determined by the Eötvös number for the two liquids, we index them o (oil) and w (water):

$$Eo = \frac{|\rho_w - \rho_o| g d^2}{8\sigma_{ow}} \tag{13.1.1}$$

The lower the Eötvös number, the more our system resembles a micro-gravity system, and the less likely it is that stratified flow will form (typically if $Eo \ll 1$).

Oil wells often produce single-phase crude oil at first, but it is common for water to occur after some time of production. The water content can be as high as 90% or more before the well becomes uneconomical and is shut in. Understanding the flow in such wellbores and the pipelines from wellhead to separation facilities does of course call for liquid-liquid models. Also, understanding the main mechanisms in both gas-liquid and liquid-liquid pipe flow is a good first step towards understanding three-phase gas-oil-water flow.

Liquid-liquid flow models have also been used to try to develop methods for transporting heavy oil by lubricating it with an annular water film between the oil and the pipe wall. That task has proved difficult, though, and there are still no known practical ways to transport very high viscosity liquids over long distances through pipelines.

From a practical point of view, the main issue in predicting the pressure drop in homogeneous liquid-liquid dispersed flow is the modeling of the mixture viscosity. That strongly depends on which of the phases are continuous (water-in-oil or oil-in-water), and this again has to do with the phase inversion phenomenon.

Liquid-liquid flow shows a greater variation in flow regimes than what we observe in gas-liquid flow, and that makes it more challenging to determine which flow regime we are likely to experience in a given situation. Figures 13.1.1 – 13.1.3, based mostly on Brauner (2003), show some observed flow regimes. In stratified flow, each regime can occur in pure form or as a dispersion in (or containing a dispersion of) the other liquid. In figure 13.1.1 f, we see that this can result in something quite similar to three-phase flow even if we start with a mixture of only two fluids.

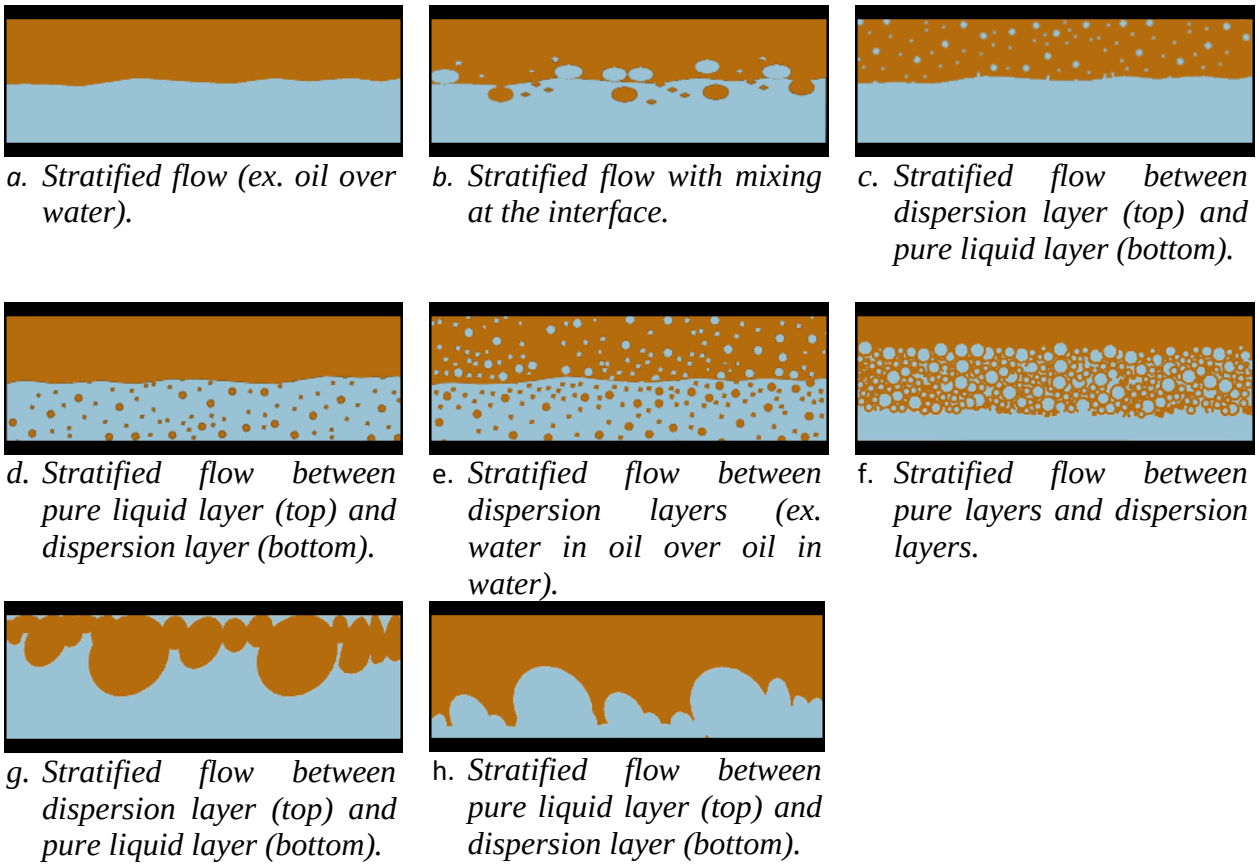

a. *Stratified flow (ex. oil over water).*

b. *Stratified flow with mixing at the interface.*

c. *Stratified flow between dispersion layer (top) and pure liquid layer (bottom).*

d. *Stratified flow between pure liquid layer (top) and dispersion layer (bottom).*

e. *Stratified flow between dispersion layers (ex. water in oil over oil in water).*

f. *Stratified flow between pure layers and dispersion layers.*

g. *Stratified flow between dispersion layer (top) and pure liquid layer (bottom).*

h. *Stratified flow between pure liquid layer (top) and dispersion layer (bottom).*

Figure 13.1.1. Various sorts of stratified flow observed in horizontal liquid-liquid flow.

When we study figures 13.1.1 – 13.1.3, we notice that either of the two liquids can act as the continuous phase while the other phase is discontinuous. The switch from one situation to the other can be quite spontaneous, and it is called *phase inversion*. That may happen under certain operating conditions under which an oil-in-water dispersion will change to water-in-oil dispersion or vice versa.

To get a feeling for how a phase inversion works, consider a pipe with single-phase oil flowing at considerable velocity. We then begin adding an increasing amount of water. At first, the water may take the form of droplets in the dispersed oil phase. When the concentration of water droplets become high enough, the droplets will more frequently collide with each other and coalesce and entrap oil in small pockets. At some point, that will cause the water to become the continuous phase while the oil becomes dispersed.

a. Annular flow (ex. oil in the center, water closest to the pipe wall).

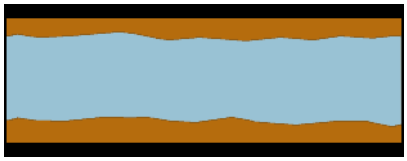

b. Annular flow (ex. water in the center, oil closest to the pipe wall).

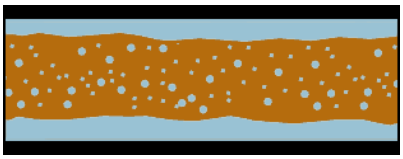

c. Annular flow with dispersion in the core

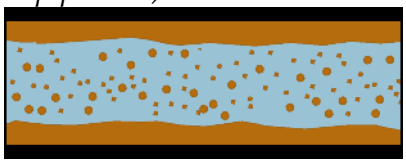

d. Annular flow with dispersion in the core

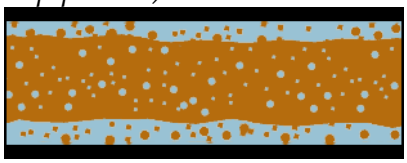

e. Annular flow of two dispersions.

Figure 13.1.2. Various sorts of annular flow observed in horizontal liquid-liquid flow.

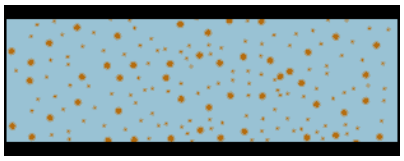

a. Dispersion of one liquid in the other (ex. oil in water).

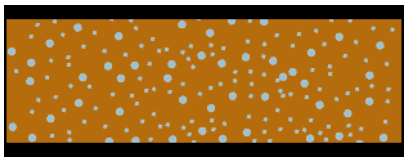

b. Dispersion of one liquid in the other (ex. water in oil).

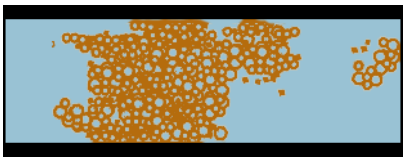

c. Intermittent flow (ex. oil dispersion in water alternating with pure water).

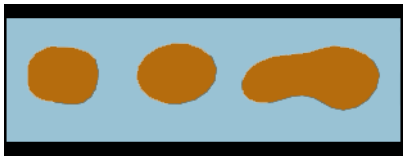

d. Large bubbles of one liquid in the other (ex. oil in water).

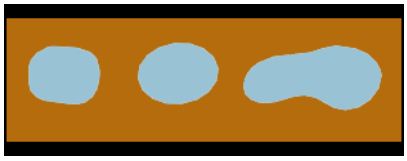

e. Large bubbles of one liquid in the other (ex. water in oil).

f. Slug-like behavior of one liquid in the other (ex. oil in water).

g. Slug-like behavior of one liquid in the other (ex. water in oil).

Figure 13.1.3. Other flow regimes observed in horizontal liquid-liquid flow.

The continuous phase's viscosity is most important for the overall mixture's friction. Since the two fluids most often have different viscosities, a phase inversion is associated with an abrupt change in the frictional pressure drop. Less obvious, but apparent in measurements (Guzhov, 1973, Valle & Utvik, 1997, and Soleimani, 1999) is the fact that viscosity shows a distinct peak around the inversion point, considerably higher than any of the liquid's single-phase viscosities. It appears as if close to the inversion point, none of the phases are continuous.

In figure 13.1.4, a somewhat simplified flow regime map shows that phase inversion can happen from various initial conditions, and predicting them accurately is not easy.

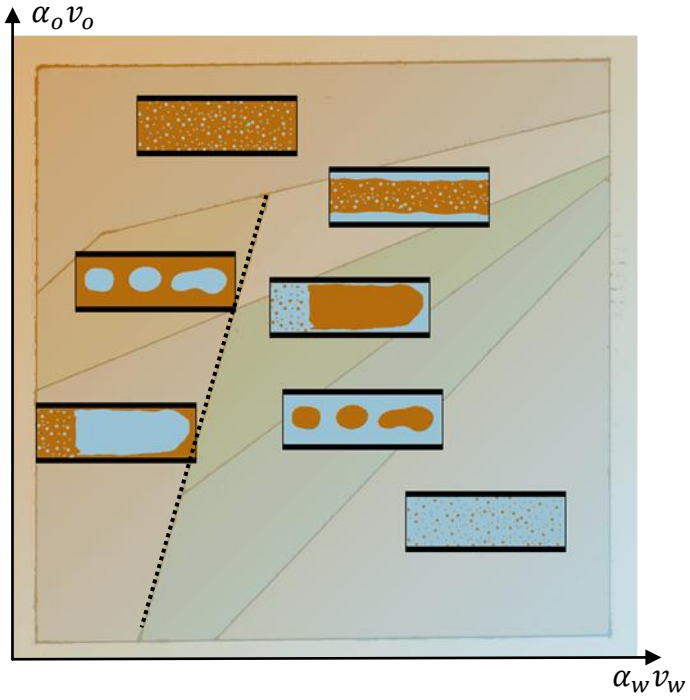

Figure 13.1.4. Flow regimes for oil and water based on Charles et al.'s (1961) measurements of horizontal flow plotted in logarithmic scale. The oil's kinematic viscosity $\mu_0 = 65 \cdot 10^{-3}\ Pa \cdot s$*.The dotted line indicates the difference between forms of water-in-oil and oil-in-water flow.*

Later works by Arirachakaran et al. (1989) and Trallero et al. (1997) have been published, but comparing the results is relatively difficult due to the lack of convenient nondimensional ways to display the flow regime diagrams. One trend is visible in all the authors' results, though: The sequence in which different flow patterns occur when increasing or reducing one liquid's superficial velocity seems to be as indicated in figure

13.1.4 for all different viscosities measured, but exactly where transition takes place depends on the viscosities, densities, and other parameters.

From a practical point of view the main issue in predicting the pressure drop in homogeneous liquid-liquid dispersed flow is the modeling of the mixture viscosity, and that again depends on identifying which phase is continuous.

13.2 Emulsion viscosity

When the slippage (velocity difference) between the dispersed and the continuous phase is significant, the mixture viscosity is normally taken as the viscosity of the continuous phase. Using index *m* for mixture, *c* for continuous, and *d* for dispersed, we set:

$$\mu_m = \mu_c \tag{13.2.1}$$

The situation changes somewhat if the dispersed droplets are very small: In a fine dispersion, sometimes called an *emulsion*, we need to take properties from both liquids into consideration when estimating the viscosity. According to Baron (1953), the dispersion should be treated as an emulsion if:

$$Re_c \left(\frac{d_D}{d}\right)^2 \frac{\rho_d}{\rho_c} < 1 \tag{13.2.2}$$

d_d is the droplet diameter of the dispersed phase. The continuous phase's Reynolds number is defined by the mixture velocity v_m as:

$$Re_c = \frac{v_m d \rho_c}{\mu_c} \tag{13.2.3}$$

The droplet diameter can be estimated by the Kolmogorow-Hinze (1955) model along the lines explained in chapter 5.7.

The emulsion viscosity is proportional to the continuous phase's viscosity, but it also depends on the dispersed phase's volume fraction α_d, the droplet diameter d_d, the

dispersed phase's viscosity μ_d, the share rate and the temperature T. Emulsifying agents – chemicals which help the emulsion to be stable and avoid separation – may also play a role (Sherman, 1968, Schramm, 1992).

The classical Einstein equation from 1906 can be used to calculate the mixture velocity for low dispersed phase volume fractions ($\alpha_d \leq 0.01$):

$$\mu_m = (1 + 2.5\alpha_d)\mu_c \; if \; \alpha_d \ll 1 \tag{13.2.4}$$

At higher dispersed phase concentrations, things become more complicated. When approaching phase inversion conditions, emulsions behave as non-Newtonian pseudoplastic fluids (see *Pipe Flow 1*, chapter 5). This gives the emulsions the remarkable property that they become less viscous as the shear rate increases. No reliable, general correlation for predicting this effect for emulsions exists, and it is necessary to perform tailor-made laboratory measurements for the emulsion in question if we need high-accuracy results (Brauner, 2003)

Even so, other, less well documented correlations exist. For higher fractions of the dispersed phase, Brinkman's (1952) correlation is frequently used:

$$\mu_m = \frac{\mu_c}{(1 - \alpha_d)^{2.5}} \tag{13.2.5}$$

This expression clearly states that there will be a sudden step in the mixture viscosity when inversion takes place, since that means both μ_c and α_d will switch which liquid they refer to. It ignores the observed peak in viscosity close to the inversion point, though.

If the phases are relatively unmixed, but the mixture viscosity still is going to be used (meaning two-phase flow is approximated as one-phase flow in the model), linear interpolation has sometimes been used. If so, we can no longer talk about one dispersed and another continuous phase. Using indexes *1* and *2* to describe the two liquids, the mixture viscosity can be expressed as:

$$\mu_m = \alpha_1\mu_1 + \alpha_2\mu_2 \tag{13.2.6}$$

Pan (1996) proposed to use a weighted average between equations 13.2.5 and 13.2.6, so that:

$$\mu_m = C_m \frac{\mu_c}{(1-\alpha_d)^{2.5}} + (1-C_m)(\alpha_1\mu_1 + \alpha_2\mu_2) \tag{13.2.7}$$

The factor C_m was called a mixing degree coefficient. He actually defined that coefficient for three-phase gas-oil-water flow, but liquid-liquid two-phase flow can be seen as a sub-case where the gas fraction is zero. Pan (1996) defined:

$$C_m = 1 - exp\frac{Re_{3p}}{K_{C_m}} \tag{13.2.8}$$

The three-phase Reynolds number was defined for:

$$Re_{3p} = \frac{(\rho_G\alpha_G v_G + \rho_o\alpha_o v_o + \rho_w\alpha_w v_w)(\alpha_G v_G + \alpha_o v_o + \alpha_w v_w)d}{\mu_G\alpha_G v_G + \mu_o\alpha_o v_o + \mu_w\alpha_w v_w} \tag{13.2.9}$$

We recognize the first parenthesis as the sum of all mass flows pr. unit area. The last is a sum of superficial velocities. The viscosity has been inserted as a weighted average of the phase viscosities. Pan (1996) found that these correlations fit his experiments remarkably well if he used $K_{C_m} = 15{,}000$.

13.3 Phase inversion criteria

Inversion can occur spontaneously so that for instance oil drops in water become water drops in oil and vice versa. As pointed out by Yeo et al. (2000), Rodrigues & Olimans (2005) and Piela et al. (2009), this phenomenon does not always take place at the same volume fraction if the fraction (of water, say) is varied from *0* to *1*, or vice-versa. It appears it occurs only if v_m is high enough to provide a good mixing of the liquids both before and after the inversion. Even so, Arirachakaran (1989) proposed the following correlation for the critical water fraction in an oil-water emulsion:

$$\alpha_w{}^* = 0.5 - 0.1108 log_{10} \frac{\mu_0}{\mu_r} \tag{13.3.1}$$

The reference dynamic viscosity $\mu_r = 10^{-3} Pa \cdot s$.

Later criteria have been developed on the basis of minimizing the total free energy. Brauner & Ullmann (2002) proposed the following for water-oil emulsions:

$$\alpha_w{}^* = \frac{\left(\frac{\sigma}{d_D}\right)_{wo} + \frac{s}{6}\sigma_{wo}\cos\beta_{wet}}{\left(\frac{\sigma}{d_D}\right)_{wo} + \left(\frac{\sigma}{d_D}\right)_{ow}} \tag{13.3.2}$$

β_{wet} is the liquid-solid surface wettability angle. For relatively large diameter pipes, or if the oil-water surface tension is the same for both oil-in-water and water-in-oil dispersions, this can be simplified to an expression containing only the density and kinematic viscosity ratios:

$$\alpha_w{}^* = 1 - \frac{\frac{\rho_o}{\rho_w}\left(\frac{v_o}{v_w}\right)^{0.4}}{1 + \frac{\rho_o}{\rho_w}\left(\frac{v_o}{v_w}\right)^{0.4}} \tag{13.3.3}$$

It has been shown that impurities and even entrained gas bubbles may have a very significant effect on $\alpha_w{}^*$ (Brauner & Ullmann, 2002). That makes it difficult to predict conditions for phase inversion accurately in practice.

13.4 Stratified flow friction modeling

For stratified flow, the theory outlined for gas-liquid flow in chapter 3.5 should in principle apply to liquid-liquid flow as well. It turns out, though, that the many possible sorts of stratified flows which may occur in liquid-liquid flows (figure 13.1.1) call for modifying the model somewhat. Brauner & Maron (1989) have found that calculating the hydraulic diameter in the way it was proposed in equations 3.5.7 and 3.5.8 should be done only when the average velocities of each phase are approximately the same. If so, we set (using index *W* for wall, index w for water):

$$\begin{aligned} d_{h\,oW} &\stackrel{\text{def}}{=} \frac{4A_o}{O_{0W}} \\ & \quad if\ v_o \sim v_w \\ d_{h\,wW} &\stackrel{\text{def}}{=} \frac{4A_w}{O_{wW}} \end{aligned} \tag{13.4.1}$$

Otherwise, they proposed that the hydraulic diameter should be calculated by:

$$\begin{aligned} d_{h\,oW} &\stackrel{\text{def}}{=} \frac{4A_o}{O_{0W} + O_{wW}} \\ & \quad if\ v_o > v_w \\ d_{h\,wW} &\stackrel{\text{def}}{=} \frac{4A_w}{O_{wW}} \end{aligned} \tag{13.4.2}$$

And:

$$\begin{aligned} d_{h\,oW} &\stackrel{\text{def}}{=} \frac{4A_o}{O_{0W}} \\ & \quad if\ v_o < v_w \\ d_{h\,wW} &\stackrel{\text{def}}{=} \frac{4A_w}{O_{0W} + O_{wW}} \end{aligned} \tag{13.4.3}$$

Similar to equations 3.5.9 and 3.5.10, the Reynolds numbers are defined for each phase separately:

$$Re_{h\,oW} \stackrel{\text{def}}{=} \frac{v_o d_{h\,oW} \rho_o}{\mu_o} \tag{13.4.4}$$

$$Re_{h\,wW} \stackrel{\text{def}}{=} \frac{v_w d_{h\,wW} \rho_w}{\mu_w} \tag{13.4.5}$$

The friction coefficients for the friction between each phase and the pipe wall is then determined as for single-phase flow. The interfacial friction coefficient is simply taken as the friction coefficient of the fastest flowing phase:

$$f_{ow} = f_{oW} \; if \; v_o \geq v_w \tag{13.4.6}$$

$$f_{ow} = f_{wW} \; if \; v_o < v_w \tag{13.4.7}$$

With these friction factors, stratified liquid-liquid flow can be simulated as for gas-liquid flow.

"Ability will never catch up with the demand for it."
Malcolm Forbes

14 Two-phase liquid-solid flow

How solids are transported in liquids:

- Liquid-solid flow regimes and how they are created
- Forces on solid particles
- Minimum mixture velocity to avoid particle accumulation

14.1 General about liquid-solid flow

Mixtures of solids and liquids are called *slurries*, and a search for that keyword on the internet generally turns up a lot of information about it. Pneumatic conveying of powders or other solids, a related phenomenon, is used in some industrial processes. Liquids, most often water, can also be used to transport sand or even gravel through pipelines. One of the first large engineering projects that involved transportation of solids by liquid was the dredging for the Suez Canal in Egypt in the 1860s. Since then, many researchers have been interested in liquid-solid flow because it can offer a convenient way to transport solids. That is different from how gas-oil multi-phase flow technology has been developed – much of it sprang out of nuclear boiler simulations - and the terminology is to some extent similarly different.

The main subject of interest here is transport of oil and natural gas, and the most frequently encountered solids when dealing with such fluids are sand or *proppant* (particles used for fracturing to increase production) coming from the well. As we will discover in chapter 18, chemical conditions can also lead to the formation of solids in the form of hydrates, wax, asphaltene, scales, or corrosion particles, and they may be of very different size and volume fraction compared to what we normally encounter in case of sand.

We would generally prefer our wells not to produce particles, and we would rather avoid sand in petroleum pipelines. Avoiding sand is not necessarily the most economical alternative, however, because the problem can be dealt with in three alternative ways:

i) Wells may be completed with downhole sand exclusion systems, or:
ii) Wells may be refitted with sand exclusion systems at a later date when sand production begins, or:
iii) We may manage rather than prevent sand production by designing the facilities to handle the sand (Dusseault et al., 1998, Dusseault & El-Sayed, 2001).

The main disadvantage with conventional downhole sand completions is that they negatively affect the overall well performance due to the additional pressure drop they generate. As a result, sand management technology is gaining attention and maximum sand free rate objectives are being superseded by maximum acceptable sand rates. This change in philosophy has the potential to improve both development and production economics, but understanding the flow properly is currently a limiting factor (see for instance Tronvoll et al., 2001, and Bello, 2008). The economic benefits are of course highest for the most capital intensive sorts of developments, which most often means deepwater fields and fields in very harsh environments. That happens to be precisely where an increasing amount of future developments are located. In such fields, it is also common to transport the well-flow from the wellhead a considerable distance to shore or offshore processing facilities, and this may create additional flow assurance challenges.

As pointed out by Gillies, et. al., (1997), most sand management operations in crude oil production are designed to keep the sand production fraction $\alpha_s < 0.05$, while in non-sand managed producing wells and flow-lines it is kept very much lower. It can be close to zero (perhaps in the order of $\alpha_s v_s \sim 5 \cdot 10^{-7} \alpha_L v_L$, Stevenson et al., 2001), or at least very low ($\alpha_s v_s \sim 2 \cdot 10^{-4} \alpha_L v_L$, Danielson, 2007). Commonly produced reservoir

sand particles are very small, typically having much smaller diameters than *1 mm* (Bello, 2008).

When we have significant amounts of sand in the flow, we need to make sure sand does not accumulate in the line to such an extent that the flow is blocked or severely restricted, and we may also need to estimate or measure sand erosion.

Solids can be transported out of the pipe by the fluid or cleaned out by pigging. If the solids are dislodged by a pig, we need to make sure the pig moves faster than the velocity necessary to move the solids. Otherwise they will accumulate in front of the pig, potentially causing it to become stuck. Knowledge of the velocity required to move solids in a pipeline is an important design parameter in a pigging program, and we will have a closer look at how to estimate it in chapter 14.3.

Another phenomenon of interest is the *black powder* occurring in natural gas pipelines. It creates flow conditions similar enough to liquid-solid flow to be mentioned here. The term 'black powder' is used as a catch-all phrase to include iron oxides, sulphide, and carbonate. Even though the name seems to indicate otherwise, the color does not have to be black – once it is scraped out, it can also appear as white or silvery. If the pipeline is operated in a corrosive condition, so that even just very thin scales flake off from the wall, considerable amounts of black powder can easily be delivered to customers, and it may also have adverse effects on the surface roughness and thereby the pipeline's capacity. Such corrosion can be of size down to $1\,\mu m$. Even particles this small can become stationary if the gas velocity or pressure (and therefore gas density) is small enough.

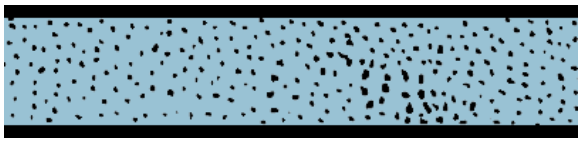

a. Homogeneous flow. The solids are evenly distributed in the liquid.

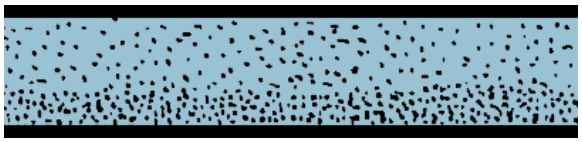

b. Heterogeneous flow. The solids are carried by the fluid, but not distributed evenly.

c. Stratified flow. The solids move, but partly along the bottom of the pipe.

d. Stationary bed flow. Some of the solids do not move.

Figure 14.1.1. Flow regimes in liquid-solid flow.

When we study the different flow regimes in figure 14.1.1, we see that the solid particles have much in common with the droplets modeled in chapter 5. Unlike droplets, though, sand particles do not tend to break up or coalesce, but the turbulence mechanism carrying the particles is similar to those carrying the droplets.

14.2 The building up of solids in the pipeline

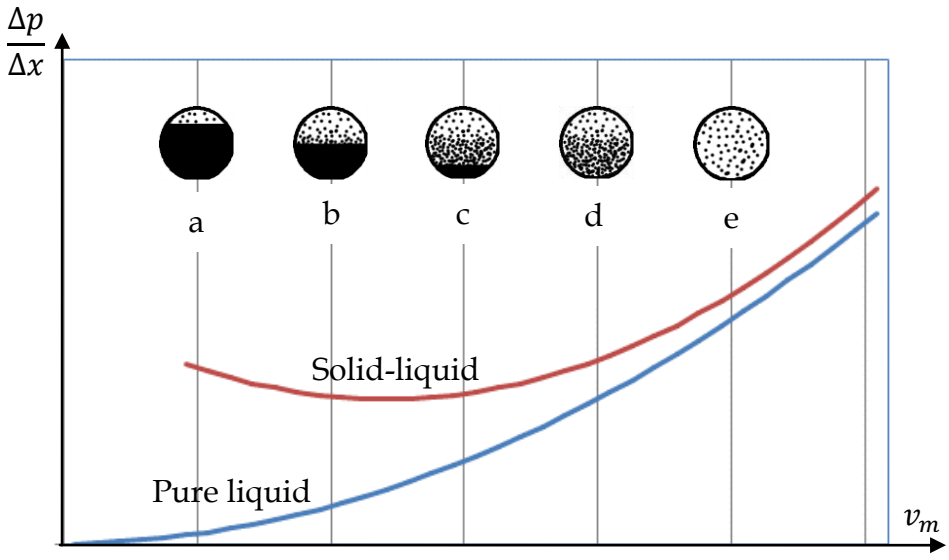

Figure 14.2.1. Flow regimes and friction loss as a function of mixture velocity.

To get a feeling for how solids may build up in a pipe, let us start by considering a horizontal pipe carrying a pure liquid – water, say. If we for simplicity ignore the fact that the Darcy-Weisbach friction factor changes somewhat with Reynolds number, we can say that the friction loss is proportional to the square of the water velocity if the flow is turbulent. That is indicated by the lower curve in figure 14.2.1. If we start adding fine sand while the water flows at a relatively high velocity, that sand will spread quite evenly in the liquid (see 14.2.1 e). Measurements show that doing so actually increases the pressure loss, even though the sand grains seem to follow the flow nicely. The grains affect the mixture density, however, and they also take part in exchanging momentum between turbulence eddies. In addition, they touch the pipe wall occasionally, and that has the total effect of moderately increasing the friction.

If we reduce the mixture velocity, the pressure drop decreases, though not as much as it would have if there was no sand. When a larger percentage of the sand is at the lower part of the pipe's cross-section, this has a greater effect on the friction, even when all the sand grains are carried by the water. Reducing the velocity further leads to sand building up at the lower part of the pipe, but a moderate velocity reduction does not stop all the sand from moving in the same direction as the water. Further reduction of the mixture velocity leads to further sand buildup, and some of the sand also becomes stationary. We therefore sooner or later reach a point where further reduction in mixture velocity leads to higher rather than lower pressure drop due to the extra sand buildup, and then there is of course a chance the pipe may get blocked. It has been suggested that operating a pipeline carrying liquid-solid flow is a bit like flying an airplane: If the velocity becomes too low, the wings stall and the plane loses altitude or worse. In the pipeline's case, too low velocity leads to drop in efficiency or blockage.

We notice, though, that there is some safety in the way a blockage builds up: If we keep the liquid mass flow constant, the local liquid velocity is going to increase as solids build up and decreases the available cross-sectional area. That increased velocity tends to reduce the chances of further buildup taking place.

14.3 Minimum transport velocity

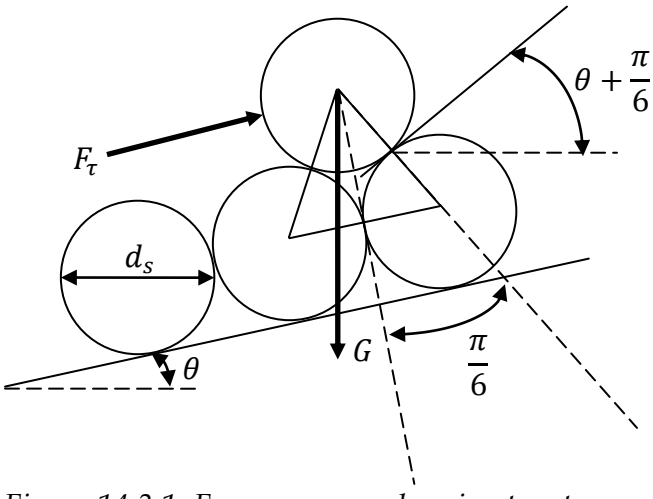

Figure 14.3.1. Forces on a sand grain at rest.

Let us at first study a simplified situation in which a spherical particle is at rest on other spherical particles in a pipe with inclination angle θ, as this is indicated on figure 14.3.1. If the sand grain lies at the bottom of the pipe, it feels the friction from the liquid passing on top of it. In *Pipe Flow 1*, equation 2.1.3, that friction shear was found to be:

$$\tau = \frac{\Delta p}{\Delta x}\frac{d}{4} \tag{14.3.1}$$

If each sand grain covers an area of $\pi {d_s}^2/4$ of the pipe's inner surface, the force on one grain becomes:

$$F_\tau = \frac{\Delta p}{\Delta x}\frac{\pi d {d_s}^2}{16} \tag{14.3.2}$$

In case very little sand has settled so that the effective pipe cross-sectional area is almost unaffected, and if we also neglect the added pressure loss due to the sand's influence on roughness, density, and turbulence, we can calculate the pressure caused by friction, $\Delta p/\Delta x$, from the Darcy-Wesibach friction factor, and we get:

$$F_\tau = f\frac{\pi {d_s}^2 \rho_L {v_L}^2}{32} \tag{14.3.3}$$

If this force is just high enough to push the sand grain at an angle $\theta + \pi/6$, see figure 14.3.1 (presuming the grain is rolling so that friction does not play a part, and also presuming the spheres have identical diameters and are stacked in the two-dimensional way shown on the figure), we get:

$$F_\tau \cos\left(\frac{\pi}{6}\right) = G \sin\left(\theta + \frac{\pi}{6}\right) \tag{14.3.4}$$

By expressing the gravity force for a sphere of density ρ_S (accounting for buoyancy), we get:

$$f\frac{\pi {d_s}^2 \rho_L {v_L}^2}{32}\cos\left(\frac{\pi}{6}\right) = \frac{\pi(\rho_S - \rho_L){d_s}^3}{6} g \sin\left(\theta + \frac{\pi}{6}\right) \tag{14.3.5}$$

We can then find the minimum average liquid velocity necessary to move a sand grain of diameter d_s. We denote it the critical velocity ${v_L}^*$ and get:

$$v_L{}^* = \sqrt{\frac{16}{3f}\frac{(\rho_S - \rho_L)}{\rho_L} g d_s \left[\frac{\sin\left(\theta + \frac{\pi}{6}\right)}{\cos\left(\frac{\pi}{6}\right)}\right]} \tag{14.3.6}$$

In case the grains slide rather than roll on top of each other, there will also be a friction force at the connection points between grains. By geometrical considerations we see that this force is:

$$F_{fs} = \mu_{fs}\left[F_\tau \sin\left(\frac{\pi}{6}\right) + G\cos\left(\theta + \frac{\pi}{6}\right)\right] \tag{14.3.7}$$

μ_{fs} is the friction coefficient between sand grains. The term $F_\tau \sin(\pi/6)$ is F_τ's component normal to the friction surface, while $G\cos(\theta + \pi/6)$ is the normal component of the gravity (compensated for buoyancy).

When this friction is taken into account, equation 14.3.4 modifies to:

$$F_\tau \cos\left(\frac{\pi}{6}\right) = G\sin\left(\theta + \frac{\pi}{6}\right) + F_{fs} \tag{14.3.8}$$

By inserting equations 14.3.7 into equation 14.3.8 and adding the friction force F_{fs} to equation 14.3.5, we get the following correlation for grains sliding against stationary grains in a liquid- or gas-filled pipe carrying sand with low sand fraction α_s:

$$\begin{aligned} f\frac{\pi {d_s}^2 \rho_L {v_L}^2}{32}\cos\left(\frac{\pi}{6}\right) \\ = \frac{\pi(\rho_S - \rho_L){d_s}^3}{6} g\sin\left(\theta + \frac{\pi}{6}\right) \\ + \mu_{fs}\left[f\frac{\pi {d_s}^2 \rho_L {v_L}^2}{32}\sin\left(\frac{\pi}{6}\right) + \frac{\pi(\rho_S - \rho_L){d_s}^3}{6} g\cos\left(\theta + \frac{\pi}{6}\right)\right] \end{aligned} \tag{14.3.9}$$

The critical velocity becomes:

$$v_L^* = \sqrt{\frac{16}{3f}\frac{(\rho_S - \rho_L)}{\rho_L} g d_s \left[\frac{\sin\left(\theta + \frac{\pi}{6}\right) + \mu_{fs}\cos\left(\theta + \frac{\pi}{6}\right)}{\cos\left(\frac{\pi}{6}\right) - \mu_{fs}\sin\left(\frac{\pi}{6}\right)}\right]} \tag{14.3.10}$$

As one would expect, equation 14.3.10 turns out to be identical to equation 14.3.6 in case the friction between grains is zero ($\mu_{fs} = 0$), which also corresponds to rolling grains. We can therefore consider equation 14.3.6 to be a special case of the more general equation 14.3.10, and the μ_{fs} can be interpreted as a factor which expresses the sand grain's resistance to moving (even if they roll, they are not completely round and may be modeled by setting $\mu_{fs} > 0$).

In case the pipe wall is nearly completely smooth compared to the grain size, the grains sliding along the wall do not need to be lifted over the neighboring grain to get moving. In that case, the angle which used to be $\pi/6$ changes to 0, and equation 14.3.10 changes to:

$$v_L^* = \sqrt{\frac{16}{3f}\frac{(\rho_S - \rho_L)}{\rho_L} g d_s \left[\sin(\theta) + \mu_{fs}\cos(\theta)\right]} \tag{14.3.11}$$

If the pipe is horizontal ($\theta = 0$), this simplifies further to:

$$v_L^* = \sqrt{\frac{16}{3f}\frac{(\rho_S - \rho_L)}{\rho_L} g d_s \mu_{fs}} \tag{14.3.12}$$

In vertical pipes, the sand particles are not going to accumulate near the bottom of the pipe, as equation 14.3.10 presumes. It therefore needs to be replaced by a simpler one based the sand grains behaving much like bubbles or droplets. We can adapt equation 8.7.3 to cover this by setting:

$$v_L^* = \sqrt{\frac{4}{3C_D} g d_s \frac{(\rho_s - \rho_L)}{\rho_L}} \tag{14.3.13}$$

The drag coefficient C_D can be estimated from equation 5.2.1 in case the sand grains are modeled as spherical.

The equations above are based on average liquid velocities (or mixture velocities, since $v_L{}^* \approx v_m{}^*$ when we have very low sand compared to liquid flow). Using an average should be a good approximation in equation 14.3.10, since the pipe wall share force (and the Darcy-Weisbach friction factor f) is defined by and well documented to be described by that average velocity. In equation 14.3.13, on the other hand, the particles are spread out across the pipe's cross section, and those in the center experience a fast velocity, while those close to the wall may experience velocities close to zero and possibly sink downwards (until turbulent eddies throw them back closer to the center). But apart from the velocity-profile effect, equation 14.3.13 is fairly uncomplicated and unhampered by uncertainty caused by tricky presumptions. Other, purely empirical correlations giving considerably different results for vertical flow and low particle loading should therefore be treated with a healthy dose of skepticism if they contradict equation 14.3.13 severely.

Note that for very small sand contents, which is what we are focusing on here, the liquid-sand mixture velocity is going to be close to the liquid velocity v_L, so $v_L{}^* \approx v_m{}^*$ (not because the sand moves at the same speed as the liquid, but because there is very little sand).

In most practical situations the grains are not all the same size, and the sand grain diameter must be interpreted as some sort of average – a problem similar to the one we experienced when discussing droplets in earlier chapters. Also, turbulence eddies result in the maximum instantaneous share force on a sand grain becoming considerably higher than the average expressed by equation 14.3.1. The grains may therefore be pushed along during those peak force times even if the time average velocity is too low to move them. Even though these effects have not been accounted for in equation 14.3.10, this simple theory catches some of the essence of liquid-solid flow:

i) There is a minimum liquid (or mixture) velocity, below which solids begin to settle.
ii) The minimum velocity is approximately proportional to the root of the density difference between the solid and the liquid, and inversely proportional to the root of the liquid density.
iii) The minimum velocity is approximately proportional to the root of the solid particles' diameters, meaning larger particles have a stronger tendency to settle than smaller ones.

iv) There is a stronger tendency for solids to accumulate in uphill than in downhill flow (but normally not in vertical or nearly vertical flow).

We notice that in case a lot of sand already has accumulated in the pipe so the effective area is reduced and no longer circular, we can use theory for non-circular pipes to estimate the shear force. This is done in a manner very similar to how we calculated it for stratified gas-liquid flow. Other authors have shown this procedure in detail (see for instance Peker & Helvaci, 2007 or Abulnaga, 2002).

Empirical formulas exist, too. Durand & Condolios (1952) derived the following equation for uniformly sized sand and gravel in horizontal pipes (and mostly applied to systems where the liquid is water):

$$v_m{}^* = K_D \sqrt{2gd\frac{\rho_S - \rho_L}{\rho_L}} \tag{14.3.14}$$

The Durand-factor K_D (Durand, 1953) was improved by Schiller & Hebich (1991) and defined for a statistical particle diameter average, so:

$$K_D = 1.3\alpha_S{}^{0.125}[1 - exp(-6.9 \cdot 10^3 d_{s\,50})] \tag{14.3.15}$$

The particle diameter average $d_{s\,50}$ is defined as the size below which half the particles would be lower than that size.

It may be a bit surprising that unlike in equations 14.3.10 and 14.3.12, equation 14.3.14 contains the pipe diameter rather than the sand grain diameter. We will soon see the equations may still give relatively similar results for horizontal flow, but less so for vertical flow.

As an example, consider water of density 998 kg/m^3 carrying sand of density 2650 kg/m^3 through a horizontal pipe of diameter 0.20 m. The average sand grain diameter $d_{s\,50} = 10^{-3}m$, and the sand volume fraction is $\alpha_S = 0.01$.

Inserting that into equation 14.3.15 gives $K_D = 0.73$, which according to equation 14.3.14 leads to the critical accumulation velocity $\boldsymbol{v_m}^* = \mathbf{1.7}\ \boldsymbol{m/s}$.

We can compare this result with the rolling sand grain model in equation 14.3.6. If the roughness relevant to the shear-force on the sand grains are described by a relative roughness $d_{s\,50}/d = 5 \cdot 10^{-3}$, and the Reynolds number is in the order of $(1.7m/s \cdot 0.2m)/10^{-6}m^2/s = 3.4 \cdot 10^{-5}$, the Darcy-Weisbach friction factor can be estimated to $f = 0.03$ (see for instance figure 2.9.1, Pipe Flow 1). For horizontal pipe ($\theta = 0$), equation 14.3.6 then leads to $\boldsymbol{v_L}^* = \mathbf{1.3}\ \boldsymbol{m/s}$.

A comparison with the sliding sand model expressed in equation 14.3.10 requires the friction factor μ_{fs} to be known. If we set it to $\mu_{fs} = 0.5$ - probably a relatively high value for a wetted sand surface - we get $\boldsymbol{v_L}^* = \mathbf{2.1}\ \boldsymbol{m/s}$.

In case the pipe is so smooth the sand grains can slide along the bottom of it without being affected by imperfections holding them back, we may use equations 14.3.11 for smooth surfaces (which is also identical to equation 14.3.12 for our horizontal pipe) and get $\boldsymbol{v_L}^* = \mathbf{1.2}\ \boldsymbol{m/s}$.

We see that these four results for horizontal flow are somewhat different, but still of the same order. The most conservative turned out to be equation 14.3.10 for this particular example, but equation 14.3.12 depends on slightly different parameters than equation 14.3.10, so we can expect the differences to become larger in other examples. The better theoretical foundation for equation 14.3.10, and its ability to account for inclined pipes as well as viscosities other than that of water, seems to make it more useful for practical calculations, even though it may not be well documented with measurements.

Interestingly, if we use equation 14.3.13 to estimate the critical velocity for vertical flow, we get C_D~0.9 and $\boldsymbol{v_L}^* = \mathbf{0.15}\ \boldsymbol{m/s}$, which is much lower than what we get for horizontal flow. This may at first seem surprising, since transporting particles upwards seems likely to take more effort than transporting them horizontally. But in vertical flow, the particles are not concentrated close to the pipe wall, they are not exposed to wall friction, and – more importantly – they are surrounded by fluid flowing much faster than that close to the wall. According to these results, this more than compensates for the extra gravitational forces working against the flow.

"The beginning of knowledge is the discovery of something we do not understand."
Frank Herbert, ca. 1950

15 Three-phase gas-liquid-liquid flow

Three-phase gas-liquid-liquid flow modeled for gas-oil-water mixtures:

- Some important flow regimes
- Dynamic models for gas-liquid-liquid flow
- Stratified and slug flow
- Some guidelines for simulations

15.1 Introduction

The general conservation equations developed in chapter 2 are just as valid for three-phase or four-phase flow as they are for two-phase flow. The problem is that the closure relationships become more complicated. In chapter 1.2 we saw that gas-liquid flow can create many different flow regimes, and liquid-liquid flow can take even more forms. In addition, we know that liquid-solid flow can occur. The number of different flow regimes we can encounter when several of these situations combine to form three-phase flow is very high, and the complexity involved in describing them increases

accordingly. Even creating and observing the many possible flow regimes in the laboratory is difficult. Combining a gas, two liquids and a solid – in practice that most often means natural gas, oil, water, and sand – creates four-phase flow. That is clearly something we can encounter in real wells. When simulating such flow, though, we most often simplify the problem down to three-phase flow, for instance by ignoring or only slightly accounting for the solids. In this chapter we are going to limit the model to three-phase flow of the gas-liquid-liquid sort. In chapter 16, we will discuss models for gas-liquid-solid flow.

One way to get an impression of the various possible flow regimes is to go back to the gas-liquid flow in figures 1.2.1 and 1.2.3, but imagining that the liquid consists of two liquids rather than one, so they occur in nearly all the forms shown in figures 13.1.1 - 13.1.3. As an example, the liquid layer in the gas-liquid stratified flow figure 1.2.1 iv) can consist of a dispersion of either liquid in the other of the sort shown in figure 13.1.3, say, or the two liquids can themselves form two or several stratified layers like those illustrated in figure 13.1.1. The same goes for slug flow, in that we can have an emulsion of the two liquids slugging with the gas, while also having one liquid carrying most of the gas dispersed as small bubbles and therefore behaving like a liquid with modified properties. That liquid can interact with the other liquid in all the ways described in chapter 13.

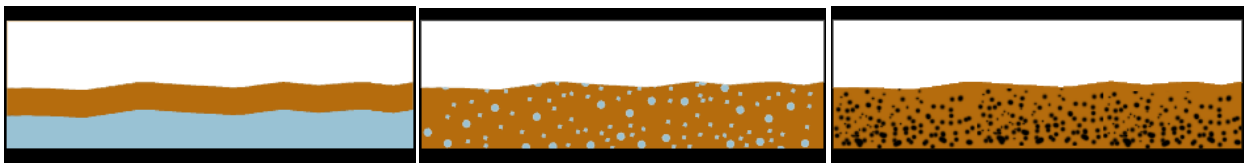

Figure 15.1.1. Three randomly chosen from many possible types of three-phase stratified flow: Separated gas-oil-water, gas over a dispersion of water-in-oil, and – as described in greater detail in chapter 16 - gas over a layer of oil carrying sand.

The stratified flows illustrated in figure 15.1.1 are not much more complicated to model for three-phase than for two-phase flow. Some of the other flow regimes, though, can be very complicated. One obvious potential way to simplify is to limit the number of possible stratified flows to one of the simplest ones even when we are dealing with more complicated types.

15.2 Main equations

All conservation equations are as described for the general case in chapter 2. For simplicity we are going to assume isothermal flow (and therefore not concern ourselves with the energy equation), as well as no phase change (the relevant terms can relatively easily be added later if needed).

We index the gas as G, while the two liquids are indexed o (oil) and w (water). Index W stands for wall. The 3 mass conservation equations become:

$$\frac{\partial(\alpha_G \rho_G)}{\partial t} + \frac{\partial(\alpha_G \rho_G v_G)}{\partial x} = 0 \tag{15.2.1}$$

$$\frac{\partial(\alpha_o \rho_o)}{\partial t} + \frac{\partial(\alpha_o \rho_o v_o)}{\partial x} = 0 \tag{15.2.2}$$

$$\frac{\partial(\alpha_w \rho_w)}{\partial t} + \frac{\partial(\alpha_w \rho_w v_w)}{\partial x} = 0 \tag{15.2.3}$$

The momentum equations become:

$$\frac{\partial(\alpha_G \rho_G v_G)}{\partial t} + \frac{\partial(\alpha_G \rho_G {v_G}^2)}{\partial x} = -\alpha_G \frac{\partial p_G}{\partial x} + (R_{Gi} + R_{GW}) - \alpha_G \rho_G g \sin\theta \tag{15.2.4}$$

$$\frac{\partial(\alpha_o \rho_o v_o)}{\partial t} + \frac{\partial(\alpha_o \rho_o {v_o}^2)}{\partial x} = -\alpha_o \frac{\partial p_o}{\partial x} + (R_{oi} + R_{oW}) - \alpha_o \rho_o g \sin\theta \tag{15.2.5}$$

$$\frac{\partial(\alpha_w \rho_w v_w)}{\partial t} + \frac{\partial(\alpha_w \rho_w {v_w}^2)}{\partial x} = -\alpha_w \frac{\partial p_w}{\partial x} + (R_{wi} + R_{wW}) - \alpha_w \rho_w g \sin\theta \tag{15.2.6}$$

The definition of fraction leads to:

$$\alpha_G + \alpha_o + \alpha_w = 1 \tag{15.2.7}$$

The density property equations are:

$$\rho_G = \rho_G(p,T) \tag{15.2.8}$$

$$\rho_o = \rho_o(p,T) \tag{15.2.9}$$

$$\rho_w = \rho_w(p,T) \tag{15.2.10}$$

The unknowns here are the fractions α_G, α_o, α_w, the densities ρ_G, ρ_o, ρ_w, the velocities v_G, v_o, v_w, and the pressure p. Therefore we have 10 equations to solve. If we use pressure correction terms, we need to establish those, too. Also, we need expressions for the friction terms.

The closure relationships depend on the flow regime in question. As already explained, there are very many possible such regimes, but we will simplify.

This transient model is based on the steady-state model presented by Zhang & Sarica (2006) and a DOE-report (2008). The model is not fully developed and documented at this stage, but it constitutes a good base for further improvements.

15.3 Three-layer stratified flow

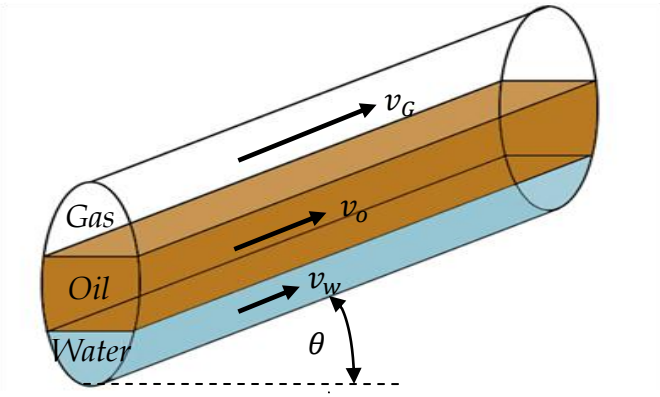

Figure 15.3.1. Gas-oil-water stratified flow

As an example, look at the stratified flow illustrated in figure 15.3.1. When we compare with the gas-liquid two-phase stratified flow model in chapters 3.4 and 3.5, we see that there are considerable similarities, and we can use the same principles to establish

frictions and stability criteria. We notice, though, that the pressure correction term, which describes the pressure difference between phases, becomes a bit more complicated. In the two-phase model, the pressure p was defined as the pressure between the phases on the only interface involved, but now we have two interfaces (between gas and oil, and between oil and water).

We choose to define the pressure p as the pressure at the surface between the gas and the uppermost liquid layer, which in our example is the oil's top surface (opposite in the much rarer situation that the oil has higher density than the water).

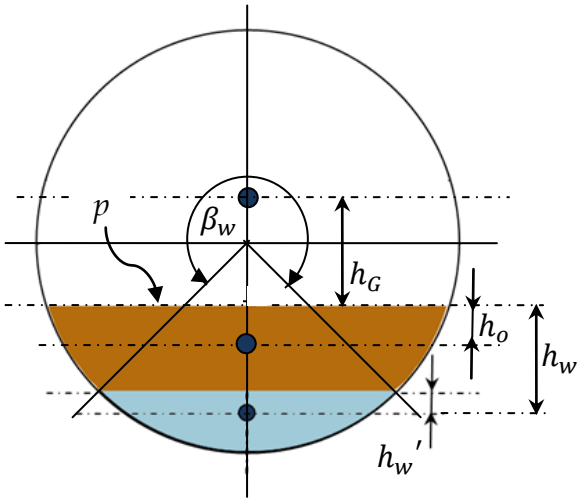

Figure 15.3.2. The different layers' center of gravity in stratified flow, with distance to upper liquid layer's elevation shown.

First, the angle to the lowest layer (the water layer) β_w is determined with equation 3.4.5 by inserting α_w (instead of α_L). It then becomes possible to calculate the distance from the surface between the water cross-section's center of gravity and the surface between the water and the oil, h_w'.

Next, calculate the distance from the oil's upper surface to the center of gravity as it would have been if the oil had covered both the oil- and the water part of the cross-section. That can be done by first calculating β_{w+o} by inserting $\alpha_w + \alpha_o$ into equation 3.4.5, and then using β_{w+o} to calculate $h_{(o\&w)}$ with equation 3.4.2. The oil's center of gravity can then be found by setting:

$$h_{(o\&w)} \cdot (\alpha_w + \alpha_o) = h_w \alpha_w + h_o \alpha_o \qquad (15.3.1)$$

And hence:

$$h_o = \frac{h_{(o\&w)} \cdot (\alpha_w + \alpha_o) - h_w \alpha_w}{\alpha_o} \tag{15.3.2}$$

Determining h_G is done by equation 3.4.1 as for two-phase flow. The gas pressure correction term is also as for two-phase gas-liquid flow, equation 3.4.3, while the liquid correction terms become:

$$\Delta p_o = p_o - p = \rho_o g h_o \tag{15.3.3}$$

$$\Delta p_w = p_w - p = \Delta p_o + \rho_w g h_w{}' \tag{15.3.4}$$

The frictions follow directly from the geometries and the definition of hydraulic diameter, equation 3.5.1. Interfacial friction factors can be estimated using equation 3.5.11 for gas-liquid and 13.3.2 and 13.4.3 for the liquid.

We can now model the stratified flow using conservation equations 15.3.1 - 15.3.10 and the above mentioned closure equations. Be aware, though, that nobody seems to have investigated in detail whether the equation system one ends up with really is hyperbolic when this procedure is followed. It seems natural that it would be, since the physics is similar to that of stratified two-phase flow. But without investigating it thoroughly with eigenvalue analysis or perturbation methods, it is difficult to be sure. If no such analysis is carried out (it is relatively laborious and complicated to do it, end the strong nonlinearities prevent the results from becoming completely general anyway) one should suspect loss of hyperbolicity to be a possibility if the simulations crash. Combining two of the three momentum equations (or even three of them) in a drift-flux fashion may in that case correct the problem.

15.4 Incompressible steady-state slug flow model

Three-phase slugs can be more complex than the two-phase ones discussed in chapter 7 and 9. If the oil and water is fully mixed, they may act much like a single liquid, reducing the problem to two-phase gas-liquid slugging, the only difference being that the liquid mixture properties have to be used instead of those of a single liquid.

If the liquids are not mixed, the slug front can look something like the one in figure 15.4.1. The front of a slug can be quite similar to the front of an ocean wave, with bubbles being mixed into the liquid. For two-phase air-water flow, such mixing was shown in figure 9.4.1.

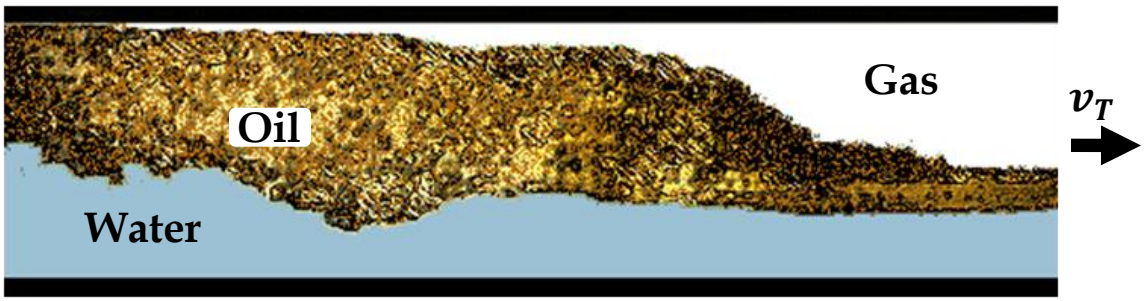

Figure 15.4.1. Slug front in horizontal gas-liquid-liquid flow. Gas bubbles are mixed into the liquids, in this illustration mostly into the oil, but we will model it as if the bubbles are distributed evenly between the liquids. The bubbles are carried by the liquids until they are released into the Taylor-bubble behind it.

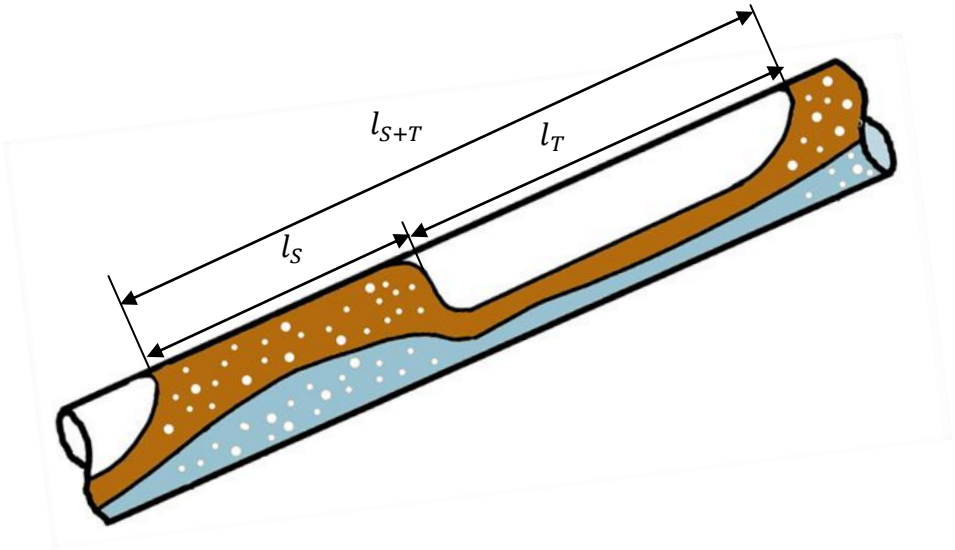

Figure 15.3.3. Slug flow with stratified liquid layers.

If the liquids are not mixed, Zhang & Sarica (2006) proposed modeling them as two stratified layers as indicated on figure 15.3.3. We will use some of their simplified steady-state theory for incompressible fluids to establish closure relationships for our dynamic model. We will not show how to include compressibility or the dynamic terms, but that can in principle be done by simply adding such terms to the ones shown

here. Their theory is only steady-state in the sense that each slug unit has constant properties when seen from outside, but since slugs by their very nature are transient, velocities and fractions must of course be allowed to vary within each unit.

The theory is similar to that in chapter 7, but the liquid phase is considered as two stratified layers (with bubbles in the liquid slug) rather than one liquid.

In case of no liquid entrainment in the gas phase, steady-state continuity for the oil phase under the Taylor-bubble (the zone of length l_T in figure 15.3.3) can be expressed as:

$$(1-\alpha_{wGS})(1-\alpha_{oS})(v_T-v_{oS})=\alpha_{oT}(v_T-v_{oT}) \qquad (15.4.1)$$

The indexes G, o, and again w symbolize gas, oil, and water, while index S points to the liquid slug-part of the pipe. Index T refers to the section where the Taylor-bubble with a liquid film below it is located. α_{wGS} is fraction of water (and bubbles in that water), so $(1-\alpha_{wGS})$ becomes the rest of the slug, which is oil with its entrapped gas bubbles. Multiply that with $(1-\alpha_{oS})$, and we have the slug oil fraction (excluding bubbles). We refer all velocities to a coordinate system moving at the slug unit (translational) velocity v_T. That is identical to the liquid slug's and Taylor bubble's velocity if the slug does not grow or shrink, but it does not equal any phase's absolute velocity. The oil's velocity compared to that system is (v_T-v_{oS}). The total product at the left-hand side of equation 15.4.1 is therefore the superficial velocity of the oil phase. In a steady-state situation, that superficial velocity must be the same under the Taylor bubble, too, which is what the right-hand side expresses.

We can write a similar continuity equation for the water-phase:

$$\alpha_{wGS}(1-\alpha_{wS})(v_T-v_{wS})=\alpha_{wT}(v_T-v_{wT}) \qquad (15.4.2)$$

For the gas-phase, we assume the small bubbles in the slug have the same velocity as the liquid that carries it. The gas fraction for the bubbles in the oil becomes $(1-\alpha_{wGS})\alpha_{oS}$, and the velocity (v_T-v_{oS}). In addition, there is a similar contribution for the bubbles in the water. In the Taylor bubble, the gas fraction is $(1-\alpha_{oT}-\alpha_{wT})$, and we get:

$$(1-\alpha_{wGS})\alpha_{oS}(v_T-v_{oS})+\alpha_{wGS}\alpha_{wS}(v_T-v_{wS})=(1-\alpha_{oT}-\alpha_{wT})(v_T-v_{GT}) \quad (15.4.3)$$

In steady-state flow, the mixture velocity must be constant. It is defined as:

$$v_M=\alpha_G v_G+\alpha_o v_o+\alpha_w v_w \quad (15.4.4)$$

In the slug, that mixture velocity can be expressed in terms of the bubble-filled oil and water fractions:

$$v_M=(1-\alpha_{wGS})v_{oS}+\alpha_{wGS}v_{wS} \quad (15.4.5)$$

In the Taylor-bubble section, we similarly set:

$$v_M=\alpha_{oT}v_{oT}+\alpha_{wT}v_{wT}+(1-\alpha_{oT}-\alpha_{wT})v_{GT} \quad (15.4.6)$$

Each phase cannot have constant fraction within the slug unit even in these 'steady-state' correlations, but the average slug train fraction must be constant for each phase. For the oil, we may write this as:

$$\alpha_o v_o=\frac{l_S}{l_{S+T}}(1-\alpha_{wGS})(1-\alpha_{oS})v_{oS}+\frac{l_T}{l_{S+T}}\alpha_{oT}v_{oT} \quad (15.4.7)$$

Similar equations for the water- and gas phases become:

$$\alpha_w v_w=\frac{l_S}{l_{S+T}}\alpha_{wGS}(1-\alpha_{wS})v_{wS}+\frac{l_T}{l_{S+T}}\alpha_{wT}v_{wT} \quad (15.4.8)$$

$$\alpha_w v_w=\frac{l_S}{l_{S+T}}[(1-\alpha_{wGS})\alpha_{oS}v_{oS}+\alpha_{wGS}\alpha_{wS}v_{wS}]+\frac{l_T}{l_{S+T}}(1-\alpha_{oT}-\alpha_{wT})v_{GT} \quad (15.4.9)$$

The total slug unit length is obviously:

$$l_{S+T} = l_S + l_T \tag{15.3.10}$$

The momentum equations can be expressed as for stratified flow. In the Taylor-bubble part of the slug unit, the model in chapter 15.3.2 is directly applicable, but it is convenient to write all velocities in terms of the moving reference. For the oil under the Taylor bubble, we can write the following steady-state momentum balance:

$$\alpha_{oT}\frac{\Delta p_{\mathrm{T}}}{l_T} = \frac{\alpha_{oT}\rho_o(v_T - v_{oT})(v_{oS} - v_{oT})}{l_T} + \frac{\tau_{GoT}S_{GoT} - \tau_{owT}S_{owT} - \tau_{oWT}S_{oWT}}{A} - \alpha_{oT}\rho_o g\sin\theta \tag{15.4.11}$$

Here we have assumed the momentum transfer from the slug to the Taylor-bubble section is mass flow 'scooped up' by the moving reference frame $\alpha_o A\rho_o(v_T - v_{oT})$ multiplied by the velocity change that mass flow experiences in the Taylor-bubble section $(v_{oS} - v_{oT})$. This momentum transfer is then inserted per unit volume Al_T. For the friction terms, we have inserted the shear stress between phases, so that for instance τ_{GoT} is shear stress from gas to oil in the Taylor-bubble section of the slug unit. Recall that index $_{\mathrm{w}}$ stands for water, while $_W$ stands for pipe wall.

We can then easily write a similar steady-state momentum equation for the water:

$$\alpha_{wT}\frac{\Delta p_{\mathrm{T}}}{l_T} = \frac{\alpha_{wT}\rho_w(v_T - v_{wT})(v_{wS} - v_{wT})}{l_T} + \frac{\tau_{owT}S_{owT} - \tau_{wWT}S_{wWT}}{A} - \alpha_{wT}\rho_w g\sin\theta \tag{15.4.12}$$

For the Taylor-bubble itself (neglecting momentum transfer from the small slug-bubbles, which is normally insignificant due to the low mass exchange compared to the friction forces), we get:

$$(1-\alpha_{oT}-\alpha_{wT})\frac{\Delta p_T}{l_T}=\frac{-\tau_{GoT}S_{GoT}-\tau_{GWT}S_{GWT}}{A}-(1-\alpha_{oT}-\alpha_{wT})\rho_G g\sin\theta \qquad (15.4.13)$$

We can establish similar equations for the two liquids in the slug:

$$(1-\alpha_{wGS})\frac{\Delta p_S}{l_S}=\frac{(1-\alpha_{wGS})\rho_o(v_T-v_{oS})(v_{oT}-v_{oS})}{l_S}+\frac{-\tau_{owS}S_{owS}-\tau_{oWS}S_{oWS}}{A}-(1-\alpha_{wGS})\rho_o g\sin\theta \qquad (15.4.14)$$

And:

$$\alpha_{wGS}\frac{\Delta p_S}{l_S}=\frac{\alpha_{wGS}\rho_w(v_T-v_{wS})(v_{wT}-v_{wS})}{l_S}+\frac{\tau_{owS}S_{owS}-\tau_{wWS}S_{wWS}}{A}-\alpha_{wGS}\rho_w g\sin\theta \qquad (15.4.15)$$

To reduce some of the computational work involved in solving the equations, we eliminate some of the variables. $\Delta p_T/l_T$ is eliminated between the Taylor-bubble equations 15.4.11 and 15.4.2, and also between 15.4.11 and 15.4.13. $\Delta p_S/l_S$ is eliminated between the two slug momentum equations 15.4.14 and 15.4.15:

$$\frac{\rho_o(v_T-v_{oT})(v_{oS}-v_{oT})}{l_T}-\frac{\rho_w(v_T-v_{wT})(v_{wS}-v_{wT})}{l_T}+\frac{\tau_{GoT}S_{GoT}-\tau_{owT}S_{owT}-\tau_{oWT}S_{oWT}}{A\alpha_{oT}}-\frac{\tau_{owT}S_{owT}-\tau_{wWT}S_{wWT}}{A\alpha_{wT}}-\rho_o g\sin\theta+\rho_w g\sin\theta=0 \qquad (15.4.16)$$

$$\frac{\rho_o(v_T - v_{oT})(v_{oS} - v_{oT})}{l_T} + \frac{\tau_{GoT}S_{GoT} - \tau_{owT}S_{owT} - \tau_{oWT}S_{oWT}}{A\alpha_{oT}} - \frac{-\tau_{GoT}S_{GoT} - \tau_{GWT}S_{GWT}}{A(1-\alpha_{oT}-\alpha_{wT})} - \rho_o g \sin\theta + \rho_G g \sin\theta = 0 \quad (15.4.17)$$

$$\frac{\rho_o(v_T - v_{oS})(v_{oT} - v_{oS})}{l_S} - \frac{\rho_w(v_T - v_{wS})(v_{wT} - v_{wS})}{l_S} + \frac{-\tau_{owS}S_{owS} - \tau_{oWS}S_{oWS}}{A(1-\alpha_{wGS})} - \frac{\tau_{owS}S_{owS} - \tau_{wWS}S_{wWS}}{A\alpha_{wGS}} - \rho_o g \sin\theta + \rho_w g \sin\theta = 0 \quad (15.4.18)$$

The three continuity equations 15.4.1 - 15.4.3 are not all linearly independent of each other, so we can only use two of them (the third does not express anything not already included in the first two). We pick 15.4.1 and 15.4.2. Similarly, of equations 15.4.7 - 15.4.9, we choose to use 15.4.8 and 15.4.9. These four equations, together with the momentum equations 15.4.16 - 15.4.18 are used in the calculations. In addition, we need to insert the slug unit's velocity v_T and the liquid slug length $l_S(= l_{S+T} - l_T)$. They can be estimated with equations 7.2.9 and 7.3.14 as before, but we need to replace α_L with $\alpha_o + \alpha_w$. The slug fractions can be determined by assuming the bubble distribution to be similar in both oil and water, and using equation 7.2.7 to determine the fractions of the two liquids together ($\alpha_{oS} + \alpha_{wS}$ replaces α_{LS} in equation 7.2.7). In the Taylor-bubble part, we do of course determine the fractions as for stratified flow.

If we include compressibility, it is possible to use a steady-state model as a basis for a dynamic model by using the unit's average values. Such a strategy has a tendency to smoothen out the slugs, however, in the way it was described for the two-phase slug models in chapter 7. Slug tracking models are therefore better.

Bonizzi & Issa (2003) have shown that horizontal three-phase slugs can be modeled using the same principles described in chapter 9. This approach is currently not realistic for commercial simulations of pipelines due to the amount of computations involved, but it may offer interesting possibilities at in the future.

15.5 Combining the different flow regimes into a unified model

Stratified- and slug flow can be modeled as explained in chapters 15.3 and 15.4. We saw that gas-liquid-liquid flow can be modeled very similarly to two-phase flow, but with extra equations for the extra phase. We also realize that flow regime criteria from two-phase gas-liquid flow theory can be used to predict onset of slugging, and emulsion viscosity and inversion criteria from the liquid-liquid theory can be used to estimate how the two liquids behave (separated or mixed, and resulting mixture properties). For slug flow, we also saw that theory from gas-liquid and liquid-liquid flow could be adapted to three-phase flow.

For annular flow, at least two different sorts of flow regimes are possible in three-phase gas-liquid-liquid flow:

1. Gas forms the central core. This may occur when we have relatively high gas content and velocities.
2. One of the liquids forms the central core, while the gas occurs as small bubbles in one or both of the liquid phases.

When the first sort of flow occurs, the high velocity makes it reasonable to assume the oil and water are well mixed and behave like a dispersion or an emulsion, see chapter 13.2 and 13.3. That reduces the modeling task to describing two-phase gas-liquid flow. In the second case, the situation is quite similar to those shown in figure 13.1.2, and the modeling effort is reduced to describing two-phase liquid-liquid flow, but with bubbles in one or both of the liquids. Droplet entrainment and deposition can be estimated as for two-phase flow.

Other types of dispersed flow – small bubbles in one or both of the liquids, say – also follow principles covered by the already described two-phase theory.

When Zhang & Sarica (2006) used this model to make steady-state simulations, they achieved reasonable agreement with some measurements, while pointing out that further verification is required.

"He who never made a mistake never made a discovery."
Samuel Smiles

16 Three-phase gas-liquid-solid flow

Three-phase gas-liquid-solid flow considerations:

- Main problems to avoid
- How to use models and correlations developed for two-phase flow
- Turbulence theory models

16.1 Introduction

As mentioned in chapter 14, some oil and gas wells produce sand or proppant. Since wells frequently produce both oil and gas together, we can often encounter three-phase gas-liquid-solid flow of the gas-oil-sand variety. When attempting to simulate such flows, we face the combined challenges of those involved in gas-liquid flow and those of liquid-solid flow, in addition to some effects caused by interaction of the three phases.

In case we have stratified flow, both fluids flow relatively slowly, and most of the sand tends to be transported by the liquid due to its higher density. In figure 11.4.1 we discovered that even moderate inclination leads to significant increases in the liquid fraction, so the liquid's average velocity goes down when where the inclination angle increases. Unsurprisingly, it has been found that slight uphill stratified flow is the most critical situation when it comes to sand deposition (Angelson et al., 1989). Other flow regimes are associated with higher velocities and therefore have better sand- carrying properties.

Codes and guidelines giving recommendations for how to size three-phase gas-liquid-solid flow-lines reflect the current lack of accurate calculation methods. The American Petroleum Recommended Practice API RP 14E, for instance, suggests sizing such flow-lines according to a simplified empirical flow equation where the maximum erosion and corrosion-safe velocity is assumed to be inversely proportional to the square-root of the gas-liquid mixture velocity. This recommendation is not convincingly documented, however.

16.2 Models and correlations

In stratified flow, which we already pointed out tends to be the most critical when it comes to sand buildup, the gas velocity is moderate and the flow relatively calm compared to other flow regimes. Most of the particles are going to be well below the liquid surface, so even if some droplets are torn off and entrained into the gas flow, it is not likely to contribute much to particle transport. Since we focus on conditions where we have very low particle fractions, both the gas and the liquid flow quite similar to what they would have in particle-free two-phase gas-liquid flow. Realizing this to be so, we immediately draw two conclusions. First, the transport of solids is not going to be significantly affected by the gas velocity directly. It will be affected indirectly, though, since increasing the gas flow increases the liquid velocity, too, due to the friction between gas and fluid. Secondly, it also follows that a moderate amount of solids will not affect the gas flow directly, and even the liquid flow is only moderately affected. This means that we can utilize the two-phase gas-liquid flow model from chapter 3 and the liquid-solid theory from chapter 14.3 to determine whether particles will start accumulating or not.

If we look back at equation 14.3.10 and the development of it, we see that the pipe diameter is not directly involved in determining the minimum liquid velocity for transporting solids. It does, however, affect the Reynolds number and therefore to some

extent the Darcy-Weisbach friction factor f. When using the definitions of hydraulic diameter outlined in chapters 3.4 and 3.5, equation 14.3.10 gives us a criterion for when sand particle accumulation may start, and we simply let the two-phase gas-liquid flow simulation program check the criterion continuously as it runs. We may even use that criterion for the other flow regimes and other phases (liquid-liquid or gas-liquid-liquid), too, since all simulation models calculate the liquid velocity for each time-step and spatial grid point.

Other criteria for gas-liquid-solid flow have also been proposed. Salama (2000) developed a model based on earlier proposals by Wicks (1971) and Oroskar (1980) for estimating the minimum mixture velocity to avoid sand deposition in multi-phase pipelines. It is built on turbulence theory, and the main principle is to require the turbulent eddies in the carrier fluid to have enough energy to balance the gravity forces and carry the particles. Danielson (2007) further modified the models and came up with the following correlation:

$$v_L{}^* = K_D \left(\frac{\mu_L}{\rho_L}\right)^{-n/(2-n)} d_s{}^{n/(2-n)} \left[gd\left(\frac{\rho_s}{\rho_L} - 1\right)\right]^{1/(2-n)} \qquad (16.2.1)$$

In measurements on a $d = 69\,mm$ nearly horizontal pipe with air or water combined with air and two different diameter sand particles, $d_s = 0.28 \cdot 10^{-3}\,m$ and $d_s = 0.55 \cdot 10^{-3}\,m$, they found this model could be fitted well to the data by setting $n = 1/5$ and $K_D = 0.23$ for inclinations in the range $-1.35^0 \leq \theta \leq 4.0^0$.

If we insert the same data as for the example at the end of chapter 14.3, we get $\boldsymbol{v_L{}^* = 0.94\ m/s}$, which is slightly lower but of the same order as the theory shown in chapter 14 for liquid-solid flow. As explained in chapter 14.3, we cannot expect this equation to give accurate results for vertical flow – something more along the lines of equation 14.3.12 is better suited for that task. But we noted that particles tend to flow more easily with the fluid in vertical pipes than in horizontal ones, so vertical flow is of lesser interest when seen from a flow assurance standpoint.

Numerous authors have also developed models for how to estimate particle transport for higher particle concentrations, including for moving sand beds, see Angelson et al. (1989), Oudeman (1993), Gilles et al. (1997), King et al. (2001), Stevenson (2001), Stevenson et al. (2002, 2003), Erian & Pease (2006), Kassab et al. (2006), Yang et al. (2007), Danielson (2007), and particularly Bello (2008). These models are well described

by the authors, and implementing them is no more difficult than implementing other multi-phase flow models. They generally take two-phase gas-liquid models as their starting point. Models for describing moving sand beds have much in common with models for gas-liquid stratified flow. Another example of how such models can be constructed is very briefly illustrated for vertical annular flow in figure 15.2.1.

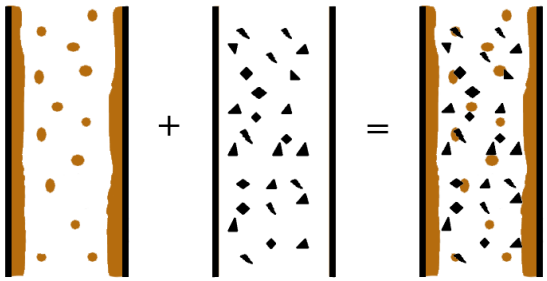

Figure 16.2.1. Vertical upwards annular gas-liquid-solid flow. This can be regarded as a combination of annular gas-liquid flow and gas-solid flow, and the mathematical model can be constructed accordingly (Erian & Pease, 2006).

As already pointed out, though, going into details regarding sand bed movement is most often not relevant for our purpose, and we are not going to outline elaborate theory for it here. Instead, we point out that looking at whether particles are going to settle or not in the stratified-flow slightly upwards inclined sections is normally sufficient for the purpose of flow assurance.

"Chemists are a strange class of mortals, impelled by an almost maniacal impulse to seek their pleasures amongst smoke and vapor, soot and flames, poisons and poverty, yet amongst all these evils I seem to live so sweetly that I would rather die than change places with the King of Persia
Johann Joachim Becher, 1667

17 Fluid properties

How to represent various fluid properties in a simulation program:

- Types of petroleum fluids
- Equation of state for single- and multi-component fluids
- Ways to model other properties

17.1 General

Any multi-phase flow model makes use of various fluid properties. We have already stated many times that a specific fluid's density is a function of pressure and temperature. In general, all fluid properties can be expressed in terms of pressure, temperature, and the fluid's composition. Knowing the fluid's composition is probably the most difficult challenge, particularly at an early project phase. Once reliable fluid samples are available, higher accuracy can be achieved, but the composition changes over time, and water break-in can lead to dramatic changes over a short period of time. Those changes can severely affect the fluid's properties, which again influence the chances of problems with various sorts of deposits, corrosion or erosion, and it can also influence the flow regimes. Fluid sampling is not going to be discussed here, but further information can be found in API RP 44, API RP 45, Ostrof (1979), and Chancey, (1987).

Determining the fluid's composition and thereby its properties accurately enough is one of the greatest challenges in a flow assurance project, particularly at early project stages.

We have seen that our simulation models also rely on properties like surface tension, enthalpy, heat capacity, thermal conductivity, Prandtl number, viscosity, and many others, including some to do with the formation of wax or hydrates (deposits are discussed in chapter 18). Describing the properties is a science in itself, a science traditionally the domain of chemists. This chapter is devoted to those who are not chemists but need to understand phenomena relevant to flow assurance calculations. It is only possible to scratch the surface in one chapter, and the focus is mainly on understanding how to use the models rather than how they have been developed.

Table 17.1.1 gives a rough classification of the different petroleum fluids we may encounter, from dry gas to heavy oil. Any component can occur both as a solid, a liquid, or a gas. 'Dry gas' is therefore obviously not going to be dry at any pressure and temperature. Table 17.1.1 simply refers to how it occurs in the (relatively hot) reservoir, but it does not tell us what happens when pressure and temperature fall on the way to the surface.

Type of fluid	Gas-oil ratio	Occurrence in reservoir
Dry gas	∞	Gas
Wet gas	> 100	Gas + tiny amount of liquid
Condensate	$3 - 100$	Gas + some liquid
Volatile oil	$1.5 - 3$	Liquid + considerable gas
Black oil	$0.1 - 1.5$	Liquid + some gas
Heavy oil	~ 0	Almost no gas

Table 17.1.1. Types of naturally occurring petroleum fluids.

Table 17.1.2 gives a further overview over what different hydrocarbon mixtures may consist of, and table 17.1.3 lists some common gas compositions with typical ranges included. We see that methane is the main component in natural gas and volatile oil, while black oil contains more of the heavier components.

Component	Gas	Gas condensate	Volatile oil	Black oil
N_2	0.3	0.71	1.67	0.67
CO_2	1.1	8.65	2.18	2.11
C_1	90.0	70.86	60.51	34.93
C_2	4.9	8.53	7.52	7.00
C_3	1.9	4.95	4.74	7.82
iC_4+nC_4	1.1	2.00	4.12	5.48
iC_5+nC_5	0.4	0.81	2.97	3.80
iC_6+nC_6	C_{6+}:0.3	0.46	1.99	3.04
C_7		0.61	2.45	4.39
C_8		0.71	2.41	4.71
C_9		0.39	1.69	3.21
C_{10}		0.28	1.42	1,79
C_{11}		0.20	1.02	1.72
C_{12}		0.15	C_{12+}:5.31	1.74
C_{13}		0.11		1.74
C_{14}		0.10		1.35
C_{15}		0.07		1,34
C_{16}		0.05		1.06
C_{17}		C_{17+}: 0.37		1.02
C_{18}				1.00
C_{19}				0.90
C_{20}				C_{20+}:9.18

Figure 17.1.2. Typical molar composition, petroleum fluids (Pedersen et al., 1989).

Gas	Composition	Range
Methane	CH_4	70-90%
Ethane	C_2H_6	0-20%
Propane	C_3H_8	0-20%
Butane	C_4H_{10}	0-20%
Pentane and higher	C_5H_{12}	0-10%
Carbon dioxide	CO_2	0-8%
Oxygen	O_2	0-0.2%
Nitrogen	N_2	0-5%
Hydrogen sulfide, carbonyl sulfide	H_2S, COS	0-5%
Argon, Helium, Neon, Xenon	A, He, Ne, Xe	traceable

Table 17.1.3. Typical composition ranges for natural gas (Speight, 2007).

A specific well fluid can consist of any combination of various components, so we cannot model all those possible mixtures directly. Instead, modeling fluid properties generally requires a theory for which behavior we expect the properties to have (such as the theory for forces between molecules underpinning the van der Waals equation of state), it requires empirical data for the components the fluid consists of (even the latest advances in molecular simulation have not removed the need for measurements, but it has reduced it, see Hamptinne & Behar, 2006), and it requires knowledge of how these properties combine to form new properties when several components are mixed. All of these steps are challenging, and in practice each of them contributes to inaccuracies in the mixture properties.

Figure 17.1.1 illustrates very roughly how different fluid types may behave. The critical points, which are explained in more detail in chapter 17.1.2, are marked with a C. The diagram shows that all different fluids can occur as gas, liquid, or a mixture of both. It also shows that black oil has the greatest tendency to occur as liquid, while 'gas', as one would expect, has the strongest tendency to occur as gas.

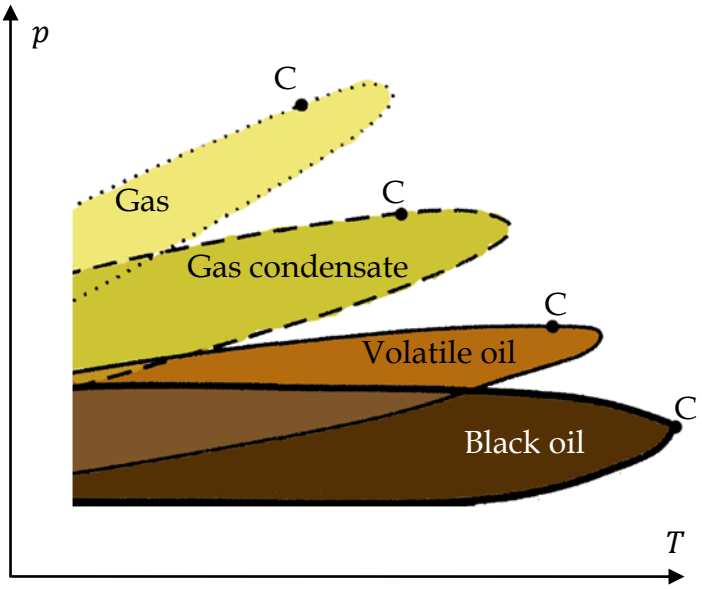

Figure 17.1.1. Typical two-phase flow envelopes for different fluid types.

If the fluid contains water, that water often has a lot of chemical compounds dissolved in it. In the reservoir, these compounds are in equilibrium with the water, but that changes as the pressure and temperature fall as it travels up the well and into the flow-line or riser. In chapter 18 we will see that this can result in various types of scales

and/or hydrates forming, and it can create or accelerate corrosion. At low water fractions, the water mostly represents chemical risk of this nature, while at high fractions, it severely affects the flow regime in ways we have discussed in previous chapters.

17.2 Equations of state

One of the most important fluid properties is the one described by an equation of state, it correlates density (or its inverse, specific volume), pressure, and temperature. There are several alternate such equations, the most used probably being the Soave-Redlich-Kwong (Soave, 1972), the Peng-Robinson (Peng & Robinson, 1976), and the Modified Peng-Robinson *PR78* (Peng & Robinson, 1978), the last of which is considered most accurate.

Before going into details for the more advanced correlations, let us first repeat the ideal gas law, which is a simplified equation of state, too simple for most realistic simulations, but it can be useful for investigating various underlying details:

$$pV = nRT \tag{17.2.1}$$

where n is a gas constant, V is the volume, and R is the universal gas constant ($R = 8.314\,472\ J\ mol^{-1}K^{-1}$). We sometimes introduce the molar volume V_m or the molar mass M_g as:

$$V_m = \frac{V}{n} = \frac{M_g}{\rho} \tag{17.2.2}$$

We can then write equation 17.2.1 as:

$$p\frac{M_g}{\rho} = RT \tag{17.2.3}$$

It turns out that for real gases, equation 7.2.3 is a reasonable approximation only for relatively low pressures. This is sometimes accounted for by introducing a dimensionless compressibility-factor Z:

$$p\frac{M_g}{\rho} = ZRT \tag{17.2.4}$$

Even if we use the modified version of the ideal state equation, we need a way to model Z in order to curve-fit empirical data. In simulation programs, we do not usually go via equation 17.2.4 at all. We simply model some function $f(p,\rho,T) = 0$ (or, alternatively, $f(p,V,T) = 0$) directly.

The van der Waals equation of state from 1873 was probably the first to perform markedly better than the ideal gas law. The Peng-Robinson equation, which is valid both for the gas- and liquid phase, is the result of a further improvement. The PR78 can be written as:

$$p = \frac{RT}{V-b} - \frac{a(T)}{\big(V+c(T)\big)(V+2c(T)+b)+\big(b+c(T)\big)(V-b)} \tag{17.2.5}$$

We see that it contains 3 'constants' (they are not completely constant for all pressures and temperatures) in addition to R. Those constants need to be determined experimentally and then tabulated for different components. We also see that it may be necessary to iterate to solve equation 17.2.5.

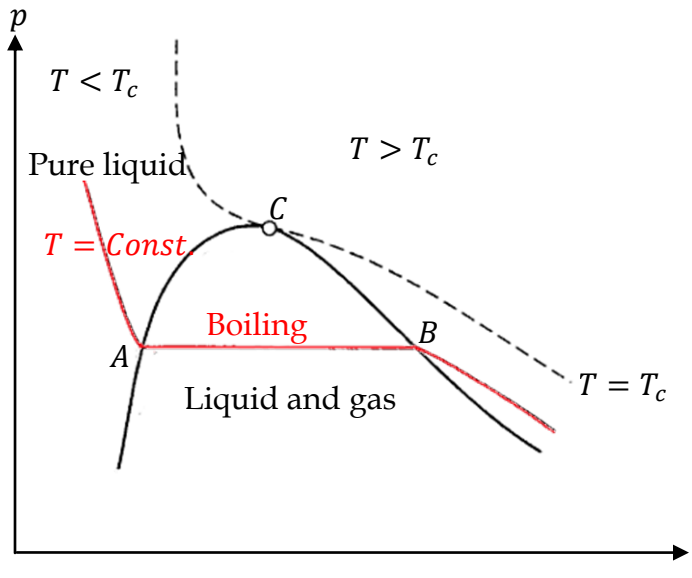

Figure 17.2.1. Pressure-volume diagram for a single-component fluid.

If we plot equation 17.2.5 in a diagram, we get results like those shown in figure 17.2.1. It is helpful when we want to understand what equation 17.2.5 expresses for a single-component fluid such as water or methane. If we start by keeping the fluid at a very high pressure, it is going to take its liquid form. If we reduce the pressure gradually by letting the liquid expand, we will sooner or later reach a point where that liquid starts to boil (point A). This point is called a *bubble point*. Since a liquid is relatively incompressible compared to a gas, the expansion is quite moderate until boiling starts. Further expansion results in all liquid boiling and becoming gas until we reach point B. For a single-component substance boiling at a constant temperature, the pressure remains constant and equal to the bubble pressure until the last drop vaporizes (point B). This point, where the vapor is in equilibrium with an infinitesimal amount of liquid is called a *dew point*. The fluid's bubble points at various temperatures form the bubble point curve, while the dew points define the dew point curve. The two curves meet at the critical point C, at the critical temperature T_c, and together they define the so-called *phase envelope*.

Hydrocarbon fluids contain a mixture of various components. For gas wells, for instance, we see from table 17.1.3 that most of the gas tends to be methane, but it is always mixed with other components. Each reservoir is unique, so we cannot tabulate the PVT-properties for every possible combination of components. Instead, we tabulate each component separately and combine them using *mixing rules.*

The classic mixing rules state that the constants a, b, and c for the mixture can be found from the constants of each component:

$$a = \sum_{i=1}^{N} \sum_{j=1}^{N} z_i z_j a_{ij} \tag{17.2.6}$$

$$b = \sum_{i=1}^{N} z_i b_i \tag{17.2.7}$$

$$c = \sum_{i=1}^{N} z_i c_i \tag{17.2.8}$$

Where z_i is mole fraction, and:

$$a_{ij} = \sqrt{a_i a_j}(1 - k_{ij}) \tag{17.2.9}$$

The parameter k_{ij} is a binary interaction coefficient, which by default is zero for hydrocarbon-hydrocarbon interactions and different from zero for interactions between a hydrocarbon and a non-hydrocarbon and between unlike pairs of non-hydrocarbons. We see that to model mixtures (rather than merely single-components), k_{ij} indicates that we need additional data to describe how the components interact with each other. Such data can be found in tables and books, but when we do simulations we must of course have it all implemented on computer-readable format, for instance in a database. Some relevant sources are McCain (1990), Danesh (1998), and Ahmed (2000).

More refined equations of state and also more refined mixing rules exist, and the development to improve them even further is ongoing. As a general rule, more refined methods yield more accurate result, but also slower calculations.

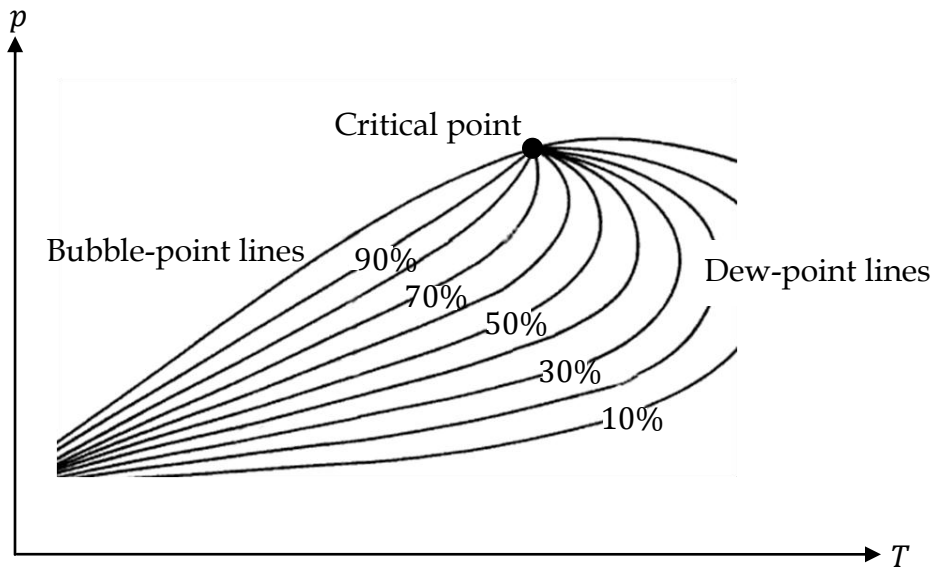

Figure 17.2.2. Phase diagram for a typical black oil with constant liquid fraction lines. The lowest shown curve represents 10% liquid, meaning 90% of the volume is taken up by gas.

If we go through a full iterative mixing and equation of state calculation for each grid-point for every time-step when we simulate multi-phase flow, these calculations easily

take more time than the rest of the calculations combined. If we know in advance that our simulations are going to use data only for a limited pressure and temperature range, we can sometimes speed up the simulations by calculating data and curve-fitting those data to simpler correlations (such as *splines*) before the actual simulations start. This strategy relies on the user specifying the required data range. Some commercially available simulation programs have that possibility integrated as a standard option.

The pressure-volume diagram for a mixture is quite different to that of a single component. If boiling is allowed to take place at constant temperature, different components evaporate unevenly, and therefore the remaining liquid (and also the already formed gas) changes composition continuously. The boiling pressure and temperature are therefore no longer constant, meaning the horizontal line in figure 17.2.1 changes shape. We can illustrate this in a different type of diagram: A $p-T$ diagram, see figure 17.2.2.

So-called *black oils* (a misleading term, since the color is not always black) are characterized by relatively low gas-oil ratios. When oils like these flow from a well through a flow-line and possibly up a riser, the pressure falls, and a larger and larger percentage of the liquid becomes gas. In multi-phase flow simulations, it is common to presume the boiling happens instantaneously as the pressure or temperature changes. Calculating how much boiling or condensation takes place in such *flash* calculations is used to estimate the amount of gas and liquid for the given data. Flash calculations determine the Γ_{ki}-term in the conservation equations directly – we normally do not consider any dynamics in the flashing itself (such as the possibility of having an under-cooled liquid, for instance).

The boiling or condensation also affects the temperature and pressure, and the flash calculations are based on determining the phase equilibrium which gives the lowest Gibbs free energy. Such calculations involve considerable effort (see for instance Ahmed, 2000).

17.3 Other properties for equation closure

17.3.1 Enthalpy

The specific enthalpy h can be expressed as:

$$h = \sum_{i=1}^{N} z_i \int_{T_{ref}}^{T} \left(C_{1,i} + C_{2,i}T + C_{3,i}T^2 + C_{4,i}T^3\right)dt - RT^2 \frac{\partial ln(\varphi)}{\partial T} \qquad (17.3.1)$$

The first term is the ideal gas enthalpy, expressed in the form of a polynomial fit to the temperature by using constants $C_{1,i}$ - $C_{4,i}$ for component i, and the last term relies on something called the *fugacity* φ. What is most important as seen from a user's perspective is that the enthalpy is always defined relative to some temperature T_{ref}, so we cannot for instance compare two different programs' estimate unless we use the same reference temperature in both programs. Also, depending on where one sets the reference temperature, it is possible to encounter negative enthalpy, something which in itself is not an indication that anything is wrong. It is quite common to use 273.15 K as reference temperature. Also, it is worth noting that the fugacity φ uses the state equation, so it is preferable to combine these calculations to minimize calculation costs.

17.3.2 Internal energy

Once the enthalpy is found, the internal energy can be calculated from equation 2.4.3 if we so wish.

17.3.3 Entropy

The entropy is calculated in a similar way to the enthalpy. It can be used to estimate the temperature change in compressors and pumps, which have constant entropy (for ideal compressors or pumps), and somewhat increasing entropy in real components. In valves, on the other hand, throttling happens at constant enthalpy.

17.3.4 Heat capacity

Heat capacity at constant pressure can easily be calculated from the enthalpy equations as:

$$c_p \overset{\text{def}}{=} \left(\frac{\partial h}{\partial T}\right)_p \approx \left(\frac{\Delta h}{\Delta T}\right)_p \qquad (17.3.2)$$

The heat capacity at constant volume can be calculated from:

$$c_v = c_p - T\left(\frac{\partial v}{\partial T}\right)_p \left(\frac{\partial p}{\partial T}\right)_v = c_p - T\left(\frac{\Delta v}{\Delta T}\right)_p \left(\frac{\Delta p}{\Delta T}\right)_v \tag{17.3.3}$$

17.3.5 Joule-Thompson coefficient

The Joule-Thompson coefficient can also be found from the enthalpy and state equation by setting:

$$\mu_J \overset{\text{def}}{=} \left(\frac{\partial T}{\partial p}\right)_h = -\frac{1}{c_p}\left(\frac{\partial h}{\partial p}\right)_T \approx -\frac{1}{c_p}\left(\frac{\Delta h}{\Delta p}\right)_T \tag{17.3.4}$$

17.3.6 Speed of sound

The speed of sound can be derived as:

$$a_s = \left\{\frac{c_p}{c_v}\frac{RT}{M_g}\left[Z + \rho\left(\frac{\partial Z}{\partial p}\right)_T\right]\right\}^{1/2} \tag{17.3.5}$$

The real gas compressibility factor Z follows from equation 17.2.4 and the equation of state, for instance equation 17.2.5. If we instead have access to density and entropy on the form

$$\begin{aligned} \rho &= \rho(p,T) \\ s &= s(p,T) \end{aligned} \tag{17.3.6}$$

Speed of sound in is defined as (when neglecting pipe elasticity):

$$a_s = \sqrt{\left(\frac{\partial p}{\partial \rho}\right)_s} \tag{17.3.7}$$

By differentiating equations 17.3.6, solving them for *ds*, and then setting *ds = 0* (since, according to equation 17.3.7, *s* shall be constant), we get:

$$d\rho\left(\frac{\partial T}{\partial \rho}\right)_p\left(\frac{\partial S}{\partial T}\right)_p-\left(\frac{\partial \rho}{\partial p}\right)_T\left(\frac{\partial T}{\partial \rho}\right)_p\left(\frac{\partial S}{\partial T}\right)_p dp+\left(\frac{\partial s}{\partial p}\right)_T dp=0 \tag{17.3.8}$$

Since everything now is expressed as function of p and T for constant s, this corresponds to setting $dp/d\rho=(\partial p/\partial \rho)_s$. By inserting this into equation 17.3.7 we end up with the alternative expression:

$$a_s=\sqrt{\frac{\left(\frac{\partial S}{\partial T}\right)_p}{\left(\frac{\partial \rho}{\partial p}\right)_T\left(\frac{\partial S}{\partial T}\right)_p-\left(\frac{\partial s}{\partial p}\right)_T\left(\frac{\partial \rho}{\partial T}\right)_p}} \tag{17.3.9}$$

All factors in equation 17.3.9 are fluid properties we can pull out of any standard PVT-program as function of pressure and temperature. Often we can also pull out a_s directly. In case of dispersed bubble flow, however, equation 17.3.9 together with the mixture properties ρ_M and s_M may offer the most convenient way of calculating the mixture speed of sound.

17.3.7 Viscosity and thermal conductivity

The viscosity model must overcome the same challenge as the equation of state in that data for the different components must be combined in order to produce the mixture viscosity. The mixture rule for one such well documented model is outlined in detail by Mo and Gubbins (1976) for viscosity and by Christensen & Fredslund (1980) and Pedesersen & Fredslund (1987) for thermal conductivity. Pedersen et al. (1984) and Pedersen & Fredenslund(1987) have developed a model for each component's viscosity, where each component is expressed as a function of a reference component, for instance methane. A similar model for thermal conductivity was developed by Hanley et al. (1975). The models are very complex and not suited for manual calculations. Like for the mixture equation of state, software implementation of viscosity and thermal conductivity properties is quite different from developing flow models, and it is in practice best done as third-party software.

17.3.8 Interfacial surface tension

Interfacial tension is a property of a fluid-fluid of fluid-solid interface, the origins of which lie in the different attractive intermolecular forces that act in the two fluid phases. The result is an interfacial energy per area that acts to resist the creation of new interfaces, while trying to make existing interfaces as small as possible. The surface tension on a raindrop falling in air tries to make the drop spherical, since that creates the smallest surface (but the air-resistance does not, so the end result is not spherical). The drop's surface tension is a property of both involved fluids (water and air), so it is strictly speaking meaningless to talk of it in terms of only one of them. As an example, we may for instance need to know the surface tension between water and air. In practice, though, water's much higher density than air's makes the water properties dominate at low pressures, so the surface tension is relatively independent of which type of gas water is in contact with. For fluids of similar density (water-oil, say), this is not the case.

Fluids between which no interfacial tension arises are said to be *miscible*. For example, salt molecules will diffuse freely across a boundary between fresh and saltwater, and there is no interfacial tension between them.

Interfacial surface tension between an oil and a gas can be calculated by a model developed by Weinaug & Katz (1943), well presented by Poling et al. (2004), which actually builds on Einstein's first, revolutionary paper from 1901. According to this theory, each component's surface tension can be expressed by a property called Parachor, a property which can be tabulated (See for instance Quayle, 1953). Weinaug & Katz' model determines how to combine each component's Parachor to calculate the surface tension for mixtures. The calculations are not very time-consuming or complicated, and they show that interfacial surface tension generally decreases when the temperature increases. At the critical point, the surface tension becomes zero as the phase interface vanishes.

As a way to associate how much the surface tension for a fluid in its liquid- and gas phase changes with temperature, the following remarkably general equation can be used:

$$\sigma_{LG} = \sigma_{0_{LG}} \left(1 - \frac{T}{T_c}\right)^{1.2} \tag{17.3.6}$$

Where $\sigma_{0_{LG}}$ is a reference surface tension for the fluid in question, and T_c is the critical temperature.

"I mixed this myself. Two parts H, one part O. I don't trust anybody!"
Stephen Wright

18 Deposits and pipe damage

Various chemical reactions which may compromise the flow:

- Hydrates, wax, asphaltenes, and scale deposits - prediction and control
- Corrosion, erosion and cavitation
- Heavy oil emulsions

18.1 Introduction

Flow assurance is to a large extent all about preventing deposits from building up inside the pipe, in addition to preventing damage due to corrosion, erosion or cavitation. The different sorts of chemical deposits depend on temperature and pressure, and determining the acceptable operational temperature limits is essential. Possible strategies may include avoiding long shutdowns, using insulation and sometimes heating, re-circulating hot fluids, and chemical injection of inhibitors. Temperature, pressure, and several other important parameters depend on how the fluid flows, so the flow models we have discussed in previous chapters are important tools when dealing with deposits. The same can be said about corrosion, erosion and cavitation. In this chapter, we will have a closer look at how these parameters are connected.

18.2 Hydrates

18.2.1 General

Hydrates are ice-like crystalline compounds which can occur when gas molecules are in contact with water at certain temperatures and pressures. They are formed by gas molecules getting into hydrogen-bonded water cages, and it happens at temperatures well above normal water freezing. A significant part of the world's gas resources occur in the form of hydrates, so they may represent an important future source of energy, and it has also been considered as an alternative to LNG for transporting gas by ship. When seen from a flow assurance perspective, though, hydrates represent a problem – often the largest problem to be dealt with in multi-phase flow-lines. Hydrate buildup can throttle the line and also cause complete blockage. Successful hydrate problem avoidance generally requires good knowledge of the fluid's composition, understanding both the fluid and the heat flow properly (having adequate simulation tools), having means of countering hydrate buildup (alternatives include injecting inhibitors, insulation, heating, or removing the hydrates), and adequate operational procedures.

It may also be possible to let hydrates form, but through various means ensure they only take the occur as small particles. A mixture of hydrate particles in oil is called hydrate slurry, and some ongoing research projects attempt to make technology for transporting relatively cold hydrate slurries through pipelines applicable. Reliable cold flow technology is not available yet, but further developments may mean it will offer a way to avoid hydrate problems in a relatively cheap way in the future. Today's most used inhibitor and temperature control based technologies are relatively expensive.

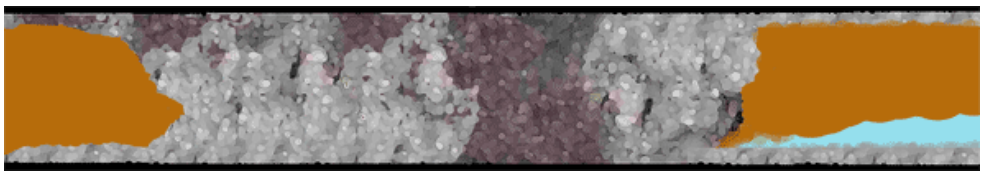

Figure 18.1.1 Hydrate plug in a flow-line, schematic.

Hydrates are formed of water and light gas molecules like methane, ethane, propane, carbon dioxide, and hydrogen sulfide. Exactly how this happens is not completely understood, but it is thought to occur at the gas water interface, and only when the temperature and pressure is within a certain range. This range can be determined from

fluid samples and empirical correlations, and one obvious strategy for avoiding problems is of course to avoid those pressures and temperatures. Formation of hydrates also releases heat, which tends to increase the temperature and hence stop or delay further hydrates from forming. Calculating this heat is like any other flash calculation and relies on knowing the relevant PVT data.

Another key question is whether the hydrates actually do create problems if and when they form. Some of the hydrates do typically not build up on the pipe wall, they may simply travel with the flow in a similar way as do other solids and not cause problems. Hydrate buildup is therefore not only affected by pressure, temperature, and chemical properties, but also by the flow conditions.

Even though significant effort goes into avoiding hydrate plugs in flow-lines, they do sometimes form. The chances of blockage are generally greatest during re-startup after flow-line shutdown, particularly if the shutdown was unintended so that extra inhibitors could not be injected first. The sections downstream from chokes are most exposed due to the Joule-Thompson effect, which can cause temperature drops down to the hydrate formation region. In *Pipe Flow 1* we saw that for single-phase systems, this temperature reduction can be investigated with relatively simple hand calculations, or we can determine it by simulations. The simulations can also be useful for tracking the injected inhibitors in order to know their concentration along the pipeline.

The most common procedure for dissociating a hydrate plug is to reduce the system pressure until it melts. It is not always possible to do this symmetrically at both sides of the plug, and that can cause violent acceleration and damaging transients when it comes loose. Dissociating hydrate plugs can take weeks or months, and avoiding them in the first place is of course the preferred strategy. Simulations can be of great help for determining acceptable procedures for clearing out hydrate plugs.

Hydrates are classified by the arrangement of water molecules in the crystal – the crystal structure. The most commonly encountered types of hydrates are called Type I and Type II. A third, less common type is called Type H. What is most important to recognize from a flow-assurance standpoint is that all three types of hydrates are relatively easy to predict for single-composition gases, and off-the-shelf fluid property software does that well. Hydrate properties for mixtures, which is what we have to deal with in practical situations, are also included in such software, but results are generally less accurate. The most reliable

Traditional hydrate prevention is based on inhibitor injection and/or temperature control.

hydrate prediction is therefore achieved by sampling and laboratory tests for the mixture in question (Sloan, 1998, Carroll, 2009). Carroll has also included some comparisons of different available software programs to emphasize this point. Sloan (2005) compared *5* named commercial software programs and concluded that their error in predicting the hydrate onset temperature is better than *1* ^0C for most of them when the composition is accurately known. That is good enough for the main problem to lie elsewhere, typically in knowing the composition accurately and also in predicting to what extent hydration creates problems if and when it happens. We are going to discuss hydrate formation dynamics further in chapter 18.2.3, but we will first discuss some traditional hydrate blockage prevention techniques.

18.2.2 Hydrate blockage prevention

Figure 18.2.1 shows a hydrate curve for a typical natural gas. Such curves depend on the gas composition, but their shape is generally similar to the one in figure 18.2.1. We see that as long as the temperature is high enough and/or the pressure low enough, hydrates do not form.

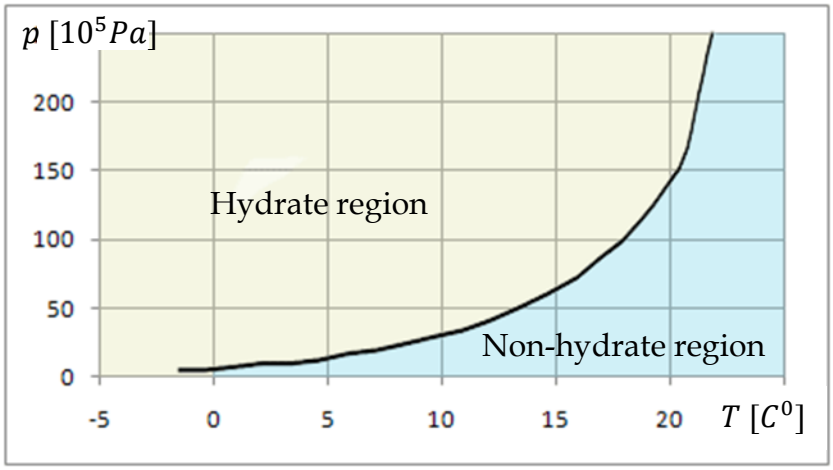

Figure 18.2.1. Typical mixture hydrate curve for a natural gas (mixture).

As already mentioned, hydrate curves like the one shown in figure 18.2.1 are calculated on the basis of the components the gas consists of. Some examples of hydrate curves for frequently encountered components are shown in figure 18.2.2. If we manage to stay in the non-hydrate region of the diagram, hydrates do not form, but we see that for temperatures encountered on the seabed (around 0 ^{0}C if the flowing fluid's temperature

falls towards the seawater temperature), the pressure needs to be unrealistically low to avoid hydrates for all of the plotted components.

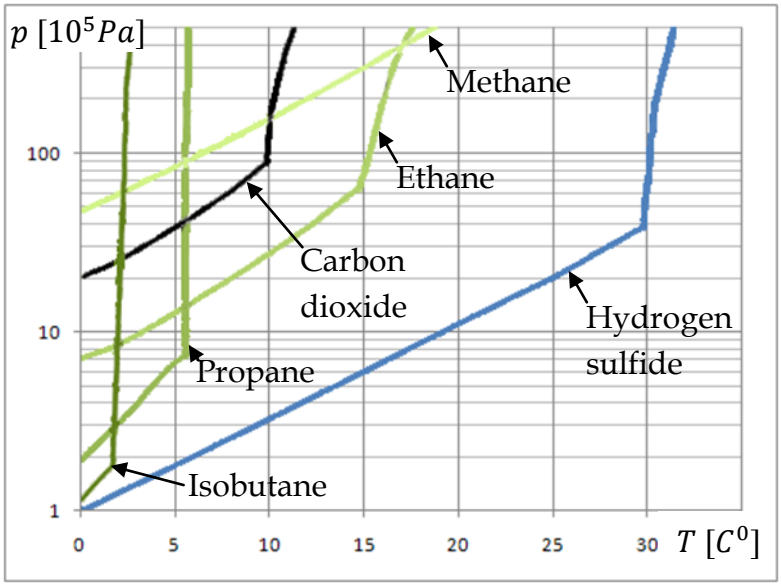

Figure 18.2.2. Hydrate curves for various pure components.

If we add methanol or monoethylene glycol (MEG), the non-hydrate region of the diagram can be made larger. Figure 10.2.3 shows the consequences of adding *10* or *20%* methanol to the water. The percentage is calculated as mass flow of methanol compared to mass flow of water and methanol combined. Gas flow – if there is any - is not included in the definition. Note that if any of the methanol is not mixed with the water it will not take part in preventing the formation of hydrates – poor mixing can obviously reduce the effect of the methanol.

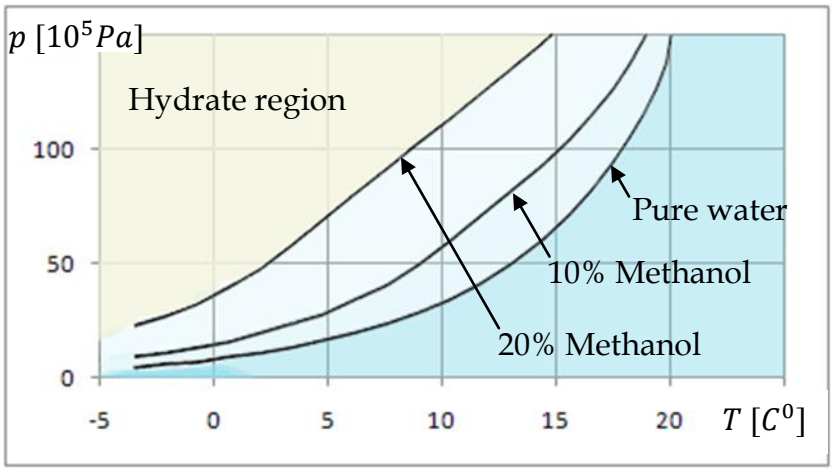

Figure 18.2.3. Hydrate curves for various amounts of methanol inhibition for one well fluid.

We may encounter situations where we need very considerable injection rates, particularly if injection is the only remedy used. Both the injection pipes and the injected fluid can constitute a large part of the total costs.

Figure 18.2.4 is created by feeding real data for a particular pipe carrying a multi-phase fluid into a commercial flow assurance software tool. As indicated by the 'Pipe states'-curve, the fluid in this example enters the pipe at around $p = 13$ *MPa* and $T = 60\ ^0C$, but both pressure and temperature fall as the fluid approaches the outlet. According to these results, if no methanol is injected, the corresponding hydrate formation curve is crossed and hydrates will start to form. We expect the danger to be greatest at the outlet end, since that is where the temperature is lowest. That is the most typical situation, since the fluid usually is hot as it enters the flow-line from the wellhead, but is cooled more and more by the surroundings the longer it remains in the line.

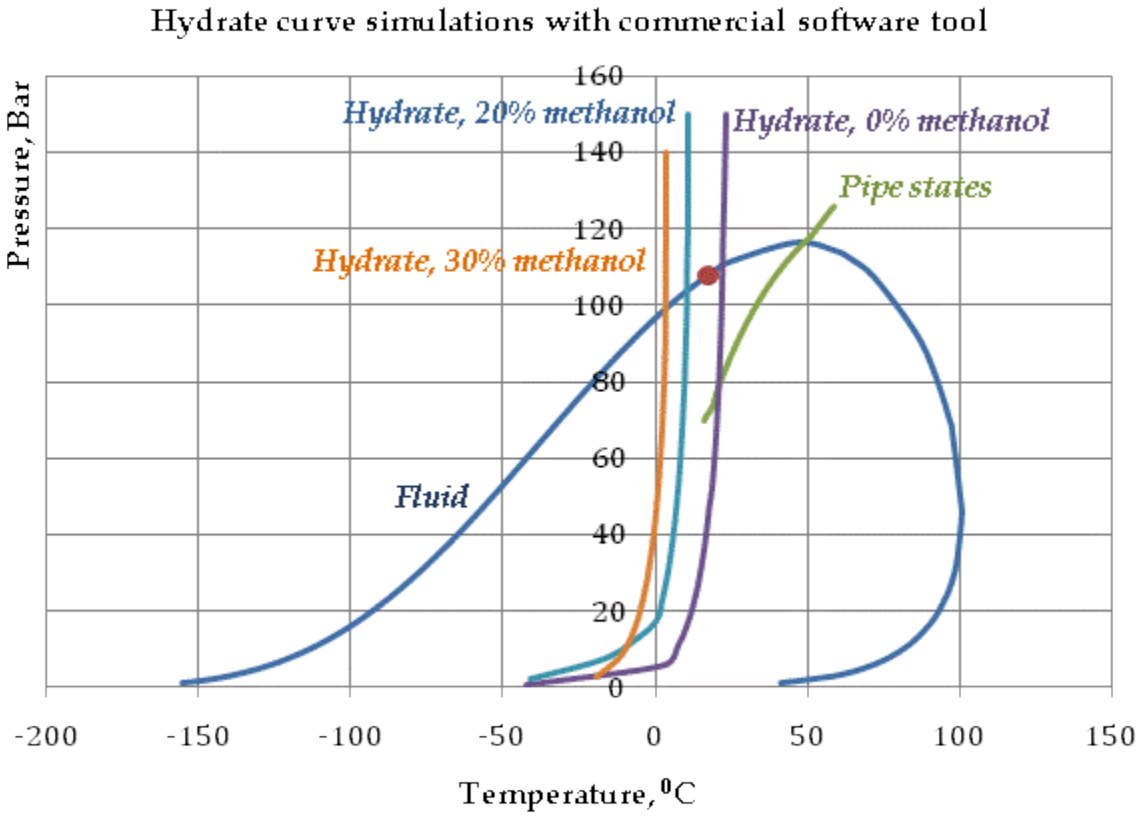

Figure 18.2.4. Hydrate curves and fluid locus for the fluid flowing through a pipe. The 'Pipe states'-curve shows the pressure the fluid will experience while flowing from pipe inlet to outlet, and it indicates that without methanol injection, hydrates can start to form.

The hydrate curve is affected both by the hydrocarbon's composition and the water composition. Adding salt to the water has the same effect on hydrates as adding methanol or MEG. Salts have negative effects, too, however, and corrosion considerations normally mean injecting salt is unacceptable.

There is also something called *kinetic hydrate inhibitors* and *anti-agglomerate inhibitors*. They can be effective at much lower dosage than methanol or MEG, but they do not work by preventing hydrates from forming. Instead, the kinetic inhibitors delay the hydrate formation, typically 24 – 48 hours. They will usually not work if the temperature falls more than 10 ^{0}C below the temperature where hydrate formation would have started without inhibitors, and after the maximum delay time they have little effect. That is not always adequate for subsea flow-lines. The anti-agglomerate inhibitors work by preventing large hydrate crystals from forming, and that tends to prevent the hydrates from sticking to the pipe wall.

Another possible strategy for preventing hydrate formation is to prevent the fluids from cooling down. Thermal insulation can help, but only if the fluid keeps flowing or if heat is added from some other source, for instance from hot water pipes embedded in the same bundle as the flow-line. Electrical heating can also be used. Gases have lower density and therefore lower heat capacity than liquids, so pipelines with a high gas fraction cool down faster than those containing liquids.

Long flow-lines are obviously harder to keep hot than shorter ones, since both the transported fluid and any external heat source have more heat loss to counter in long lines.

Recent research by Aspenes et al. (2009) indicates that the pipe surface's wettability is important to the hydrate's tendency to stick to the surface. Low wettability, as measured by droplets' tendency to wet the surface (low wettability means droplets tend to remain relatively circular and stay on top of the surface) is favorable. At this stage their results cannot be transformed into realistic hydrate prediction calculations, but the model seems to indicate that as a surface changes (due to surface treatment flaking off or due to corrosion, say), we can expect the hydrate tendency to change, too. As we will discover in the next chapter, increased surface roughness, which we know in most situations leads to higher friction, causes more stirring and faster hydrate formation. This, and the fact that the fluid's composition tends to change over time, can lead to the hydrate conditions for the same flow-line changing during its lifetime.

18.2.3 Hydrate formation rate prediction

Hydrates do not become problematic instantly even if we temporarily drop into the hydrate region of the transported fluids. Hydrate formation is a transient phenomenon, and understanding it enables estimation of how fast hydrates build up. It turns out the formation rate depends on the nature of crystal growth, which generally is relatively difficult to describe. We know from reactor experiments that the amount of stirring affects that process. In a pipeline, the stirring can be caused by turbulent eddies and the interaction between phases in the different flow regimes. This means that hydrate formation is affected by how the fluids flow. There are in fact three different parameters affecting hydrate formation and dissociation rate: The mixing rate, the surface area between the hydrocarbon-rich phase and the aqueous phase, and the temperature. The model presented below is mainly that of Turner et al. (2005) and Boxall et al. (2008, 2 papers) used in the OLGA commercial simulation program's so-called CSMHyK-module, but with comments and correlations based on additional sources.

According to Matthews et al. (2000), the formation of hydrates by nucleation is nearly instantaneous when the sub-cooling is around *3.6* ^0C below the onset temperature (for instance as determined from a diagram of the sort shown in figure 18.2.1) for the pressure and liquid in question.

The reaction rate for a chemical reaction of this sort is by chemists described by:

$$\frac{dm_G}{dt} = -A_S k_1 \exp\left(\frac{k_2}{T}\right)(T^* - T) \qquad (18.2.1)$$

Where dm_G/dt is the gas mass flow consumed by the forming hydrates, A_S is the surface area between the hydrocarbon-rich phase and the aqueous phase (total area, including water droplets if relevant), T^* is the critical absolute temperature where hydrates start to form, and k_1, k_2 are rate constants which depend on the fluid's composition and on whether hydrate forms or melts.

Vsyniauskas & Bishnoiand (1983, 1985) and Englezos et al. (1987) measured k_1 and k_2 for mixed methane and ethane hydrates for so-called structure II hydrate formation to be $k_1 = 7.355 \cdot 10^{17}$ and $k_2 = -13.6\,K$. For the inverse process, when the hydrate melts, Kim et al.'s (1987) date for Structure I dissociation was adapted by Turner et al. (2005) to yield $k_1 = -1.530 \cdot 10^{25}$ and $k_2 = -13.6\,K$. For melting, A_S was taken as the area of the hydrate particles, which in effect were presumed to exist in the liquid hydrocarbon

phase only. When using this in a simulation model, it has been necessary to tune k_1 and k_2 to get good agreements with laboratory experiments.

We notice that equation 18.2.1 does not explicitly contain the mixing velocity, even though that is known to have an effect (Lippmann et al, 1995, Mork & Gudmundsson, 2001). Mork & Gudmundsson proposed taking this into account by presuming the mixing to be driven by the friction, since friction is what creates turbulent eddies. What they proposed for a homogeneous, bubbly mixture of gas, oil and water can be expressed by the mixture velocity v_M as:

$$\frac{dm_G}{dt} = -k_3 p \alpha_G \rho_G v_M \left(\frac{f {v_M}^3}{2d}\right)^{k_4} (T^* - T)^{k_5} \tag{18.2.2}$$

Mork & Gudmundsson (2001) did not achieve accurate prediction capabilities with their equation, but it is still worth examining. We see that if k_3 is expressed as a function of contact area, equations 18.2.1 and 18.2.2 have some similarities. What is clearly different, though, is that equation 18.2.2 includes a term which takes into account the turbulence's effect (increased velocity means increases friction, turbulence and reaction velocity), something equation 18.2.1 ignores. Boxall et al. (2008) also reported that the conversion rate increased when the velocity increased, but they did not modify equation 18.2.1 accordingly. The flow's ability to transport the formed hydrates, however, increased with increasing speed, so the overall clogging effect of increasing the speed can in principle go either way. Even though we will build our model on equation 18.2.1, equation 18.2.2 seems to contain useful ideas when developing future improvements to the overall model. Having to tune k_1 and k_2 to each different system, as is now often necessary, makes accurate hydrate formation rate predictions at an early project stage difficult. Still, tuning is possible and can be used once the pipe is operational and more data becomes available, and equation 18.2.1 is commonly modified to include only one tunable parameter, namely k_6:

$$\frac{dm_G}{dt} = -A_S k_6 (T^* - T) \tag{18.2.3}$$

When estimating the viscosity for the liquid hydrocarbon phase (index o for oil) with hydrates in it (index h for hydrate), that mixture was treated as a slurry with viscosity according to Mills (1985) and Camargo & Palermo (2002):

$$\mu_{oh} = \frac{1 - \alpha_{h\,eff}}{\left(1 - \frac{\alpha_{h\,eff}}{\alpha_{h\,max}}\right)^2} \tag{18.2.4}$$

Where $\alpha_{h\,eff}$ is the effective hydrate volume fraction in the slurry (meaning it uses the slurry area as reference, not the total pipe cross-sectional area), and $\alpha_{h\,max}$ is the maximum volume fraction (also defined by the slurry area), assumed to be 4/7. $\alpha_{h\,eff}$ is estimated by setting:

$$\alpha_{h\,eff} = \alpha_h \left(\frac{d_A}{d_M}\right)^{3-f_{frac}} \tag{18.2.5}$$

The parameters d_A and d_M are aggregated and monomer hydrate particle sizes, and f_{frac} is the fractal dimension, assumed to be 2.5. Turner et al. (2005) used Vsyniauskas & Bishnoi's (1983) model, but corrected the hydrate particle size according to Cournil & Henri (2002) and found the mean hydrate particle size of the particles forming spontaneously due to sub-cooling to be $d_M = 40 \cdot 10^{-6} m$. They used that result in all simulations. The diameter relation was determined by Camargo & Palermo's (2002) correlation, also well described and documented by Sinquin et al. (2004):

$$\left(\frac{d_A}{d_M}\right)^{4-f_{frac}} - \frac{F_A \left[1 - \frac{\alpha_h}{\alpha_{h\,max}} \left(\frac{d_A}{d_M}\right)^{3-f_{frac}}\right]^2}{{d_M}^2 \mu_o \dot{\gamma} \left[1 - \alpha_h \left(\frac{d_A}{d_M}\right)^{3-f_{frac}}\right]} = 0 \tag{18.2.6}$$

F_A is attractive van der Waals-force between hydrate particles (a necessary, measured input property to the model. Some results are available in Yang, 2003) and $\dot{\gamma} = \partial v / \partial x$ is shear rate.

The so-called *Hamaker*-constant is:

$$F_A = \frac{A_H d_M}{6\Delta S^2} \tag{18.2.7}$$

ΔS is the distance separating two hydrate spheres, both of diameter d_M.

We see that this hydrate kinetic simulation model relies on knowing the surface between the oil and the water. In stratified flow, that interface can be determined relatively easily the way it was described in chapter 3.4. When droplets or bubbles are present, the model in chapter 4 can provide the necessary areas, and the slug models can be adapted similarly. When doing so, the model can tell us where the hydrate formation rate is likely to be highest, and that is also where we expect hydrate plugs to be most likely to form. It is more difficult to predict exactly how much hydrate needs to form before the whole pipe cross-section is clogged, but being able to approximate the formation rate is at least a start.

18.3 Waxes

Some oils contain wax molecules, and at sufficiently low temperature they will form wax particles. Waxy oils tend to deposit wax on the walls when the fluid is being cooled, and the oil can also get a gel-like structure.

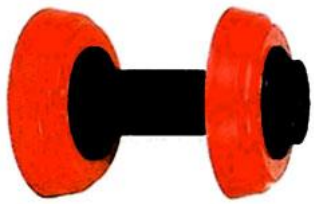

Figure 18.3.1. Cleaning pig.

The problem of wax deposition is – as seen from a flow assurance standpoint – in some ways similar to that of hydrates, but the chemistry involved is different. Both types of problems can normally be controlled by keeping the temperature high enough and/or by using inhibitors, but wax deposits tend to build up gradually so that regular, frequent pigging can more conveniently be used as an important method of mitigating the problem.

Shut-down may have to be kept short to avoid problems due to cool-down, particularly if it was unintended and not prepared by extra inhibitor injection. Startup can also increase the chances of deposits occurring due to the pressure alteration it creates.

Hydrates tend to form if water and gas are present, while wax problems are mainly encountered while transporting waxy oils.

When the temperature of crude oil is reduced,

the heavier components (carbon numbers C_{18}-C_{60}) precipitate and deposit on the pipe wall, and it can cause blockage. Even relatively small deposits tend to increase the pipe surface roughness and thereby the friction. This can sometimes be used to detect the buildup at an early stage, depending on where in the friction factor diagram the flow takes place (the Darcy-Weisbach friction factor is only sensitive to surface roughness in part of the modified Moody diagram).

The *cloud point*, sometimes called the *wax appearance temperature,* is the temperature below which wax starts to form for the specific pressure and oil composition. It is one of the central parameters in characterizing wax deposition. When oil flows out of a well, the lighter components tend to flash off as the pressure is reduced, and the higher concentration of heavier components in the remaining fluid increases the tendency to wax formation. As long as boiling occurs, however, the waxing tendency is lower than what we anticipate compared with 'dead' oil at the same temperature and pressure, so we get conservative results if we use static equilibrium oil data. As an example, the wax appearance temperatures of most paraffin North Sea oils and condensates are in the *30* to *40°C*-range. (Tordal, 2006).

When wax starts to form on the pipe wall, the wax crystals trap oil and form a wax-oil gel. Further temperature reduction causes the wax layer to grow, and it will finally trap all the oil and thereby stop the flow if no action is taken. Several oil pipelines worldwide have had to be abandoned due to wax problems.

If we reach temperatures as low as the wax appearance temperature, we must either inject more inhibitors or use other sorts of inhibitors. Sometimes the cheapest solution may simply be to make sure pigging is done very frequently. If it is not done often enough, the buildup can become so large that the pig gets stuck, particularly in relatively small diameter pipes. Also, wax tends to become harder over time, so it is easiest to get out a relatively short time after it formed.

Wax control strategies are similar to those used for hydrate control, but the chemistry involved is different. Frequent pigging to remove the wax layer before it creates problems can also be effective, a less suited option against hydrates.

The wax porosity – the fraction of oil occluded in the wax – is affected by the pigging process itself because the oil tends to be squeezed out of the wax in front of the pig. This, too, makes the wax harder and increases the chances of the pig getting stuck.

There are very many types of cleaning pigs on the market, and some of them have built-in bypass to allow some wax to escape past the pig in case the buildup becomes too high. In the North Sea, pigging frequencies for wax removal can vary between 2 - 3 days to 3 – 4 months.

Simple geometry dictates that if a pipe has a layer of wax with a thickness δ_{wax}, diameter d and length l, the wax volume would be approximately $\pi d \delta_{wax} l$, corresponding to a wax plug of length:

$$l_{wax\ plug} = \frac{4\delta_{wax} l}{d} \tag{18.3.1}$$

As an example, pigging a 200 mm pipeline with a 1.2 mm layer of wax deposits would according to equation 18.3.1 lead to the wax plug length increasing by $24\ m$ for each pigged kilometer. Since the wax is compressed and some wax may escape past the pig, the actual buildup is going to be somewhat less, but wax buildup in front of the pig of more than a kilometer has been reported (Tordal, 2006.)

Equation 18.3.1 also helps us understand why pigs get stuck much more easily in small diameter pipes compared to those of larger diameter: Larger diameter leads to shorter wax plugs pr kilometer of pigging for the same wax layer thickness. The frictional area for a certain length of plug, on the other hand, is proportional to the diameter. In addition, the force available to push the pig is obviously proportional to the pig's (and therefore the pipe's) cross-sectional area, which again is proportional to the square of the pipe diameter. All in all, that should make the chances of the pig getting stuck due to wax buildup inversely proportional to d^2.

Wax inhibitors can reduce the wax appearance temperature by as much as 10 ^{0}C (Groffe et al., 2001), and they can also to some extent reduce anti-sticking properties so formed wax to a greater extent is carried by the flow instead of building up. Wax inhibitors should be added at a temperature at least $10°C$ higher than the wax appearance temperature, preferably as high as possible.

The chances of a pig getting stuck are approximately inverse proportional to d^2, and therefore small diameter pipes are much more likely to suffer this problem than large diameter pipes.

Wang et al. (2003) tested eight different commercially available wax inhibitors and found they were only effective on waxes of

relatively low molecular weight, though not on those in the C_{35}-C_{44}-range. They reduced the total amount of wax buildup, but the formed wax was harder and more difficult to remove.

Simulating the wax deposition rate is relatively difficult, and current models are not very accurate. Several mechanisms are believed to contribute to wax formation, but the mechanisms responsible for wax deposit growth are widely debated (Benallal, 2008). One of the most accepted mechanisms, though, is that of molecular diffusion. In those cases where the pipe wall is colder than the flowing fluid – the most common situation – the wax concentration becomes lowest near the wall, since some of the wax there already has been deposited. The mass transfer can then be described by Fick's law:

$$\frac{dm_w}{dt} = \rho_w D_w A_w \frac{dC_w}{dr} \tag{18.3.2}$$

m_w is wax mass, ρ_w is wax density, D_w is diffusion coefficient for liquid wax, A_w is the deposition area, dC_w/dr is the wax concentration gradient. The diffusion coefficient was by Burger et al. (1981) found to be a function of a constant characterizing the wax, K_w, and the oil's dynamic viscosity:

$$D_w = A_w \frac{K_w}{\mu_o} \tag{18.3.3}$$

Another mechanism tending to transport wax particles toward the pipe wall is called *shear transport*, which is caused by the flow's shear rate. It can be characterized by the dispersion coefficient as:

$$D_s = \frac{{d_w}^2 \dot{\gamma} \alpha_w}{10} \tag{18.3.4}$$

d_w is the wax particles' diameter, $\dot{\gamma}$ is the shear rate at the pipe wall, and α_w is the volume fraction of wax out of the solution at the wall. We can use this to modify equation 18.3.3 by replacing D_w with $D_w + D_s$.

We see that this model is incomplete, since it fails to outline in detail how to quantify the different parameters in equations 18.3.2 - 18.3.4. That, as well as more refined models for wax growth, is outlined in Correra et al. (2008) and Edmonds et al. (2008). Since current models are not very accurate, basing wax management on predicting the growth rate theoretically is problematic. This technology will likely improve in the future as the simulation tools become more refined, but as the technology stands now, the uncertainties in the wax buildup estimation make it wise to start out with a high pigging frequency, and rather reduce it as more experience with the particular pipe in question becomes available. As seen from equation 18.3.1, the acceptable layer of wax before pigging is highly dependent of pipe diameter and length, but a typical limit may for instance be *2 mm* or less.

Uncertainties in the wax buildup estimates make it wise to use a high pigging frequency until experience indicates otherwise.

18.4 Asphaltenes

Asphaltene solids are dark brown or black. Unlike hydrates and waxes, they do not melt when heated. Like hydrates and waxes, though, it is temperature, pressure and composition which determine whether they form or not. Decreased pressure, as we experience when the fluid flows towards the surface, tends to work against any asphaltenes forming. But once the pressure becomes low enough for gas to separate from the oil, the remaining oil's composition changes in an unfavorable direction, and the chance of asphaltenes forming increases. The most unstable pressure is therefore typically that around the bubble pressure. Reduced temperature also works to increase the likelihood of asphaltenes forming.

Asphaltenes are defined as the compounds in oil which are insoluble in n-pentane or n-hexane, but solutable in toluene or benzene. The so-called *solubility parameter* of the asphaltenes, together with the solubility parameter for the crude oil, will determine how much asphaltene is solutable in the oil. The more similar they are, the more asphaltene the oil can hold. When the asphaltenes are at equilibrium with the crude oil, the so-called *Flory-Huggins theory* states the maximum volume fraction of asphaltenes in the oil is:

$$\alpha_{a\,max} = exp\left\{\frac{V_a}{V_o}\left[1 - \frac{V_o}{V_a} - \frac{V_o}{RT}(\delta_a - \delta_o)\right]\right\} \quad (18.4.1)$$

In this equation, the asphaltene volume fraction is defined by ignoring the gas part of the pipe's cross section and defining the asphaltene fraction as part of the oil-asphaltene mixture (see Hirschberg et al., 1984, Burke et al., 1990). Index a denotes asphaltene, and o denotes oil. V are molar volumes, T is temperature, and R is the ideal gas constant. The solubility parameters δ_a and δ_o are calculated from the components they consist of in a similar fashion to how other mixture properties are constructed, a job which is best left to dedicated software.

The most important thing to remember as seen from a flow assurance standpoint is that like hydrates and waxes, asphaltenes can form as the pressures, temperatures and possibly oil composition change. It is therefore best to check this at points along the pipe when we do simulations. We also need to keep in mind that asphaltene formation and correlations to describe it is a field under development, and improved equations of state for asphaltene formation are likely to appear in the future. (Vargas et al., 2009).

Asphaltene prevention is done in similar ways as for waxes: By keeping the pressures and temperatures where they do not form, by injecting additives, or by cleaning the pipes with cleaning pigs. Asphaltenes are harder than waxes, so the pigs must obviously be designed to cope with that. Also, asphaltene buildup is even more difficult than waxes to predict accurately, so we may opt for a relatively high pigging frequency to make sure we do not run into problems due to too high asphaltene buildup. In wellbores, wireline, or coiled tubing systems may be used for cleaning. It is possible to draw an asphaltene diagram similar to that shown for hydrates in figure 18.2.3 (see for instance Vargas et al., 2009). Still, determining which chemicals to inject is more difficult for asphaltenes, and some chemists recommend testing them on the oil in question (rather than trying to predict it from the oil's composition) before using them.

Asphaltene control is quite similar to wax control, but accurate prediction is more difficult.

18.5 Scales

Scales form from the inorganic chemicals present in produced water. The main and most common scales are inorganic salts like barium sulphate ($BaSO_4$), strontium sulphate ($SrSO_4$), calcium carbonate ($CaCO_3$), though some may also be partly organic (naftenates, MEG-based etc.). Sulphate scales are mainly due to mixing of chemically incompatible waters (like sea water and formation water) while carbonate scales are due to pressure release of waters containing high concentrations of bicarbonate. Carbonate scales tend to form when the pressure is reduced or the pH-value increased.

Sulfate scales can occur if production from different wells is mixed in gathering networks . It is also possible for this to happen in one well due to inflow at multiple points in the well, particularly when seawater injection is used to maintain formation pressure.

Carbonate-scales often form inside tubing due to CO_2 escaping and causing increased pH. It can cause increased surface roughness, reduced cross-sectional area or complete blockage, and it can also cause problems to valves, pumps, and other components in the flow-path.

The main means of scale control is chemical inhibition. Continuous chemical injection may be used, and in wells it can be useful to squeeze scale inhibitors into the formation at regular intervals. As for asphaltenes, testing and selecting the right inhibitor for the fluid in question is critical (Yuan, 2003, Rosario & Bezerra, 2001). But, unlike for asphaltenes, water is the fluid to sample when we consider scale. Produced water tends to increase over time, so scale problems are also typically of more concern later in a well's life. Dedicated software is best suited to predict the onset of scales and also to select the best inhibitors from available sample analysis.

The main means of scale control is chemical inhibition.

Scales can be quite hard, and removing them once formed can be difficult. Pigging is one possibility, using aggressive chemicals like acids is another.

18.6 Corrosion, erosion, and cavitation

18.6.1 General

External corrosion is nearly always a concern for pipelines, and very often internal corrosion is, too. The corrosivity inside pipelines depends on the presence of water, and concentrations of CO_2 and H_2S. The pipe material is of course important, too, and so is coating. In addition, flow-dependent parameters like temperature, pressure, flow-regime, and flow-rates play a role. The corrosion rate is easiest to predict on bare steel exposed to well-defined compounds, but less so when the surface is protected by coating.

Gas pipelines can be prone to corrosion after commissioning if the water used for pressure testing and cleaning is not dried out properly. The chemistry of corrosion is very complex and worthy of many books on its own, so we will not attempt to go into it in full detail. What we can say, though, is that the flow simulation models can be used to calculate some of the parameters required as input to the corrosion simulation models. The same can be said about erosion: The flow model can be used to estimate the velocity of sand or other particles, and that is useful when we want to determine under which conditions particle or droplet erosion is likely to become a problem.

Corrosion generally increases with increased temperature and increased pressure, and higher velocity and better mixing also seems to increase corrosion. Increased velocity tends to result in thinner protective films of iron carbonate scale and/or inhibitors, limiting such films' ability to slow down further corrosion. It is therefore common to experience more corrosion in areas where we have slugging compared to areas of stratified flow.

Corrosion inhibitors are sometimes used to slow down corrosion rates. Describing the effect of corrosion inhibitors is not a straight forward task. Published models vary enormously in complexity, stretching from simple *inhibitor factor-based* to complicated *molecular modeling* techniques. Some models assume the degree of protection to be directly proportional to the fraction of steel surface covered by the inhibitor. These types of models rely on establishing a correlation between surface coverage, inhibitor concentration, and flow conditions. Many investigators have shown that the so-called *Frumkin Isotherm* – a well-known concept to chemists - can be used to model the degree of protection offered by an inhibitor. When the adsorption of the inhibitor from the solution phase onto the pipe's metal surface happens at the same rate as the desorption of it back into the flow, we have equilibrium, and the covered fraction of the surface, θ_S, is described by:

Corrosion increases with temperature and pressure, and higher velocity and better mixing also seem to have the same effect.

$$\frac{\theta_S}{1-\theta_S} = \frac{k_a}{k_d} c\, exp(-g\theta_S) \qquad (18.6.1)$$

k_a and k_d are the rate constants for the adsorption and desorption process, c is the concentration of inhibitor in the aqueous phase, and the g-factor indicates lateral interactions between the adsorbed molecules. Further details on how to use equation 18.6.1 can be found in Nesic et al. (1995).

Cavitation, another related problem, is caused by gas bubbles collapsing nearly instantly when the pressure suddenly increases. The Bernoulli energy equation can explain one of the primary reasons why cavitation sometimes occurs. When the velocity increases, for instance due to reduced cross-section, the pressure is reduced. Local high velocities inside valves and pumps can cause the pressure to fall down to boiling pressure. Once the velocity is reduced again some distance downstream, the bubbles collapse. The low pressure side of valves and pumps - in the unit itself or in the pipe immediately downstream of it - are therefore areas to watch.

Cavitation can cause small pieces of the surface to be knocked off and in time weaken the surface where the bubbles collapse. When inspected, the surface may look as if somebody had been hacking on it with a needle. Pressure surges due to valve opening or closure, or pump startup or stoppage can obviously also cause cavitation, but the much shorter exposure times rarely causes pitting damages of the sort characteristic to cavitation. Low instantaneous pressure combined with high outside pressure can cause the pipeline to buckle inwards or even implode, though. Avoiding damage due to outside overpressure is an important design criterion, particularly for subsea pipelines.

Erosion can be caused by particles or droplets. It is generally accepted that sand or proppant is the most common source of erosion problem in hydrocarbon systems, even though droplet corrosion can occur at very high velocities. Particle erosion depends on how fast the particles move, the solid fraction, and how large, hard and sharp the grains are. Erosion tends to attack hardest on places where the grains are pressed against the wall, such as in bends or valves.

A well's sand production rate is determined by a complex combination of geological factors and can be estimated by various techniques, for example those described by Marchino (2001). New wells often produce a large amount of sand and proppant, but then stabilize at a relatively low level before increasing again as the well ages and the

reservoir formation deteriorates. If a well produces less than $2 - 5 \cdot 10^{-5} kg/s$, it is often regarded as being 'sand-free', but it does not eliminate the possibility of sand erosion taking place.

Gas systems often run at high velocities ($> 10\ m/s$) making them more prone to erosion than liquid systems. In wet gas systems sand particles tend to be trapped and carried in the liquid phase. Slugging in particular can generate periodically high velocities that may significantly enhance the erosion rate. If the flow is unsteady or operational conditions change, sand may accumulate at times of low flow, only to be flushed through the system when high flows occur. If the sand production rate is known, this can generally be simulated quite accurately with the model outlined in chapters 14 and 16.

It is well known that erosion can work together with corrosion to produce a worse effect than the two would have done separately. This is because the iron carbonate scale and/or inhibitor layer normally slowing down the corrosion process is less wear-resistant than the steel itself and tends to be more easily removed by erosion, allowing corrosion to accelerate. The same problem goes for internal coatings: Erosion can remove them, and this accelerates corrosion. This is in fact one of the main problems with internal coatings if we are unable to control liquid quality. In pipelines carrying refined gas to customers, the coating should be able to survive for a long time. In flow-lines, however, it can come off more rapidly. It can be difficult to select appropriate internal coating and also to predict how long it survives in flow-lines.

Erosion can work together with corrosion to produce a worse effect than the two would have done separately.

The relative role of corrosion and erosion determines to which extent the velocity of the fluid in contact with the pipe wall affects the corrosion rate. Lotz (1990) expressed it in this way:

$$Erosion + Corrosion \sim v^n \tag{18.6.2}$$

n can be found from table 18.6.1.

This correlation shows the corrosion rate increases no more than proportional to the velocity, sometimes less, as long as corrosion occurs without influence of erosion. The presence of particles can make the velocity-dependence much higher, and the exponent

can become as high as 3. Droplet impingement and cavitation is even more velocity dependent. Note that the velocity of relevance in equation 18.6.2 is velocity close to where the damage takes place, meaning close to the pipe wall. Since the flow regime may change when we increase or decrease the mixture velocity, knowing the flow regime becomes essential when trying to predict corrosion-erosion rates.

Mechanism of metal loss	n
Pure corrosion	0-1
Erosion due to solid-particle impingement	2-3
Erosion due to liquid droplet impingement in high-speed gas flow	5-8
Cavitation attack	5-8

Table 18.6.1. Velocity exponent for corrosion-erosion rates.

Particle size has a somewhat surprising connection to erosion rate: It is the medium-sized particles which are most dangerous. Very small particles ($< 10\,\mu m$) are carried with the fluid and do not hit walls hard enough to cause significant damage. Very large particles ($> 1\,mm$) tend to move slowly or settle out of the carrying fluid and are unlikely to do much harm. The influence of particle hardness is more intuitive, and as one would expect, hard particles cause more erosion than soft ones.

Salama & Venkatesh (1983) stated that solids-free erosion (in practice that means droplet-erosion) only occurs at very high velocities. High velocities cause unacceptably high pressure losses, therefore the conditions required for droplet erosion are unlikely to occur in correctly designed pipelines. They defined an acceptable velocity limit to avoid significant liquid impingement erosion to be (here converted to SI-units):

$$v_{max} = \frac{366\left[\sqrt{kg/ms^2}\right]}{\sqrt{\rho_L}} \tag{18.6.3}$$

We see that for water of density $10^3\ kg/m^3$, this leads to a velocity limit of *11.6 m/s*. This is very conservative compared to values they published in tables, where the limit varies from *26* to *118 m/s* depending on steel quality. Shinogaya et al. (1987) published test data suggesting threshold velocities of about 110 m/s for water droplet impingement on stainless steel. Svedeman & Arnold (1993) stated that droplet erosion does not occur

at velocities less than 30 m/s. We see that published data varies enormously, but taken as a whole, they seem to suggest (as some of the guidelines do) that droplet erosion is not a concern in well designed pipelines.

Some traditional sand erosion prediction models, such as recommendations in API 14E, have a similar form as equation 18.6.3, but with a different proportionality factor. Many more recent models have been developed, and the one proposed by Salalma (1998) suggests the erosion rate in a bend where gas and liquid polluted by sand particles, measured in *mm erosion per kg of sand*, can be estimated as:

$$E_p = \frac{1}{S_p}\frac{{v_M}^2 d_s}{\rho_M d^2} \tag{18.6.4}$$

The mixture velocity v_M is defined as $v_M = v_G + v_L$, and the mixture density $\rho_M = (\rho_G v_G + \rho_G v_G)/v_M$. d_s is sand particle diameter, and d is as always pipe diameter. The factor S_p is a geometrical constant to do with bend radius, and it has been estimated by Barton (2003) to be around 2000.

We see that equation 18.6.4 does not take into account many of the facts already stated to be important for sand erosion, and its validity is – as for other similarly simple equations – limited.

The presence of crude oil in the transported fluid has a somewhat similar protective effect as corrosion inhibitors. The crude oil entrains the water and prevents it from wetting the steel surface. This effect and how to model it is discussed in great detail by Cai et al. (2003). Also, certain crude oil components – not present in all crude oils - reach the steel surface by direct contact or by first partitioning into the water phase, and they can create a protective layer. In an extensive study Mendez et al. (2001), Hernandez et al. (2001), and Hernandez et al. (2003) have outlined how to model this effect when it is caused by saturates, aromatics, resins, asphaltenes, nitrogen, and even sulphur.

In natural gas pipelines, condensation of water vapor occurs if the temperature falls down to the dew-point for the actual pressure, and pure water droplets form on the pipe wall. The water usually contains CO_2, and the pH is typically lower than 4. High condensation rates lead to lots of acidic water flowing down the pipe walls and create a very corrosive environment which can result in so-called *top-of-the-line* corrosion. If the condensation rates are slow, the water film renewal is also slow, and enough iron atoms

is released to increase pH significantly. That leads to the formation of a protective carbonate scale in some cases. This is less likely to happen for lower condensation rates, and therefore higher condensation rates are more dangerous.

The upper part of the pipeline is most difficult to protect with inhibitors, and that is why top-of-the-line corrosion is difficult to prevent and therefore quite common. Further details on this can be found in Gunaltun & Larrey (2000) and Vitse et al. (2003).

Glycol and methanol injected primarily to prevent hydrates is also thought to reduce the corrosion rate significantly, but the mechanisms are not fully understood (Nesic, 2007).

18.6.2 Corrosion simulation models

A host of different mathematical CO_2-corrosion models have been developed over the years, and many of them have been adapted for internal pipe corrosion prediction. Some of the models are described in open literature, others are proprietary models. We must expect the latter to be variations of the publicly available models, in some cases probably calibrated against additional laboratory or field data.

The different models can roughly be classified as *empirical corrosion models*, *semi-empirical corrosion models*, and *mechanistic corrosion models*. The empirical models rely on little or no theoretical background and the formulas used are simply curve-fits to empirical data. These models work best close to the conditions where the data they rely on originated. They have also been used very successfully when interpolating between the measurements. Extrapolating outside verified areas, however, is likely to lead to misleading results. As we have seen, corrosion is a very complicated phenomenon affected by many parameters, so using purely empirical corrosion models – like the early multi-phase models – requires great care to make sure one stays within their validity area. As seen from table 18.6.2, we have chosen to put the NORSOK-model in this category. The standard contains very detailed calculation methods, though, and it has clear statements of validity range for all of the input parameters. Those parameters are most of those we have seen take part in the flow calculations, in addition to some additional chemical properties.

Semi-empirical models are partly based on theoretical hypotheses, and that should in principle make them more reliable. Probably the most utilized model of this sort is the one developed by de Ward et al. (1975 - 1995). Mechanistic corrosion models, like the one proposed by Nesic & Lee (2003) and briefly outlined below, have strong theoretical

Name	Year	Availability	Model type	Flow	Reference
de Waard et al.	1975-1995	Open	Semi-empirical	Multi-phase	de Waard et al. (1995)
HYDROCOR	1995	Closed	Empirical	Extends to slug	Pots (1995)
Tulsa	1995	Restricted	Mechanistic, no scale formation	Single-phase	Dayalan et al. (1995)
LIPUCOR	1979-1996	Closed	Empirical	Gas and oil single-phase	Gunaltun (1996)
KSC	1998	Restricted	Mechanistic with scale formation	Single-phase	Nyborg et al. (2000)
DREAM	1996-2000	Restricted	Mechanisitc, no scale formation	Downhole gas wells	High et al. (2000)
IFE	2000	Restricted	Semi-empirical De Waard and NORSOK-based	Multi-phase, OLGA for input	Nyborg et al. (2000)
PREDICT	1996-2000	Restricted	Semi-empirical De Waard-based	Multi-phase	Jangama et al. (1996)
USL	1984-2000	Restricted	Unknown	Gas-conden-sate wells	Garber et al. (1998)
Ohio	1995-2001	Restricted	Mechanistic and empirical with scale formation	Multi-phase	Zhang et al. (1998), Jepson et al. (1997)
Cassandra	2001	Closed	Mechanistic	Multi-phase	Bill Hedges (2001)
Transport & electrochemical	2003	Open	Mechanistic	Multi-phase	Nesic & Lee, 2003
NORSOK M-506	1998-2005	Open	Empirical, based on measurements at IFE	Single-phase	Norwegian Technology Standards Institution (1998)

Table 18.6.2. Comparison of CO_2 corrosion prediction models for carbon steel. Based on the original papers, in addition to Wang et al. (2002) and Nesic (2007). The categorization is kept very basic for simplicity, and it is emphasized that not all authors necessarily agree with the considerations done in this table.

background and can be expected to be somewhat more general. That does not mean that they are easier to use, and they cannot escape all difficulties involved in the flow models underpinning them – the flow models discussed in the other chapters of this book, for instance. Generally it is also difficult to account accurately for any added corrosion enhanced by erosion. As for the flow models, knowing the chemical properties for the corrosion models sufficiently accurately is always a challenge.

CO2	Dissolved carbon dioxide
H_2CO_3	Carbonic acid
HCO_3^-	Bicarbonate ion
CO_3^{2-}	Carbonate ion
H^+	Hydrogen ion
OH^-	Hydroxide ion
Fe^{2+}	Iron ion
CL^-	Chloride ion
Na^+	Sodium ion
K^+	Potassium
Ca^{2+}	Calcium ion
Mg^{2+}	Magnesium ion
Ba^{2+}	Barium ion
Sr^{2+}	Strontium ion
CH3COOH (HAc)	Acetic acid
CH_3COO^- (Ac^-)	Acetate ion
HSO_4^-	Bisulphate ion
SO_4^{2-}	Sulphate ion

Table 18.6.3. Species typically found in oilfield brines according to Nesic & Lee (2003).

We are going to go through the most important steps in Nesic & Lee's 2003 model, even though not all theory and data will be repeated here. When creating a computer program, the original publication and its references should be utilized. The purpose here is more modest than creating a simulation program: We simply try to gain some insight into how a mechanistic corrosion model might work and how it interacts with the flow model.

When a surface corrodes, certain species in the solution appear at the steel surface (typically Fe^+), while others are depleted (typically H^+) by the electrochemical reactions. The concentration gradients this leads to create diffusion of these species towards or away from the surface. This can be formulated as:

Reaction		Equilibrium constant
Dissolution of carbondioxide	$CO_2(g) \Leftrightarrow CO_2$	$K_{sol} = \frac{C_{CO_2}}{P_{CO_2}}$
Water dissociation	$H_2O \underset{K_{b,wa}}{\overset{K_{f,wa}}{\rightleftharpoons}} H^+ + OH^-$	$K_{wa} = C_{H^+}C_{OH^-}$
Carbonoxide hydration	$CO_2 + H_2O \underset{K_{b,hy}}{\overset{K_{f,hy}}{\rightleftharpoons}} H_2CO_3$	$K_{hy} = \frac{C_{H_2CO_3}}{C_{CO_2}}$
Carbonic acid dissociation	$H_2CO_3 \underset{K_{b,ca}}{\overset{K_{f,ca}}{\rightleftharpoons}} H^+ + HCO_3^-$	$K_{ca} = \frac{C_{H^+}C_{HCO_3^-}}{C_{H_2CO_3}}$
Bicarbonate anion dissocation	$HCO_3^- \underset{K_{b,bi}}{\overset{K_{f,bi}}{\rightleftharpoons}} H^+ + CO_3^{2-}$	$K_{bi} = \frac{C_{H^+}C_{CO_3^{2-}}}{C_{HCO_3^-}}$
Acetic acid dissociation	$HAc \underset{K_{b,ac}}{\overset{K_{f,ac}}{\rightleftharpoons}} H^+ + Ac^-$	$K_{HAc} = \frac{C_{H^+}C_{Ac^-}}{C_{HAc}}$
Hydrogen sulphate anion dissociation	$HSO_4^- \underset{K_{b,HSO_4}}{\overset{K_{f,HSO_4}}{\rightleftharpoons}} H^+ + SO_4^{2-}$	$K_{HSO_4^-} = \frac{C_{H^+}C_{SO_4^{2-}}}{C_{HSO_4^-}}$

Table 18.6.4. Chemical reactions for oil and gas field brines and their equilibrium constants according to Nesic & Lie (2003). Values for the constants can be found in Nordsveen et al. (2003).

$$\frac{\partial(\varepsilon c_j)}{\partial t} = \frac{\partial}{\partial x}\left(\varepsilon^{1.5} {D_j}^{eff} \frac{\partial c_j}{\partial x}\right) + \varepsilon R_j \qquad (18.6.5)$$

ε is the scale's porosity, c_j *[kMol/m³]* is concentration of species j, ${D_j}^{eff}$ *[m²/s]* is effective diffusion coefficient of species j (including both molecular and turbulent diffusion), and R_j *[kMol/(m³s)]* is source or sink of species j due to chemical reactions.

One such transport equation can be written for each of the species in table 18.6.4. The boundary conditions at the steel surface are defined by the flux of species, which again can be determined from the electrochemical reactions. In electrochemical models, the cathodic current density i_c *[A/m²]* is commonly found by combining the charge transfer control current density i_{ct} *[A/m²]* and the limiting current density i_{lim} *[A/m²]* as:

$$\frac{1}{i_c} = \frac{1}{i_{ct}} + \frac{1}{i_{lim}} \tag{18.6.6}$$

In case of direct H_2O reduction, $i_{lim} = 0$ (for other situations, see Vetter, 1967 Revie 2000, Nesic & Lee, 2003), while:

$$i_{ct} = i_o \cdot 10^{-\frac{\eta}{b_c}} \tag{18.6.7}$$

And:

$$i_a = i_{o(Fe)} \cdot 10^{-\frac{\eta}{b_a}} \tag{18.6.8}$$

i_{ct} *[A/m²]* is charge transfer component of the total current density, i_o *[A/m²]* is exchange current density, i_a *[A/m²]* is anodic current density, η *[V]* is overpotential, b_a and b_c *[V/decade]* are so-called *anodic and cathodic Tafel slope*.

The corrosion potential and current were then found from:

$$\sum i_c = i_a \tag{18.6.9}$$

For the liquid some distance away from the pipe wall, the equilibrium concentrations of species is obtained by solving the set of equilibria in table 18.6.4. As initial conditions it is common to use a bare metal surface with the solution in chemical equilibrium.

Once this set of equations is solved for a given time-step, the corrosion rate *CR [mm/year]* can be calculated as the flux of Fe^{2+}. The homogeneous chemical reaction is calculated as:

$$R_j = k_f \prod_{r=1}^{n_r} c_r - k_b \prod_{p=1}^{n_p} c_p \tag{18.6.10}$$

R_j *[kMol/m³s]* is source or sink of species *j* due to chemical reactions, c_r and c_p *[kMol/m³]* are concentration of reactants and products, while k_f and k_b is forward and backward reaction rate constants.

The rate of precipitation of iron carbonate can be described as:

$$R_{FeCO_{3(s)}} = \frac{S}{V} \cdot f(T) \cdot f(S_s) \tag{18.6.11}$$

Where *S/V [m⁻¹]* is surface area to volume ratio, *T [K]* is temperature, and *f()* denotes some function of. *Super-saturation* is defined as:

$$S_s = \frac{c_{Fe^{2+}} + c_{CO_3{}^{2-}}}{K_{sp}} \tag{18.6.12}$$

K_{sp} is solubility limit. A mass balance equation for solid iron carbonate can then be expressed in the form of volumetric scale porosity:

$$\frac{\partial \varepsilon}{\partial t} = -CR\frac{\partial \varepsilon}{\partial x} - \frac{M_{FeCO_{3(s)}}}{\rho_{FeCO_{3(s)}}} R_{FeCO_{3(s)}} \tag{18.6.13}$$

M [kg/kMol] is molar mass, ρ *[kg/m³]* is as always density, and $R_{FeCO_{3(s)}}$ *[mm/year]* is precipitation rate of iron carbonate. We notice that some of the parameters involved in these equations depend on the flow conditions. Surface to volume rate depends on flow regime, turbulent diffusion depends on velocity, concentrations depend on contact times and so on. When such data is pulled from the flow simulation model, equation 18.6.13 can be solved together with the transport equation 18.6.5 and the electrochemical equation 18.6.9. That enables direct calculation of porosity, thickness and protective properties of the carbonate scales.

The time scales involved in corrosion are much longer than the ones we focus on when simulating pipe flow, so it does not make sense to solve the corrosion equations for each time-step in the flow model. Instead, we use the flow model to determine typical flow conditions in various parts of the pipeline and use that as input to the corrosion model.

Even though we have not given all model details here, we can see that corrosion simulations are possible, if not easy, and not necessarily very accurate. Nesic (2007) has produced an overview of current state of art when it comes to corrosion prediction in pipelines. He believes the electrochemistry of mild steel dissolution largely has been understood and can be modeled quite accurately now. There are lots of outstanding issues, though, and different steels, as well as the influence of H_2S, HAc, glycol, and methanol cannot currently be predicted reliably. Localized CO_2 corrosion attack, probably the most dangerous type of CO_2 attack, is also difficult to predict with current technology.

18.7 Heavy oil and emulsions

Large molecules may cause the oil to be very viscous and difficult to transport in pipes. As explained in chapter 13, two liquids can form emulsions, and those emulsions can under certain conditions lead to very high overall viscosity. The result can be a gel with non-Newtonian properties, and transporting it can be as difficult as for very viscous oil. Predicting whether such emulsions are likely to occur, and evaluating whether that can cause serious problems typically involves both chemical analysis and flow calculations.

"Design is not just what it looks like and feels like. Design is how it works."
Steve Jobs

19 Various subjects

Some subjects of relevance to the flow assurance engineer:

- Multi-phase flow measurement and estimation
- Gas lift
- Slug catchers

19.1 Multi-phase flowmeters and flow estimators

We have seen that mathematical models can be used to simulate the flow in multi-phase pipelines. The simulations produce data for pressure, flow, temperature, and many others when they run. This means that if a simulator runs in parallel with a real pipeline, we can pull out such data from the simulator instead of doing it from transmitters on the physical pipeline. We have also observed that the models rely on boundary conditions at the pipeline's inlet and outlet, and those boundary conditions must obviously be fed into the simulator, possibly from transmitters. The boundary conditions at the inlet have to include temperature and either pressure or mass flow fraction for each phase. Multiphase mass or volumetric flow is more difficult to measure than pressure and temperature, so the flow measurements are less accurate and more susceptible to failure than the others. New subsea multiphase field developments are sometimes equipped with transmitters for all of these parameters nowadays, and that

makes it possible to use the simulator to check them against each other. Should a flowmeter fail, it is also possible to estimate the flow based on the other measurements. If several wells produce to the same flow-line, estimation becomes more complicated and less accurate, but it is still possible to do it. Transmitters and flow simulators complement each other, but they also overlap, so having both provides some redundancy. Such technology has now been used successfully on several offshore fields. In chapter 1.8 in *Pipe Flow 1*, the Ormen Lange-development was described as an example of this.

A three-phase multi-phase flowmeter normally provides the following outputs:

- Oil, water and gas flow rates, on volume-format (as $A\alpha_G v_G$, $A\alpha_o v_o$, and $A\alpha_w v_w$) and/or on mass flow format (as $A\alpha_G \rho_G v_G$, $A\alpha_o \rho_o v_o$, and $A\alpha_w \rho_w v_w$).
- Phase volume fractions α_G, α_o and α_w.
- Pressure p and temperature T.

Multi-phase flow meters are more demanding than single-phase meters, and they rely on some input data from the user. They depend somewhat on the measurement principles used by the specific meter, but the list may look like this:

- Each phase's density.
- Water conductivity.
- Oil permittivity.
- Linear attenuation coefficient or mass attenuation coefficient for each phase.
- Viscosity for each phase.

The uncertainty varies depending on how the meter is designed, and the designs again vary depending on the fractions it is designed to measure. Uncertainties can often be as high as 5 – 10%. That is not good enough for fiscal metering, but it can be very useful for testing each well individually when the flow from several wells is lead into the same flow-line.

Some meters are designed only for dry gas, others can handle some liquid content. We generally need to have a fair idea of the expected mass flow fractions in order to select an appropriate multi-phase flowmeter. A simple overview over available technologies and how to utilize them can be found in Corneliussen et al. (2005).

19.2 Gas lift

19.2.1 General

Subsea multi-phase pumping is now considered a relatively well proven technology, but further improvements will be needed with increased transport distances and water depths. This involves increased pressure boosting and capacity as well as the ability to handle more complex fluids (viscous crude).

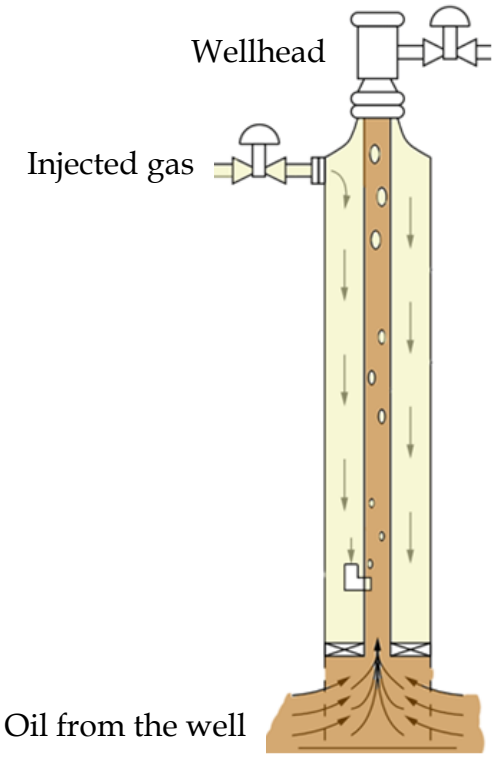

Figure 19.2.1. Oil-producing well with gas lift.

One of the most common 'pumping'-challenges is to reduce well pressure by injecting gas down the annulus as illustrated on fig. 19.2.1. If the well produces single-phase liquid, for instance oil, the added gas is going to reduce the average density for the fluid mixture in the tubing, but it is also going to produce two-phase flow. That flow's behavior is of course as for any other two-phase flow, and the flow regimes will be as outlined in chapters 1 and 11. At high gas injection rates, annular flow is the most likely flow regime, and the flow arriving at the wellhead will be fairly constant. At lower injection rates, slugging occurs, something which is unfavorable both to the receiving

end of the flow (be that a riser, a gathering pipe network, or a flow-line) and to the well itself. Slugging can be avoided by making sure the injection rate is high enough. That is an effective stabilization strategy, but it sometimes means we have to inject more gas than needed for the lifting process, and it is also costly in terms of compressor power. Therefore it can be attractive to use lower injection rates, and to stabilize the flow by actively controlling the injection and production chokes. This strategy can lead to remarkably stable flow even if slugging is not necessarily prevented. The controller can use the wellhead and downhole pressures as inputs, and only a standard PID-controller is required. In some cases stable pressure has been achieved even with the Integrator and Derivative gain settings in the controller adjusted to zero, meaning it in reality is reduced to a Proportional-controller.

We do not always have access to the downhole pressure, either because we have not installed a pressure sensor, or because the harsh environment in the well leads to short sensor survival time. It is known from control theory that it sometimes is possible to estimate some of the state variables we lack by using a so-called *Kalman filter*. A Kalman filter is a mathematical model of the system, and it uses available measurements to estimate parameters which are not measured directly. If the model is linear, we can transform state variable correlations and get real-time estimates rapidly. Since multi-phase flow follows very complicated, nonlinear laws and requires spatial discretization when we want to simulate it, we may at first expect designing a workable Kalman-filter to be difficult. Eikrem et al. (2003) have shown, though, that a very simplified model of only the mass conservation equations is sufficient for the purpose of constructing the Kalman filter and estimating the downhole pressure accurately enough to enable very significant reduction in the slug-generated pressure pulses.

Achieving stable gas injection is similar to achieving stable normal flow for two-phase gas-oil or gas-water production in wells where no gas is injected, the difference being that we cannot throttle the gas separately (since the gas and the liquid already is mixed). Still, very stable flow has been achieved on many fields by using the same technique (see for instance Godhavn et al., 2005).

19.2.2 Oil & water-producing well with gas lift: Simulation example

As an example of what a steady-state simulation with a commercially available steady-state simulation program can be used for, we consider the oil and water producing well in figure 19.2.2.

If no gas is injected, the well produces oil with 10% water in it (10% water cut). Injecting gas through annulus reduces the average density in the out-flowing fluid, and depending on flow regime and liquid fractions, we can expect more or less increase in production. The problem here is to determine how much gas should be injected.

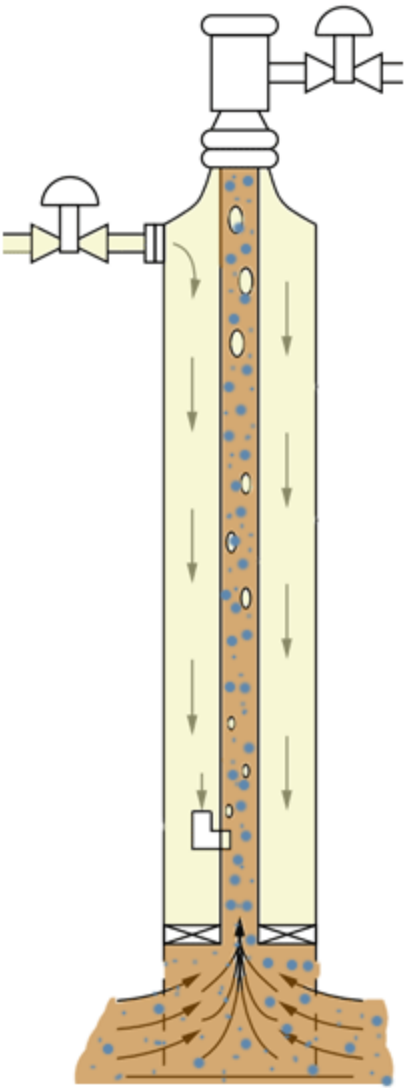

Figure 19.2.2. Oil and water-producing well with gas lift.

The gas flow down annulus is of course single-phase and therefore relatively easy to model, but after it is mixed with the oil and water in the tubing, it creates three-phase flow there.

For simplicity, we only include the part of the well which is above the gas injection point, and we consider the tubing pressure constant at that point. This is of course an approximation, since a somewhat flow-dependent pressure loss upstream of the injection point is likely.

The input data to the simulation program is given in table 19.2.1. When running the simulations with the given boundary conditions for a series of gas injection rates, we can plot the resulting oil and water flow as a function of injection rate. It is the oil flow we are most interested in, and we have plotted it as a function of the injected gas flow in figure 19.2.3.

Note that the gas flow is given in standard cubic meters per second, meaning as it would have been if the pressure was one atmosphere and the temperature 15 ^{0}C. Since the pressure is much higher, the actual volumetric gas flow is lower.

The oil production reaches a maximum at a particular gas injection rate. This is in some ways the optimum gas injection rate, though not necessarily the one we would use in practice. The problem is that at low gas rates, we tend to get slugs, and that does not lead to a smooth flow out of the wellhead. For a well as small as this, the problem may not necessarily be serious enough to require any stabilization of the sort discussed in

chapter 19.2.1 or increased gas injection in order to make the flow annular, but in some cases we may have to do that.

Well temperature (at injection point)	**T=100**	**^{0}C**
Tubing pressure (at injection point)	p_{in}=16.0	MPa
Oil density	ρ_o=874	Kg/m^3
Water density	ρ_v=998	Kg/m^3
Gas density (injected gas) at standard pressure	ρ_G=0.978	Kg/m^3
Water content, % of oil volume at inlet	10	%
Well depth (the vertical part included in the study)	l=2500	m
Tubing inner diameter	d_1=62	mm
Tubing outer diameter (annulus inner diameter)	d_2=73	mm
Casing inner diameter (annulus outer diameter)	d_3=161	mm
Heat transfer coefficient oil/water/gas-tubing	U=4.2 ·10^8	W/(m^{2}K)
Heat transfer coefficient gas-casing	U=8.4 ·10^8	W/(m^{2}K)
Tubing relative roughness, inner side	k_s/d=9.8·10^{-4}	
Tubing relative roughness, outer side	k_s/d=8.3·10^{-4}	
Casing relative roughness, inner side	k_s/d=3.8·10^{-4}	
Pressure at receiving end	p_{out}=1.0	MPa

Table 19.2.1. Input data to the gas lift simulations.

Since this is a steady-state analysis, it does not directly tell us if stability is going to be a problem, although it indirectly gives us some information about it since it indicates when the flow is expected to become intermittent. But in general, we cannot use a steady-state simulation program to design and tune a choke regulator in the way it was explained in chapter 19.2.1.

It is worth noting that the documentation for the simulation program used to produce these results does not clarify how it deals with three-phase flow. It appears likely that a simplified average mixture model of the oil and gas is used so that oil and gas is treated as one phase. The resulting gas-oil/water flow appears to be simulated as quasi-two-phase. Also, some of the flow regime maps produced during the many simulations necessary to create figure 19.2.3 did actually include a part called stratified flow, a type of flow which does not occur in vertical pipes! As we saw examples of in *Pipe Flow 1*, results from the commercial software packages need to be checked as thoroughly as possible, and for important calculations, it is recommended comparing simulation results in some of the points along the pipe with manual calculation according to

correlations for flow regime and friction given by other sources. Using more than one simulation program is also useful.

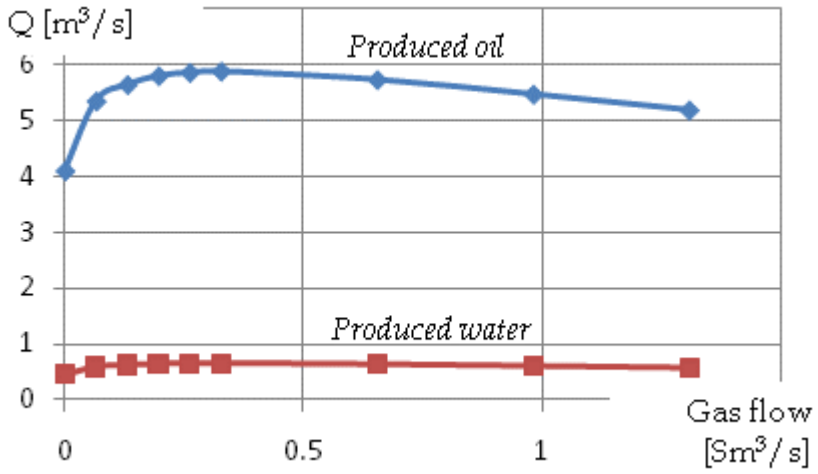

Figure 19.2.3. Produced oil and water as a function of injected gas flow. Very high gas injection rates do not increase oil production and are costly, but produce more stable flow. Stabilizing the flow with active regulation rather than excessive injection rates is more economical.

19.3 Slug catchers

Slugs can cause the amount of liquid in a multi-phase pipeline to arrive at very uneven rates. As already mentioned, such slugs can be caused by the hydrodynamic conditions in the pipe, or by the terrain. Pigging can also cause slugs, since the pig tends to push the liquid in front of it, and it is not uncommon for such slugs to be the largest ones occurring.

A slug catcher is a vessel with sufficient buffer volume to store the largest slugs expected to arrive at the receiving end of the flow-line. The slug catcher is located between the outlet of the line and the processing equipment. The buffered liquids can be drained to the processing equipment at a much slower rate to prevent overloading the system. A slug catcher can be designed as a large tank, but since the pressure often is high, it is usually cheaper to construct it from pipes which are connected together as 'fingers'. Slug catchers can be quite costly, particularly if they have to be located offshore, and sizing them may be one of the most important flow assurance tasks.

Figure 19.2.1. Finger slug catcher.

A slug catcher's effectiveness is not only determined by its size. Giozza (1983) has simulated vessel-type slug catchers, and Sarica et al. (1990) have developed a useful model for designing finger slug-catchers. The finger slug catcher model is also well presented in Shoham's book (Shoham, 2005). Results seem to indicate the finger slug catchers generally are more efficient than those of the vessel type, and the fingers should slope a few degrees downwards.

"It is possible to store the mind with a million facts and still be entirely uneducated."
Alec Bourne

Suggested reading

Wallis, G. B. (1969): **One-Dimensional Two-Phase Flow**. McGraw-Hill Book Co. Inc.
This is one of the earliest attempts to analyze two-phase flow, and has served numerous engineers well. It is still used as a reference, but having been published in 1959 it is a bit outdated. Paradoxically, the book has partly become a victim of its own success in that its most useful content has found its way into many other, later multi-phase books.

Govier, G. W., Aziz, K. (1972): **The flow of complex mixtures in pipes**. R.E. Krieger Publishing Co., Inc. Malabar, Florida.
This is another early attempt to deal with two-phase flow. It shows the derivation of the conservation equations for two-phase flow and discusses important phenomena like slippage and holdup.

Ishii, M. (1975): **Thermo Fluid Dynamic Theory of Two-Phase Flow**. Eyralles Press, Paris, France.
This is Ishii's much-referenced PhD theses. After publishing a book with nearly the same title together with Hibiki in 2006 (see below), Ishii's 1975 book is now less relevant.

Chaudhry, M. H. (1979): *Applied Hydraulic Transients.* Van Nostrand Reinhold Company.
This book is mostly about single-phase liquid flow, but its chapter on column separation is still of considerable pedagogical value.

Hetsroni, G. (1982): **Handbook of Multi-phase Systems.** McGraw Hill.
This general book on multi-phase flow contains quite a bit of information, but much of it is less relevant to flow assurance. Only one of its 10 chapters deals with gas-liquid two-phase flow, and many of the other books deal with that in greater detail. It has an extensive chapter on multi-phase measurement principles.

Streeter, V.L., Wylie, E.B., (1983, earlier editions exist): **Fluid Transients.** FEB Press.

This book is the probably most-used popular reference for single-phase liquid transient simulations, and its way of presenting the method of characteristics should be familiar to most people in this field. Its relevance to multi-phase flow is somewhat limited, though.

Frisch, U. (1995): *Turbulence*. **The Legacy of A. N. Kolmogorov.** Cambridge University Press.
This book is mentioned as one example of the many on turbulence, and is included mainly to remind the reader that turbulent phenomena plays a major role in nearly everything to do with flow regime change, friction, droplet deposition, bubble dispersion. A basic understanding of turbulence is essential to understanding multi-phase pipe flow.

Crowe, C. T., Sommerfeld, M., Tsuji, Y. (1997): **Multi-phase Flows with Droplets and Particles.** CRC Press LCC.
The book primarily focuses on droplets, solid particles, and bubbles. It can be useful for those attempting to improve flow assurance methods related to hydrodynamics of dispersions.

Brill, J. P., Mukherjee, H. (1999): **Multi-phase Flow in Wells.** *Henry L. Doherty Memorial Fund of AIME, Society of Petroleum Engineers.*
This book is useful to anyone involved in well flow. It summarizes the methods utilized most for steady-state well flow calculations, and contains a welth of correlations and diagrams.

Levy, S. (1999): ***Two*-Phase Flow in Complex Systems.** John Wiley & Sons, Inc.
This book on two-phase flow focuses mostly on nuclear power plants and climate systems, but it also contains quite a lot on flow assurance, including descriptions of important phenomena like flow patterns.

Toro, E. F. (1999): **Riemann Solvers and Numerical Methods for Fluid Dynamics. A practical Introduction.** Springer Verlag.
Solving the conservation equations numerically is not trivial, and the development in the field of relevant numerical methods runs at a fast pace. Of the many books on numerical methods available, Toro's is one of the most useful to flow assurance engineers and academics. It contains a thorough overview of the methods available today, and prepares the reader to be able to make sense of the constant flow of new publications in the field.

Hasan, A. R., Kabir C. S. (2002): **Fluid Flow and Heat Transfer in Wellbores.** Society of Petroleum Engineers, Richardson, Texas.
Describes how to model multi-phase flow heat transfer for a large variety of wellbore operating conditions. Drilling and gas lift problems are treated thoroughly.

Naterer, G. F. (2003): **Heat Transfer in Single and Multi-phase Systems.** CRC Press.
Contains chapters on many relevant subjects, including turbulence, boiling and condensation, gas-liquid-solid flow, with a general focus on heat transfer.

Brennen, C. E. (2005): **Fundamentals of Multi-phase Flow.** Cambridge University Press. *This book presents a mixture of pipe flow and multidimensional calculations. As the name suggests, it takes a fundamental approach, and as such, it does not go all the way to explaining how to simulate in practice. It contains a lot of useful correlations, though.*

Guo, B., Song, S., Chacko, J., Ghalambor, A. (2005): **Offshore Pipelines.** Elsevier.
Although this book mainly discusses pipeline design and installation methods, it has also found room for chapters on flow assurance with emphasis on hydrate formation as well as descriptions of pigging operations. Two appendixes on gas-liquid multi-phase flows in pipelines and steady and transient solutions for pipeline temperature are also very readable and useful.

Liu, H. (2005): **Pipeline Engineering**. Lewis Publishers. **(Book)**
Contains chapters on pipe flow, including solid liquid and solid gas mixtures as well as non-Newtonian fluids. Its main strength, as seen from a flow assurance stand-point, may lie in the many practical considerations and operational conditions in outlines.

Kolev, N. I. (2005): **Multi-phase Flow Dynamics 1. Fundamentals.** Springer, 2002, 2005.
Kolev, N. I. (2005): **Multi-phase Flow Dynamics 2. Thermal and Mechanical Interactions.** Springer, 2002, 2005.
Kolev, N. I. (2005): **Multi-phase Flow Dynamics 3.** *Turbulence, Gas Absorption and Release, Diesel Fuel Properties*. Springer, 2002, 2005, 2007.
Kolev, N. I. (2006): **Multi-phase Flow Dynamics 4.** *Nuclear Thermal Hydraulics*. Springer, 2006.
These four books form one of the most extensive collections of flow assurance-relevant correlations and models. Kolev has in many ways done a great job, the books are very useful as reference for nearly everything we know about multi-phase flow. A considerable part of it is specifically about pipe flow. Each chapter has its own nomenclature, but some readers may find it problematic that those nomenclatures are generally incomplete, sometimes leaving the reader to seek out other sources to decipher the equations.

Crowe, C.T. (2006): **Multi-phase Flow Handbook.** CRC.

This large collection of multi-phase flow subjects written by invited lecturers includes chapters relevant to flow assurance, including the normal two-phase flow regime maps and some very detailed droplet considerations. It also discusses details relevant to various multi-phase flow measurements.

Ishii, M., Hibiki, T. (2006): Thermo-Fluid Dynamics of Two-Phase Flow. Springer.
This book appears to be partly built on Ishii's PhD Theses, which has served as a cornerstone in the field of multi-phase flow for what in this relatively new field must count as a long time. It contains many chapters on different ways of averaging, and that part may be too theoretical to most practicing engineers. Both Ishii and Hibiki have published a lot of measurements on multi-phase pipe flow during the years, and many of their results are included in the book. It may serve more as reference for researchers than a practical tool for commercial flow assurance work.

Shoham, O. (2006): Mechanistic Modeling of Gas-Liquid Two-Phase Flow in Pipes. Society of Petroleum Engineers.
This highly useful and well written book focuses on steady-state mechanistic models for two-phase gas-liquid flow in pipelines and well-bores. It is written by a well respected scientist who has worked in the field of flow assurance together with equally competent colleagues for a long time. The book comes with a CD and two simulation programs, one to predict flow patterns, and one to predict liquid fraction and pressure drop in a pipeline. It also contains numerous examples and problems, and that makes the book more pedagogical than most. To the flow assurance engineer, it is also a clear advantage that this book focuses on pipe flow, without getting lost in such interesting, but to flow assurance less relevant subjects as multidimensional flow or nuclear boiler peculiarities. Transient models are only briefly discussed.

Wilson, K. C., Addie, G. R., Sellgren, A., Clift, R. (2006): Slurry Transport using Centrifugal Pumps. Springer.
Packed with both theoretical and practical considerations on pipe flows where particles are transported by a liquid. It discusses central questions when dealing with slurry flow, particularly whether one gets settling and what the pressure loss becomes.

Prosperetti, A., Tryggvason, G. (2007): Computational Methods for Multi-phase Flow. Cambridge University Press.
Some of the chapters in this generally well-written book are highly relevant to flow assurance engineers, even though most of it is dedicated to 2D and 3D computations. Of the books mentioned here, this is the one that takes the numerical mathematics most seriously, a subject essential to both developers and practicing engineers.

Datta, A. (2008): Process Engineering and Design Using Visual Basic. CRC Press.
Even though its name seems to suggest otherwise, this book does in fact contain a lot on multi-phase flow, mostly on chemical reactor flow, but also results from simulations with the well-known OLGA software.

Jacobsen, H. A. (2008): Chemical Reactor Modeling, Multi-phase Reactive Flows. Springer.
This very extensive book of more than 1,200 pages contains a lot of fundamental multi-phase flow theory. As the title suggests, the main focus is reactor modeling, and the book may not cover much of the semi-empirical knowledge essential to flow assurance practitioners. Still, the thoroughness with which averaging, turbulence models and numerical solution methods are treated make this book useful to researchers in the field, particularly those who want to experiment with multidimensional simulations.

Zaichik, L. I., Alipchenkov, V. M., Sinaiski, E. G. (2008): Particles in Turbulent Flows. Wiley-VCH.
It covers motion of particles in turbulent flows, with relevance to droplets and bubbles, particularly dispersion and clustering. The theories are mostly relevant to flow assurance model developers.

Bratland, O (2009): Pipe Flow 1, Single-phase Flow Assurance. Available at drbratland.com.
This is the first book in a series of two, and precedes the one you are currently reading. It presents a survey of different commercially available flow assurance software tools for both single- and multi-phase flow. It also presents various friction and flow models as well as simulation and verification methods for single-phase pipe flow.

Carroll, J. (2009): Natural Gas Hydrates. A Guide for Engineers. Second Edition.
This very readable and practical book is one of the most updated on this subject and probably the one best suited to most flow assurance engineers. It has thorough explanations on different types of hydrates, how they are formed, and how to model them. The book comes with some free software, downloadable from the internet site at members.shaw.ca/hydrate.

"Get the facts, or the facts will get you."
Thomas Fuller, 1732

References

Jeffreys, H. (1926): *On the Formation of Water Waves from Wind*, Proc. Royal Soc., London, A110, 241.

Sieder, E.N., G.E. Tate. (1936): *Heat transfer and pressure drop of liquids in tubes*, Ind. Eng. Chem, 28, 1429.

Dumitrescu, D. T. (1943): *Strömung an Einer Luftblase im Senkrecten Rohr (in German)*. Z. Angew. Math. Mech. 23, 139.

Weinaug, C. F., Katz, D. L. (1943): *Surface Tensions of Methane-Propane Mixtures*. Ind. Eng. Chem. 35, pp. 239-246.

Sverdrup, H. U., Munk, W. H. (1947): *Wind, Sea and Swell: Theory of Relations for Forcasting.* US NaVY Hydrographic Office Pub. No. 601.

Davies, R. M., Taylor, G. (1950): *The Mechanics of Large Bubbles rising through Extended Liquids and through Liquids in Tubes*. The Royal Society, London, Series A, 200, No. A1062, 375-390.

Durand, R., Condolios, E. (1952): *Communication de R. Durand et E. Condolios, Compte Rendu des Deuxiemes Journees de L'Hydraulique*. Paris, Societe Hydrotechnique de France, pp. 29–55, June.

Baron, T., Sterling, C. S., and Schueler, A. P. (1953): *Viscosity of Suspensions - Review and Applications of Two-Phase Flow.* Proceedings 3rd Midwestern Conference Fluid Mechanics. University of Minnesota, Minneapolis 103-123.

Durand, R. (1953): *Basic relationships of the transportation of solids in pipes-experimental research.* Proceedings of the Fifth Minneapolis International Hydraulics Convention, Minneapolis, MN, pp. 89–103.

Hinze, J.O. (1955): *Fundamentals of the hydrodynamics mechanisms of splitting in dispersion process*. AIChE J. 1 289–295.

Dengler, C. E., Addoms, J. N. (1956): *Heat Transfer Mechanisms of Vaporization of Water in Vertical Tubes.* Chem. Eng. Proc. Symp. Series 52, 95.

Stepanoff, A.J. (1957): *Centrifugal and Axial Flow Pumps. Theory, Design and Applications.* John Wiley & Sons, Inc. **(Book)**

Harmathy, T. Z. (1960): *Velocity of Large Drops and Bubbles in Media of Infinite or Restricted Extent.* AIChE J. 6, 281.

Charles, M. E., Govier, G. W., Hodgson, G.W. (1961): *The Horizontal Pipeline Flow of Equal Density Oil-Water Mixtures.* The Canadian Journal of Chemical Engineering, February.

Collier, J. P., Pulling, D. J. (1962): *Heat Transfer to Two-Phase Gas-Liquid Systems, Part II: Further Data on Steam-Water Mixtures in Liquid Dispersed Region in an Annulus.* Trans. Inst. Chem. Engineers 29, 174.

Nicklin, D. J., Wilkes, J. O., Davidson, J.F. (1962): *Two-phase Flow in Vertical Tubes.* Trans. Inst. Chem. Engineers 40, No. 1, 61.

Wisner, P. (1965): *On The Role of The Froude Criterion for The Study of Air Entrainment in High Velocity Flows.* In: Proc. 11th IAHR Congress, Leningrad, USSR, paper 1.15 (in French).

API RP 44 (1966): *API Recommended Practice for Sampling Petroleum Reservoir Fluids*. American Petroleum Institute.

Rajaratnam, N. (1967): *Hydraulic jumps.* Adv. Hydrosci. 4, 197–280.

Bridkey, R. S. (1967): *The Phenomena of Fluid Motion.* Addison-Wesley Press, Boston.

API RP 44 (1966): *Recommended Practice for Sampling Petroleum Reservoir Fluids.* American Petroleum Institute.

Benjamin, T. B. (1968): *Gravity Currents and Related Phenomena*. J. Fluid Mech. 31, part 2, 209.

Sherman, P. (1968): Emulsion *Science*. Academic Press, New York.

Wallis, G. B. (1969): *One-Dimensional Two-Phase Flow*. McGraw-Hill Book Co. Inc. **(Book)**

Turner, R. G., Hubbard, M. G., Dukler, A. E. (1969): *Analysis and Prediction of Minimum Flow Rate for the Continuous Removal of Liquid from Gas Wells*. McGraw-Hill Book Co. Inc.

DeGance, A. E., Atherto, R. W. (1970): *Transferring Heat in Two-Phase Systems, Pert 3*. Chem. Eng. May, 113.

Wicks, M. (1971): *Transport of Solids at Low Concentration in Horizontal Pipes.* Advances in Solid-Liquid Flow in Pipes & Its Application, I. Zandi, ed., Pergamon Press, pp. 101–124.

Govier, G. W., Aziz, K. (1972): *The flow of complex mixtures in pipes*. R.E. Krieger Publishing Co., Inc. Malabar, Florida. **(Book)**

Soave, G. (1972): *Equilibrium constants for a modified Redlich-Kwong equation of state*. Chem. Eng. Sci, 27, 1197-1203.

Beggs H. D., & Brill J. P., (1973): *A study of two-phase flow in inclined pipes.* Journal of Petroleum Technology, Transactions, 25, 607-617, May 1973.

Chisholm, D. (1973): *Two-Phase Flow in Pipelines and Heat Exchangers*. George Godwin, London and New York in association with the Institution of Chemical Engineers, New York.

Sevik, M., Park, S.H. (1973): *The splitting of drops and bubbles by turbulent fluid flow*. Trans. ASME J. Fluids Eng. 95, 53–60.

de Waard, C., Williams, D. E. (1975): *Carbonic Acid Corrosion of Steel.* Corrosion, 31, 177.

Hanley, H. J. M., McCarty, R.D., Haynes, W. M. (1975): *Equation for the Viscosity and Thermal Conductivity of the Individual Gases.* Cryogenics 15, 1975, 413.

Ishii, M. (1975): Thermo *Fluid Dynamic Theory of Two-Phase Flow*. Eyralles Press, Paris, France. **(Book)**

Ishii, M., Grolmes, M.A. (1975): *Inception criteria for droplet entrainment in two-phase concurrent film flow*. AIChE J. 21, 308–318.

Gnielinski, V. (1976): *New Equations for Heat and Mass Transfer in Turbulent Pipe and Channel Flow.* Int Chem Eng Vol. 16 p. 10.

Henstock, W. H., Hanratty, T. J. (1976): *The interfacial drag and the height of the wall layer in annular flows*. AIChE J. 22, 990–1000.

Mo, K. C., Gubbins, K. E. (1976): *Conformal Solution Theory for Viscosity and Thermal Conductivity of Mixtures.* Mol. Phys. 31, 825.

Peng, D.Y. and D.B. Robinson (1976): *A new two-constant equation of state.* Ind. Eng. Chem. Fundam., 15, 59-64.

Taitel Y., & Duckler A. E., (1976): *A Model For Predicting Flow Regime Transitions in Horizontal and Near-Horizontal Gas-Liquid Flow*. AIChE Journal, 22/1, 47-55.

Yuen, M. C., Chen, L. W. (1976): *On Drag of Evaporating Droplets.* Combust. Sci. Technol. 14, 147-54.

Gregory, G. A., Nicholson, M. K., Aziz, K. (1978): *Correlation of Liquid Volume Fraction int the Slug for Horizontal Gas-Liquid Slug Flow.* Intl. J. Multi-phase Flow 4, 33.

Liles, D. R., Reed, W. H. (1978): *A Semi-implicit Method for Two-phase Fluid Dynamics.* J. Comput. Phys. 26:390-407.

Peng, D. Y., Robinson, D. B. (1978): *The Characterization of the Heptanes and Heavier Fractions for the GPA Peng-Robinson Programs.*, GPA Research Report RR-28, 1978.

Chaudhry, M. H. (1979): *Applied Hydraulic Transients.* Van Nostrand Reinhold Company. **(Book)**

Ishii, M., Zuber, N. (1979): *Drag Coefficient and Relative Velocity in Bubbly, Droplet or Particular Flows.* AIChE Journal, vol. 25, pp. 843-855.

Nigmatulin R. I. (1979): *Spatial Averaging in the Mechanics of Heterogeneous and Dispersed Systems.* Int. J. Multi-phase Flow, 5, 353-385.

Ostrof, A. G. (1979): *Introduction to Oilfield Water Technology.* Second Edition, National Association of Corrosion Engineers, Houston.

Barnea, D., Shoham, O., Taitel, Y., Dukler, A. E. (1980): *Flow Pattern Transition for Steady Upward Gas-Liquid Flow in Vertical Tubes.* AIChE J. 26, No. 3, 345-354.

Christensen, P. L., Fredenslund Aa. (1980): *A Corresponding States Model for the Thermal Conductivity of Gases and Liquids.* Chem. Eng. Sci. 35, p. 871.

Oroskar, A. R., and Turian, R. M. (1980): *The Critical Velocity in Pipeline Flow of Slurries.* AIChE. J., Vol. 26, No. 4, pp. 550–558.

Taitel, Y., Barnea, D., Dukler, A. E. (1980): *Modelling Flow Pattern Transition for Gas-Liquid Flow in Horizontal and Inclined Pipes, Comparison of Experimental Data with Theory*. Intl. J. Multi-phase Flow 6, 217.

Burger, E. D., Perkins, T. K., and Striegler, J. H. (1981): *Studies of Wax Deposition in the Trans Alaska Pipeline.* Journal of Petroleum Technology, 33.

Barnea, D., Shoham, O., Taitel, Y. (1982): *Flow-Pattern Transition for Downward Inclined Two-Phase Flow; Horizontal to Vertical.* Chem. Eng. Sci. 37, 735.

Barnea, D., Shoham, O., Taitel, Y. (1982): *Flow-Pattern Transition for Vertical Downward Two-Phase Flow.* Chem. Eng. Sci. 37, 741.

Hetsroni, G. (1982): *Handbook of Multi-phase Systems.* McGraw Hill. **(Book)**

Malnes, D. (1982): *Slug flow in vertical, horizontal and inclined pipes.* V. Inst. for Energy Tech., Kjeller, Norway. Report IFE/KR/E-83/002.

Nigmatulin, B. I, Netunaev, S. B., Gorjunova, M.Z . (1982): *Investigation of moisture entrainment processes from the liquid film surface in air–water upflow*. Thermophys. High Temp. 20 (1982) 195–197.

Shoham, O., Dukler, A. E., Taitel, Y. (1982): *Heat Transfer during Intermittent Slug Flow in Horizontal Tubes.* Ind. Eng. Chem. Fundam. 21, No. 3, 312.

Drew D. A. (1983): *Mathematical modeling of two-phase flows.* Annual Review of Fluid Mechanics, 15, 261-291.

Giozza, W. F. (1983): *Simulation of Gas-Oil Separator Behavior under Slug Flow Conditions.* MS Thesis, University of Tulsa, USA.

Gnielinski, V. (1983): *Single-Phase Convective Heat Transfer*, Ch. 2. 5, section 1-1 to 2-9, Hemisphere Publishing Corporation.

Kataoka, I., Ishii, M., Mishima, K. (1983): *Generation and size distribution of droplets in annular two-phase flow.* Trans. ASME J. Fluids Eng. 105, 230–238.

Salama, M. M., Venkatesh, E. S. (1983): *Evaluation of API RP14E Erosional Velocity Limitations for Offshore Gas Wells.* OTC 4484, OTC Conference, Houston, May 2 – 5, pp371 – 376.

Streeter, V.L., Wylie, E.B., (1983): *Fluid Transients.* FEB Press. **(Book)**

Vysniauskas, A., Bishnoi, P. R. (1983): *Kinetics of Methane Hydrate Formation*. Chem. Eng. Sci. 38: 1061-1072

Bendiksen, K. H., (1984): *An Experimental Investigation of The Motion of Long Bubbles in Inclined Tubes.* Intl. J. Multi-phase Flow 10, 467.

Hirschberg, A., deJong, L. N. J., Schipper, B. A., Meijer, J. G. (1984): *Influence of Temperature and Pressure on Asphaltene Flocculation.* SPE Journal, June.

Pedersen, K. S., Thomassen, P., Fredenslund, A. A (1984): *Thermodynamics of Petroleum Mixtures Containing Hydrocarbons. 2. Flash and PVT Calculations with the SRK Equation of State.* Ind. Eng. Chem. Proc. Des. and Dev., 23, 566-573.

Stewart, H. B., Wendroff, B. (1984): *Two-phase Flow: Models and Methods*. J. Comput. Phys. 56:363-409.

Asali, C., Hanratty, T. J., Andreussi, P., (1985): *Interfacial Drag and Film Height for Vertical Annular Flow*. AIChE J. 31, 895–902.

Azzopardi, B. J. (1985): *Drop-Sizes in Annular Two-Phase Flow*. Exp. Fluids 3, 53-59.

Barnea, D., Shoham, O., Taitel, Y., Dukler, A. E. (1985): *Gas Liquid Flow in Inclined Tubes: Flow-Pattern Transition for Upward Flow*. Chem. Eng. Sci. 40, 131.
Mills, P., J. (1985): *De Physique Letters.* 46: L601-309.

Vysniauskas, A. and Bishnoi, P. R. (1985): *Kinetics of Ethane Hydrate Formation*. Chem. Eng. Sci. 1985; 40: 299-303.

Oliemans, R. V. A., Pots, B. F. M., Trompe, N. (1986): *Modeling of Annular Dispersed Two-Phase Flow in Vertical Pipes.* Intl. J. Multi-phase Flow 12, No.5, 711.

Andritsos, N., Hanratty, T. J. (1987): *Influence of Interfacial Waves in Stratified Gas-Liquid Flow.* AIChE J., 33, 444-454.

Chancey, D. G. (1987): *Measuring, Sampling, and Testing Crude Oil.* Petroleum Engineering Handbook. Society of Petroleum Engineers.

Englezos, P., Kalogerakis, N., Dholabhai, P. D., Bishnoi, P. R. (1987): *Kinetics of Gas Hydrate Formation from Mixtures of Methane and Ethane.* Chem. Eng. Sci. 42(11): 2659-2666

Pedersen, K.S. and Fredenslund, A. (1987): *An Improved Corresponding States Model for Prediction of Oil and Gas Viscosities and Thermal Conductivities.* Chem. Eng. Sci., 42, 182-186, (1987).

Kim, H. C., Bishnoi, P. R., Heidemann, R. A., Rizvi, S. S. H. (1987): *Kinetics of Methane Hydrate Decomposition.* Chem. Eng. Sci. 1987; 42 (7): 1645-1653.

Rezkallah, K. S., Sims, G. E. (1987): *An Examination of Correlations of Mean Heat Transfer Ceoefficients in Two-Phase and Two-Component Flow in Vertical Tubes.* AIChE Symposium Series 83, 109.

Shinogaya, T., Shinohara, T., Takemoto, M. (1987): *Erosion of metals in high speed mist flow evaluation of velocity by acoustic emission system.* International Congress on Metallic Corrosion,. Vol IV: Sessions 14-19, Madras, India, 7-11 Nov.

Smith, P. R., Van Laan, T. J. (1987): *Piping and Pipe Support Systems, Design and Engineering.* McGraw Hill. **(Book)**

Lahey Jr. R. T., Drew D. A. (1988): *Three Dimensional Time and Volume Averaged Conservation Equations of Two-Phase Flow.* Advances in Nuclear Science Technology, 20, 1-69.

Andreussi, P., Bendiksen, K. (1989): *An investigation of void fraction in liquid slugs for horizontal and inclined gas–liquid pipe flow.* Int. J. Multi-phase Flow 15, 937–946.

Angelson, S., Kvernvold, O., Linglem, M. and Oslen, S. (1989): *Long Distance Transport of Unprocessed Hydrocarbon: Sand Settling in Multi-phase Flow-lines.* Proc. 4th Int. Conf. on Multi-phase Flow, Paper D2, BHRA, Nice, 1989. France.

Arirachakaran S., Oglesby K. D., Malinowsky M. S., Shoham O., Brill J. P. (1989): *An Analysis of Oil/Water Flow Phenomena in Horizontal Pipes*. SPE Paper 18836, SPE Production Operations Symposium, pp. 155-167, Oklahoma, March 13-14.

Brauner, N., Moalem Maron, D. (1989): *Two-Phase Liquid-Liquid Stratified Flow*. PCH Physico Chemica, Hydrodynamics 11(4):487-506.

Ishii, M., Mishima, K. (1989): *Droplet Entrainment Correlation in Annular Two-Phase Flow.* Intl. J. Heat Mass Transfer, 32, No. 10, 1835.

Kuznecov, Y.N. (1989): *Heat Transfer in Problems related to Nuclear Reactor Safety.* Energoatomizdat, Moscow. (In Russian).

Jepson, D. M., Azzopardi, B. J., Whalley, P. B. (1989): *The Effect of Gas Properties on Drops in Annular Flow.* Journal of Multi-phase Flow 15 327-339.

Pedersen, K. S., Fredenslund, Aa., Thomassen, P. (1989): *Properties of Oils and Natural Gases.* Gulf Publishing Inc., Houston.

Scott, S. L., Shoham, O., Brill, J. P. (1989): *Prediction of Slug Length in Horizontal Large-Diameter Pipes*. SPEPE Aug., 335.

Burke, N. E., Hobbs, R. E., Kashou, S. (1990): *Measurement and Modeling of Asphaltene Precipitation*. JPT, Nov.

Hewitt , G. F., Govan, A. H. (1990): *Phenomenological modeling of non-equilibrium flows with phase change*. Int. J. Heat Mass Transfer 33, 229–242.

Mao, Z. S., and Dukler, A. E. (1990): *The Motion of Taylor-bubbles in Vertical Tubes. A Numerical Simulation for the Shape and Rise Velocity of Taylor-bubbles in Stagnant and Flowing Liquid*. J. Computational Physics, 91, 132-160.

McCain, W. D. (1990): *Petroleum Fluids*. PennWell Publishing Company. **(Book)**

Nessyahu, H., Tadmor, E. (1990): *Non-oscillatory Central Differencing for Hyperbolic Conservation Laws*, Journal of Comput. Phys. 87, 408.

Lotz, U. (1990): *Velocity Effects in Flow Induced Corrosion*. Proceedings of Symposium on Flow-Induced Corrosion; NACE, Houston, USA.

Sarica, C., Shoham, O., Brill, J. P. (1990): *A New Approach for Finger Slug Catcher Design*. Offshore Technology Conference, Houstojn, May.

Taital, Y., Barnea, D. (1990): *Two-Phase Slug Flow*. Advances in Heat Transfer, Vol. 20,Academic Press Inc., San Diego, CA, 83-132.

Ambrosini, W., Andreussi, P., Azzopardi, B. J. (1991): *A physically based correlation for drop size in annular flow*. Int. J. Multi-phase Flow 17, 497–507.

Bendiksen, K. H., Malnes, D., Moe, R., Nuland, S. (1991): *The Dynamic Two-Fluid Model OLGA: Theory and Application*. SPE Production Engineering, 6, 171-80.

de Waard, C., Lotz, U., and Milliams, D. E. (1991): *Predictive Model for CO2 Corrosion Engineering in Wet Natural Gas Pipelines*. Corrosion, 47, 750.

Nigmatulin, R. I. (1991): *Dynamics of Multi-phase*. Media, Hemisphere, New York.

Nydal, O.J., Andreussi, P. (1991): *Gas entrainment in a long liquid slug advancing in a near horizontal pipe*. Int. J. Multi-phase Flow 17, 179–189.

Schiller, R. E., and P. E. Herbich (1991): *Sediment transport in pipes*. Handbook of Dredging, Edited by P. E. Herbich. New York: McGraw-Hill.

Schramm, L. L. (1992): *Emulsions Fundamentals and Applications in the Petroleum Industry. Advances in Applications in the Petroleum Industry, Advances in Chemistry.* Series 231, American Chemical Society.

Andreussi, P., Bendiksen, K., Nydal, O. J. (1993): *Void Distribution in Slug Flow.* J. of Multi-phase Flow 19, 817-828.

Averick, B. M., More, J. J., Bischof, C. H., Carle, A., Griewank, A. (1993): *Computing Large-Sparse Jacobian Matrices Using Automatic Differentiation.* Center for Research on Parallell Computing, Rice University, Houston. CRPC-TR93362.

de Waard, C., and Lotz, U. (1993): *Prediction of CO2 Corrosion of Carbon Steel.* Corrosion, paper No. 69, NACE International.

Mahaffy, J. H. (1993): *Numerics of Codes: Stability, Diffusion and Convergence.* Nucl. Eng. Dec. 1945:131-145.

Oudeman, P. (1993): *Sand Transport and Deposition in Horizontal Multi-phase Trunklines of Sub-sea Satellite Developments*. SPE 25142.

Svedeman, S. J., Arnold, K. E. (1993): *Criteria for sizing multi-phase flow lines for erosive/corrosive service.* SPE 26569, 68th Annual Technical Conference of the Society of Petroleum Engineers, Houston, Texas, 3-6 Oct.

Colella, P., Puckett, E. G. (1994): *Modern Numerical Methods for Fluid Flow.* University of California, Berkeley.

Pauchon C., Dhulesia H., Binh Cirlot G., and Fabre J., (1994): *TACITE: A Transient Tool for Multi-phase Pipeline and Well Simulation*, SPE 28545, SPE Annual Technical Conference, New Orleans, LA, USA.

Zheng, G., Brill, J., Taitel, Y. (1994): *Slug Flow Behavior in a Hilly Terrain Pipeline.* Int. J. Multi-phase Flow, Vol. 20, No.1, pp. 63-79.

Dayalan, E., Vani, G., Shadley, J. R., Shirazi, S. A., and Rybicki, E. F. (1995): *Modeling CO2 Corrosion of Carbon Steels.* Corrosion, paper No. 118, NACE International.

De Henau V. and Raithby G.D. (1995): *A transient two-fluid model for the simulation of slug flow in pipelines, 1-Theory.* Int. J. Multi-phase Flow, 21, 335–349.

de Waard, C., Lotz, U., and Dugstad, A. (1995): *Influence of Liquid Flow Velocity on CO2 corrosion: A Semi-empirical Model.* Corrosion, Paper No.128, NACE International.

Frisch, U. (1995): *Turbulence. The Legacy of A. N. Kolmogorov.* Cambridge University Press.

Manolis, I.G. (1995): *High Pressure Gas–Liquid Slug Flow.* Imperial College, London, UK. **(PhD Thesis)**

Nesic, N., Wilhelmsen, W., Skjerve, S., Hesjevik, S. M. (1995): *Testing of Inhibitors for CO_2 Corrosion using the Electrochemical techniques.* Proceedings of the 8th European Symposium on Corrosion Inhibitors, Ann. Univ. Ferrara, N. S., Sez. V, Suppl. N. 10.

Pots, B. F. M. (1995): *Mechanistic Models for the Prediction of CO2 Corrosion Rates under Multi-phase Flow Conditions.* Corrosion, paper No. 137, NACE International, 1995.

Thomas, J. W. (1995): *Numerical Partial Differential Equations.* Springer, Berlin. **(Book)**

Tomiyama, A., Kataoka, I., Fukuda, T., Sakaguchi, T. (1995): *Drag Coefficient of Bubbles. 2nd Report, Drag Coefficient for a Swarm of Bubbles and its Applicability to Transient Flow.* Trans. Jpn. Soc. Mech. Eng. B, 46–53.

Adams, C.D., Garber, J.D. Singh R.K. (1996): *Computer Modeling to Predict Corrosion Rates in Gas Condensate Wells Containing CO2.* Corrosion paper No: 31, NACE International.

Barnea D., & Taitel Y., (1996): *Stratified three-phase flow in pipes – Stability and transition.* Chemical Engineering Communication, Vols. 141-142, 443-460.

Bendiksen, K. H., Malnes, D., Nydal, O. J. (1996): *On the Modeling of Slug Flow.* Chem. eng. com. 141: 71-102.

Chanson, H. (1996): *Air Bubble Entrainment in Free-surface Turbulent Shear Flow.* Academic Press.

Dennis, J. E., R. B. Schnabel, R. B. (1996): *Numerical Methods for Unconstrained Optimization and Nonlinear Equations.* SIAM, Philadelphia, PA.

Gunaltun, Y. M. (1996): *Combine Research and Field Data for Corrosion Rate Prediction.* Corrosion, paper No. 27, NACE International.

Nigmatulin, R. I. , Nigmatulin, B. I., Khodzhaev, Y. D., Kroshilin, V. E. (1996): *Entrainment and deposition rates in a dispersed film flow.* Int. J. Multi-phase Flow 22, 19–30.

Nydal, O. J., Banerjee, S. (1996): *Dynamic slug tracking simulations for gas-liquid flow in pipelines.* Chem. Eng. Commun. 141—142, 13—39.

Shampine, L. F., Hosea, M.E. (1996): *Analysis and implementation of TR-BDF2.* Applied Numerical Mathematics 20, 21-37.

Viviand H. (1996): *Modèle simplifié d'écoulement dans les conduites pétrolières.* Technical Report RSY, 43 069 02, Principia, France.

Patault S., Tran, Q.H. (1996): *Modèle et schéma numérique du code TACITE-NPW.* Technical Report 42415, Institut Français du Pétrole, France.

Azzopardi, B.J. (1997): *Drops in annular two-phase flow*. Int. J. Multi-phase Flow 23 (Suppl.), 1–53.

Clarke, A., Issa, R. I. (1997): *Numerical Model of Slug Flow in Vertical Tubes*. Computers & Fluids, 26 (4), 395-415.

Crowe. C.T. (1997): *Multi-phase Flows with Droplets and Particles*. CRC. **(Book)**

Gillies, R. G., Mckibben, M. J. and Shook, C. (1997): *Pipeline flow of gas, liquid and sand mixture at low velocity*. J. Canadian. Petroleum Technology, 36, 36-42.

Hanratty, T. J., Dykhno, L.A. (1997): *Physical Issues in Analyzing Gas-Liquid Annular Flows*. Proceedings of the 4th World Conference on Experimental Heat Transfer, Fluid Mechanics and Thermodynamics. Brussels, vol. 2.

Jangama, V. R. and Srinivasan, S. (1997): *A Computer Model for Prediction of Corrosion of Carbon Steels.* Corrosion paper No. 318, NACE International.

Jepson, W. P., Stitzel, S., Kang, C., and Gopal, M. (1997): *Model for Sweet Corrosion in Horizontal Multi-phase Slug Flow.* Corrosion, paper No. 11, NACE International.

Kawaji, M., DeJesus, J. M., Tudose, G. (1997): *Investigation of Flow Structures in Vertical Slug Flow*. Nuclear Enginering and Design," 175, 37-48.

Spedding, P.L., Hand, N.P. (1997): *Prediction in stratified gas–liquid co-current flow in horizontal pipelines.* Int. J. Heat Mass Transfer 40, 1923–1935.

Trallero, J. L., Sarica, C., Brill J. P. (1997): *A Study of Oil/Water Flow Patterns in Horizontal Pipes*. SPE Production & Facilities, August.

Valle A., Utvik O. H. (1997): *Pressure Drop, Flow Pattern and Slip for Two-Phase Crude Oil/Water Flow: Experiments and Model Predictions*. International Symposium on Liquid-Liquid Two-Phase Flow and Transport Phenomena, ICHMT, Antalya, Turkey.

Zhang, R., Gopal, M., and Jepson, W. P. (1997): *Development of a Mechanistic Model for Predicting Corrosion Rate in Multi-phase Oil/Water Flows,* Corrosion paper No 601, NACE International.

Cortes J, Debussche A, Toumi I. (1998): *A Density Perturbation Method to study the Eigenstructure of Two-Phase Flow Equation Systems.* J Comput Phys 1998;147:463–84.

Danesh, A. (1998): *PVT and Phase Behaviour of Petroleum Reservoir Fluids.* Elsevier Science & Technology Books. (Book)

Fossa, M., Pisoni, C., Tagliafico, L. A. (1998): *Experimental and theoretical results on upward annular flows in thermal non-equilibrium*. Exp. Therm. Fluid Sci. 16, 220–229.

Fukano, T., Furukawa, T. (1998): *Prediction of the effects of liquid viscosity on interfacial shear stress and frictional pressure drop in vertical upward gas–liquid annular flow*. Int. J. Multi-phase Flow 24, 587–603.

Lopez de Bertodano, M.A., Assad, A. (1998): *Entrainment rate of droplets in the ripple-annular regime for small vertical ducts*. Nucl. Sci. Eng. 129, 72–80.

Masella, J. M., Tran, Q. H., Ferre, D., Pauchon, P. (1998): *Transient Simulation of Two-Phase Flows in Pipes.* Institut Français du Pétrole, France.

Nyborg, R., Nordsveen, M., Stangeland, A. (1998): *Kjeller Sweet Corrosion V, Final Report.* Institute for Energy Technology, No. 75.

High, M. S., Wagner, J., and Natarajan, S. (2000): *Mechanistic Modeling of Mass Transfer in the Laminar Sublayer in Downhole Systems.* Corrosion, paper No. 62, NACE International.

Ouyang, L.-B. (1998): *Single Phase and Multi-phase Fluid Flow in Horizontal Wells.* Stanford University, Stanford, CA. **(PhD Thesis)**

Salama, M. M. (1998): An *Alternative to API 14E Erosional Velocity Limits for Sand Laden Fuids.* OTC 8898, OTC Conference, Houston, May 4 – 7 1998, pp721 –733.

Sloan, E. D (1998): *Clathrate Hydrates of Natural Gases*. 2nd edition, NY: Marcel Dekker.

Zaichik, L. I. (1998): *Estimation of time between particle collisions in turbulent flow*. High Temperature, vol 36 no 3 (translation from Russian).

Zaichik, L. I. (1998): *Transport and Deposition of Inertial Particles in Trubulent Pipe Flow*. ERCOFTAC Bull. 36, 16-19.

Zaichik, L. I., Nigmatulin, B. I., Alipchenkov, V. M. (1998): *Droplet Deposition and Film Atomization in Gas-Liquid Annular Flow*. Third International Conference on Multi-phase Flow, Lyon, France.

Biberg, D (1999): *An Explicit Approximation for The Wetted Angle in Two-Phase Stratified Pipe Flow.* The Canadian Journal of Chemical Engineering, vol. 77, pp 1221-1224

Brill, J. P., Mukherjee, H. (1999): *Multi-phase Flow in Wells. Henry L. Doherty Memorial Fund of AIME, Society of Petroleum Engineers.* **(Book)**

Kim, D., Ghajar, A.J., Dougherty, R.L., and Ryali, V.K. (1999): *Comparison of 20 Two-Phase Heat Transfer Correlations with Seven Sets of Experimental Data, Including Flow Pattern and Tube Inclination Effects.* Heat Transfer Engineering, vol. 20, no. 1, pp. 15–40.

Levy, S. (1999): *Two-Phase Flow in Complex Systems.* John Wiley & Sons, Inc. **(Book)**

Soleimani A. (1999): *Phase Distribution and Associated Phenomena in Oil-Water Flows in Horizontal Tubes*. Imperial College, University of London. **(PhD Thesis)**

Toro, E. F. (1999): *Riemann Solvers and Numerical Methods for Fluid Dynamics. A practical Introduction.* Springer Verlag. **(Book)**

Zaichik, L. I., Alipchenkov, V. M. (1999): *Interaction time of turbulent eddies and colliding particles*. Thermophys. Aeromech. 6, 493–501.

Zaichik, L. I., Nigmatulin, B. I., Alipchenkov, V. M. (1999): *Droplet entrainment in vertical gas–liquid annular flow.* Proceedings of the 2nd International Symposium on Two- Phase Flow Modelling and Experimentation, Rome, vol. 2.

Baker Jardine (2000): *PIPESIM 2000 User Guide.*

Ahmed, T. (2000): *Reservoir Engineering Handbook*. Gulf Professional Publishing. **(Book)**

Azzopardi, B. J., Zaidi, S. H. (2000): *Determination of Entrained Fraction in Vertical Annular Gas/Liquid Flow.* Trans. of ASME Journal of Fluids Eng., Vol. 122, March 2000.

Bouchut F, Brenier Y, Cortes J, Ripoll J. F. (2000): *A hierarchy of models for two-phase flows.* J Nonlinear Science 10:639–60.

Fore, L. B., Beus, S. G., Bauer, R. C. (2000): *Interfacial friction in gas–liquid annular flow: analogies to full and transition roughness*. Int. J. Multi-phase Flow 26, 1755–1769.

Gunaltun, Y. M., Larrey, D., (2000): *Correlation of Cases of Top Of Line Corrosion with Calculated Water Condensation Rates.* Corrosion paper No. 71, NACE International.

High, M. S., Wagner, J., and Natarajan, S. (2000): *Mechanistic Modeling of Mass Transfer in the Laminar Sublayer in Downhole Systems.* Corrosion, paper No. 62, NACE International.

Kurganov, A., Tadmor, E. (2000): *New High-Resolution Central Schemes for Nonlinear Conservation Laws and Convection-Diffusion Equations*, Journal of Comp. Phys., 160, 214–282.

Matthews, P. N., Notz, P. K., Widender, M. W., Prukop G. (2000): *Flow Loop Experiments Determine Hydrate Plugging Tendencies in the Field*. Annals of New York Academy of Science. 330-338

Nyborg, R., Anderson, P., and Nordsveen, M. (2000): *Implementation of CO2 Corrosion Models in a Three-Phase Fluid Flow Model.* Corrosion paper No. 48 (Houston, TX: NACE International, 2000)

Revie, R. W. (2000): *UHLIG's Corrosion Handbook.* John Wiley & Sons. **(Book)**

Salama, M. M. (2000): *Sand Production Management*. Journal of Energy Resources, Vol. 122, 29-33, March.

Yeo, L.Y., Mater, O.K., Perez de Ortiz, E.S., Hewitt, G.F. (2000): *Phase inversion and associated phenomena.* Multi-phase Science & Technology, 12:51-116.

Zabaras, G. J. (2000): *Prediction of Slug Frequency for Gas-Liquid Flows.* SPEJ, Sept, 252.

Groffe, D., Groffe, P., Takhar, S., Andersen, S.I., Stenby, E.H., Lindeloff, N., Lundgren, M. (2001): *A Wax Inhibition Solution to Problematic Fields: A Chemical Remediation Process.* Petroleum Science and Technology, Vol. 19, Nos. 1 & 2.

Hedges, B., Paisley, D., Wollam, R. (2001): *The corrosion inhibitor availability model.* NACE.

Hernandez, S., Duplat, S., Vera, J. Baron, E. (2001): *A Statistical Approach for analyzing The Inhibiting Effect of Different Types of Crude Oil in CO2 Corrosion of Carbon Steel.* Corrosion No. 293, NACE International.

King, M. J. J., Fairhurst, C. P. and Hill, T. J. (2001): *Solids transport in multi-phase flows: applications to high viscosity systems*. Journal of Energy Resources, 123, 200-204, Sept.

Marchino, P. (2001): *Best practice in sand production prediction.* Sand control & Management, London, 15- 16 Oct.

Mendez, C., Duplat, S., Hernandez, S., Vera, J. (2001): *On the Mechanism of Corrosion Inhibition by Crude Oils.* Corrosion paper no. 44, NACE International.

Mork, M., Gudmundsson, J. S. (2001): *Rate of Hydrate Formation in Subsea Pipelines.* 12th Int. Oil Field Chemistry Symposium, Geilo, Norway.

Rosario, F. F., Bezerra, M. C. (2001): *Scale Potential of a DeepWater Field –Water Characterisation and Scaling Assessment.* SPE 3rd International Symposium on Oilfield Scale, Aberdeen.

Stevenson, P. (2001): *Particle transport in pipes by two-phase flows*. University of Cambridge, Cambridge, United Kingdom. **(PhD Thesis)**

Stosic, Z. V., Stevanovic, V. D. (2001): *A Comparative Analysis of Bubbly Flow Void Fraction based on Different Approaches for Interfacial Drag Force.* 5th World Conference on Experimental Heat Transfer, Fluid Mechanics and Thermodynamics, Thessaloniki, Greece, Sept. 24-28.

Zaichik, L. I., Alipchenkov, V. M. (2001): *A statistical model for transport and deposition of high-inertia colliding particles in turbulent flow*. Int. J. Heat Fluid Flow 22, 365– 371.

Abulnaga, B. (2002): *Slurry Systems Handbook.* McGraw Hill. **(Book)**

Anglart, H., Podowski, M. Z. (2002): *Fluid Mechanics of Taylor-bubbles and Slug Flows in Vertical Channels.* Nuclear Science and Engineering, 140, 165-171.

Brauner, N., Ullmann, A. (2002): *Modeling of Phase Inversion Phenomenon in Two-Phase Pipe Flow*. International Journal Multi-phase Flow 28, 1177-1204.

Camargo, R., Palermo, T. (2002): *Flow Properties of Hydrate Suspensions in Asphaltenic Crude Oil*. Proc. 4th Intnl. Hydrates Conf., Yokohama. 880-885.

Cournil, M., Herri, J. M. (2002): *Asymptotic Modelling of Crystallization in Two Layers Systems. Application to Methane Hydrate Formation in Batch Reactor.* Proc. 4th Intnl. Hydrates Conf., Yokohama. 819-824

Hasan, A. R., Kabir C. S. (2002): *Fluid Flow and Heat Transfer in Wellbores*. Society of Petroleum Engineers. **(Book)**

Frankel, M. (1996, 2002): *Facility Piping Systems Handbook.* Second Edition, McGraw-Hill.

LeVeque, R. J. (2002): *Finite Volume Methods for Hyperbolic Problems.* Cambridge University Press. **(Book)**

Stevenson, P. and Thorpe, R. B. (2002): *Method calculates sand velocity, hold-up in flow-lines.* Oil and Gas Journal, 100 (30), 47-50.

Stevenson, P., Thorpe, R.B. and Davidson, J.F., (2002): *Incipient motion of a small particle in the viscous boundary-layer at a pipe wall.* Chemical Engineering Science, 57, 4505-4520.

Stevenson, P. and Thorpe, R.B., (2002): *The velocity of isolated particles along a pipe in smooth stratified gas – liquid flow.* AIChE. Journal, 48, 963-969.

Wang, H., Cai, J., Jepson, W. P. (2002): *CO_2 Corrosion Mechanistic Modelling and Prediction in Horizontal Slug Flow.* Corrosion, paper No. 02238, NACE International.

Bagchi, P., Balachandar, S. (2003): *Effect of Turbulence on Drag and Lift of a Particle*. Physics of Fluids, Vol. 15, No. 11.

Barton, N. A. (2003): *Erosion in Elbows in Hydrocarbon Production Systems: Review document.* TÜV NEL Limited, report 115.

Bonizzi, M., Issa, R. I. (2003): *A Model for simulating Gas Bubble Entrainment in Two-Phase Horizontal Slug Flow.* J. of Multi-phase Flow 29 1685-1717.

Bonizzi, M., Issa, R. I. (2003): *On the simulation of three-phase slug flow in nearly horizontal pipes using the multi-fluid model.* J. of Multi-phase Flow 29 1719-1747.

Brauner, N. (2003): *Liquid-Liquid Two-Phase Flow Systems.* School of Engineering, Tel-Aviv University, Israel.

Cai, J., Nesic, S., de Waard, C.. (2003): *Modelling of Water Wetting in Oil-Water Pipe Flow.* Corrosion, paper No. 663, NACE International.

CO-LaN Consortium (2003): *Documents 1.0 Documentation Set* (freely available from colan.org).

Daniels L. C., Guardino C., and Thompson C. P. (2003): *An Implicit Two-Phase Compressible Flow Solver For Pipelines.* Multi-phase Science and Technology, 21 (3), 335-349.

Gaard, S., Isaksen, O.T. (2003): *Experiments with Different Drag-Reducing Additives in Turbulent Flow in Dense Phase Gas Pipelines.* PSIG 03B3, Pipeline Simulation Interest Group.

Hernandez, S., Bruzal, J., Lopez-Linares, F., Luzon, J. (2003): *Isolation of Potential Corrosion Inhibiting Compounds in Crude Oils.* Corrosion paper No. 330, NACE International.

Imsland, L., Eikrem, G. O., Foss, B. (2003): *State Feedback Control of a Class of Positive Systems: Application to Gas Lift Control.* ECC 03, Cambridge, UK.

Imsland, L., Eikrem, G. O., Foss, B. (2003): *Stabilization of gas lifted oil wells without downhole measurements.* Adchem 2003.

Issa, R. I., and Kempf, M. H. W. (2003): *Simulation of Slug Flow in Horizontal and Nearly Horizontal Pipes with the Two-Fluid Model.* International Journal of Multi-phase Flow, 29, 69.

Kelley, C. T. (2003): *Solving Nonlinear Equations with Newton's Method.* Society for Industrial and Applied Mathematics.

Naterer, G. F. (2003): *Heat Transfer in Single and Multi-phase Systems.* CRC Press. **(Book)**

Nesic, S, Lee, A. (2003): *A Mechanistic Model for CO_2 Corrosion of Mild Steel in the presence of Protective Iron Carbonate Scales – Part O: Scale Growth Model.* Corrosion 59, 616.

Scott, S. L., Barrufet, M. A. (2003): *Worldwide Assessment of Industry Leak Detection Capabilities for Single & Multi-phase Pipelines.* Texas A&M University, Department of Petroleum Engineering.

Van der Vorst, H. A. (2003): *Iterative Krylov Methods for Large Linear Systems.* Cambridge University Press. **(Book)**

Vitse, F., Nesic, S., Gunaltun, Y., Larrey de Torreben, D., Dunchet-Suschau, P. (2003): *Mechanistic Model for the prediction of Top-Of-The-Line Corrosion Risk.* Corrosion No. 59, 1075.

Wang, K. S., Wu, C. H., Creek, J. F., Shuler, P. J., and Tang, Y. C. (2003): *Evaluation of Effects of Selected Wax Inhibitors on Paraffin Deposition.* Petroleum Science and Technology, Vol. 21, Nos. 3 & 4.

Worner, M. (2003): *A Compact Introduction to the Numerical Modeling of Multi-phase Flows.* Forschungszentrum Karlsruhe in der Helmholtz-Gemeinschaft, FZKA 6932.

Yang, S., Kleehammer, D. M., Huo, Z., Sloan, E. D., Miller, K. T. (2003): *Micromechanical Measurements of Hydrate Particle Attractive Forces.* Colorado School of Mines, USA.

Yuan, M., Williamson, D.A., Smith, J. K., Lopez, T. H. (2003): *Effective Control of Exotic Mineral Scales Under Harsh System Conditions.* SPE International Symposium on Oilfield Chemistry, Houston.

Zaichik, L. I., Alipchenkov, V. M. (2003): *Pair dispersion and preferential concentration of particles in isotropic turbulence.* Phys. Fluids 15, 1776–1787.

Zaichik, L. I., Simonin, O., Alipchenkov, V. M. (2003): *Two statistical models for predicting collision rates of inertial particles in homogeneous isotropic turbulence.* Phys. Fluids 15, 2995–3005.

Alipchenkov, V.M. , Nigmatulin, R.I., Soloviev, S.L., Stonik, O. G., Zaichi, L. I., Zeigarnik, Y. A., (2004): *A three-fluid model of two-phase dispersed-annular flow.* International J. of Heat and Mass Transfer 47, 5323–5338.

Eikrem, G. O., Imsland, L., Foss, B. (2004): *Stabilization of Gaslifted Wells based on State Estimation.* The International Federation of Automation Control (IFAC).

Ellul, I.R., Saether, G., Shippen, M.E. Goodreau, M.J. (2004): *The Modelling of Multi-phase Systems under Steady-State and Transient Conditions – A Tutorial.* Pipeline Simulation Interest Group PSIG 0403.

Knoll, D. A., Keyes, D. E. (2004): *Jacobian-free Newton–Krylov methods: a survey of approaches and applications.* J. of Computational Physics 193, 357–397.

Omgba-Essama, C. (2004): *Numerical Modeling of Transient Gas-Liquid Flows, Application to Stratified & Slug Flow Regimes.* Cranfield University, School of Engineering. **(PhD Thesis)**

Poling, B. E., Prausnitz, J. M. O'Connel, P. O. (2004): *The Properties of Gases and Liquids*. Fifth Edition Connell McGraw-Hill **(Book)**

Quayle, O. R. (1953): *The Parachors of Organic Compounds. An Interpretation and Catalogue.* Chem. Rev. 53: 439.

Sinquin, A., Palermo, T., Peysson, Y. (2004): *Rheological and Flow Properties of Gas Hydrate Suspensions.* Oil & Gas Science and Technology – Rev. IFP, Vol. 59 No. 1, pp. 41-57.

Shea, R., Eidsmoen, H., Nordsveen, M., Rasmussen, J. Xu, Z., Nossen, J. (2004): *Frequency Prediction Method Comparison.* BHRG Multi-phase Production Technology Proceedings, Bannf, Canada.

Society of Petroleum Engineers (2004): *Offshore Multi-phase Production Operations – 1.* SPE Reprint series No. 58.

Brennen, C. E. (2005): *Fundamentals of Multi-phase Flow.* Cambridge University Press. **(Book)**

Corneliussen, S., Couput, J. P, Dahl, E., Dykesteen, E., Frøysa, K. E., Malde, E., Moestue, H., Moksnes, P. O., Scheers, L., Tunheim, H. (2005): *Handbook of Multi-phase Flow Metering.* Norwegian Society for Oil and Gas Measurement. **(Book)**

Evje, S., Flåtten, T. (2005): *A family of Central Schemes for Nonlinear Hyperbolic Conservation Laws.* RF-Rogaland Research, Stavanger, Norway, and Centre of Mathematics for Applications, Oslo, Norway.

Ghajar, A. J. (2005): *Non-Boiling Heat Transfer in Gas-Liquid Flow in Pipes – a tutorial.* J. of the Braz. Soc. Of Mech. Sci. & Eng. Vol IIVII, No. 1 Jan.-March.

Godhavn, J. M., Strand, S., Skofteland, G. (2005): *Increased Oil Production by Advanced Control ff Receiving Facilities*. The International Federation of Automation Control (IFAC).

Guo, B., Song, S., Chacko, J., Ghalambor, A. (2005): *Offshore Pipelines*. Elsevier. **(Book)**

Han, H. (2005): *A Study of Entrainment in Two-phase Upward Cocurrent Annular Flow in A Vertical Tube.* University of Saskatchewan, Department of Mechanical Engineering. **(PhD Theses, part of)**

Invensys/Simsci-Esscor (2005): *PIPEPHASE 9.0 Keyword Manual.*

Invensys/Simsci-Esscor (2005): **T***acite 4.1 User's Guide.*

Kolev, N. I. (2005): *Multi-phase Flow Dynamics 1. Fundamentals*. Springer, 2002, 2005. **(Book)**

Kolev, N. I. (2005): *Multi-phase Flow Dynamics 2. Thermal and Mechanical Interactions*. Springer, 2002, 2005. **(Book)**

Kolev, N. I. (2005): *Multi-phase Flow Dynamics 3. Turbulence, Gas Absorption and Release, Diesel Fuel Properties*. Springer, 2002, 2005, 2007. **(Book)**

Liu, H. (2005): *Pipeline Engineering.* Lewis Publishers. **(Book)**

Mandil, C. (2005): *Oil & Gas Technologies for the Energy Markets of the Future. Resources to Reserves.* International Energy Agancy. OECD/IEA.

Norwegian Technology Standards Institution (1998, 2005): *CO2 Corrosion Rate Calculation Model.* NORSOK Standard No. M-506, available at www.standard.no/petroleum (free to download at the time of this writing).

Rodrigues, O. M. H., Oliemans, R. V. A. (2005): *Experimental Study on Oil-Water Flow in Horizontal and Slightly Inclines Pipes.* J. Multi-phase Flow 32 (2006) 323-343.

Sloan, E. D. (2005): *A Changing Hydrate Paradigm – From Apprehension to Avoidance to Risk Management.* Fluid Multi-phase Equilibria 228-229, 67-74.

Turner, D., Yang, S., Boxall, J., Kleehamer, D., Koh, C., Miller, K., Slaon, E. D., Xu, Z., Matthews, P., Talley, L. D. (2005): *Development of a Hydrate Kinetic Model and its Incormporation Into the OLGA2000 Transient Mulit-Phase Flow Simulator.*5th International Conf. on Gas Hydrates, Trondheim, Norway, p.1231-1240.

Wegmann, A. (2005): *Multi-phase Flows in Small Scale Pipes.* Swiss Federal Institute of Technology Zurich. **(PhD Thesis)**

Crowe, C.T. (2006): *Multi-phase Flow Handbook.* CRC. **(Book)**

Erian, F. F., Pease, L. F. (2006): *Three-phase Flow in a Vertical Pipe.* Int. J. of Multi-phase Flow 33, 498-509.

Ghajar, A., Kim, J., Tang, C. (2006): *Two-Phase Flow Heat Transfer Measurement and Correlation for the Entire Flow Map in Horizontal Pipes.* School of Mech. & Aerospace Eng., Oklahoma State Univ.

Hemptinne, J. C., Behar, E. (2006): *Thermodynamic Modeling of Petroleum Fluids.* Oil & Gas Science and Technology – Rev. IFP, Vol. 61 (2006), No. 3, pp. 303-317

Ishii, M., Hibiki, T. (2006): *Thermo-Fluid Dynamics of Two-Phase Flow.* Springer. **(Book)**

Issa, R. I., Bonizzi, M., Barbeau, S. (2006): *Improved Closure Models for Gas Entrainment and Interfacial Shear for Slug Flow Modelling in Horizontal Pipes.* Int. J. of Multi-phase Flow 32, 1287-1293.

Jassim, E. W., Newell, T. A., Chato, J. C. (2006): *Probabilistic Flow Regime Map Modelling of Two-Phase Flow.* University of Illinois at Urbana-Champaign.

Kassab, S. Z., Kandil, H. A., Warda, H. A., Ahmed, W. H. (2006): *Experimental and Analytical Investigations of Airlift Pumps Operating in Three-Phase Flow.* Chemical Eng. J. 131, 273-281.

Moran, M.J., Shapiro, H.N. (2006): *Fundamentals of Engineering Thermodynamics*, John Wiley & Sons Ltd.

Shoham, O. (2006): *Mechanistic Modeling of Gas-Liquid Two-Phase Flow in Pipes.* Society of Petroleum Engineers. **(Book)**

Tordal, A. (2006): *Pigging of Pipelines with High Wax Content*. Pigging Products & Services Association, Aberdeen, UK.

Wilson, K. C., Addie, G. R., Sellgren, A., Clift, R. (2006): *Slurry Transport using Centrifugal Pumps.* Springer. **(Book)**

Zhang, H. Q., Sarica, C. (2006): *Unified Modeling of Gas/Oil/Water-Pipe Flow – Basic Approaches and Preliminary Validation.* 2005 SPE Annual Technical Conference & Exhibition, Dallas. Revised 2006.

Aarvik, A., Olsen, I., Vannes, K., Havre, K., Krogh, E., C. (2007): *Design and development of hte Ormen Lange flow assurance simulator*. 13th International Conference on Multi-phase Production technology, p.47-64.

Danielson, T. J. (2007): *Sand transport in multi-phase pipelines.* Proceedings of the Offshore Technology Conference, Houston, USA, OTC 18691.

Geracia, G., Azzopardia, B. J., van Maanen, H.R.E., (2007): *Effect of inclination on circumferential film thickness variation in annular gas/liquid flow.* Chemical Engineering Science 62, 3032 – 3042.

Kjolaas, J. (2007): *Plug Propagation in Multi-phase Pipelines.* NTNU Theses 2007:140. **(PhD Thesis)**

Lapiga, E. J., Sinaiski, E. G. (2007): *Separation of Multi-phase, Multi-component Systems.* Wiley-VCH. **(Book)**

Neotechnology Consultants Ltd. (2007): *PIPEFLO7 Help and FORGAS / FOROIL User Manual.*

Nesic, S. (2007): *Key Issues related to Modelling of Internal Corrosion of Oil and Gas Pipelines.* Corrosions Science 49, 4308-4338.

Peker, S. M., Helvaci, S. S. (2007): *Liquid-solid Two Phase Flow.* Elsevier. **(Book)**

Pourafshary, P. (2007): *A Coupled Wellbore/Reservoir Simulator to Model Multi-phase Flow and Temperature Distribution.* The University of Texas at Austin. **(PhD Thesis)**

Prosperetti, A., Tryggvason, G. (2007): Computational *Methods for Multi-phase Flow.* Cambridge University Press. **(Book)**

Quarteroni, A., Sacco, R., Saleri, F. (2007): *Numerical Mathematics*. Springer. **(Book)**

Ramberg, R. M. (2007): *Multi-phase Pump Performance Modelling.* NTNU Theses 2007:117. **(PhD Thesis)**

Renault, F. (2007): *A Lagrangian slug capturing scheme for gas-liquid flows in pipes.* Norwegian University of Science and Technology Faculty of Engineering Science and Technology Department of Energy and Process Engineering. **(PhD Thesis)**

Shaikh, A., Al-Dahhan, M. H. (2007): *A Review on Flow Regime Transition in Bubble Columns.* Internation Jounrnal of Chemical Reactor Engineering, Vol. 5, Review R1.

Speich, J. G. (2007): *Natural Gas: A Basic Handbook.* Gulf Publishing Company. **(Book)**

Woldesemayat, M. A., Ghajar, A. J. (2007): *Comparison of void fraction correlations for different flow patterns in horizontal and upward inclined pipes.* International Journal of Multi-phase Flow 33, 347–370.

Yang, Z. L., Ladam, Y., Laux, H., Danielson, T. J., Goldszal, A., Martins, A. L. (2007): *Simulation of Sand Transport in a Stratified Gas-Liquid Two-Phase Pipe Flow.* Proceedings of the BHR Multi-phase Production Technology Conference, Edinburgh, UK.

Zhong, W. (2007): *Entropy Stable Approximations of Nonlinear Conservation Laws and Related Fluid Equations.* Faculty of the Graduate School of the University of Maryland, College Park **(PhD Thesis)**

Bello, O. O. (2008): *Modelling Particel Transport in Gas-Oil-Sand Multi-phase Flows and its Applications to Production Operations.* Faculty of Energy and Economics Sciences, Clausthal University of Technology. **(PhD Thesis)**

Benallal, A., maurel, P., Agassant, J. F., Darbouret, M., Avril, G., Peuriere, E. (2008): *Wax Deposition in Pipelines: Flow-Loop Experiments and Investigations on a Novel Approach.* Society of Petroleum Engineers 115293.

Boxall, J., Nicholas, J., Koh, C., Sloan, E. D., Turner, D., Talley, L. (2008): *Hydrate Blockage Potential in an Oil-Dominated System studied using a Four Inch Flow Loop.* Proc. 6th International Conf. on Gas Hydrates ICGH 2008, Vancouver, Cananda.

Boxall, J., Davis, S., Sloan, E. D., Koh, C. (2008): *Predicting When and Where Hydrate Plugs Form in Oil-Dominated Flow-lines.* Offshore Technology Conf. Houston, USA.

Bratland, O. (2008): *Update on commercially available flow assurance software tools: What they can and cannot do and how reliable they are.* 4th Asian Pipeline Conference & Exposition 2008, Kuala Lumpur.

Cheng, N. S. (2008): *Comparison of Formulas for Drag Coefficient and Settling Velocity of Spherical Particles.* School of Civil and Environmental Engineering, Nanyang Technological University.

Correra, S., Fasanoy, AFusiy, L., Primicerioy, M. (2008): *Modelling Wax Diffusion in Crude Oils: The Cold Finger Device.* Journal of Petroleum Technology.

Datta, A. (2008): *Process Engineering and Design Using Visual Basic.* CRC Press. **(Book)**

Dharmaraja, S., Wang, Y., and Strang, G. (2008): *Optimal Stability for Trapezoidal-Backward Dierence Split-Steps.* Department of Mathematics, MIT, Cambridge, USA.

DOE Award No. DE-FC26-03NT15403 (2008): *Development of Next Generation Multi-phase Pipe Flow Prediction Tools.* Final Report. Office of Fossil Energy, US Deperatment of Energy.

Edmonds, B., Moorwood, T., Szczepanski, R., Zhang, X. (2008): *Simulating Wax Deposition in Pipelines for Flow Assurance.* Energy & Fuels, 22, 729–741.

Haoues, L., Olenkhnovitch, A., Teyssedou, A. (2008): *Numerical Study of the Influence of the Internal Structure of a Horizontal Bubbly Flow on the Average Void Fraction.* Nuclear Engineering and Design 239, 147-157.

Jacobsen, H. A. (2008): *Chemical Reactor Modeling, Multi-phase Reactive Flows.* Springer. **(Book)**

Sawant, P., Sihii, M., Mori, M. (2008): *Droplet Entrainment Correlation in Vertical Upward Co-current Annular Two-Phase Flow.* Nuclear Engineering and Design, 238 1342-1352.

Zaichik, L. I., Alipchenkov, V. M., Sinaiski, E. G. (2008): *Particles in Turbulent Flows.* Wiley-VCH. **(Book)**

Al-Safran, E. (2009): *Investigation and Prediction of Slug Frequency in Gas/Liquid Horizontal Pipe Flow*. To be published in J. if Petroleum Sci. and Eng.

Aspenes, G., Hoyland, S., Barth, T., Askvik, K. M. (2009): *The Influence of Petroleum Acids and Solid Surface Energy on Pipeline Wettability in relation to Hydrate Deposition.* J. of Colloid and Interface Science 333, 533-539.

Bratland, O (2009): *Pipe Flow 1, Single-phase Flow Assurance*. Available at drbratland.com.

Carroll, J. (2009): *Natural Gas Hydrates. A guide for Engineers.* Gulf Professional Publishing. **(Book)**

Lucas, G.P., Penagiotopulos, N. (2009): *Oil Volume Fraction and Velocity Profiles in Vertical, Bubbly Oil-In-Water Flows.* Flow Measurement and Instrumentation, 20, 127-135.

Piela, K., Delfos, R., Ooms, G., Westerweel, J., Oliemans, R. V. A. (2009): *Phase Inversion in the Mixing Zone between Water Flow and an Oil Flow through a Pipe.* J. Multi-phase Flow 35, 91-95.

Vargas, F. M., Gonzalez, D. L., Hirasaki, G. J., Chapaman, W. G. (2009): *Modeling Asphaltene Phase Behavior in Crude Oil Systems Using the Perturbed Chain Form of the Statistical Associating Fluid Theory (PC-SAFT) Equation of State.* Energy & Fuels, 23, 1140-1146.

Nomenclature

Latin letters

a	Constant in general linear equation, see equation 12.1.1	
a_s	Speed of sound	[m/s]
A	Cross-sectional area	[m²]
A	General square matrix	
b_a	Anodic Tafel slope	[V/decade]
b_b	Cathodic Tafel slope	[V/decade]
c_j	Concentration of species j	[kMol/m³]
c_v	Spesific heat at constant volume	[J/kg·K]
c_p	Spesific heat at constant pressure; concentration of reactants	[J/kg·K]; []
c_r	Concentration of products	[]
C_D	Drag coefficient	Dimensionless
C_{GR}	Hinze's particle response coefficient	Dimensionless
C_0	Factor defined in equation 5.3.12	Dimensionless
C_μ	Kolmogorov-Prandtl constant	Dimensionless
CR	Corrosion rate	[mm/year]
d	Inner pipe diameter	[m]
d_D	Droplet diameter	[m]
$d_{D\Delta v}^{*}$	Maximum stable droplet diameter	[m]
d_h	Hydraulic pipe diameter, as defined by equation 3.1.1	[m]
d_i	Inner annular diameter, as defined in figure 3.4.1	[m]
d_o	Outer annular diameter, as defined in figure 3.4.1	[m]
d_s	Sand particle diameter	[m]
D_j^{eff}	Effective diffusion coefficient of species j	[m²/s]
D_S	Diffusion coefficient	[m²/s]
D_W	Outer annular diameter, as defined in figure 3.4.1	[m²/s]
e_F	Maximum accepted error norm	Not defined
E	Volume-specific power	[W/m³]
E_s	Energy pr. unit mass	[J/kg]
E_0	Eötvös number	Dimensionless
E_{0B}	Bubble Eötvös number	Dimensionless
f	Darcy-Weisbach friction factor	Dimensionless
f_S	Slug frequency	[s⁻¹]
F_S	Shape factor defined by equation 10.3.3	Diemsnionless
F	Force; Volume-specific force, Primary variables derivative	[N]; [N/m³]

	vector	
Fr	Froude number	Dimensionless
g	Gravitational acceleration	[m/s^2]
G	Gravity parameter defined by equation 5.1.13; Sand grain weight	Dimensionless; [N]
h	Specific enthalpy	[J/kg]
h_L	Liquid height, as defined in figure 11.2.1	[m]
h_w	Wave height for waves on the liquid surface in stratified flow	[m]
H	Hurst exponent, in this book's context used to characterize surfaces	Dimensionless
i_a	Anodic current density	[A/m^2]
i_c	Total cathodic current density	[A/m^2]
i_{ct}	Transfer control current density	[A/m^2]
i_{lim}	Limiting current density	[A/m^2]
i_o	Exchange current density	[A/m^2]
J	Jacobi-matrix	
k_b	Backward reaction rate constant	Dimensionless
k_f	Correction parameter defined by equation 5.1.14; Forward reaction rate constant	Dimensionless
k_G ,k_L	Constants defined in equations 3.6.1 and 3.6.2; Turbulence energy (eq. 5.6.7)	[kg/(m^{2}s)]; [m^4/s^2]
k_s	Sand grain roughness, equivalent sand grain roughness	[m]
k_W	Constant characterizing the wax in equation 18.4.2	[kg·m^2/s^2]
K_{sp}	Solubility limit	Diemsnionless
l	Length, total pipe length unless specified otherwise	[m]
l_S	Slug length	[m]
l_T	Taylor-bubble length	[m]
m	Mass	[kg]
$\dot{m}$	Mass flow	[kg/s]
M	Molar mass	[kg/kMol]
$\dot{M}_B$	Shredding rate of dispersed bubbles at the slug tail	[kg/s]
n	Number of droplets	Dimensionless
N	Number of phases; number of equations	Dimensionless
Nu	Nusselt number	Dimensionless
N_x	Number of grid points or cells (ghost-cells not included)	Dimensionless
m_n	Friction factor used in Manning's formula	[m$^{1/3}$·s]
O	Wetted surface area, used in the definition of hydraulic diameter	[m^2]
p	Pressure	[Pa]
Pr	Prandtl number	Dimensionless

q	Volume-specific heat	[W/m³]
Q	Flow	[m³/s]
Q	Heat transfer rate	[W]
r	Inner pipe radius	[m]
R	Universal gas constant	[J/(K·mol)]
R_g	Characteristic gas constant for a particular ideal gas	[J/kg·K]
R_j	Source or sink of species *j* due to chemical reactions	[kMol/(m³s)]
R_{ki}	Volume-specific friction force from other phases on phase k	[N/m³]
R_{kW}	Volume-specific friction force from the pipe wall on phase k	[N/m³]
Re	Reynolds number	Dimensionless
Re_{3p}	Three-phase Reynolds number	Dimensionless
S	Surface; Surface tension force	[m²]; [N/m³]
$S_G(d_D)$	Zaichik et al.'s velocity structure function	[s²/m⁴]
S_s	Supersaturation	Dimensionless
t	Time	[s]
$t_{D\,i}$	Eddy droplet interaction time	[s]
$t_{D\,R}$	Droplet dynamic response time	[s]
t_E	Eulerian time microscale	[s]
t_{Lag}	Lagrangian time scale	[s]
$t_{\Delta D\,i}$	Time scale for velocity difference between a droplet's 2 sides	[s]
T	Absolute temperature	[K]
u	Specific internal energy; general variable (equation 12.2.1)	[J/kg]; [-]
u_s	Surface structure uniformity factor	Dimensionless
U	Heat transfer coefficient; general vector (equation 12.4.1)	[W/(m²K)];[-]
$v'_{G\,r}$	Radial intensity of gas velocity fluctuations	[m/s]
v	Fluid velocity	[m/s]
V	Volume; Vector used in Newton-Krylov iteration	[m³]; [-]
w	Volume-specific work	[J/m³]
We	Weber number	Dimensionless
x	Axial direction; integration variable defined by equation 2.8.18	
y	Distance from pipe wall (= d/2 – r)	[m]
Y	Primary variables vector	
z	Elevation from reference level	[m]
Z	Compressibility factor for real gas	Dimensionless
$\bar{Z}$	Averaged compressibility factor for real gas	Dimensionless

Greek letters

α	Volume fraction	
α	Thermal diffusivity	[m2/s]

β	Angle defined in figure 3.4.1.	[rad]
δ	Relative iteration error	Dimensionless
δ_l	Laminar sub-layer thickness	[m]
δ_s	Solubility parameter used in equation 18.4.1	[MPa]
ε	Scale porosity	Dimensionless
ε	Energy dissipation per unit mass	[m^2/s^3]
ϵ	Small number used in developing Newton-Krylov iteration	Dimensionless
η	Overpotential	[V]
$\Phi_{LW\,B}$	Malnes' slug friction modification, equation 9.3.6	Dimensionless
γ	Number between 0 and 1 used in equation 12.6.3	[$kg/(m^3 s)$]
$\dot{\gamma}$	Shear rate	[s^{-1}]
Γ	Mass transfer per unit volume and time	[$kg/(m^3 s)$]
Γ_{ki}	Mass transfer per unit volume and time into phase k from other phases	[$kg/(m^3 s)$]
Γ_{kw}	Mass transfer per unit volume and time into phase k from the pipe wall (through perforations)	[$kg/(m^3 s)$]
κ	Ideal gas isentropic exponent	Dimensionless
λ	Eigenvalue	Dimensionless
π_{fS}	Dimensionless group defined by equation 7.2.1	Dimensionless
$\pi_{h_{LS}}$	Dimensionless group defined by equation 7.2.2	Dimensionless
μ	Dynamic viscosity (= $\nu\rho$)	[$kg/(m \cdot s)$]
μ_{fs}	Friction coefficient between sand grains	Dimensioness
μ_J	Joule-Thomson coefficient, as defined by equation 14.2.1	[$kg/(m \cdot s)$]
ν	Joule-Thomson coefficient, as defined by equation 14.2.1	[m^2/s]
ρ	Density	[kg/m^3]
ρv	Area-specific mass flow	[$kg/s \cdot m$]
σ	Surface tension, generally given between two fluids/materials	[N/m]
τ	Shear stress	[N/m^2]
τ_w	Shear stress between fluid and pipe wall	[N/m^2]
θ	Pipe elevation angle, positive is upwards in positive flow direction	Radians

Subscripts

a	Asphaltene
B	Bubble
D	Droplet
G	Gas
i	Spatial discretization No.; Internal (between phases); Inner (pipe layer)
j	Time-step No. (for integration), species No. (for corrosion)

k	Phase No.
L	Liquid
M	Mixture
o	Oil; Outer
S	Superficial (Ex. v_{LS} is liquid superficial velocity); Slug
T	Taylor-bubble (also used for the section of the pipe where the Taylor-bubble occupies the upper part of the pipe)
w	Water; Wax
W	Wall
τ	Relating to shear
1,2,3..	Wall

Superscripts

*	Critical value
1	First step in multistep calculation

Index

- A -

- B -

- C -

- D -

- E -

- F -

- G -

- H -

- I -

- J -

- K -

- L -

- M -

- N -

- O -

- P -

- R -

- S -

- T -

- U -

- V -

- W -

The author, Dr. Ove Bratland, was awarded his PhD from the Norwegian Institute of Technology in 1985. He has 28 years of experience in the petroleum industry as lecturer, consultant, and manager, and has worked in various countries in Europe and Asia. His technical qualifications cover an unusually broad range of skills, including hydraulics and pneumatics, pipe flow with special emphasis on flow assurance, flow measurement, dynamic simulations, software development, dynamic system analysis, and automation. He has worked hands-on with most systems common to the upstream petroleum industry, particularly those found on oil rigs and subsea in the Norwegian sector of the North Sea.

This book is the final in a series of two, and it deals with multi-phase pipe flow assurance. It progresses from single phase theory in the first book, and its purpose is to assist flow assurance engineers.

- Explores topics essential to dealing with gas, oil, water, and particles flowing in pipes and wells.
- Builds on the very latest from fluid mechanics, thermodynamics, mechanical engineering, chemical engineering, discrete mathematics, computer sciences, and automation.
- Goes through theory for two-phase, three-phase, and (partly) four-phase flow, and discusses the main issues to be dealt with from a flow assurance perspective.
- The main emphasis is on transient simulations, but steady-state methods are also discussed.
- Includes an extensive list of **Suggested Reading**.
- Resources for the book, including some simulation programs, can be found at www.drbratland.com

Pipe Flow 2

Multi-phase Flow Assurance

The only book binding together all the main subjects multiphase flow assurance rests on, which makes it a uniquely invaluable reference for engineers and developers involved with multi-phase pipe- and well-flow in the petroleum industry.